Molecular Mechanisms of Inhibition of Histone Acetyltransferases: Implications in Antineoplastic Therapy

A Thesis

Submitted for the Degree of

Doctor of Philosophy

By

Arif

To

Molecular Biology and Genetics Unit

Jawaharlal Nehru Centre for Advanced Scientific Research,

Jakkur, Bangalore- 560064, India

March-2009

DECLARATION

I hereby declare that the work embodied in this thesis entitled *"Molecular Mechanisms of Inhibition of Histone Acetyltransferases: Implications in Antineoplastic Therapy"* has been carried out by me under the supervision of Prof. Tapas K. Kundu, Molecular Biology and Genetics Unit, Jawaharlal Nehru Centre for Advanced Scientific Research, Bangalore and that it has not been submitted for any degree or diploma to any other institution. Following prevalent scientific practice, acknowledgement has been accorded wherever due.

Arif *Arif*

Bangalore

Date: 24/3/09.

iii

572
P09

Prof. Tapas K. Kundu

Transcription and Disease Laboratory

Molecular Biology and Genetics Unit

Jawaharlal Nehru Centre for Advanced Scientific Research,

Bangalore-560064

Certificate

I hereby declare that the work embodied in this thesis, entitled, *"Molecular Mechanisms of Inhibition of Histone Acetyltransferases: Implications in Antineoplastic Therapy"* has been carried out by Arif under my supervision at Molecular Biology and Genetics Unit, Jawaharlal Nehru Centre for Advanced Scientific Research, Bangalore and that it has not been submitted for any degree or diploma to any other institution.

Prof. Tapas K. Kundu

Date: Bangalore-64
March 24, 2009

Acknowledgements

I wish to express my deep gratitude to Prof. Tapas. K. Kundu not only for being my mentor but also for my mental and scientific growth. His natural ability to address problems with clarity, organizing ability and optimism is beyond comparison. I am indebted to him for all the stimulating discussions and criticisms, ingenious ideas and encouragement. His agreeable ways made working a reinvigorating experience.

I would like to thank Prof. Dipak Dasgupta (SINP, Kolkata) and Prof. Chandrabhas Narayana for the crucial suggestions that had helped me to give shape to my work.

My sincere thanks is also for Prof. M.R.S. Rao for his critical comments on the work. I would also like to thank all the Faculty members of the MBGU, JNCASR for all their help, support and encouragement. I thank Prof. Udaykumar Ranga for his constant help and for allowing me to use his lab facilities. I also thank Prof Hemalatha Balaram for stimulating discussions.

I profoundly thank all my teachers, learning from them was enriching and enlightening. They always satisfy my curiosity.

I am thankful to the academic section, computer lab., library and administrative staff.

I am indebted to my previous and present lab-mates Dr. Swaminathan, Dr. Chandrima Das, Dr. Kishore, Dr. Kiran Batta, Dr. Altaf, Radhika, Srikanth, Jayasha, Selvi, Sujata, Dr. Karthikeyan, Dr.Mohan, Thanuja, Vedamurthy, Ashok, Ramesh, Snehajyoti, Senthil Dr. K. Mantelingu, Dr.Beneka Prasad, Dr. Ravindra, Dr. Thimmegowda for being very helpful in laboratory. Their invaluable support helped me tide over many difficult situations. They are wonderful people and learning from them was very fruitful. Our group meetings, discussions, birthday parties will always remind me of my second home in JNC.

Contents

Contents

Contents

Abbreviations

kDa:	kilo Dalton
bp:	base pair
ng:	nanogram
µg:	microgram
pmol:	pico mole
nmol:	nano mole
pM:	pico Molar
nM:	nano Molar
mM:	mili Molar
ml:	mililitre
µl:	microlitre
min(s):	minute(s)
h (s):	hour(s)
CPM:	counts per minute
Rpm:	revolutions per minute
FACS:	Fluorescence Activated Cell Sorting
UV:	ultraviolet
DNA:	Deoxyribonucleic acid
RNA:	Ribonucleic acid
cDNA:	Complementary Deoxyribonucleic acid
PBS	Phosphate buffered saline
DTT:	Dithiothreitol
EDTA:	Ethylene diamine tetraacetic acid
PMSF:	Phenyl Methyl Sulphonyl Fluoride
SDS:	Sodium Dodecyl Sulphate
TEMED:	N,N,N'N'-Tetramethyl-ethylene diamine
TCA:	Trichloroacetic acid

Abbreviation

TE:	Tris-EDTA
PAGE:	Polyacrylamide Gel electrophoresis.
EtOH:	Ethanol
Ph-OH:	Phenol
$CHCl_3$:	Chloroform
DEPC:	Diethyl pyrocarbonate
RT:	Room temperature
E. coli	*Escherichia coli*
IPTG	Isopropyl β-D-thiogalactoside
LB	Luria Bertini Broth
MALDI-TOF	Matrix Assisted Laser Desorption/Ionisation- Time Of Flight
Ni-NTA	Nickel-nitrilotriacetic acid
NAD^+	β -Nicotinamide Adenine Dinucleotide (oxidized form)
PCR	Polymerase chain reaction
CD	Circular Dichroism
p300HD	p300 HAT domain
SERS	Surface Enhanced Raman Spectroscopy
GAPDH	Glyceraldehyde 3-phosphate dehydrogenase
HAT Assay	Histone Acetyltransferase Assay
HMT Assay	Histone Methyltransferase Assay
HDAC Assay	Histone Deacetylase assay
KAT	K(lysine) acetyltransferase
CBP	CREB Binding Protein or KAT3A
PCAF	p300/CBP-associated factor or KAT2B
H&E staining	Hematoxylin and eosin staining
IHC	Immunohistochemistry
i.p	Intraperitoneal
HATi	Histone Acetyltransferase inhibitor

Chapter **1**

This chapter introduce to dynamic organization of chromatin which is regulated by several factors including reversible acetylation of chromatin proteins. The consequences of aberrant acetylation in disease manifestation, specially cancer has also been highlightens.

1. Introduction:

Reversible covalent modification of histone and non-histone proteins plays an important role in the regulation of gene expression and cellular homeostasis in eukaryotes. Any dysfunction in the transcription regulation of genes could lead to diseases. Hence a proper balance between different signaling events in the chromatin context is important. Histone-modifying enzymes are one of the main epigenetic regulators in cells whose malfunctioning has been linked to several diseases including cancer. This provides an opportunity for the therapeutic intervention using small molecule modulators of these enzymes.

1.1. Chromatin: A dynamic nucleoprotein organization:

The organization of DNA into chromatin and chromosome structures plays a central role in many aspects of cell biology and developments in eukaryotes. Chromatin is the physiological template for nuclear processes involving genomic DNA, including transcription by RNA polymerase II (Pol II). The structural unit of chromatin, the nucleosome, comprises 147 bp of DNA wrapped around an octamer of core histone proteins (two copies each of H2A, H2B, H3, and H4) in ~1.7 turns (Figure 1.1) (Richmond and Davey, 2003). Chromatin exists in multiple, functionally distinct

structural states that are defined by their protein composition and level of compaction (e.g., transcriptionally active euchromatin and transcriptionally repressed heterochromatin (Horn and Peterson, 2002; Woodcock and Dimitrov, 2001). The dynamic interconversion between these different chromatin states can play an important role in transcriptional regulation (Horn and Peterson, 2002; Woodcock and Dimitrov, 2001).

The establishment of distinct chromatin domains can be achieved through (1) specific covalent modification of histones (e.g., acetylation, methylation), (2) nucleosome assembly with histone variants (e.g., H2A.Z, CENP-A), or (3) incorporation of nucleosome binding non-core histone proteins, such as the linker histone H1, the heterochromatin-associated protein HP1, poly(ADP-ribose) polymerase-1 (PARP-1) and PC4 (Brown, 2003; Horn and Peterson, 2002; Kellum, 2003; Kim et al. 2004; Das et al. 2006). The effects of H1 and HP1 incorporation on chromatin structure have been well defined, with both factors causing the condensation of chromatin into compact, transcriptionally repressed higher-order structures that form discrete chromatin domains (Brown, 2003; Horn and Peterson, 2002; Kellum, 2003). The formation and disruption of higher-order chromatin structures is regulated by the same histone-modifying enzymes (e.g., acetyltransferases, deacetylases) and chromatin remodeling complexes (e.g., SWI/SNF family) that act locally to modify individual nucleosomes at promoters (Horn and Peterson, 2002). Thus, chromatin is a heterogeneous nucleoprotein filament whose structure and activity is modulated by its constituent proteins, as well as a diverse group of regulatory enzymes.

1.2. Nucleosome: The Fundamental Unit of Chromatin:

The most fundamental and well-characterized structural unit of the chromosome is the nucleosome (Kornberg, 1974; McGhee and Felsenfeld, 1980) (Figure 1.1). The nucleosome/ chromatin structures play critical roles in the regulation of various genomic events; the nucleosome restricts the access of regulatory proteins and prevents the progress of enzymatic reactions along the DNA (Felts et al., 1990; O'Neill et al., 1992).

Not only the nucleosome structures but also the higher-order arrangement of the nucleosome array plays important roles in a number of genome functions; transcriptional regulation is known to be tightly coupled with the dynamic structural changes of the nucleosomal arrays (Ding et al., 1997).

The nucleosome core contains 147 bp of DNA supercoiled in 1.67 left-handed turns around a core histone octamer (Richmond and Davey, 2003). The core histone octamer consists of two copies of each H2A, H2B, H3 and H4. X-ray
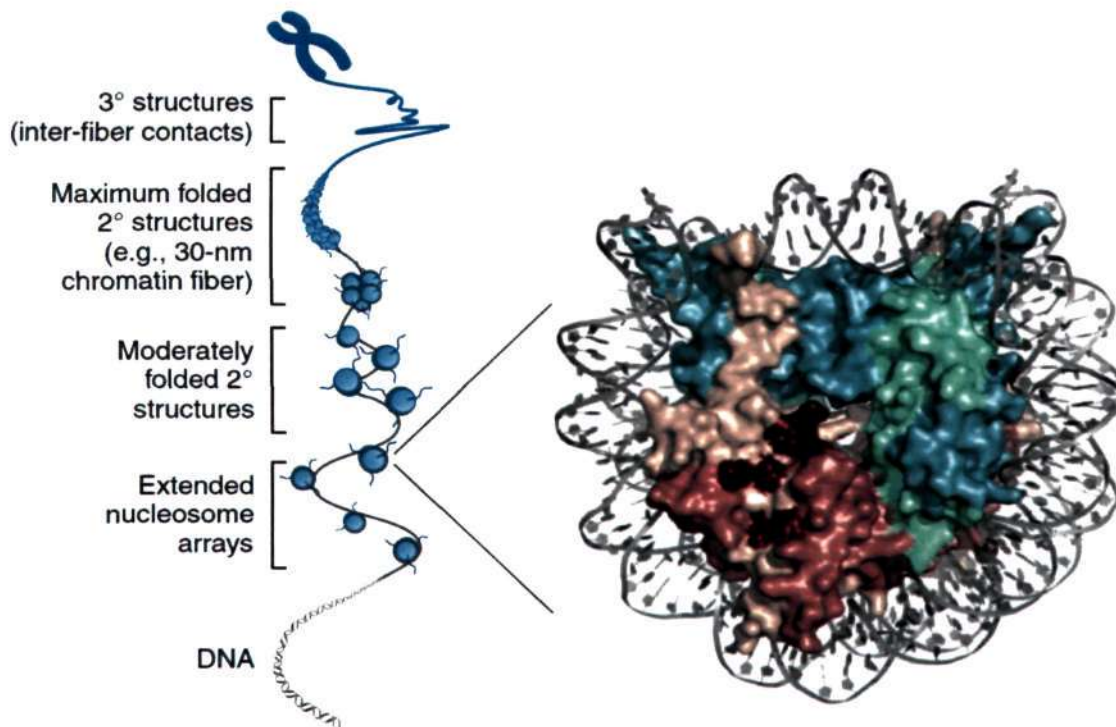
Figure 1.1: Multiple levels of chromatin structure: Left, schematic of various levels of chromatin compaction, from extended nucleosome arrays to folding of secondary chromatin structures exemplified by the 30-nm chromatin fiber to poorly characterized higher-order structures. There are ten histone tails protruding from each nucleosome core. Right, detail of nucleosome surface showing histones H2A (yellow), H2B (light red), H3 (blue) and H4 (green). Residues comprisingthe charged pocket are shown in dark red. (Taken from Caterino et al, 2007)

crystallography has revealed that histone octamer has a disk-like shape with the diameter of 6.5 nm and the thickness of 6.0 nm (Arents et al., 1991). The tails of H2A and H4 stick out of the disk-shaped nucleosome and the tails of H3 and H2B extend between DNA

gyres (Luger et al., 1997). DNA wrapping around the octamer (nucleosomal DNA) has a helical pitch of 10.2 bp per turn (Satchwell et al., 1986), which is shorter than that of free B-type DNA (10.5 bp per turn) (Rhodes and Klug, 1981). Therefore, about 1 positive supercoiling is introduced by one nucleosome assemble (Germond et al., 1975; Keller, 1975), because 146 bp of DNA wraps around the octamer.

Core histones are evolutionary conserved basic proteins, and consist of unstructured, flexible N-terminal tails, and globular C-terminal domains that make up the nucleosomal scaffold. All histones have a common motif, called the histone
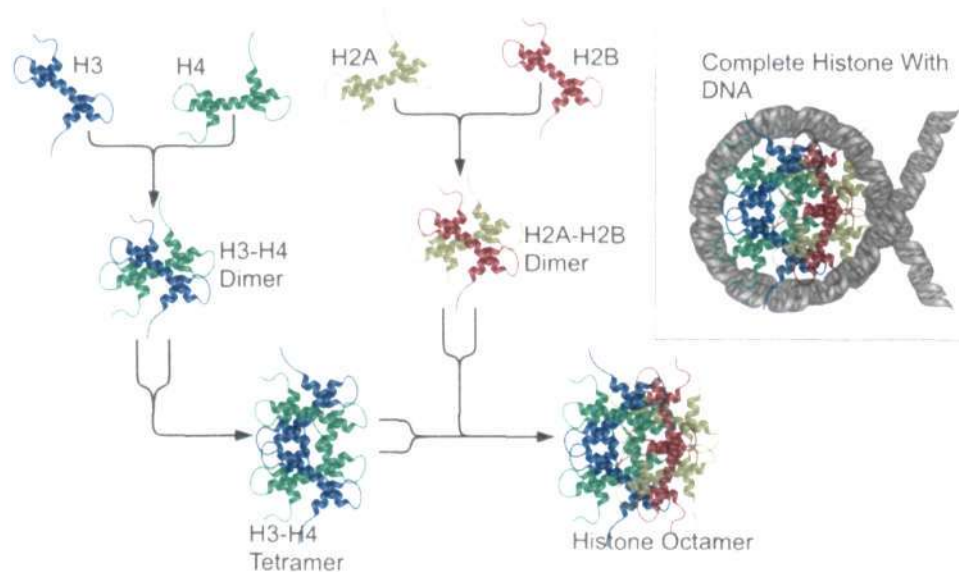
Figure 1.2: Structural organization of a nucleosome : The steps of chromatin assembly involve formation of a H3-H4 tetramer followed by H2A-H2B dimer. Finally there is formation of the core octamer with a double stranded DNA wrapped around it. Histone H1 (not shown here) is positioned at the dyad axis of the nucleosome forming the chromatosome.

fold domain made up of three α helices connected by loops (Figure 1.2). These regions are involved in the formation of the heterodimers, H3-H4 and H2A-H2B. Under physiological condition, H3-H4 stably oligomerize into a tetrameric structure, while H2A and H2B remains as a dimmer. Intramolecular hydrogen bondings between the charged groups buried in the helix bundle occurs and hydrophobic interactions within the dimmers also contributes to the stability (Figure 1.2). The assembly of nucleosomes takes

place in two step process. The initial step is the deposition of the H3-H4 tetramer onto the DNA followed by the deposition of a pair of H2A-H2B dimmers, resulting in reconstitution of the nucleosome (Figure 1.2). This step is generally mediated by a class of protein called histone chaperones.

The tetramer binds to the central 60bp of the nucleosomal DNA. The H2A-H2B dimmers are tethered to one half of the histone H4-H4 tetramer (Figure 1.2). Each dimmer organizes 30 bp towards the ends of the DNA and each histone fold pair leaves a 4 bp linker between the units. The distortion of the DNA helix is brought about by the interaction between the structures regions of the histone protein and the minor groove of the DNA over 14 different locations (Luger, 1997). The unstructured histone tails protrude out of the core particle through the gyres of the DNA super helix. Histone tails do not contribute to the stability of the core particle structure but may contribute to the higher order chromatin structure. The internucleosomal interactions between the histone tails, results in further compaction of the nucleosomal structure into the solenoid structure i.e 30n.m fiber, which could form the physiological template in vivo (Figure 1.1). The solenoid remains attached to the chromosomal scaffold through the scaffold attachment region (SARs), forming loops of variable lengths. This structure can be further altered locally by the association with different non-histone chromatin proteins (e.g. HMGs).

Control of higher-order structures is thought typically to involve the modulation of histone tail interactions with DNA. However, recent work suggest that a distinct mechanism exist which shows that a histone protein surface far from the DNA in the nucleosome also has a key role in modulating chromatin structure (Zhou et al. 2007; Chodaparambil et al. 2007). Recent work on the crystal structure of an oligonucleosome (a compact tetranucleosome) at 9A ° resolution shows that linker DNA zigzags back and forth between two stacks of nucleosome cores, which form a truncated two-start helix, and does not follow a path compatible with a one-start solenoidal helix (Schalch et al. 2005).

1.3. Higher order chromatin structure:

The multifaceted hierarchical complex chromatin is made up of the most basic repeating subunit of chromatin, the nucleosome. Individual nucleosomes can block association of trans-acting factors with DNA and thus contribute to the regulation of specific genes. However, it is becoming clear that regulation of 'higher-order' chromatin structures, beyond the level of the nucleosome, is a key aspect of the control of transcription and other nuclear processes (Figure 1.1).

Histone H1 plays an important role in the organization of the higher order chromatin structure. The structure of H1 reveals a central globular domain with N- and C- terminal extensions. H1 interacts with the nucleosome ina 1:1 ratio, without any specificity towards the underlying DNA sequence. H1 binds at or near the nucleosomal dyad exis and interacts with the linker region (Bustin et al. 2005). It is known that H1 is highly dynamic in its interactions with the nucleosome which suggests that H1 plays mainly a regulatory role than a structural one.

There are several nonhistone chromatin proteins which help in the maintenance of chromosomal structure. Among these, PARP-1 plays role in regulation of chromatin structure and gene expression in response to specific cellular signals. The targets of PARP-1 enzymatic activities are PARP-1 itself (primary *in vivo* target), core histones, linker histone H1 and a variety of transcription related factors (Ogata *et al*, 1981; Huletsky *et al*, 1989; Kraus and Lis, 2003). Auto ADP ribosylation of PARP-1 leads to a dramatic reduction in its DNA binding ability and hence leads to a loss of compact chromatin structure.

Myeloid and erythroid nuclear termination stage specific protein (MENT) is a developmentally regulated and a highly abundant nuclear protein found in terminally differentiated avian blood cells belonging to serine protease inhibitor (serpin) family. This protein is found in the condensed chromatin fraction chiefly in the heterochromatin (Grigoryev *et al*, 1999). MENT can bind to naked DNA and form tramline structure wherein two or more DNA molecules come to the proximity. It can also bind to the nucleosomes but in a histone-tail independent manner. The protein oligomerization plays a major role in MENT-dependent chromatin condensation. MENT induces formation of higher order chromatin structure of 30-50 nm diameter with the entry-exit sites of the DNA always oriented towards the center of the fibre ultimately leading to the formation

6

of stacks or coils of chromatin. MENT induced chromatin compaction occurs through the formation of a zipper-like structure bridging the DNA molecules similar to histone H1.

DEK was first isolated as part of a fusion protein expressed in a subtype of acute myeloid leukemia (AML) with chromosomal translocations (von et al, 1992). It is a proto-oncogene, which alters the DNA structure by introducing supercoils (Alexiadis et al, 2000). The change in DNA topology, as introduced by DEK, was only observed with chromatin (but not with naked DNA) and depends on the presence of H2A-H2B dimer (Alexiadis et al, 2000). It can oligomerize and thereby alter chromatin architecture in a phosphorylation-dependent manner.

Human transcriptional coactivator PC4 is a highly abundant multifunctional protein. In our laboratory we have found that PC4 is a bona fide component of chromatin with distinct chromatin organization ability (Das et al. 2006). PC4 was found to selectively interact with core histones H3 and H2B which led to PC4-mediated chromatin condensation. Recent works also suggest the role of post translational regulation of chromatin binding ability of PC4. It has been observed that acetylation reduces the ability of PC4 to compact the chromatin (unpublished data).

1.4. Nuclear dynamics and chromosome territories:

A striking feature of nuclear architecture is the existence of distinct structural and functional compartments (Figure 1.3). Understanding of nuclear architecture is important for understanding the cell-type dependent orchestration of active and silent genes and other nuclear functions like DNA replication, transcription, splicing and repair (Cremer et al. 2006). Each chromosome maintains its individuality during the cell cycle and occupies a spatially limited volume, known as a chromosome territory (CT). These discrete regions can be visualized in vivo as roughly spherical domains of about 2 micrometers in diameter (Cremer et al. 2006). As a result of different compaction levels, different chromosome segments adopt a complex organization and topography within their chromosome territory (Croft et al. 1999; Edelmann et al. 2001; Zink et al. 1998)Well

characterized nuclear substructures include the nuclear lamina, nucleoli, PML(promyeolocytic leukaemia RING-finger protein) and Cajal bodies, and nuclear speckles as shown in the schematic (Figure 1.3).
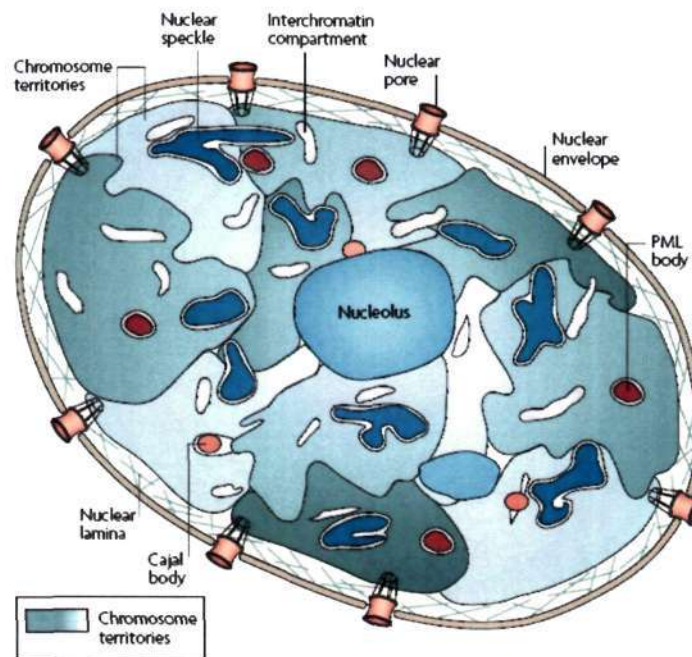
Figure1.3: Model of functional nuclear architecture : Structural features that support the chromosome-territory–interchromatin-compartment (CT–IC) model are shown. The nucleus is characterized by a compartmentalized distribution of functional components. The nuclear envelope contains pores and rests on a meshwork of intermediate filaments, the nuclear lamina. CTs have complex folded surfaces. A giant chromatin loop with several active genes expands from the CT surface into the IC space. CTs have variable chromatin density (dark brown, high density; light brown, low density). Loose chromatin expands into the IC, whereas the most dense chromatin is remote from the IC. Higher-order chromatin structures built up from a hierarchy of chromatin fibres. active genes are at the surface of convoluted chromatin fibres. Silenced genes may be located towards the interior of the chromatin structure. Chromatin is organized in distinct CTs. Also depicted are nuclear speckles, PML bodies and Cajal bodies located in wider IC lacunas The CT–IC model predicts that the IC contains complexes and larger non-chromatin domains for transcription, splicing, DNA replication and repair. (Taken from Lanctôt et al. 2007)

CTs are built up from a hierarchy of chromatin fibers starting from 10nm to 130nm chromosome fibers. Although the exact nature of the higher-order folding of the

chromatin structure is not clear (Cremer and Cremer 2001). There are three basic hypothesis regarding the structure and organization of CTs : (1) higher order chromatin structure (rosettes) are originated from small scale chromatin loops(SLs) (50-200kb long) and are essential building blocks of CTs; (2) CTs are originated from giants loops (GLs) comprising 1-2Mbps DNA; (3) involvement of short and giants loops in the formation of CTs. The SL model supports the existence of CTs separated by interchromatin-compartment (IC). The active genes are located at the periphery of the CTs, in order to allow a functional interaction with various components of the IC. The CT surface can undergo folding, in order to exposé the active genes buried in the interior of CTs, resulting in looping out of CTs into IC. The GL model proposes an existence of chromatin fiber of several Mb DNA (GL) that is separated from the next GL in the same CT by a 200 kb chromatin linker. Modulation of the size of GLs or linkers affect chromatin compactness (Cremer and Cremer 2001).

The interiors of chromosome territories are permeated by highly branched, interconnected networks of channels. These make the genome sequences deep inside accessible to regulatory factors such as gene activators and inhibitors (Figure 1.3). In addition, the structure of the DNA within chromosome territories is nonrandom, as the chromosome arms are mostly kept apart from each other and gene-rich chromosome regions are separated from gene poor regions. This arrangement probably contributes to the structural organization of the chromosome, and might also help in regulating particular sets of genes in a coordinated manner. Recent studies indicate that although there is a correlation between open chromatin structure and high gene density but it does not corroborate with high gene expression. This is because of the fact that there is presence of some active genes in more compact and silent genes in more open chromatin loci, indicating that open or closed chromatin conformation are not the only determinant of gene expression. Interestingly, role of RNA has been suggested in the organization of chromatin in maintaining higher order folded chromatin architecture beyond 30nm fiber (Worcel et al.1972; Zamore et al. 2005; Ohniwa 2007).

1.5. Euchromatin and Heterochromatin:

The nuclear organization of chromatin exists in a highly dynamic functional organization with regions with varying gene expression. Transcriptionally active regions of high gene expressions are known as euchromatin unlike the heterochromatin regions which is structurally more compact with more silenced genes. Heterochromatin is characterized by silenced chromatin loci e.g. centromere and telomere regions. Chromatin in this region is hypoacetylated on histones and hypermethylated on the DNA. The nucleation of heterochromatin formation at a particular locus begins with the requirement of sequence-specific DNA binding proteins at the silencer regions. In case of the telomeres, the Rap1p protein binds to the telomere repeats (Luo et al. 2002). These proteins then recruit the Sir proteins which in turn recruits the Sir3p and the Sir2p histone deacetylase, which deacetylates H4K16, promoting the spread of this complex.

In case of the centromeric regions, short stretch of repetitive DNA is activated by RNAi pathway leading to the recruitment of Suv29H1, a histone methyltransferase. Further, H3K9 gets methylated and creates a docking site for HP1 which results in the silencing (Maison et al. 2004; Nielsen et al. 2001). H3K9me is further enhanced by the removal of H3K9 and H3K14 acetylation by the HDAC complex. The euchromatin-heterochromatin boundary is efficiently maintained by the insulator elements. H4K16 acetylation has been shown to demarcate the heterochromatin boundaries. The acetylase Sas2p is responsible for the maintenance of this histone mark globally, thereby defining boundaries for the heterochromatin (Suka et al. 2002).

1.6. Transcription from Chromatin template:

The complex eukaryotic genome are complex of up to 25 000 genetic loci in human and are organized within compact nucleoprotein structures called chromatin. The mechanisms by which individual genes get expressed involve the coordinated action of many specialized proteins and protein complexes in a spacio-temporal manner called transcription (Roeder 2005).

Eukaryotic cells contain RNA polymerase-specific general initiation factors that, despite the structural complexity of the enzymes (14, 12 and 17 subunits in RNA polymerases I, II and III, respectively), are necessary for accurate transcription initiation on corresponding core promoter elements by purified RNA polymerases (Roeder 2003; Roeder 2005). These factors include TFIIIC and TFIIIB for RNA polymerase III; TFIIA, TFIIB, TFIID, TFIIE, TFIIF and TFIIH for RNA polymerase II; and several factors for RNA polymerase I. Further, core promoter recognition factors which include TFIIIC for class III and TFIID for class II promoters were discovered. At the same time mechanistic studies revealed pathways for the ordered assembly of initiation factors and RNA polymerases into corresponding preinitiation complexes (PICs). The structural
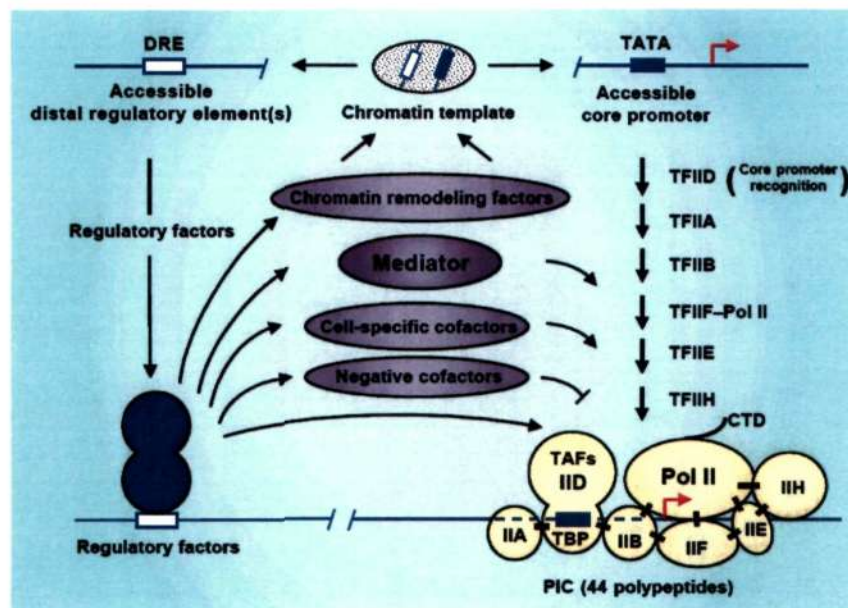
Figure 1.4: PIC assembly pathway of class II genes and the general initiation factors: A model for the regulation of PIC assembly and function involves, sequential binding of regulatory factors to distal control elements. This is followed by the regulatory factor interactions with cofactors that modify chromatin structure and facilitate binding of additional factors. Finally the regulatory factor interact with cofactors that act after chromatin remodeling to facilitate, through direct interactions, recruitment or function of the general transcription machinery. TAFs, TBP-associated factors. (Taken from Roeder, 2003)

11

complexity of the basic preinitiation complexes (~25 and 44 polypeptides, respectively, for RNA polymerases III and II) is remarkable which is proved by a variety of biochemical and genetic analyses and which provided a detail picture regarding the structure and function of the individual polypeptides during PIC formation and during subsequent steps of transcription events . In the case of RNA polymerase II, additional insights into PIC formation and RNA polymerase function have been provided by structural studies of TBPTATA and higher order complexes (Nikolov et al. 1997) and of RNA polymerase II itself (Cramer 2002; Cramer et al. 2001) (Figure 1.4).

The pathways leading to productive PIC assembly at the promoter region has been intensively studied in great detail. In vitro transcription experiments performed with chromatographic fractions derived from HeLa cells suggests that PIC could be assembled in a stepwise manner. Further, the hierarchical nature of GTF assembly at the promoter region was further defined. (Buratowski et al,1989). Thus suggesting an order-of-addition model for PIC formation. Specifically, TFIID first recognizes the TATA box, followed in a stepwise manner by the entry of TFIIA, TFIIB, pol II and TFIIE. Once all of the GTFs were identified and purified to near homogeneity, The stepwise GTF assembly pathway was updated as: TFIID first binds to the promoter region, followed by the entry of TFIIA and TFIIB that help stabilize promoter-bound TFIID, and then the recruitment of pol II/TFIIF. After formation of a stable TFIID-TFIIA-TFIIB-pol II/TFIIF-promoter complex, TFIIE is then recruited, with the subsequent entry of TFIIH. This stepwise manner of PIC assembly became known as the sequential assembly pathway (Figure 1.4).

Further with the discovery that pol II could be purified as a preassembled holoenzyme complex SRBs (suppressors of RNA polymerase B mutations) (Kim et al., 1994; Koleske and Young, 1994), with or without a subset of GTFs; and other proteins involved in chromatin remodeling, DNA repair, and mRNA processing (reviewed in Thomas et al. 2006) led to the concept of alternative pathway for PIC formation. Further, the identification of a TFIID-deficient pol II holoenzyme complex suggests that TFIID, as a core promoter-binding factor, may facilitate the entry of pol II holoenzyme to the promoter region.

1.7. Chromatin regulation during transcription:

The complex of DNA and protein into nucleoprotein structure, chromatin, imposes obstacles on all aspects of transcription that are mediated by RNA polymerase II. The dynamics of chromatin structure are tightly regulated by several mechanisms including histone modification, chromatin remodeling, histone exchange and variant incorporation (Li et al. 2007). The presence of nucleosomes is now known to affect all stages of transcription from activator binding and PIC formation to elongation (Workman and Kingston, 1998).During the process of transcriptional activation direct interaction of sequence-specific transcriptional activators with coactivators are achived. Coactivators coordinate the modification and remodeling of chromatin with the assembly of a preinitiation complex (PIC) (Li et al. 2007).

It is well known that histone acetylation is closely linked to gene transcription. Numerous studies have shown that chromatin acetylation generally precedes transcription (Cosma, 2002; Reinke and Horz, 2003).The identification of histone acetyltransferases (HATs) and the large multiprotein complexes in which they reside has yielded important insights into how these enzymes regulate transcription. The demonstration that HAT complexes interact with sequence-specific activator proteins further illustrates how these complexes target specific genes (Brown et al. 2000). The highly related metazoan HATs, p300 and CBP, act as coactivators for a wide variety of transcriptional activators including GAL4-VP16, p53, and nuclear receptors (Roth et al. 2001). The HAT activity of p300 is targeted to chromatin by activators in vitro and is necessary for p300-dependent transcription from chromatin in vitro and in vivo (Kundu et al., 2000; Roth et al., 2001) (Figure 1.5). In addition to histones, p300 acetylates activators, nonhistone chromatin- associated proteins, and itself, a phenomenon termed autoacetylation (Roth et al. 2001). These acetylation reactions influence transcriptional activity in vitro and in cells (Black et al. 2006; Black et al. 2008)

The affect of different histone modifications on transcription is now well documented (Li et al. 2007). Modifications that are associated with active transcription, such as acetylation of histone 3 and histone 4 (H3 and H4) or di- or trimethylation (me)

of H3K4, are commonly referred to as euchromatin modifications. Similarly, modifications that are localized to inactive genes or regions, such as H3 K9me and H3 K27me, are termed as heterochromatin modifications. Most modifications are distributed in distinct localized patterns within the upstream region, the core promoter, the 5' end of the open reading frame (ORF) and the 3' end of the ORF. Indeed, the location of a modification is tightly regulated and is crucial for its effect on transcription (Li et al. 2007). This is evident from the fact that Set2- mediated methylation of histone H3K36 normally occurs within the ORF of actively transcribed genes. However, if Set2 is mistargeted to the promoter region through artificial recruitment, it represses transcription (Landry et al., 2003; Strahl et al., 2002). Similarly the distribution of histones can also affect the rate of transcription. Presence of histone variant H2A.Z at the promoter region can negatively affect the rate of transcription. In addition, transcription activation can trigger deposition and removal of H3.3 from the Drosophila genome (Schwartz and Ahmad, 2005). Further H2ABbd, a H2A histone variant can lead to transcriptional activation. Similarly, macroH2A localized in the Inactive X chromosome can cause X chromosome inactivation while H2A.X, that becomes phosphorylated upon DNA damage that lead to gene repression.

Recent works suggest the role of chromatin remodeling complexes in stimulating binding of TFs (transcription factors) to nucleosomal sites (Utley et al., 1997). It has also been predicted that there is a low-level nucleosome occupancy at functional TF-binding sites and that there are more stable nucleosomes at the nonfunctional sites. Therefore, it seems that eukaryotic cells tend to position sequence-specific TF-binding sites within accessible regions. Thus, the first step of gene activation (activator binding) could be more responsive to signaling pathways than it would be if the binding sites were sequestered (Li et al. 2007). Consistent to this, high levels of histone H3K4/79 methylation and H3 acetylation were found to be strict prerequisites for binding of the Myc transcription activator, which implies that chromatin modifications can actually regulate TF binding (Guccione et al., 2006).

During transcription initiation, activators bind to the promoter and trigger a cascade of recruitment of coactivator complexes. Coactivators (such as chromatin-remodeling complexes, histone-modification enzymes, and mediator) not only facilitate

stronger binding of activators to DNA but also make nucleosomal DNA elements more accessible to GTFs. However, it has been demonstrated that acetylation of H3 and H4 peaks sharply at active yeast promoters and that, when normalized to nucleosome density, the level of acetylation is proportional to the transcription rate (Pokholok et al., 2005). Consistent with this observation, Robert et al. reported that the HATs Gcn5 and Esa1 are both generally recruited to promoters genome wide (Robert et al., 2004). Similarly, SAGA is recruited to the promoter through direct interaction between its Tra1 subunit and a bound activator (Brown et al., 2001). SAGA recruitment and histone acetylation occur prior to PIC formation at the GAL1 promoter (Bhaumik and Green, 2001).

In case of trancscription elongation, Pol II releases from GTFs and travels into the coding region which signals the recruitment of the elongation machinery, which includes different factors involved in polymerization, mRNA processing, mRNA export, and chromatin function (Hahn, 2004).During this process cells uses specific set of factors to control chromatin architecture during elongation, and the events and factors required at the beginning of the gene differ significantly from those required at the end. This is done not only to promote efficient RNA synthesis but also to ensure the integrity of the chromatin structure while Pol II travels through the body of the gene. The dynamics of chromatin during elongation in yeast is determined by the factors associated with different forms of Pol II called PAF. PAF facilitates the binding of FACT, COMPASS, and Rad6/Bre1 to the Ser5-phosphorylated CTD, which results in H2B ubiquitination and accumulation of trimethylation of H3K4 at the 5' end of ORF. The histone methyltransferase, Set2 directly interacts with Ser2-phosphorylated CTD, thus methylating H3K36 at the 3' end (Li et al. 2007) (Figure 1.5).

It has been observed that when Pol II migrates into promoter-distal regions, where the influence of activator-dependent HATs is diminishing, Pol II requires other HATs (elongators or those associated with Pol II) to acetylate the nucleosome in front of elongation machinery. The movement of Pol II causes histone displacement. Subsequently, these histones are redeposited onto the DNA behind Pol II via concerted actions of histone chaperones. Alternatively, the free forms of histones in the nucleus are also available for reassembly. These newly deposited nucleosomes are somehow hyperacetylated and are immediately methylated by Set2. Methylation of H3K36 is then
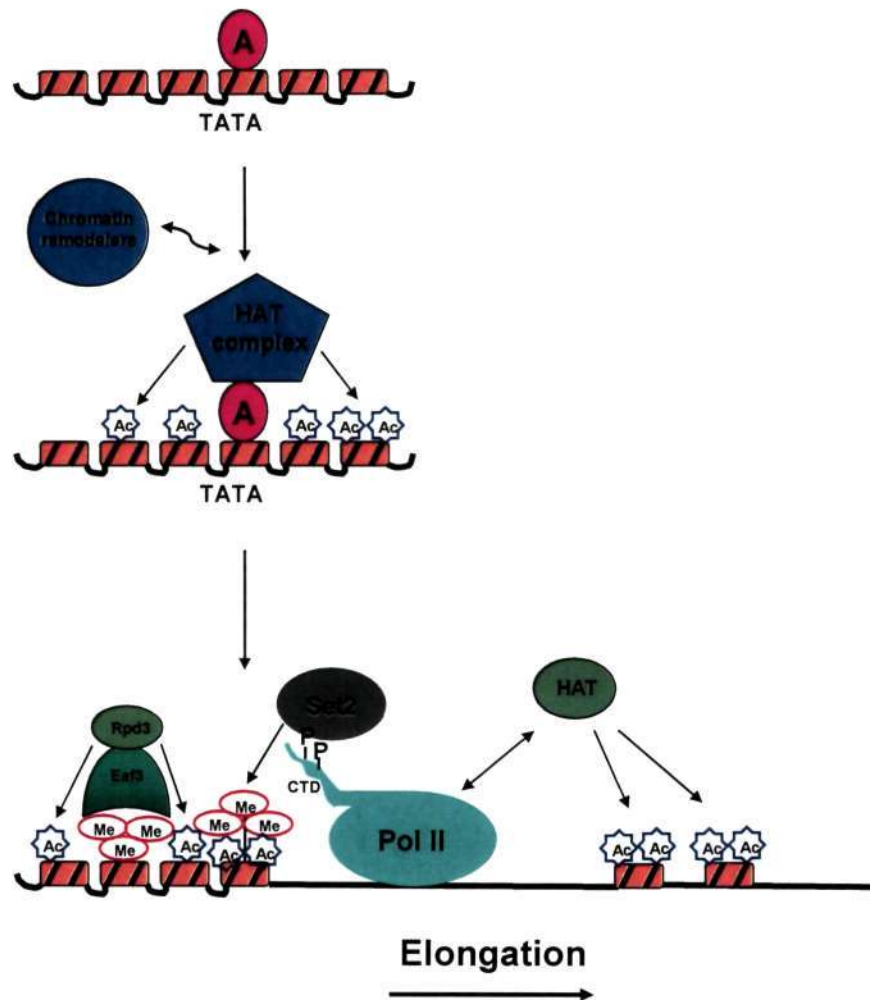
Figure 1.5: Chromatin regulation during transcription and a possible mechanism of HAT targeting to promoter. Activator protein (A) binds to its binding site upstream of a promoter. The activator subsequently recruits activators recruit various coactivators (such as Swi/Snf or SAGA). HAT complex (e.g. SAGA) that acetylates the nucleosomal histones at promoter-proximal regions. Further other transcription factors or general transcriptional machinery gain the access to the promoter (TATA box) leading to the pre-initiation complex (PIC) formation and strart of transcription. Set2 directly interacts with Ser2-phosphorylated CTD, thus methylating H3K36 at the 3'end. During elongation HATs (elongators or those associated with Pol II) acetylate the nucleosome in front of elongation machinery. Histones are displaced during the Pol II movement. Subsequently, these histones are redeposited onto the DNA behind Pol II with the help of histone chaperones which are methylated by Set2. Methylation of H3K36 is then recognized by the chromodomain of Eaf3, which in turn recruits the Rpd3S deacetylase complex (not shown). For detail see text.

16

recognized by the chromodomain of Eaf3, which in turn recruits the Rpd3S deacetylase complex. Rpd3S removes the acetyl marks and leaves the nucleosome in a stable state. Methylation of H3K36 is eventually eliminated by a histone demethylase when the gene turns off (Li et al. 2007) (Figure 1.5).

1.8. Role of Post-translational modifications (PTMs) :

PTMs provide a dynamic means to modify intracellular proteins and to elicit changes in cellular function. PTMs are recognized by a wide array of modular interaction domains, which read the state of the proteome. In combination, the large set of PTMs and corresponding interaction domains provide a versatile mechanism to orchestrate cellular behavior. Predominantly reversible phosphorylation and acetylation play pivotal role in transcriptional regulation and the other functions of the cellular proteins.

Protein phosphorylation and phosphorylation-dependent interactions are one of the most well documented post-translational modifications involved in many cellular phenomena. It affect different biological processes like growth, metabolism, division, differentiation, motility, organelle trafficking, membrane transport, muscle contraction, immunity, learning and memory (Manning et al. 2002). It is known to alter the biological function and subcellular localization of proteins. Presently around 1000 different protein kinases and around 500 phosphates are known to be encoded by human genome. Further, imbalances in the state of phosphorylation are known to cause of many diseases. Phosphorylation of histones plays a critical role in chromatin dynamics and thereby regulates cellular death, mitosis, transcription, DNA repair, replication and recombination .

Among protein methylation, histone methylation on lysine or arginine residues (Kouzarides. 2007; Shilatifard. 2006) are well known. Histone arginine methylation can occur in the mono- or dimethylated form at specific positions on histone H3 and histone H4 in higher eukaryotes. Histone lysines can be mono-, di-, or trimethylated on lysines 4, 9, 27, 36 and 79 of histone H3 and Lys20 of histone H4. Unlike HATs, which can be promiscuous in their histone substrate specificity and can

modify several residues within the same or different histones, histone methyltransferases are typically more specific about their histone targets (Bhaumik et al. 2007).

Histones may also be modified by the attachment of multiple anionic ADP-ribose monomers. The resultant poly(ADP-ribose) chains are generated by the catalytic action of poly(ADP-ribose) polymerases (PARPs). Using NAD^+ as a substrate, PARPs transfer successive ADP-ribose moieties to glutamic acid or aspartic acid residues of substrate proteins. This results in an increased negative charge that alters the biological properties of the histone and affects condensation of the chromatin fiber. PARP-1 is involved in transcription, replication, recombination, genomic stability, cell death and DNA-damage signaling and repair (Huletsky et al. 1989; Hassa et al. 2006).

Like histone acetylation, histone ubiquitination is important in the regulation of gene expression. In fact, several early studies showed an abundance of ubiquitinated histones at transcriptionally active gene loci. In vivo all the histones can be ubiquitylated at lysine residues; however H2A and H2B ubiquitylation is most common Ubiquitination of protein in general lead to protein degradation (Keppler et al. 2008). Further, lysine residues can also undergo a related modification upon the addition of small ubiquitin-related modifiers (SUMO) called ubiquitylation. SUMO moieties share only 18% sequence identity to ubiquitin, however, they possess similar secondary and tertiary structural elements. SUMOylation, though, does not translate into a degradation signal as does ubiquitylation but rather serves solely as a regulatory signal (Shiio et al. 2003).

1.8.1. Acetylation:

The acetylation of proteins by acetyltransferases is increasingly considered a biologically relevant regulatory modification like phosphorylation (Kouzarides.2000). Acetyltransferases transfer acetyl groups from acetyl-coenzyme A (AcCoA) either to the α-amino group of the amino-terminal residue (N-acetyltransferases) or to the ε-amino group of specific lysine residues (histone/factor acetyltransferases) of substrate proteins (1). The reverse reaction is catalyzed by deacetylases that remove acetyl groups from

specific acetyllysine residues in their substrates. The reversible lysine acetylation of histones and nonhistone proteins plays a vital role in the regulation of many cellular processes including chromatin dynamics and transcription (Kuo et al. 1998; Kouzarides. 1999; Knoepfler et al. 1999; Wolffe et al. 2000), gene silencing (Bestor et al. 1998; Razin et al. 1998), cell cycle progression (Marzio et al. 2000; Takahashi et al. 2000; Morris et al. 2000; Zhang et al. 2000), apoptosis (Fu et al. 2004; Roh et al. 2004; Iyer et al. 2004), differentiation (Koipally et al.1999; Wang et al. 1999; Zhou et al. 2000; Sartorelli et al 2001; Miska et al 2001), DNA replication (Iizuka et al. 1999; Aggarwal et al. 2004), DNA repair (Gu et al. 1997; Sakaguchi et al. 1998; Liu et al. 1999; Abraham et al. 2000; Rubbi et al. 2003; Bernardi et al. 2004), nuclear import (Madison et al. 2002; Blander et al. 2002; Gay et al. 2003), and neuronal repression (Huang et al. 1999; Roopra et al. 2000; Boutillier et al. 2003). More than 20 acetyltransferases and 18 deacetylases have been identified so far, but the mechanistic details of substrate selection and site specificity of these enzymes is still not clear for most of these enzymes. Over 40 transcription factors and 30 other nuclear, cytoplasmic, bacterial, and viral proteins have been shown to be acetylated in vivo (Sterner et al.2000; Polevoda et al. 2002), and the investigation of protein acetylation continues (Dormeyer et al. 2005). A detail overview of the Biological implications of protein acetylation is given in Table 1.1.

1.8.1. a Role of acetylation of proteins in cellular function:

Lysine side chains can be acetylated, methylated (mono-,di or trimethylation), ubiquitinated (mono- or polyubiquitination), sumoylated and ADP-ribosylated (Merrick and Duraisingh, 2007). These rivalling and reversible posttranslational modifications are regulated by a complex interplay of different enzymes. Reversible acetylation of lysine ε-amino groups crucially modulates protein function and cellular networks. In eukaryotic cells, acetylation is among the most common covalent modifications and ranks similar to the important master switch phosphorylation (Kouzarides, 2000). Acetylation apparently shows a broader substrate spectrum than phosphorylation, and far fewer acetylases than

kinases have been described. Intriguingly, no acetylation cascades have been described (Ref from Staphinie).

Hundreds of proteins are known to be modified by acetylation. Acetylation can change protein characteristics and functions enormously. In general, acetylation changes the electrostatic state of lysine from positive to neutral and increases the size of the amino acid side chain. Acetylation can affect enzymatic activities, as acetylated lysines exhibit slightly different preferences for secondary structures than unacetylated lysines. Different covalent modifications can furthermore compete for the same lysines important for signalling or the subcellular localisation of a protein (Kim et al., 2006). Additionally, the acetylation of lysines can create new docking sites for protein–protein interactions, for example via recognition by the bromodomain. Hence, acetylation can determine protein function at multiple levels. Acetylation can affect signaling pathways and thereby alter cell fate and function mRNA splicing, mRNA transport, mRNA integrity, translation, protein activity, protein localisation, protein stability and interactions are regulated by acetylation. Hence, acetylation can interfere with different levels of regulatory processes from signaling to transcription to protein degradation.

The process of gene expression has been closely linked to acetylation. In addition to histone acetylation, the acetylation of non-histone proteins is important. For example, acetylation of transcription factors within their DNA-binding domain has been described. In the cases of E2F1, YY1 and many more, this results in altered DNA binding affinity (Table 1.1) (Lamonica et al., 2006; Martinez- Balbas et al., 2000). However, acetylation can equally inhibit the DNA binding of transcription factors, providing an explanation why HDAC inhibitors do not generally increase gene expression many folds. Not all proteins are regulated by acetylation of the protein itself. For example, HDAC6-mediated Hsp90 deacetylation enables activation of the glucocorticoid receptor by ligands (Kovacs et al., 2005).

The inducible transcription factor NF-κB plays a central role in immune responses, inflammation, cell survival, differentiation and proliferation. The NF-κB/Rel family consists of p50, p52, p65 (RelA), c-Rel and RelB, which form homo- or heterodimers (Xiao, 2004). Posttranslational modifications of NF-κB dimers have been

shown to alter their interactions with co-activators. Phosphorylated p65 preferentially interacts with p300/CBP, resulting in p65 acetylation at multiple sites. Acetylation of K221 and K310 is associated with an increased transcription of NF-κB target genes (Chen and Greene, 2004).

Table 1.1: Biological implications of protein acetylation. (Modified from Stephanie, 2008)

Biological implication	Proteins affected by acetylation	
Protein stability	*Acetylation increases stability* p53, p73, Smad7, c-Myc, Runx3, AR, H2A.z, E2F1, NF-E4, ER81, SREBP1a, HNF6, BACE1	*Acetylation decreases stability* GATA1, HIF-1α, pRb, SV40 T-Ag
Gene expression	*Transcriptional activation* p53, HMG-A1, STAT3, AR, ERα (basal), GATA,PC4 EKLF, MyoD, E2F1, p65(NFκB), GR, p73, PGC1α, MEF2D, GCMa, PLAG1, PLAGL2, Bcl-6, α-Catenin, KLF5, Sp1, BETA2, Cart1, RIP140, TAF(I)68	*Transcriptional inactivation* Erα (ligand-bound), HIF-1α, STAT1, FOXO1, FOXO4, RIP140
DNA binding	*Increased DNA binding* p53, SRY, STAT3, GATA ,PC4, E2F1, p50 (NFκB), Erα, p65 (NFκB), c-Myb, MyoD, HNF-4, NF-E2, KLF13 AML1, BETA2, , TAF(I)68, AP endonuclease	*Decreased DNA binding* YY1, HMG-A1, HMG-N2, p65 (NFκB), DEK, KLF13, SATB1
Enzymatic activity	*Enhanced* p300, ATM	*Decreased* PTEN, HDAC1, Mdm2, ACS, Polβ
Protein interactions	*Enhanced* STAT3, AR, EKLF, Importin A, STAT1, TFIIB, α-Tubulin, actin, cortactin	*Decreased* p65(RelA), Ku70, Hsp90
mRNA stability	*Increased* p21, Brm	*Decreased* Tyrosinhydrolase (Th), eNOS
Localisation	*Nucleus* PCAF, SRY, CtBP2, POP-1, HNF-4, PCNA	*Cytosol* c-Abl, PAP

Acetylation can prevent ubiquitination and proteasomal degradation (Table 1.1). Acetylation regulates protein stability in a sophisticated manner and by surprisingly diverse mechanisms (Sadoul et al., 2008). Acetylation of lysines can block ubiquitination at the same residue thereby preventing proteasomal degradation. This was first suggested for p53, which is tightly controlled by the Mdm2 E3 ligase driving proteasomal degradation of p53. PCAF and p300/CBP catalyse acetylation of C-terminal p53 lysine residues (K320, K370, K372, K373, K381 and K382), which overlap with ubiquitination sites. It was shown that acetylation abrogates complex formation between p53 and Mdm2. (Ito et al., 2002).

Further it is also known that aberrant acetylation levels of proteins not only lead to the dysfunction of these proteins but also cause disturbances in cellular processes thereby leading to several diseases. There are several reports of aberrant acetylation in diseases like cancer, diabetes, cardiac hypertrophy and viral diseases. For example, in hyperglycemic conditions HIF1 degradation is increased because of enhanced HIF1 acetylation by a factor acetyl transferase ARD1, which makes it susceptible to proteosomal degradation (Jeong et al. 2002). Insulin receptor substrate proteins (IRS) are the key regulators of insulin action. IRS1 is acetylated and the acetylation enhances its phosphorylation, which mediates the down stream insulin dependent signaling. IRS1 is associated with HDAC2 and HDAC2 mediated deacetylation have the reverse effect. HDAC2 specific small molecular inhibitors may elevate insulin sensitivity in otherwise insulin resistant conditions (Kaiser and James, 2004). Link between HAT and diseases will be discussed in section 1.8.2.

1.9. Chromatin and Disease:

Disease pathogenesis may result from genetic alterations and/or a more diverse group of epigenetic changes. While events such as DNA methylation are well established, there is significant interest in nucleosome remodeling, RNA interference and histone modifications, as mechanisms that underlie epigenetic effects. While genetic mutations are permanent, epigenetic changes can be transitory. The potential to reverse epigenetic

changes has led to the development of therapeutic strategies targeting chromatin-modifying enzymes.

Chromatin structure affects gene expression as well as replication, recombination and DNA repair. Several human diseases are linked to or are even based on defects in the machinery maintaining and/or modifying chromatin structure. For instance, DNA methylation patterns are severely altered in tumors with a bias for overall hypomethylation of the genome and hypermethylation of specific CpG rich regions (Herman et al. 2003; Jones et al. 2002).

In many cancers and other diseases, epigenetic mechanisms, working in concert with genetic alterations, may alter histone modifications, sending transcriptional control into disarray. Epigenetic mechanisms of transcriptional control, unlike genetic changes, include changes in gene expression that occur independently of any change in DNA sequence integrity (Jones et al. 2002). A number of cellular processes are affected by epigenetic dysregulation including cell growth, proliferation, differentiation, DNA repair, cell cycle control and apoptosis. Therefore, from a therapeutic standpoint, targeting the reversible epigenetic changes may be a more attractive approach than targeting the more stable genetic mutations. In fact, certain cancers, for example, display specific histone modification profiles. Recent studies have shown that specific histone modifications can serve as markers for cancer prognoses (Kurdistani et al. 2007) and can even be used to predict clinical outcome and probability of relapse (Seligson et al. 2005).

1.9.1 Chromatin-modifying enzymes as therapeutic targets:

Chromatin regulation is a highly dynamic process and chromatin accessibility is strictly supervised by chromatin-modifying machinery (Workman et al. 1998). Depending on the type and combination of potential histone modifications a variety of multi-protein complexes will be recruited, thus allowing for tightly regulated transcriptional control. In addition, these enzymes can be triggered to act either locally, recruited by specific transacting factors to individual nucleosomes, or globally, targeting almost all nucleosomes throughout the genome (Keppler et al. 2008). Depending on the cellular

stimuli, histones can be modified to either loosen chromatin and allow for transcriptional initiation or condense chromatin and deny promoter access. The enzymes which carry out these modifications include histone acetyl transferases (HAT), histone deacetylases (HDAC), histone methyl transferases (HMT), histone demethylases (HDM), kinases, E3 ubiquitin ligases, small ubiquitin-related modifier (SUMO)-cojugating enzymes and ADPribosyl transferases (ADPRT). ATP-dependent nucleosome remodeling complexes do not covalently alter histones but they do play a role in regulating DNA accessibility. Together, these enzymes work in concert to compose distinctive signals which can trigger either the recruitment or denial of any number of additional regulatory transcriptional elements. Because this high level of precise control is required to maintain transcriptional fidelity, any alteration in regulation can have a profound effect as is seen in many disease states (Kepler et al. 2008). It was observed that manipulating histone-modifying enzymes with agonists or antagonists is a promising therapeutic approach which is the basis of the present study.

1.9.2 HATs and Diseases:

Histone acetylation is a modification that neutralizes the positive charge of the target lysine, and it occurs at specific lysines on the four core histones (Figure 1.6). It has been proposed that histone acetylation can alter histone-DNA interactions, creating a more open chromatin architecture (Shahbazian et al. 2007). This modification is catalyzed by histone acetyltransferases (HATs) through the transfer of the acetyl moiety from acetyl-coenzyme A to the ε-amine of target lysine residues.

The newly acetylated lysine can then be recognized by specific bromo domain-containing proteins, leading to a cascade of additional modifications often culminating in increased transcriptional activity. Histone acetylation can be reversed by the enzymatic action of the histone deacetylases (HDACs). The interplay between HAT and HDAC activities thus regulates cellular histone acetylation levels. HATs are categorized into two groups based on their cellular localization. Type A HATs are nuclear and acetylate nucleosomal histones and other chromatin-associated proteins,

24

whereas type B HATs exist in the cytoplasm to acetylate newly synthesized histones. Unlike type A, type B HATs have no direct influence on transcription. Group A HATs
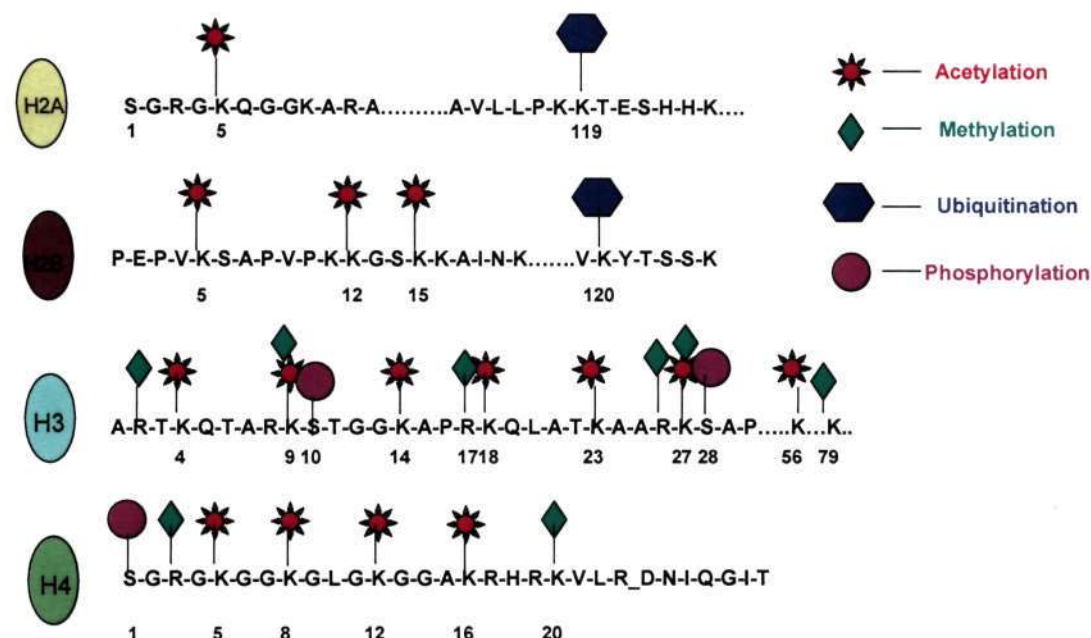
Figure 1.6: Post-translational modifications of human nucleosomal histones. The modifications include acetylation, methylation, phosphorylation and ubiquitination. Most of the known histone modifications occur on the N-terminal tails of histones, with some exceptions including ubiquitination of the C-terminal tails of H2A and H2B and acetylation and methylation of H3 within the globular domain.

may be further grouped into five different families; GNAT (GCN5 (general control of nuclear-5)-related N-acetyl transferases), MYST (MOZ (monocytic leukaemia zinc-finger protein), YBF2 (yeast binding factor 2)/SAS3 (something about silencing 3), SAS2, TIP60 (Tat interactive protein-60)), p300/CBP (CREB (cAMP response element binding protein)- binding protein), nuclear receptor co-activators and general transcription factors (Table 1.2). Due to their involvement in so many cellular regulation pathways, it has been found that genes encoding a number of HATs are mutated and/or their protein expression levels and activities are altered in many diseases, especially in a variety of cancers. For example, GCN5 dysregulation is found in genetic diseases and cancers and p300 and p300/CBP associated factor (PCAF) are linked to cancer due to their roles in myogenic differentiation (MyoD)-dependent cell cycle arrest (Puri et al.

1997). In addition, some HATs, such as p300 and CBP, have been characterized as tumour suppressors and act as transcriptional cofactors for a variety of oncoproteins (p53, pRB, Myb, Jun, Fos) (Yang et al. 2004) . p300 was first implicated in oncogenic pathways when it was originally identified as an adenovirus E1A oncoprotein binding partner (Stein et al. 1990) . Similar observations were made when mutations in the gene encoding p300 are found in breast, colorectal, gastric and epithelial cancers. Glioblastoma and other malignancies can also arise as a result of loss of heterozygosity at the p300 locus (Gayther et al. 2000). CBP mutations rendering the HAT enzymatically

Table1.2: Histone acetyltransferase (HAT) families and specificities (Major HATs are shown):

HATs	Histone substrate specificity
GNAT family	
GCN5	H2B; H3-K9, -K14, -K18, -K23, -K27; H4-K8, -K16
PCAF	H3-K14; H4-K8
MYST family	
TIP60	H2A-K5; H3-K14; H4-K5, -K8, -K12
MOZ	H3; H4
p300/CBP family	
p300	H2A-K5; H2B-K12, -K15, -K20; H3-K14, -K18, -K23; H4-K5, -K8, -K12
CBP	H2A-K5; H2B-K12, -K15, -K20; H3-K14, -K18, -K23; H4-K5, -K8
Nuclear receptor coactivators	
AIB1	H3; H4
General transcription factors	
TAF$_{II}$250	H3; H4

inactive are seen in leukaemogenesis and Rubenstein–Taybi syndrome, a developmental disorder associated with childhood cancers of neural crest origin (Petrij et al. 1995). Loss of CBP function, caused by mutated polyglutamine proteins, is also found in

Huntington's disease, Alzheimer's disease, amytropic lateral schlerosis and spinal and bulbar muscular atrophy (Rouaux et al. 2004). In the MYST family of HATs, Tip60
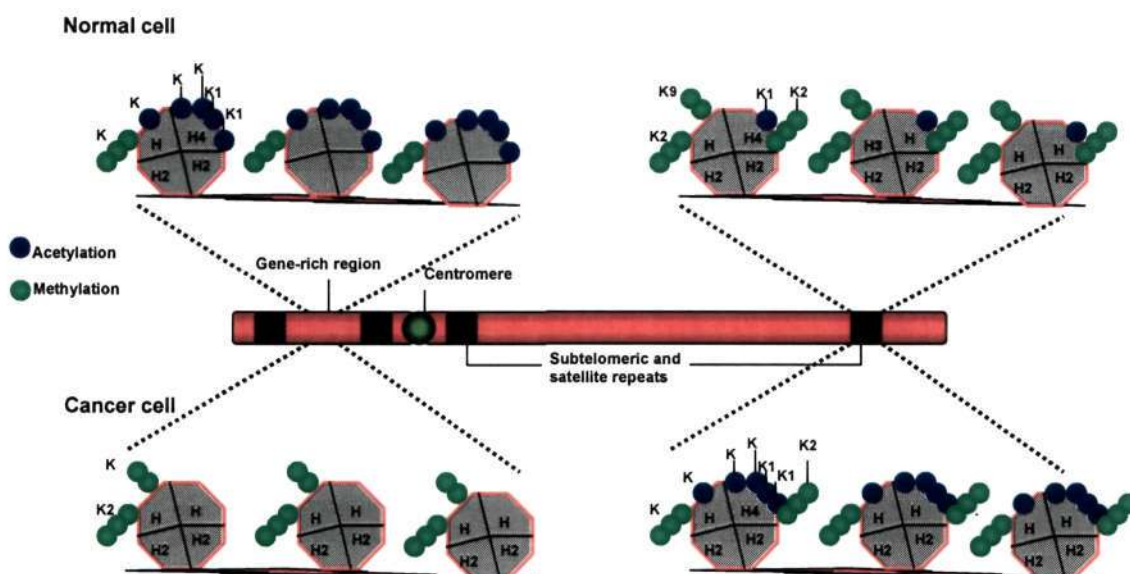
Figure 1.7 : Chromatin-modification maps for a typical chromosome in normal and cancer cells. Nucleosomal arrays are shown in the context of chromosomal location and transcriptional activity. Octamers consisting of histones H2A, H2B, H3 and H4 are represented as grey cylinders. Histone acetylation and methylation (di- and tri-) are shown. In 'normal' cells, genomic regions that include the promoters of tumour-suppressor genes are enriched in histone modification marks associated with active transcription, such as acetylation of H3 and H4 lysine residues (for instance K5, K8, K9, K12 and K16) and trimethylation of K4 of H3. In the same cells, DNA repeats and other heterochromatic regions are characterized by trimethylation of K27 and dimethylation of K9 of H3, and trimethylation of K20 of H4, which function as repressive marks. In transformed cells, this scenario is disrupted by the loss of the 'active' histone marks on tumour-suppressor gene promoters, and by the loss of repressive marks such as the trimethylation of K20 of H4 or trimethylation of K27 of histone H3 at subtelomeric DNA and other DNA repeats. This leads to a more 'relaxed' chromatin conformation in these regions.

mutations nullifying acetyl transferase activity disable the cell's DNA double strand break repair system. The resulting cells lose their ability to apoptose, even after gamma-irradiation, thus allowing for proliferation of DNA-damaged cells (Ikura et al. 2000). Nuclear receptor co-activators possessing HAT activity, such as amplified in breast cancer-1 (AIB1), have also been linked to cancer. AIB1, a member of the steroid receptor coactivator-1 (SRC-1) family of transcriptional coactivators, is amplified and

overexpressed in a number of estrogen receptor-positive breast and ovarian cancer cell lines (Anzick et al. 1997). HAT regulation can also be interrupted as a result of chromosomal translocations as observed in acute myeloid leukaemia (AML), a hematological malignancy. In AML, a fusion protein is created in which CBP is fused with a MYST domain-containing MOZ (Yang. 2004; Borrow et al. 1996) . This CBP–MOZ chimaera, possessing protein interacting domains from both the p300/CBP and MYST families of HATs, exhibits gain of function characteristics leading to unchecked hyperacetylation and aberrant transcriptional activation.
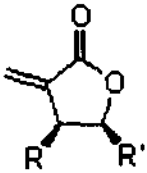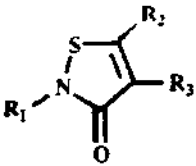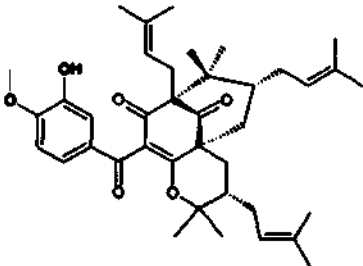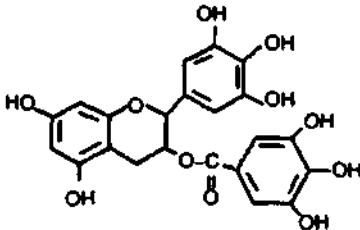
So far, little is known about the patterns of histone modification disruption in human tumours (Esteller. 2007). It is known that the promoter CpG-island hypermethylation in cancer cells is associated with a particular combination of histone marks: deacetylation of histones H3 and H4, loss of histone H3 lysine K4 (H3K4) trimethylation, and gain of H3K9 methylation and H3K27 trimethylation (Fahrner et al. 2002; Ballestar et al. 2003; Vire et al. 2006) (Figure1.7). It is also recognized that certain genes with tumour suppressor- like properties, such as p21WAF1, are silent at the transcriptional level in the absence of CpG island hypermethylation when hypoacetylated and hypermethylated histones H3 and H4 are present (Richon et al. 2000). Recently a post-translational modifications of histone present (Richon et al. 2000). Recently a post-translational modifications of histone H4 have now been profiled at a global level in a comprehensive panel of normal human tissues, cancer cell lines and primary tumours (Fraga et al. 2005). In this study, cancer cells were shown to exhibit a loss of monoacetylated and trimethylated forms of histone H4. Interestingly, these changes appear early and accumulate during the tumorigenic process, as shown in a mouse model of multistage skin carcinogenesis (Fraga et al. 2005). The finding that these changes in histone modification patterns occur so soon in the course of tumorigenesis, similar to the manner in which CpG-island hypermethylation precedes KRAS mutations in small colorectal adenomas (Esteller et al. 2004)), indicates that they might be relevant steps in the transformation process. By mass spectrometry, these losses were found to occur predominantly at the acetylated K16 and trimethylated K20 residues of histone H4, and were associated with the well characterized hypomethylation of DNA repetitive sequences (Figure 1.7). Similar data have been obtained in breast and liver tumorigenesis

Table 1.3: Types of HAT inhibitors:

HAT inhibitor	Structure	Enzyme specificity
Lysyl CoA,		p300
H3 CoA 20		PCAF
Anacardic acid		p300, PCAF
Garcinol		p300, PCAF,
Curcumin		p300/CBP

572
P09

29

γ- butyrolactones	R: Me, Ph R': alkyl	CBP/Gcn5
Isothiazolones		p300/PCAF
LTK14		p300
epigallocatechin-3-gallate (EGCG)		p300/CBP, PCAF, Tip60

(Tryndyak et al. 2006; Pogribny et al. 2006), indicating that the global loss of monoacetylation and trimethylation of histone H4 might be a common hallmark of human tumour cells (Esteller et al. 2007).

Despite the involvement of dysregulated HATs in some many disease states, only a limited number of HAT inhibitors have been reported (Table 1.3) against the large number of HDAC inhibitors (Table 1.4). The observation that polyamine-CoA conjugates inhibited acetyl transferase activity in cell extracts was

pioneer in the field of HAT inhibitors (Cullis et al. 1982). Two bisubstrate analogs specific for p300 and PCAF, Lys-CoA and H3-CoA-20, respectively, were synthesized and proved useful in blocking in vitro HAT activity, however, their low metabolic stability and cellular impermeability were significant drawbacks (Lau et al. 2000). Naturally-occurring small-molecule HAT inhibitors have also been described. Anacardic acid (Balasubramanyam et al. 2003) and garcinol (Balasubramanyam et al. 2004) are p300 and PCAF inhibitors and curcumin (Balasubramanyam et al. 2004) is a p300-selective inhibitor. Unfortunately anacardic acid, isolated from cashewnut shell liquid,

Table 1.4: Classification of HDAC inhibitors:

HDAC inhibitors					
Hydroxamic acid derivatives	**Cyclic tetrapeptides**	**Short chain fatty acids**	**Synthetic pyridyl carbamate derivative**	**Synthetic benzamide derivatives**	**Ketones**
-Trichostatin (TSA)	-Depsipeptide (FK228, FR901228)	-Valproic acid (VA)	- MS-275	- CI-994 (N-acetyldianiline)	- Trifluoromethyl ketone a-ketomides
- Suberoylanilide hydroxamic acid (SAHA)	- Apicidine	- Phenyl butyrate (PB)			
- M-carboxy cinnamic acid bis-hydroxamide (CBHA)	- Trapoxin	- Phenyl acetate (PA)			
- Azelaic bis-hydroxamic acid (ABHA)	- HC-toxin	- Sodium butyrate (SB)			
- NVP-LAQ824	- Chlamydocin	- AN-9 (Pivanex)			
-LBH 589	- Depudesin				
- Oxamflatin	- CHAPS				
-PXD101					
-Scriptaid					
- Pyroxamide					

and some synthetic amide derivatives displayed permeability problems in cell culture (Table 1.3). But recently, self fluorescent nanoparticles were used to deliver the first known p300 activator (HAT activator) in the cell and animal system (Selvi et al. 2008). On the other hand, garcinol, a polyisoprenylated benzophenone derivative from Garcinia

indica fruit rind, was shown to be an equally active HAT inhibitor both in vitro and in vivo. Garcinol inhibited histone acetylation and induced apoptosis in HeLa cells, making it the first ever reported cell permeable HAT inhibitor (Balasubramanyam et al. 2004). One of the garcinol derivative, LTK 14 (Table 1.3) was found to inhibit p300 specifically and inhibited the HIV multiplication in cell culture (Mantelingu et al. 2007). Curcumin has also demonstrated therapeutic value as it has been shown to prevent hyperacetylation in cancers and exhibit anti-HIV activity (Balasubramanyam et al. 2004). Additional synthetic HAT inhibitors possessing anticancer activity have been reviewed (Mai et al. 2007). Although some of the more recently discovered small molecules have exhibited cell permeability and potencies that rival the natural products, a gold-standard HAT inhibitor has yet to be discovered (Keppler et al. 2008). Finally, HATs can also contribute to global levels of histone modifications by acetylating non-histone proteins. p300 and PCAF, for example, have been found to acetylate a number of transcriptional regulators, tumour suppressors, cell cycle regulators and other proteins such as p53, p73, E2F1, c-Jun, MyoD, Rb and HIV Tat, among others (Roth et al. 2001) . Like the histone code, this pattern of non-histone protein acetylation can be predictive of disease states. When targeting HATs in therapies, therefore, their roles in acetylating both histones and non-histone proteins must be considered.

1.9.2 a. HAT and Cardiac hypertrophy:

Cardiac hypertrophy is an increase in size of the cardiomyocytes which in turn results in increase in the size of the heart. It can also occur in response to an increase in hemodynamic pressure or volume, the heart may undergo compensatory hypertrophy. Cardiac hypertrophy can further also be stimulated by small molecules such as endothelin and phenylephrine and causes the cardiomyocytes to increase their rates of protein synthesis, resulting ultimately in an increase in the size of individual cardiomyocytes and, consequently, an enlargement of the heart. Prolonged hypertrophy is ultimately deleterious and results in dilated cardiomyopathy and heart failure (Bilsen et al. 1993). Therapeutic use of some molecules used for the treatment of like ischemia/reperfusion

injury of heart are hampered by the fact that it also induces hypertrophy (reviewed in ref. Latchman et al. 2002). Different studies have shown the involvement of HAT p300 in cardiac hypertrophy and development. It has been shown that Phenylephrine (PE) could activate p300 and CBP through p42/p44 MAPK (Gusterson et al. 2002). The importance of p300 in normal cardiac transcription was further illustrated by p300 knockout mouse embryos that have reduced expression of muscle structural proteins such as myosin heavy chain and α-actinin, and, as a consequence, cardiac structural defects (Yao et al. 1998). In contrast, role of the related protein, CBP was found to be less important in cardiovascular development (Shikama et al. 2003; Tanaka et al. 2000). Transgenic studies have also shown that it is the HAT activity of p300 that is essential for heart formation (Shikama et al. 2003). It was also demonstrated that p300 transcriptional activity is increased during PE-induced hypertrophy (Gusterson et al. 2002). and that inhibition of p300, either by using antisense or dominant negative mutant constructs, inhibits PE-induced hypertrophy (Gusterson et al. 2003). Similarly, overexpression of p300 was sufficient to induce hypertrophy, but the HAT domain of p300 was found to be required for this activity (Gusterson et al. 2003).The above study clearly suggested the importance of p300 in regulating the hypertrophic program in response to PE . These studies also suggested a possibility of p300 HAT as a target. Recently, it was shown that Anacardic acid (AA), a potent inhibitor of p300 and PCAF histone acetyltransferase (HAT) activities (Balasubramanyam et al. 2003). could suppress the induction of cardiomyocyte hypertrophy by inhibiting p300 HAT activity (Davidson et al. 2005). This raises the possibility of treatment of cardiac hypertrophy using HAT inhibitors.

1.9.2. b. HAT and Diabetes:

Diabetes is a complex multigenic syndrome primarily due to beta-cell dysfunction associated with a variable degree of insulin resistance (Gray et al. 2005). Recent advances in the field have led to new developments with regard to our understanding of the mechanisms that regulate insulin transcription. It is proposed that the activities of HATs/histone deacetylases (HDACs) affect the regulation of transcription of genes

33

critical for beta-cell function and metabolic homeostasis, and therefore may play a crucial role in the pathogenesis and/or management of diabetes (Gray et al. 2005). Increasing evidence links possible dysregulation of these mechanisms in the pathogenesis of diabetes, with important therapeutic implications. In a mutant mouse model of a HAT, mice heterozygous for the CBP demonstrated an increase insulin sensitivity and glucose tolerance even while demonstrating a marked lipodystrophy of white adipose tissue (Yamauchi et al. 2002). More recently, it was also demonstrated that the regulation of expression of insulin by glucose is under the control of histone hyperacetylation, suggesting an important role for HATs and HDACs in the regulation of this critical gene (Gray et al. 2001; Chakrabarti et al. 2003; Mosley et al. 2003). Expression of glucokinase and glucose-6-phosphatase (Glc-6-Pase) have been shown to be intimately regulated at the promoter level by histone acetylation. In the case of glucokinase, a complex involving HIF-1, HNF-4, and p300 was identified as necessary for insulin-dependent transcription of this gene (Roth et al. 2004). Further the role of HDAC in the pathogenesis of diabetes is also shown where genome wide scanning for both type 1 and type 2 diabetes loci was performed. Interestingly, significant linkage has been observed for region 6q21, where HDAC2 is also located (Gray et al. 2001; Nerup et al. 2001; Xiang et al. 2004).

1.9.2. c. HAT and Neurodegeneration diseases:

The molecular basis of selective neuronal apoptosis during neurodegenerative diseases has revealed the role of acetylating and deacetylating agents during the process. Several studies have now successfully manipulated neuronal vulnerability by influencing the dose and enzymatic activity of histone acetyltransferases (HATs) and histone deacetylases (HDACs), enzymes regulating acetylation homeostasis within the nucleus, thus focusing on the importance of balanced acetylation status in neuronal vitality (Saha et al. 2006). It is now increasingly becoming clear that acetylation balance is greatly impaired during neurodegenerative conditions. During normal conditions, protein concentration (availability) and enzymatic activity of HATs (like CBP and p300) and HDACs remain in a state of balance where adequate active molecules from either group are present to

effectively regulate chromatin and TF acetylation in a controlled manner . Such equilibrium manifests neuronal homeostasis and is responsible for regulated gene expression leading to normal neurophysiological outputs like long-term potentiation, learning and memory (Saha et al. 2006). It is found that the acetylation homeostasis alter significantly during neurodegenerative circumstances when histone acetylation level in neuron decreases globally, (Rouaux et al. 2003) which reflects a malfunctioning acetylation apparatus. Such malfunction, as suggested by several observations, is manifested by comprehensive loss of HATs like CBP and p300 during various neurodegenerative challenges (Rouaux et al. 2003; Jiang et al. 2003). As reflected by the deacetylation of histones in apoptotic conditions where this loss is an early event during apoptosis (Rouaux et al. 2003) and is specific for affected neurons only. In one study, immunocytological detection of CBP with oxidative stress-challenged murine cortical neurons was done which revealed the presence of CBP only in the nucleus of neurons surviving the hypoxic stress, whereas in the condensed or fragmented nuclei, representing neurons undergoing apoptosis, the HAT was not present (Jin et al. 2001). Furthermore, the critical nature of the loss of HAT is illuminated by several overexpression studies of CBP, all of which demonstrate enhanced neuronal viability in response to various challenges (Rouaux et al. 2003; Nucifora et al. 2001; McCampbell et al. 2001; Taylor et al. 2003). It may be mentioned here that, among all HATs, loss of CBP appears to be pivotal in facilitating neurodegenerative cascade of events. Various mechanisms are now known to reduce CBP HAT availability in several models of neuronal insult. Nuclear translocation of expanded polyglutamine-containing neurotoxins (like mutated huntingtin protein), implicated in at least nine neurodegenerative diseases, selectively enhance ubiquitination and degradation of CBP by proteosomal pathway (Jiang et al. 2003). Additionally, during Alzheimer's disease progression, Presenilin-1- dependent epsilon-cleavage product N-Cad/CTF2 binds to CBP and facilitates its proteosomal degradation (Marambaud et al. 2003). Alternatively, CBP is redistributed from their normal nuclear location into Huntington aggregates, which compromises their availability for normal functions (Nucifora et al. 2001). Furthermore, caspase-6-dependent CBP proteolysis has been reported in low K^+ shock model of neurodegeneration (Rouaux et al. 2003). Active caspase-6 is also reported in neuropil threads, neuritic plaques and neurofibrillary tracts

of Alzheimer brain, suggesting that CBP may be lost in Alzheimer's disease by caspase cleavage. Like CBP, p300 protein level also decreases during neurodegenerative conditions (Rouaux et al. 2003). However, the mechanism behind such loss is not well known (ref review). These result suggest that small molecule activators HAT p300/CBP like CTPB (Selvi et al. 2008; Balasubramanyam et al. 2003) may be useful in therapeutic intervention of the disease.

1.9.2.d. HAT and Asthma:

There is increasing evidence that histone acetylation, controlled by HATs and HDACs plays a critical role in the regulation of inflammatory genes and in mediating the anti-inflammatory effects of corticosteroids in asthma patients (Mroz et al. 2007). It was observed that the HAT activity in higher in asthmatic patients which leads to increased expression of multiple inflammatory genes that are regulated by proinflamatory factors, such as NF-κ B. Further reduction in HDAC activity, secondary to oxidative and nitrative stress and severe inflammation, may account for the amplified inflammation in chronic obstructive pulmonary disease (COPD) (Cosío et al. 2004; Thompson et al. 2003). It is known that corticosteroids switch off inflammatory genes through the inhibition of HAT activity and by recruiting HDAC2 to the activated transcriptional complexes. These observations were supported from the fact that in bronchial biopsies and in alveolar macrophages obtained from patients with asthma, there was an increased HAT activity and small reduction in HDAC1 expression, while that of HDAC2 and HDAC3 levels were normal compared with the normal airways (Cosío et al. 2004). Little is known about the mechanism of activation of inflammatory genes in asthma and COPD. It has been found that in the presence of IL-1β, tumour necrosis factor, or endotoxin, the inflammatory gene expression increases, such as granulocyte-macrophages colony stimulating factor (GM-CSF) in the human epithelial cell lines (Mroz et al. 2007). This can be explained by activation of NF-κ B which results in acetylation of lysine 8 and 12 on histone H4. (Ito et al. 2000) These observations also suggest a possibility of therapeutic interventions using HAT inhibitors.

1.10. Crosstalk of different Histone Modifications:

When considering the therapeutic targeting of histone residue-specific modifications, however, the existence of crosstalk (one histone modification promoting the generation of another) between chromatin modifications and chromatin modifying enzymes must be taken into consideration.

1.10.1 Cross-talk between histone acetylation and methylation:
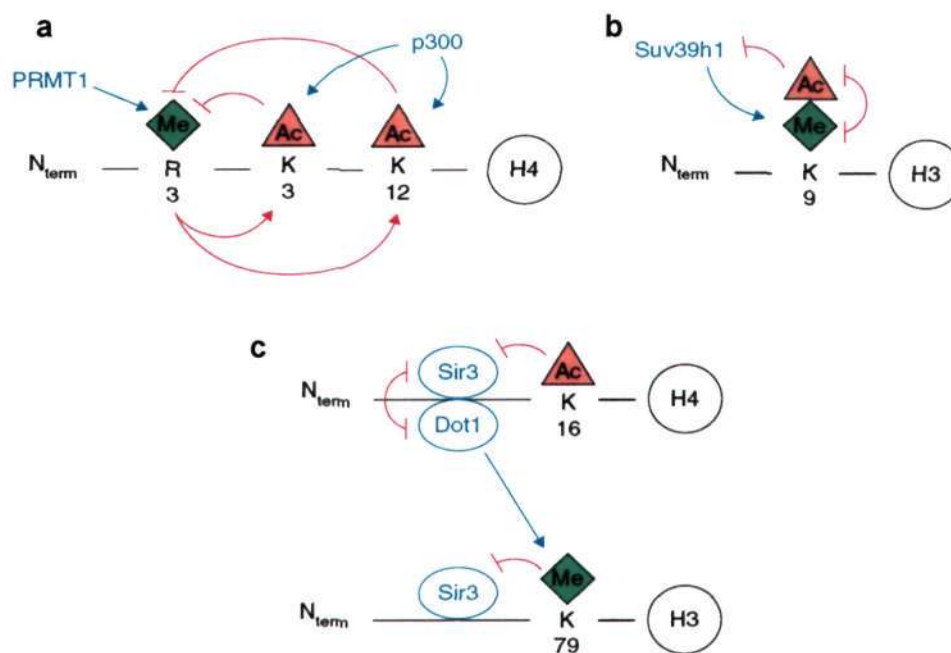
Figure 1.8: Cross-regulation between histone acetylation and methylation : a. Methylation and acetylation are coupled in a negative feedback loop. b. Interplay between acetylation and methylation on the same histone residue determines whether a gene is silenced or activated. c. Acetylation of histone H4 determines methylation of histone H3 as Sir3 and Dot1 compete for the same binding sites. Enzymes and their directed action are indicated in blue. Induction and inhibition are indicated in red. Taken from (Keppler et al. 2008).

Methylation-induced acetylation has been found to occur on histone H4 (Figure 1.8a). PRMT1 (Protein arginine methyl transferase 1), an H4-R3 methylase, induces p300-mediated H4 acetylation and transcriptional activation and is involved in nuclear cytoplasmic shuttling (An et al. 2004). This H4 acetylation in turn inhibits H4 methylation. (Figure 1.8a).

It is also observed that methylating and acetylating enzymes targeting the same histone residue can be indirectly inhibitory towards one another. For example, acetylated lysine 9 on histone H3 will inhibit Suv39h1 (Suppressor of variegation 3 – 9 homologue1)-mediated methylation of the same residue (Figure 1.8b). Similarly, methylated H3-K9 will prevent acetylation. These two mutually exclusive modifications have this effect on one another because of their opposing transcriptional outcomes as H3-K9 methylation results in gene silencing whereas H3-K9 acetylation induces gene activation (Keppler et al. 2008).

Furthermore, the methyl transferase disruptor of telomeric silencing-1 (Dot1) is known to cross-talk with the heterochromatin protein silent information regulator-3 (Sir3), a member of the SIR complex that also includes Sir4 and the NAD-dependent H4-K16 HDAC Sir2 (Figure 1.8c) (Altaf et al. 2007) . The SIR complex is associated with transcriptional repression, gene silencing, cell cycle progression and chromosome stability (Brachmann et al. 1995) . Misregulation of Dot1 is linked with leukemogenesis (Okada et al. 2005) and is responsible for methylating histone H3 at lysine 79 within the globular domain. This methylation is dependent on the ability of Dot1 to interact with a short basic region on the N-terminal tail of histone H4. Sir3, known to associate with unmodified H3 and H4 tails, competes with Dot1 by interacting with the same basic region on H4 and by binding H3 adjacent to K79. GCN5-mediated H4-K16 acetylation displaces Sir3 on H4, thereby allowing Dot1 to interact with H4 and subsequently methylate H3-K79 (Figure1.8c). H3-K79 methylation in turn further blocks Sir3–H3 interactions. This series of events serves to define a heterochromatin boundary and allow for transcriptional elongation.

1.10.2 Cross-talk between histone acetylation and phosphorylation:

Histone phosphorylation is known to modify nucleosomal structure. H3 phosphorylation is synergistically coupled to histone acetylation, thereby adding additional levels of complexity and control to transcriptional regulation (Cheung et al. 2000). Combinations of phosphorylated and acetylated histones is believe to display different recruitment signals for transcription factors and regulatory complexes than a singly modified histone.

Figure 1.9: Cross-talk between phosphorylation and acetylation: a. The synergistic model. H3K14 acetylation is enhanced by H3S10 phosphorylation. Enzyme actions are indicated by blue arrows. Induction is indicated by the red arrow. b. The parallel-independent model. Lysine acetylation occurs equally on both phosphorylated and unmodified histones. Taken from (Keppler et al. 2008).

However, the precise mechanism and physiological roles of this multifaceted cross-talk relationship is not fully understood but two models have been proposed: the synergistic model and the parallel-independent model (Figure 1.9) (Biel et al. 2005). A number of HATs is known to preferentially acetylate H3-S10 phosphorylated forms of their substrates as opposed to the unmodified forms, thus giving rise to the synergistic model. For example, Msk1/2-mediated H3-S10 phosphorylation enhances the binding affinity of the HAT general control of nuclear-5 (GCN5) to H3, which in turn leads to H3-K14 acetylation and transcriptional activation (Figure 1.9a) (Lo et al. 2000). In the parallel-

independent model, H3-S10 phosphorylation does not necessarily inevitably lead to H3-K14 acetylation, and the absence of H3 phosphorylation does not necessarily decrease levels of H3 acetylation (Figure 1.9b). This model is supported by the observation that, at times under certain conditions, Msk1/2 mutations or inhibition resulting in decreased H3-S10 phosphorylation do not affect levels of histone acetylation (Keppler et al. 2008).

1.10.3 Cross-talk between acetylation, methylation and phosphorylation:

Phosphorylation, acetylation and methylation machinery is also known to function together in a cross-talk tertiary loop (Figure 1.10). For example, histone H3K9
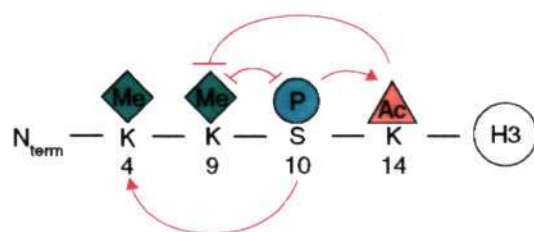
Figure 1.10: Tertiary cross-talk between acetylation, methylation and phosphorylation: On histone H3, S10 phosphorylation facilitates gene activation by blocking K9 methylation and facilitating K4 methylation and K14 acetylation. K14 acetylation, in turn, serves to further block K9 methylation and allow for chromatin decondensation. Induction and inhibition are indicated in red. Taken from (Keppler et al. 2008).

methylation inhibits S10 phosphorylation to repress gene transcription. On the other hand, in the case of gene activation, S10 phosphorylation facilitates K4 methylation, inhibits K9 methylation and enhances K14 acetylation, which in turn helps to further inhibit K9 methylation (Figure 1.10) (Cheung et al. 2000; Rea et al. 2000; Zhang et al. 2001). The absence of a repressive methyl group on K9 then allows for K9 acetylation and further chromatin decondensation. These modifications work in concert to compose distinct histone codes, which are recognized by specific chromatin-interacting proteins in order to precisely drive the necessary physiological processes in the cell (Keppler et al. 2008).

1.11. p300/CBP

p300 and/or CBP homologues are present in many multicellular organisms, including flies, worms and plants, but not in lower eukaryotes such as yeast (Champagne et al. 1999b; Bordoli et al. 2001b; Yuan and Giordano, 2002). The histone acetyltransferase p300 is the most thoroughly studied among different HAT families. It is a highly potent enzyme that acetylates histones and several other proteins (factor acetyltransferase, FAT)
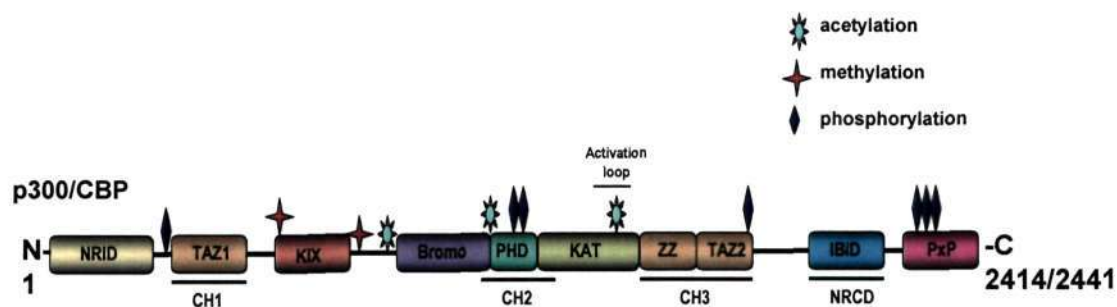
Figure 1.11: Schematic of p300 domain organization and its covalent modifications: As mammalian p300 and CBP are functionally interchangeable in many in vitro assays, the term p300/CBP is used to refer to one or the other. The functional domains in p300 are indicated, including the cysteine/histidine-rich domains CH1, CH2 and CH3, the KIX domain and the bromodomain (Br). The N- and C-terminal domains of p300/CBP can act as transactivation domains, and the acetyl-transferase domain is located in the central region of the protein i.e. HAT or KAT domain. Domain abbreviations include the following: Bromo, bromodomain; CH1, Cys- and His-rich domain 1; IBiD, IRF-3 binding domain; KIX, kinase-inducing domain (KID) binding region; NRCD, nuclear receptor coactivator binding domain (synonymous to IBiD); NRID, nuclear receptor-interacting domain; PxP, prolinerich domain (no known function); TAZ1, transcriptional adaptor zinc finger; and ZZ, zinc finger near the dystrophin WW domain. (Modified from Yang et al, 2008)

(Ogryzko et al. 1996; Bannister et al. 1996). CBP was originally isolated as a coactivator of the transcription factor CREB (Chrivia et al. 1993), and p300 was cloned as a protein interacting with the transforming adenoviral E1A protein (Eckner et al. 1994), both proteins were subsequently shown be interchangeable for these functions (Arany et al. 1995; Lee et al. 1996). CBP and p300 are ubiquitously expressed during mouse development (Partanen et al. 1999). Comparison of the amino acid sequences of these

multidomain proteins from different species revealed the presence of numerous regions of near identity, including three cysteine-histidine rich regions (CHI, −2 and −3), the binding site for the CREB transcription factor, referred to as the KIX domain, the bromodomain and the HAT domain while other regions are poorly conserved (Arany et al., 1994) (Figure 1.11).

p300 acts as a transcriptional coactivator through the direct interaction with a diverse set of transcription factors and RNA polymerase II transcription machinery(Goodman et al. 2000). The intrinsic HAT activity of p300 plays an important role in the transcriptional coactivation of CREB, c-Jun, c-Fos, c-Myb, p53, Stats, nuclear receptors, RelA GATA, p73, etc(Shikama et al. 1997; Ogryzko et al. 1996; Costanzo et al. 2002; Zhou et al. 2004). These interactions occur through an N- and C-terminal activation domain. In addition, CBP and p300 can bind to a variety of diverse transcription factors, and other proteins, through their CHI, CH3, KIX and NRCD domains (Figure 1.11) (Chan and La Thangue, 2001; Vo and Goodman, 2001). By interacting simultaneously with the basal transcription machinery and with one or more upstream transcription factors, CBP and p300 function as physical bridges or scaffolds and thereby stabilize the transcription complex. Interestingly, several of these protein-protein interactions can be regulated by the same post-translational modifications that chromatin is subject to, such as phosphorylation (Janknecht and Nordheim, 1996; Ait-Si-Ali et al., 1998, 1999;), sumoylation (Girdwood et al., 2003) methylation (Xu et al., 2001; Chevillard-Briet et al., 2002), indicating that CBP and p300 are themselves targets of signalling cascades.

1.11.1 Function of p300/ CBP:

Although p300 and CBP share extensive homology, genetic and molecular analyses suggest that they perform not only overlapping but also unique functions. The p300-/-, Cbp-/- and p300+/- Cbp+/- mice show similar, embryonic lethal phenotypes (Yao et al., 1998), together with similar defects in growth and neural tube closure (Yao et al., 1998) which suggests that p300 and CBP have overlapping roles during embryonic

42

development. Furthermore, some *p300* and *Cbp* heterozygous mice suffer early lethality (Yao et al., 1998), indicating that p300/CBP gene dosage, and therefore the level of p300/CBP proteins, is probably important during development. Consistent with this idea are the findings that the haplo-insufficient RTS syndrome is heterozygous for mutation in the Cbp allele (Petrij et al., 1995) and that Cbp heterozygous mice also show skeletal abnormalities reminiscent of RTS (Tanaka et al., 1997). Overall, it appears that p300 and CBP have overlapping roles, but that in addition they perform unique tasks in certain physiological processes (Chan et al. 2001).

CBP/p300 is known to contribute in diametrically opposed cellular processes. It is shown that it participate in various tumor-suppressor pathways. It has been shown that mice engineered to contain a null mutation in one CBP allele developed a variety of hematological abnormalities, including extramedullary myelopoiesis and erythropoiesis, lymph node hyperplasia, and splenomegaly (Goodman et al. 2000) which also supported from the fact that human patients with the Rubinstein-Taybi syndrome (RTS), due to CBP heterozygosity, also have an increased incidence of malignancy (Goodman et al. 2000). It ends with the demonstration that these coactivators are essential for the actions of many oncogenes. Whether CBP and p300 promote apoptosis or cell proliferation appears to be highly context dependent.

Cell proliferation and growth is also known to get influenced by p300/CBP activity (Stein et al., 1990; Yao et al., 1998) which is supported by the fact that p300-/- embryos are significantly smaller than their wild-type littermates and show defects in cell proliferation (Yao et al., 1998). Further it is also shown that p300/CBP-pCAF protein complex can arrest cell cycle progression (Yang et al., 1996) and might regulate target genes that are involved in controlling the G1/S transition, such as p21WAF1 (Missero et al., 1995).

1.11.2 p300/CBP and cancer:

Chromosomal translocations complete or partial deletions and point mutations in one copy of the CBP gene result in a congenital developmental disorder named Rubinstein–

Taybi syndrome (RTS). The syndrome is characterised by retarded growth and mental function, broad thumbs, broad big toes and typical facial abnormalities (Rubinstein and Taybi, 1963). Furthermore, RTS patients have an increased risk to develop tumours, particularly in the nervous system including oligodendroglioma, medulloblastoma, neuroblastoma, and meningioma (Miller and Rubinstein, 1995). The genetic aberrations found in RTS patients are always de novo, meaning that the parents are not affected. Haploinsufficiency of CBP is the likely cause of RTS in humans, since no clear phenotypic differences were observed between patients with a complete deletion of one CBP allele or those with a single heterozygous point mutation were found (Kalkhoven et al., 2003). These finding are also supported by the fact that in mice, heterozygous deletion or truncation of CBP also leads to an RTS-like phenotype (Tanaka et al., 1997; Oike et al., 1999; Kung et al., 2000).

Until recently RTS was only linked to the CBP gene, but recent work has shown that the p300 gene was affected in some RTS patients (Roelfsema et al., 2005). In all the cases it was predicted to result in loss of the HAT function of p300. Furthermore, bi-allelic somatic mutations in the p300 gene have also been observed in gastric, colon and breast cancers, and mutations in p300 that result in truncated proteins were detected in primary tumours and tumour cell lines (Muraoka et al., 1996; Gayther et al., 2000).

The p300/CBP genes are also involved in various chromosomal translocation events during haematological malignancy and might contribute to aberrant growth control possibly through a gain of function mutation. For example, an MOZ-CBP fusion resulting from a translocation between MOZ (for monocytic leukaemia zinc finger protein) and CBP was reported in AML (acute myeloid leukemia; Borrow et al., 1996). Similarly, a second translocation of the CBP gene to the MLL (mixed lineage leukaemia) gene occurs in chronic myeloid leukaemia and myelodysplastic syndrome (Sobulo et al., 1997), which arise as a consequence of cancer therapies. In another case, a patient suffering from therapy related AML was identified as having an in-frame fusion of MLL with p300 (Ida et al., 1997). Since both MOZ and MLL have been implicated in chromatin remodeling, these fused proteins could deregulate gene expression, thereby preventing proper differentiation (Chan et al. 2001).

1.11.3 p300: Structures, mechanisms and specificities

Recently the crystal structure of the p300 HAT domain in complex with a Lys-CoA bisubstrate inhibitor has been solved and an accompanying biochemical analysis of the enzyme has also been done (Figure 12) (Liu at al. 2008). The structure reveals an elongated globular domain containing a central seven strand β-sheet surrounded by nine α-helices and several loops (Figure 1.12). One side of the Lys-CoA inhibitor is positioned

a   b

c

Figure 1.12: Structure of p300 HAT domain and enzymatic mechanism: (a) The protein binding site groove is present at the middle of the shown figure with negative patch area, shown in red. An electrostatic surface of p300 is shown with positive, negative, and neutral charged surfaces shown in blue, red, and white, respectively. Lys-CoA is shown in yellow stick representation. (b) A cartoon representation of the same figure as in A. (c) Schematic representation of the Theorell–Chance (hit and run) catalytic mechanism of p300. (Taken from Liu *et al*, 2008)

roughly in the middle (between β4 and β5) and against the wide edge of the β-sheet and the C- terminal ends of two helices (α3 and α4). A long ~25 residue loop (L1), called the substrate binding loop, encapsulates the opposite side of the Lys-CoA inhibitor (Figure1.12). A comparison with the Gcn5/ PCAF and MYST HATs shows structural conservation within the central core region associated with acetyl-CoA cofactor binding despite the lack of sequence homology, but significant structural divergence flanking the central core region. Despite the similarities among the HATs within the domain associated with Ac- CoA cofactor binding, the L1 substrate binding loop is a unique feature of the p300 HAT domain, burying about one-third of the CoA portion of the Lys-CoA inhibitor and mediating about one-half of the CoA interactions (Liu at al. 2008, Marmorstein et al. 2008). Further it was found that the electrostatic surface proximal to the lysine portion of the Lys-CoA inhibitor is electronegative which is apolar in the corresponding regions of Gcn5/ PCAF and MYST HATs . On the basis of mutagenesis studies of this electronegative site it was shown that this site was important for protein substrate binding by p300. These studies were further support the observation that p300/CBP has a wider substrate specificity (Thompson et al. 2001, Liu et al. 2008).

A detail mutagenesis and kinetic analysis in the above work also been able to show that p300 follows an unusual the hit-and-run (Theorell-Chance) mechanism of enzyme action (Liu et al. 2008) that is distinct from the catalytic mechanisms employed by the Gcn5/PCAF and MYST HAT families (Figure 1.12). The observation that p300 is inhibited potently by the Lys-CoA inhibitor but poorly by bisubstrate analogs with longer peptide moieties; and the longer peptides are better substrates for p300 than lysine further supported this fact. Further it was shown that p300 gets extensively autoacetylated in an intermolecular fashion, which is highly cooperative in nature. Autoacetylation of multiple lysines at the proteolytic sensitive loop was found to be important for the regulation of its catalytic activity (Liu et al. 2008). It was also proposed that this highly basic loop sits in the electronegative substrate binding site is released from this site upon autoacetylation (Liu et al. 2008).

A very recent report about the crystal structure of Rtt109 bound to Ac-CoA(Tang et al. 2008) show a striking and unexpected overall structural similarity to

p300. This includes a structurally conserved central seven stranded β-sheet, surrounding helices and L1 substrate binding loop that plays an analogous role in Ac-CoA interaction. A detail study suggest that the Rtt109 and p300/CBP HATs diverge significantly at the functional level like substrate binding site is not as electronegative as it is in p300 and that Rtt109 employs a distinct catalytic mechanism (Tang et al. 2008).

Since, the complete structure of p300 is not yet solved and the unstructured nature of p300 and the problem associated in obtaining large amount of highly pure p300 full length seems to further affect such an attempt. So in order to have insight into the structure of full length p300 surface-enhanced Raman scattering (SERS) studies on p300 full length in solution was performed. Vibration spectral analysis has been performed in an attempt to understand the structure of the p300 in the absence of its crystal structure. The detail of the SERS study of p300 full length and that of it's HAT domain makes up the 4th chapter of this thesis.

1.11.4 Regulation of p300/CBP function:

p300 and its homolog CREB binding protein (CBP) are transcriptional coactivators that physically or functionally interact with over 320 mammalian and viral proteins and participate in a myriad of cellular functions, including DNA repair, inflammation, cell growth, differentiation, and apoptosis (Goodman and Smolik, 2000). CBP and p300 mediate communication between transcription factors and the transcriptional machinery and thus appear to be important for gene transcription (Chan and La Thangue, 2001). The number of signal transduction pathways that require the activity of CBP and p300 is so large that the availability of these proteins can be envisioned as a limiting factor for the appropriate execution of many biological processes. Competition between different transcription factors for CBP or p300 has been proposed to play a role in the coordination of gene expression in response to signaling (Kamei et al., 1996). One of the most remarkable examples of this phenomenon is the reciprocal functional antagonism between p53 and NF-kB through competition for CBP or p300 (Ravi et al., 1998; Webster and Perkins, 1999). CBP/p300 are functional integrators of multiple signal

transduction pathways because diverse transcription factors compete with each other to interact with a limiting amount of CBP/p300 within the cell (Fronsdal et al., 1998; Horvai et al., 1997; Lemasson and Nyborg, 2001; McKay and Cidlowski, 2000). The most important paradox in CBP and p300 functions is their capability to regulate diametrically opposite processes: cell proliferation and cell growth arrest. The ability of CBP and p300 to serve as mediators for cell proliferation or growth arrest has been proposed to be highly context dependent (Goodman and Smolik, 2000). All the above facts suggest that protein-protein interactions between p300/CBP and other factors can influence its function influencing its HAT activity, substrate specificity, and protein binding preferences. All these can be very context dependent as said above. This also indicates that different signaling pathways can interfere with one another through modulating the availability of p300/CBP for a particular transcriptional complex via posttranslational modifications.

1.11.4.a Posttranslational modifications of p300/CBP:

Several posttranslational modifications have been reported to regulate CBP activity. Phosphorylation of CBP or p300 at an unidentified site near the carboxyl terminus by MAPK and CaMKIV has been reported to increase their HAT and transcriptional activity during neuronal differentiation (Figure 1.13) (Ait-Si-Ali et al., 1999; Impey et al., 2002). In one study it is also found that Akt-dependent p300 phosphorylation at Ser-1384 can increase p300 HAT activity and contribute to inflammatory gene expression by TNF-α (Huang and Chen, 2005). However, phosphorylation of p300 at Ser-89 by PKCα and PKCδ appears to repress its transcriptional activity, probably leading to cell growth inhibition (Yuan et al., 2002; Yuan and Gambee, 2000). Besides phosphorylation, methylation by CARM1 (Xu et al., 2001) and sumoylation by Ubc9 (Girdwood et al., 2003) have also been reported to regulate the transcriptional activities of CBP and p300. p300/ CBP methylation by coactivator- associated arginine methyltransferase 1 (CARM1) causes a transcriptional switch from CREB-regulated to nuclear hormone receptor-regulated gene expression (Xu et al., 2001). A recent work indicated that IKKα-mediated phosphorylation of CBP not only changes its protein binding preference but

also is required for its HAT and intrinsic transcriptional activities (Figure 1.13). However, blockage of IKKα or substitution of CBP Ser- 1382/Ser-1386 with Ala could not completely abolish the HAT activity, suggesting that IKKα mediated phosphorylation
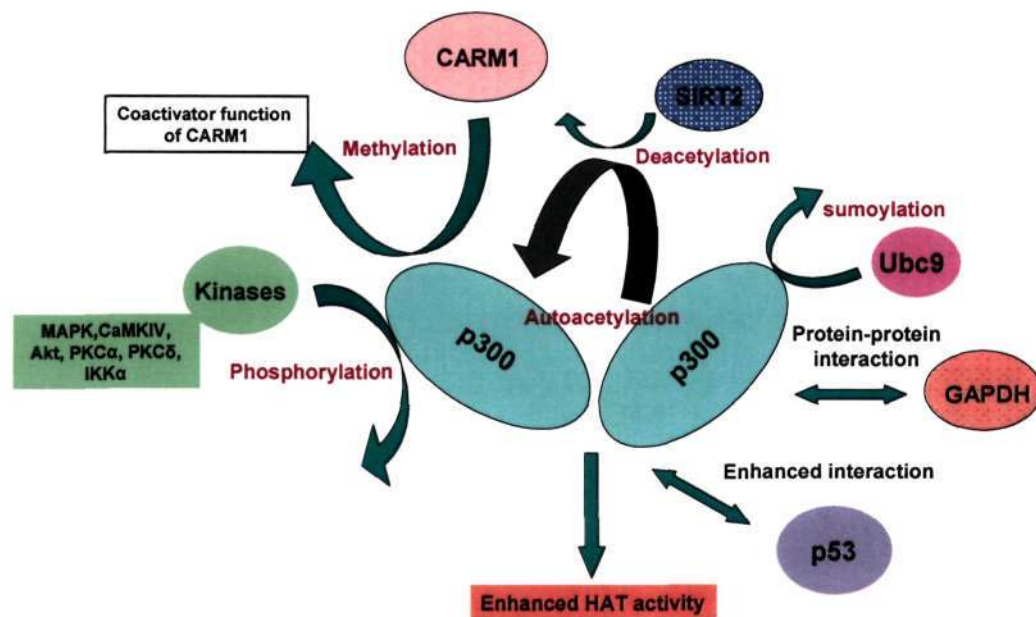
Figure 1.13: Regulation of p300/CBP function: Schematic of various ways of regulation of p300/CBP HAT function. Protein-protein interaction and/or post translational covalent modifications influencing its HAT activity, substrate specificity, and protein binding preference. See text for the detail.

of CBP might act in concert with other covalent modifications to establish the ''p300/CBP code'' (Gamble and Freedman, 2002), then influencing its HAT activity, substrate specificity, and protein binding preference. In a similar line of work, Philip cole lab has shown that p300/ CBP get autoacetylted and the autoacetylation enhances the HAT activity of the enzyme (Figure 1.13) (Thompson et al. 2004). Role of p300/CBP autoacetylation and function is given in the next section.

1.11.4.b Autoacetylation of p300/CBP:

Like phosphorylation of kinases and phosphatases, acetyltransferases and deacetylases themselves are acetylated. It was found that p300 gets extensively autoacetylated in an intermolecular fashion (Figure 1.13), which is highly cooperative in nature as mentioned earlier. Autoacetylation of multiple lysines at the proteolytic sensitive loop was found to be important for the regulation of its catalytic activity. It was also proposed that this highly basic loop sits in the electronegative substrate binding site is released from this site upon autoacetylation (Thompson et al., 2004). An attractive model is that DNA-binding proteins recruit p300 and bring two or more p300 molecules into physical proximity, leading to intermolecular acetylation and enzymatic activation. Consistent with this idea, many transcription factors stimulate the acetyltransferase activity of p300 and CBP. Moreover, recruitment to DNA is important for p300 activation (Doman et al., 2003). This model was suggested to be reminiscent of the way in which ligands activate membrane receptors (Yang et al. 2008). It was also suggested that autoacetylation of p300 induces a conformational change that facilitates the transition between chromatin modification and preinitiation complex assembly mediated by the activator VP16 (Black et al., 2006). Autoacetylation causes p300 to dissociate from complexes it forms with GAL4- VP16 and Mediator. (Black et al., 2006). In addition, acetylation occurs at the tandem sumoylation sites upstream from the p300 bromodomain to block sumoylation and relieve transcriptional repression (Girdwood et al., 2003). Both sites are conserved in homologs from zebrafish to humans (Yang et al. 2008). p300 and CBP are also phosphorylated and methylated at multiple sites (Figure 1.13) (Legube and Trouche, 2003). It will be interesting to decipher how acetylation coordinates with phosphorylation, sumoylation, methylation, and ubiquitination to regulate p300 and CBP activities in a concerted fashion. In one study ATF-2 b-ZIP interaction with the p300 HAT domain was examined and it was shown that p300 HAT autoacetylation can enhance the binding affinity (Karanam et al. 2007). In another study it was shown that p300 is susceptible to acetylation in cultured tumor cells and that its acetylation status is affected by histone deacetylase inhibitor trichostatin A. Further it was found that

acetylated p300 possesses enhanced ability to interact with p53 (Stiehl et al. 2007). Taken together it can be said that the acetylation of p300/CBP may contribute to the dynamic regulation of their complex formation with various interacting partners. In a very recent work it was found that nitric oxide (NO)-induced nuclear translocation of glyceraldehyde-3-phosphate dehydrogenase (GAPDH) mediates cell death through p300/CBP–p53 pathway. In this study it was shown that GAPDH activates the p300/CBP autoacetylation and thus its HAT activity by directly interacting with the HAT. It was also shown that acetylation og GAPDH at a single lysine residue is important for the interaction (Sen et al. 2008)

Recently attempts were made to identify a p300 deacetylase in extracts from HeLa cells. It was found that out of the seven mammalian NAD^+-dependent deacetylases, the Sirtuin family, only SIRT2 was uniquely capable of deacetylating autoacetylated p300 in vitro. Further knockdown of SIRT2 increased cellular acetylated p300 levels and affected activation of a model gene. These observation suggest that p300 undergoes a dynamic cycle of acetylation and deacetylation. It should be noted that deacetylation of p300 by SirT2 was first observed by cole group(Thompson et al. 2004) and we have also shown this affect in an in vitro study using recombinant p300 HAT domain (Selvi et al. 2008).

The discoveries of different posttranslational modification of chromatin-modifying complexes like G9a is automethylated, Rsc4 is acetylated, and PARP-1 is auto-ADPribosylated, represents an additional level of transcriptional control. It is predicted that these modifications will be recognized by additional effector proteins utilizing the same domains that recognize epigenetic marks on histone tails (Black et al. 2008), as is the case where automethylated G9a is recognized by the HP1 chromodomain (Sampath et al., 2007).

1.12. Cancer:

Tumorigenesis is a multistep process that requires several integrated events to allow a cell to grow rapidly without the input of extraneous growth-stimulating signals, and to

overcome growth-inhibitory signals and host immune responses. Tumour cells must also be able to circumvent apoptosis, replicate indefinitely and sustain growth and survival by maintaining a sustainable oxygen and nutrient supply .Mutations that result in constitutive activation of oncogenes or functional inactivation of tumour-suppressor genes are important tumorigenic events(ref 1).Although these mutations can affect several cellular pathways in the absence of de novo protein synthesis, aberrant gene expression — which is often downstream of these mutations — also has an important role in tumour initiation and progression. In addition, mutations within gene promoter or enhancer regions, or epigenetic changes, can induce abnormal expression of genes that regulate cellular differentiation, the cell cycle and apoptosis, thereby enhancing the potential for cellular transformation. Moreover, aberrant transcription of the genes that are needed to initiate the host antitumour immune response and induce neovasculature can result in tumour immune escape and angiogenesis — events that are essential for cancer progression.

1.12.1. Head and neck squamous cell carcinoma (HNSCC) and Oral Cancer:

Head and neck squamous cell carcinoma (HNSCC) is one of the most common types of human cancer, with an annual incidence of more than 500,000 cases worldwide. HNSCC is associated with severe disease- and treatment-related morbidity and has a 5-year survival rate of approximately 50%; this rate has not improved in more than 2 decades (Mao et al., 2004; Forastiere et al., 2001). HNSCC is a complex disease arising in various organs, including the oral cavity, pharynx, and larynx. Tumors from these different sites have distinct clinical presentations and clinical outcomes, and are treated with different strategies, which may include surgery, radiotherapy, and chemotherapy. Recent molecular studies have advanced our understanding of the disease and provided a rationale to develop novel strategies for its early detection, classification, prevention, and treatment (Mao et al., 2004).

Oral squamous cell carcinoma (OSCC) is one of the most common head and neck carcinomas, which affects chronic smokers, drinkers and betel

squid chewers (Yuen et al. 1999). It is one of the most common cancers in developing countries. The prevalence of oral cancer is particularly high among men. It is the eighth most common cancer worldwide. In south-central Asia, cancer of the oral cavity ranks among the three most common types of cancer. In India, the age standardized incidence rate of oral cancer is 12.6 per 100 000 population. Patients often present symptoms at a late stage, and there is a high recurrence rate after treatment (Yuen et al. 1997). Local and regional recurrences account for 90% of treatment failures post surgery and radiotherapy (Yuen et al. 1997). The overall survival rate decreases as the carcinoma stage increases, from 75% for Stage 1 to 22% for Stage IV (Yuen et al. 1997). Tumor invasion and metastasis are main causes of tumor recurrence, which are commonly associated with poor prognosis. Metastasis is the result of several multi-step processes whereby highly motile tumor cells lose cell–cell contact and invade to the surrounding tissue (Partin et al. 1989; Aznavoorian et al. 1993; Liotta et al. 2001). Rearrangement of cytoskeletal microfilaments is the major morphological alteration by the actions of cross-linking proteins for the invasive tumor cells (Otto et al. 1994; Matsudaira et al. 1994; Tilney et al. 1998).

1.12.2. Etiology of Oral cancer:

Through a large number of epidemiologic studies, a strong link has been established between the use of tobacco and an increased risk for HNSCC. Alcohol is another independent risk factor for the disease that may have a synergistic effect when combined with tobacco. The risk for development of oral cancer is 3 to 9 times greater in those who smoke or drink and as much as 100 times greater in those who both smoke and drink heavily than in those who neither smoke nor drink (Neville and Day, 2002). Mutations of p53 have been found more frequently in the HNSCC of smokers and drinkers than in those of other patients (Brennan et al., 1995), suggesting that inactivation of the p53 tumor suppressor gene is important in tobacco- (and possibly alcohol-) induced HNSCC tumorigenesis (Mao et al., 2004).

Recently it is shown that Human papillomavirus (HPV) may play an important role in the etiology of HNSCC, particularly for tumors of the oropharynx (Gillison et al., 2000). It is shown that E6 protein found in the oncogenic high-risk types of HPV, such as HPV-16, can bind to the p53 protein and accelerate its degradation, thereby limiting its ability to inhibit growth of, induce apoptosis in, or cause substantial genetic damage to cancer cells.

Other risk factors for HNSCC include poor hygiene in the oral cavity; environmental contaminants such as paint fumes, plastic byproducts, and gasoline fumes; gastroesophageal reflux disease; dietary factors; and use of marijuana. In patients with HNSCC who lack clear exposure to the common risk factors, the identification of the etiology of HNSCC will be critical to develop strategies to prevent and treat the disease (Mao et al., 2004).

1.12.3. Histologic and clinical classification:

HNSCC is graded histologically as well, moderately, or poorly differentiated carcinoma. It was found that the well-differentiated tumors contain orderly stratification and heavy keratinization in a pear formation. While moderately differentiated tumors have prickle cells, some stratification, and less keratinization. Poorly differentiated tumors are still recognizable as squamous cell carcinomas but manifest prominent nuclear pleomorphisms and atypical mitosis. However, although the histologic differentiation status is required in pathology reports of HNSCC, it provides limited information to guide treatment decisions because a strong association between differentiation status and clinical outcome or treatment response is lacking. The anatomic location of HNSCC is important for their clinical classification because tumors arising from different locations often have distinct clinical outcomes and different functional considerations. For example, tumors in the hypopharynx have a higher probability of metastasizing compared to tumors in the oral cavity or larynx (Mao et al., 2004). By contrast, laryngeal tumors metastasize infrequently, and patients with these tumors often receive no or minimal

surgery but do receive chemoradiotherapy in order to retain their speech function (Forastiere et al., 2003).

1.12.4. Prevention of Oral cancer:

The development of HNSCC requires accumulation of genetic and epigenetic alterations, and thus can theoretically be interrupted, delayed, or reversed through the use of natural or synthetic agents in a process known as chemoprevention (Hong and Sporn, 1997). The goal of cancer chemoprevention is to slow, block, or reverse the process of carcinogenesis through the use of natural or synthetic compounds. For a variety of reasons naturally occurring dietary substances over synthetic agents are preferred by patients to prevent cancer. This approach has largely focused on targeting deregulated intracellular pathways that have been implicated in abnormal cellular function. As a result there has been an increasing interest in dietary compounds that have an innate ability to modify these pathways thereby delaying process of carcinogenesis (Khan et al. 2006). For example,pre-clinical studies of curcumin have shown the ability to inhibit carcinogenesis in cell lines that include breast, cervical, colon, gastric, hepatic, leukemia, oral epithelial, ovarian, pancreatic, and prostate cancer (Aggarwal et al. 2003). Supporting this idea the epidemiological research has suggested the possible role of curcumin to prevent or delay the diagnosis of colorectal cancer as evidenced by ethnic groups that consume curcumin (Johnson et al. 2007) .

It was shown that the high-dose retinoids have established efficacy in the reversal of early oral premalignant lesions but are associated with mucocutaneous toxicity (Hong et al., 1986). The efficacy of retinoids on moderately and severely dysplastic lesions were also addressed with a combination of interferon-α, α-tocopherol, and 13-cis-retinoic acid (Papadimitrakopoulou et al., 1999). The possibility of preventing second primary tumors was further suggested by a randomized, double-blinded, placebo-controlled trial of high-dose 13-cis-retinoic acid taken for 1 year by patients whose original HNSCC were curatively treated (Hong et al., 1990). However, these results were

not confirmed by studies with low-dose 13-cis-retinoic acid (Khuri et al., 2003) or with different retinoids (van Zandwijk et al., 2000).

New strategies in chemoprevention include targeting p53 abnormalities, selective cyclooxygenase-2 inhibitors, EGFR kinase inhibitors, and the epigallocatechin gallate component of green tea. Therefore it is the need of hour to design newer studies to treat lesions with a higher genetically defined risk for cancer development, such as aneuploidy or loss of heterozygosity at specific tumor suppressor loci in oral premalignant lesions (Sudbo et al., 2001; Mao et al., 1996b; Partridge et al., 2000; Rosin et al., 2000) or patients with certain cyclin D1 polymorphisms (Izzo et al., 2003).

Aim and scope of the present study:

p300/CBP functions as a transcriptional coactivator in multiple, signal dependent transcription events. The p300/CBP genes are also involved in various chromosomal translocation events during haematological malignancy and might contribute to aberrant growth control possibly through a gain of function mutation. Earlier observations from our laboratory showed that the polyisoprenylated benzophenone, garcinol isolated from *Garcinia indica* (an edible fruit), is a potent nonspecific inhibitor of histone acetyltransferase p300. Further it was shown that among several garcinol derivatives some were specific towards p300 (e.g. LTK14) and some were not (e.g. isogarcinol). The present study was initially aimed to study the biochemical and biophysical reasons for the differential nature of inhibition brought about by these HAT inhibitors. Such a detail study will provide a precise enzymatic inhibitory mechanism of these small molecule inhibitors which will be useful in designing future therapeutic molecules. Given the therapeutic potential of p300/CBP inhibitors in cancer, cardiac disease, diabetes mellitus and HIV, it is important to understand the molecular mechanism of the HAT inhibition. The next objective of this study was to find out the structure-function relationship of p300 full length and small molecule inhibitors. Using Surface Enhanced Raman Scattering (SERS) it was possible to identify modes related to various functional groups of the protein, which would provide a key to understand protein-inhibitor interactions. We have also utilized SERS as an effective probe to determine the subtle structural change in p300 HAT domain after autoacetylation.

Recently, we have observed that histones are predominantly hyperacetylated in oral patient samples and which is positively correlated to the upregulation of NPM1 (B23) and GAPDH expression. This prompted us to study the molecular mechanisms involved in this phenomenon. Results from this study clearly suggest the role of nitric oxide (NO) for the hyperacetylation of H3. We also investigated the enzymatic mechanism of the hyperacetylation. Incidentally, we have discovered a novel water soluble HAT inhibitor, CTK7A. We have explored the possibility of targeting the p300 mediated hyperacetylation by the water soluble HAT inhibitor as a putative therapeutic agent.

Chapter **2**

> *This chapter presents the materials and experimental methods used in the research work done for this thesis*

2.1. General methods:

2.1.1. Preparation of competent cells:

E. Coli. strains BL21 DE3 and DH5α cells were grown overnight in 5 ml of Luria Bertani (LB) medium (10 gm/L tryptone, 5 gm/L yeast extract and 10 gm/L NaCl) at 37°C without any antibiotics. Cell streaking was done with the overnight culture and grown in a 37°C incubator. A single colony was inoculated in 5 ml of LB and cultured overnight at 37°C. Secondary inoculation was done with overnight culture in to 500 ml of medium A (500 ml LB containing 10 mM $MgSO_4$ and 11 mM glucose) and grown till the OD_{600} reached to 0.3. The precooled culture was pelleted by centrifugation at 4°C, 2000 rpm for 10 mins. The pellet was resuspended in medium A at 4°C. The cells were pelleted again and resuspended in 25 ml of storage buffer B (36% Glycerol, 12 mM $MgCl_2$, 12 gm of PEG 8000 in 100 ml) aliquoted and stored at -80°C.

2.1.2. Transformation:

Competent cells were thawed on ice for 5 mins just before the addition of 100 ng of DNA to be transformed followed by incubation on ice for 30 mins. Heat shock was given for 90 seconds at 42°C and immediately incubated on ice for 5 mins. 1 ml of LB was

added to the cells and cells were grown for 45 mins at 37°C. The cells were then pelleted down and plated on LB agar plate containing appropriate antibiotic and grown at 37°C overnight.

2.1.3. DNA purification:

DNA was isolated from *E. Coli*. DH5α cells that were transformed with individual plasmid or clone constructs, using Mini prep kits according to the protocol supplied by manufacturers (QIAGEN).

PCR products were purified using QIAGEN-PCR purification kit according to the manufacturer's protocol. DNA was also gel eluted from agarose gels using QIAGEN gel elution kit according to the manufacturer's protocol. DNA was gel eluted from poly acrylamide gels by crushing the gel into pieces in TE buffer (10 mM Tris, 1mM EDTA) and incubated at 37°C overnight. The mixture was centrifuged and the supernatant was phenol-chloroform extracted twice and the DNA was alcohol precipitated.

2.1.4. Isolation of total RNA:

RNA was isolated from mammalian cells using Trizol reagent (Invitrogen). Cells harvested from 30 mm dish were resuspended in 100 μl of Trizol reagent by vortexing thoroughly and incubated at room temperature for 5 mins. 27 μl of chloroform was added to the supernatant obtained after centrifugation of the suspension at 12,000 rpm for 10 mins and incubated at room temperature after vigorous shaking for 15 mins. The upper phase was taken after centrifugation at 12,000 rpm for 10 mins and reextracted with chloroform (200 μl) twice. RNA was precipitated by the addition of equal amount of isopropanol to the upper phase taken followed by centrifugation at 12,000 rpm for 20 mins. The RNA was resuspended in 70 μl of DEPC treated water and was reprecipitated with 7 μl of 3M sodium acetate (pH 5.7) and 77 μl of isopropanol. The resultant RNA precipitate was further washed with 80% ethanol, air dried for 10 mins and dissolved in

deionized MQ water and used for further experiments. All the steps were done at 4°C. Isolated RNA was checked on 1% agarose gel (See figure 2.2.a).

2.1.5. cDNA synthesis:

3.0 μg of total RNA was used for synthesis of 20 μl cDNA. 3 μg RNA was taken in to 12 μl reaction containing 40 pico moles of oligo dT and incubated at 70°C for 10 mins followed by immediate incubation on ice for 10 mins. Reaction was initiated by the addition of 10 mM DTT, 0.5 mM dNTPs, 4 μl of 5X First strand synthesis buffer and 1 μl superscript RT (Invitrogen). The reaction was incubated for 60 mins at 42°C followed by heat inactivation at 70°C for 10 mins. The cDNA was then used for real time or normal PCR analysis using specific set of primers.

2.1.6. Estimation of Nucleic acids and proteins:

a. Nucleic acids concentration was estimated spectrophotometrically by measuring the absorbance of DNA solution diluted in 10 mM Tris 1 mM EDTA at 260 nm wavelength (A_{260}). The concentration was calculated according to Beer-Lamberts law.

$$C = A_{260} \times \theta$$

C is the concentration of nucleic acid in ng/μl. For DNA θ is 50 ng/μl. In case of oligonucleotide θ is 33 ng/μl. In case of RNA θ is 40 ng/μl.

b. Estimation of proteins: The concentration of protein in cell lysates was estimated with Biorad-Protein estimation reagent according to the protocol supplied by manufacturer using BSA as standard. Recombinant purified proteins were estimated by running different concentrations of BSA along with protein of interest on a SDS-PAGE gel.

2.1.7. Agarose gel electrophoresis:

Agarose gel electrophoresis was performed to analyze DNA/RNA samples. Indicated percentage of agarose was added to 1X TBE (0.09 M Tris Borate and 0.002 M EDTA) /0.5X TBE and dissolved by melting in hot air oven. Samples were prepared in 1X loading buffer (0.25 % Bromophenol blue, 0.25% Xylen cyanol in 40% sucrose) and loaded on to the gel. Samples were elecrophoresed at different voltages for varying time periods as mentioned, in 1X TBE/0.5X TBE. Gels were stained with EtBr (10 µg/100 ml H_2O) or SYBR green (1:10,000 dilutions in H_2O) with gentle rocking. Nucleic acids were visualized on U.V. lamp in gel documentation system (Biorad).

2.1.8. Poly Acrylamide Gel Electrophoresis (PAGE):

SDS-PAGE: SDS-PAGE was performed to separate the proteins according to molecular weight and also to analyze the purity of the protein samples. Separating gels were made in various percentages of acrylamide (Stock: 30%, Acrylamide: Bis acrylamide 29:1) along with 0.375 M Tris pH 8.8, 0.1% SDS, 0.1% APS and 8% TEMED. Stacking gels were made with 5% acrylamide along with 0.375 M Tris pH 6.8, 0.1% SDS, 0.1% APS and 8% TEMED above the separating gel. Protein samples were made in 1X sample buffer (50 mM Tris-HCl pH 6.8, 100 mM DTT, 0.1% bromophenol blue, 10% glycerol) boiled at 90°C for 10 mins before loading on to the gel. Gels were electrophoresed using Tris-Glycine buffer (25 mM Tris, 250 mM Glycine pH 8.3, 0.1% SDS). Gels were visualized by staining with coomassie (45% methanol, 10% Acetic acid, 0.25 % bromophenol blue) followed by destaining with destaining solution (30% methanol, 10% acetic acid in H_2O).

2.1.9. Western blot analysis:

The separated proteins on a 12% SDS-PAGE gel were blotted to PVDF/Nitrocellulose membrane using semidry western apparatus. Initially the gel was

washed with transfer buffer (25 mM Tris, 192 mM glycine, 0.038% SDS, 20% methanol v/v) for 30 mins on a rocker. The PVDF membrane was activated by soaking in methanol for 1 min followed by washes with transfer buffer. The proteins were transferred to the membrane at 25V for appropriate time period according to the size and nature of the protein. The nonspecific sites were blocked using 5% skimmed milk or 1% BSA at 4°C overnight or at room temperature for 3 hours. The blot was then incubated with primary antibody in 2.5% skimmed milk or 1% BSA in PBS for 3 hours or overnight at 4°C depending on the antibody. The blot was washed with wash buffer according to standardized conditions for each primary antibody. Further the blot was incubated with appropriate secondary antibody conjugated with HRP in 2.5% skimmed milk or 1% BSA in PBS for 3 hours at 4°C or at room temperature for 1.5 hours. The membrane was washed and the blot was developed using Pierce Super Signal West Pico Chemiluminiscent kit as described by the manufacturer. The blot was exposed to TMS (Kodak) films for different time points and developed using GBX-Developer-Fixer Kit (Sigma).

For doing western with tissues, tissues were first homogenized in RIPA (Tris-HCl 50 mM, pH 7.4 NP-40 1%, Na-deoxycholate 0.25%, NaCl 150 mM, EDTA 1 mM, Phenylmethylsulfonyl fluoride (PMSF), 1 mM, Aprotinin, leupeptin, pepstatin 1 μg/ml each, Na_3VO_4 1 mM, NaF 1 mM) in liquid nitrogen. Following that the tissue lysate is incubated on ice for 3 hrs and mixing with the pipette every 15 minutes. Proteins were analysed by western blotting using the indicated antibodies.

2.1.10. Mammalian Cell culture:

HeLa, KB, H1299, A549 and HEK293T cells were maintained at 37°C in Dulbecco's modified Eagle medium (DMEM) supplemented with 10% fetal bovine serum (Invitrogen) and appropriate antibiotics in 5% CO_2 incubator. For cell storage, approximately 2 million cells were suspended in 1 ml of 90% FBS and 10% DMSO. The temperature of the cells was bought down gradually to -80°C with the help of thermo cooler and finally cells were stored in liquid nitrogen for long term storage. Cell revival

was done by keeping the cells at 37°C for 3 minutes followed by washing with 10 ml of DMEM to remove DMSO. Cells were further seeded in 25 mm flask for maintenance.

2.1.11. Culturing Insect cells, Sf21:

The *Spodoptera frugiperda* ovarian cell line Sf21 was cultured in the commercial TC100 medium (Sigma), supplemented with 0.1% Pluronic F-68 solution (Sigma), 10μg/ml Gentamycin (Sigma) and 10% FBS (Hyclone) at 27°C in a BOD incubator. After attaining confluency, the cells were dislodged from the substratum using a cell scraper and subcultured in a 1:3 ratio. For cell storage, approximately 2 million cells were suspended in 1 ml of 90% FBS and 10% DMSO. The temperature of the cells was bought down gradually to -80°C with the help of thermo cooler and finally cells were stored in liquid nitrogen for long term storage. Cell revival was done by keeping the cells at 37°C for 3 minutes followed by washing with 10 ml of TC100 to remove DMSO. Cells were further seeded in 25 mm flask for maintenance.

2.1.12. Immunofluorescence Protocol:

Cells were grown on cover slips coated with poly-Lysine at 37°C in a 5% CO_2 incubator. After the indicated treatment of cells were washed with PBS and fixed with 4% paraformaldehyde (in PBS) for 20 mins at room temperature. Cells were then permeablized using 1% Triton X-100 (in PBS) for 10 mins and subsequently washed with PBS for 10 mins, 3 times. Nonspecific sites were blocked using 5% FBS (in PBS) for 45 mins at 37°C. Immunostaining was done with primary antibody at appropriate dilutions for 1 hour at room temperature. The cells were washed with wash buffer (1% FBS in PBS) 4 times, 3 mins each. Primary antibody stained cells were incubated with secondary antibody tagged with fluorescent dye at appropriate dilutions for 1 hour at room temperature. After washes with wash buffer the nuclei were stained with Hoechst

(1:10,000 dilution) for 20 mins. Two times PBS washed cover slips were inverted on to a microscopic slide over a 2 µl of 70% glycerol (in PBS) and visualized using confocal microscopy.

2.1.13. Whole cell extract preparation:

Cells were harvested in to a 1.5 ml or 15 ml tube by pelleting cells at 6,000 rpm for 5 mins at 4°C. Cell pellet was washed with cold PBS and resuspended 10 times packed volumes of cell pellet in RIPA (Tris-HCl 50 mM, pH 7.4 NP-40 1%, Na-deoxycholate 0.25%, NaCl 150 mM, EDTA 1 mM, Phenylmethylsulfonyl fluoride (PMSF), 1 mM, Aprotinin, leupeptin, pepstatin 1 µg/ml each, Na_3VO_4 1 mM, NaF 1 mM) or TNN (50 mM Tris-HCl, pH 7.4; 100 mM NaCl, 5 mM EDTA, 0.5% NP-40, 1 µg pepstatin per ml, 200 µM PMSF, 0.5 mM dithiothreitol (DTT), 1 µg of leupeptin per ml) buffer. Homogenization wad done using pipette tip and homogenate was incubated at 4°C for 30 mins. Lysates were cleared of debris by centrifuging at 13,000 rpm for 5 mins and the supernatant was used for further experiments.

2.1.14. Acid extraction of histones:

Cells (3 x 10^6 cells per 90-mm dish) were seeded overnight, and histones were extracted from the cells after 24 h of compound treatment. In all the cases serum was added after a period of 2 h of compound treatment. Cells were harvested, washed in ice-cold buffer A (150 mM KCl, 20 mM HEPES, pH 7.9, 0.1 mM EDTA, and 2.5 mM MgCl2) and lysed in buffer A containing 250 mM sucrose and 1% (v/v) Triton X-100. Nuclei were recovered by centrifugation, washed, and proteins were extracted (on ice) for 1 h using 0.25 M HCl. Chromosomal proteins were precipitated with 25% (w/v) trichloroacetic acid and sequentially washed with ice-cold acidified acetone (20 µl of 12 N HCl in 100 ml of acetone), and acetone, air-dried, and dissolved in the sample buffer (5.8 M urea, 0.9 M glacial acetic acid, 16% glycerol, and 4.8% 2-mercaptoethanol). The

protein was quantified using a protein assay reagent (Bio-Rad). This was later used for immunoblotting analysis to assay the in vivo histone modification status.

2.1.15. Raising polyclonal antibody against Lysine-1499-acetylated-p300 antibody and affinity purification of antibodies by protein G- sepharose:

Polyclonal antibodies are produced by immunizing rabbits with a synthetic acetylated peptide (KLH-coupled) corresponding to residues surrounding Lysine-1499 of human p300 or Lys1535 of human CBP as earlier reported (Thompson et al. 2004) (Figure 2.11). Antibodies are purified by protein G chromatography.

Regular immunization schedules were followed to raise the antibody against the ac-p300 in rabbit. Briefly 100 µg of p300 hepta-acetylated- p300 peptide in PBS (172 mM NaCl, 2.7 mM KCl, 8.1 mM Na_2HPO_4, 1.76 mM KH_2PO_4) was emulsified with equal volume of Freund's Complete Adjuvant and injected subcutaneously into rabbit. This was followed by first booster doses after 2 weeks when 50 µg p300 peptide in PBS was emulsified with equal volume of Freund's Incomplete Adjuvant and similar subcutaneous injection was given. After 3 weeks, the second booster was given with 50 µg p300 peptide in PBS emulsified with equal volume of Freund's Incomplete Adjuvant injected subcutaneously. After 3 weeks of second booster heart puncture was done to collect the immunized blood and serum was extracted from it. The antibody titre was checked after the first injection as well as booster doses. The rabbit polyclonal antibody was purified by Protein G-Sepharose and used for the immunofluorescence experiment as well as other biochemical studies. Preimmune Serum (PIS) was used as negative control. Antibody dilution of 1:1000 was used which recognized the purified p300 protein from KB cell lysate pull down assay (see text, Chapter5). It also recognizes the autoacetylated p300 HAT domain in vitro (Figure 2.11).

The specificity of ac-p300 antibody was verified by western blotting using p300HD. In this case p300HD was first fully autoacetylated followed by

deacetylation with SirT2 in concentration dependent manner. Specificity was also confirmed by peptide competition assay as shown below (Figure 2.11).
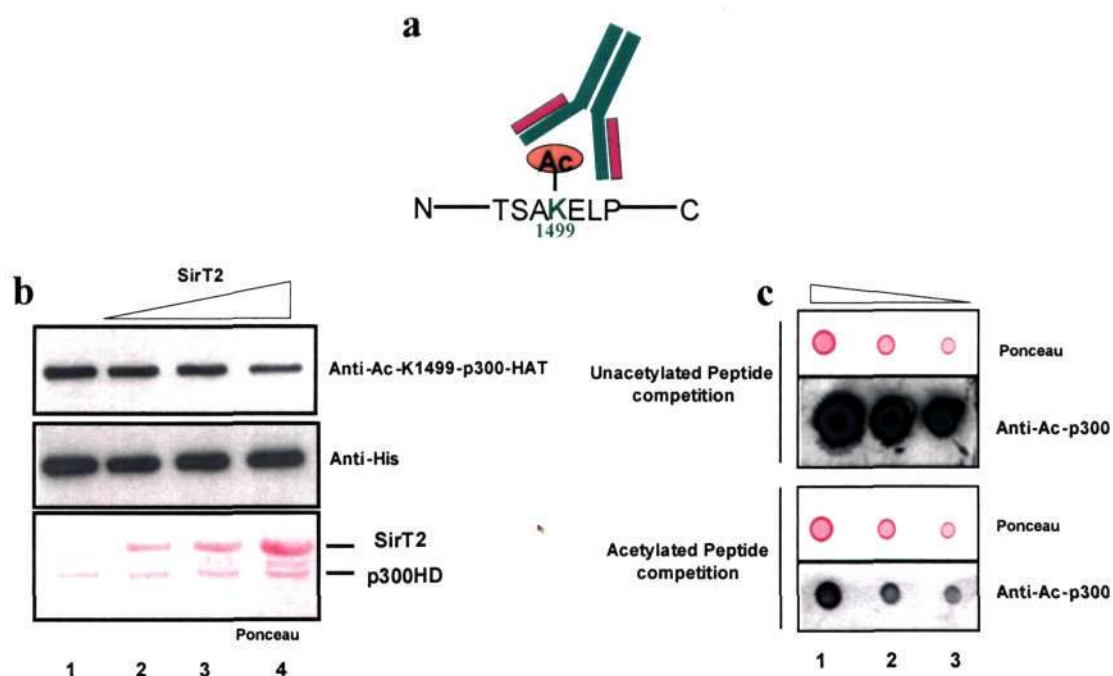
Figure 2.11. Antibody characterization. (a) Schematic of p300 hepta acetylated peptide used for antibody generation. b. The specificity of anti-Ac-K1499-p300 antibody was verified by western blotting using recombinant hexa histidine tagged p300 HAT domain (aa1284-1673). HAT domain was hyperacetylated and was further deacetylated using increasing concentration of recombinant SirT2. As can be seen from the figure, SirT2 deacetylates the hyperacetylated p300 HAT domain in a dose dependent manner (lane 1 vs. 2, 3 and 4). The gradual decrease in the level of acetylation could be recognized by the antibody, suggesting the antibody specificity. c. Peptide competition assay for the specificity of anti-Ac-K1499-p300 antibody. Top and bottom panel; decreasing concentration acetylated peptide were blotted onto the nitrocellulose membrane (lane 1=1µg and three fold diluted in subsequent lanes . In parallel ac-p300 antibody was mixed with both acetylated and unacetylated antibody in cold room for 4 hr and were used for western blotting.

2.1.16. General procedure for the synthesis of CTK7A:

Synthesis of CTK7A is done in two steps. Firstly CTK7 (see scheme I) (Shim et al. 2002) is made followed by CTK7A (see scheme II) as mentioned below:

Scheme I: General procedure for the synthesis of 4-(3,5-bis(4-hydroxy-3-methoxystyryl)-4,5-dihydropyrazol-1-yl)benzoic acid (CTK 7):

Curcumin (1) (200mg, 0.54mmol) was dissolved in methanol (10 ml) and 4-hydrazionobenzoic acid (2) (412 mg, 2.71 mmol) and triethylamine (377µl, 2.71 mmol) were added to the solution. After 5 minutes of stirring catalytic amount of acetic acid to the reaction mixture was added and refluxed at 70-80° C for 7 hrs with stirring. The progress of the reaction was monitored by thin layer chromatography ($CHCl_3$:CH_3OH - 6:1). After completion of the reaction the solvent was evaporated under vacuum and the residue was quenched with 10 ml of distilled water. The product was extracted with ethyl acetate and dried over anhydrous sodium sulphate and the solvent was evaporated under vaccum to get a gummy product. The crude product was purified by column chromatography using 220-400 mesh silica gel ($CHCl_3$: CH_3OH) gave CTK 7 as a dark orange powder (145 mg, 55%) which was analyzed by mass spectrometry [M+H] [+]: 486.17. Melting point of CTK7 was found to be 165° C ± 3° C.

Scheme II: General procedure for the synthesis of Sodium-4-(3,5-bis(4-hydroxy-3-methoxystyryl)-4,5-dihydropyrazol-1-yl)benzoate (CTK 7A):

4-(3,5-bis(4-hydroxy-3-methoxystyryl)-4,5-dihydropyrazol-1-yl)benzoic acid (CTK 7) (100 mg, 0.206 mmol) was dissolved in methanol (5 ml) and kept for stirring at room temperature. After 5 minutes sodium ethoxide (14 mg, 0.205mmol) was added and stir the reaction mixture for 1-2 hr. The reaction mixture was filtered using watmann filter paper. The filterate was evaporated in vaccum. Finally the product obtained Sodium 4-(3,5-bis(4-hydroxy-3-methoxystyryl)-4,5-dihydropyrazol-1-yl)benzoate CTK7A was washed with hexane and then with ethyl acetate. A dark brownish solid (56 mg, 53%) was obtained which was analyzed by mass spectrometry [M+H] [+]: 507.0. Melting point of CTK7A was found to be 90° C ± 3° C.

Scheme I.

CTK 7

Scheme II.

CTK 7 → (C₂H₅ONa, CH₃OH, Stir at RT 1-2 hrs) → CTK 7A
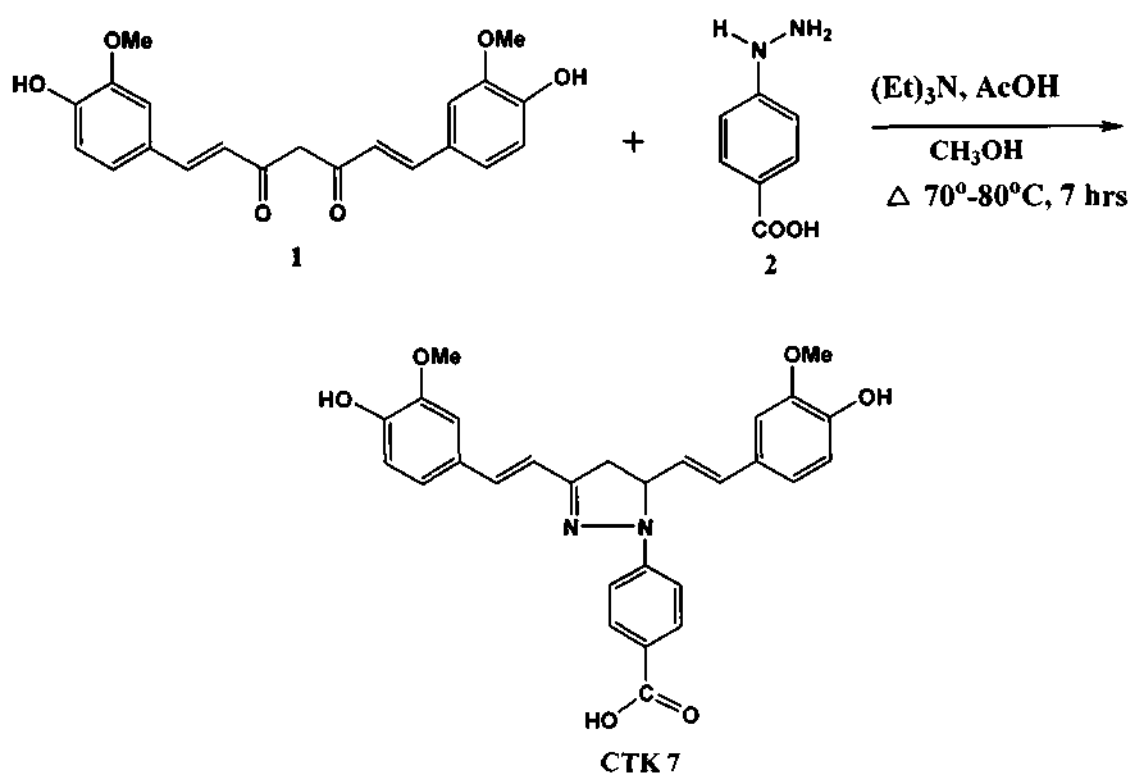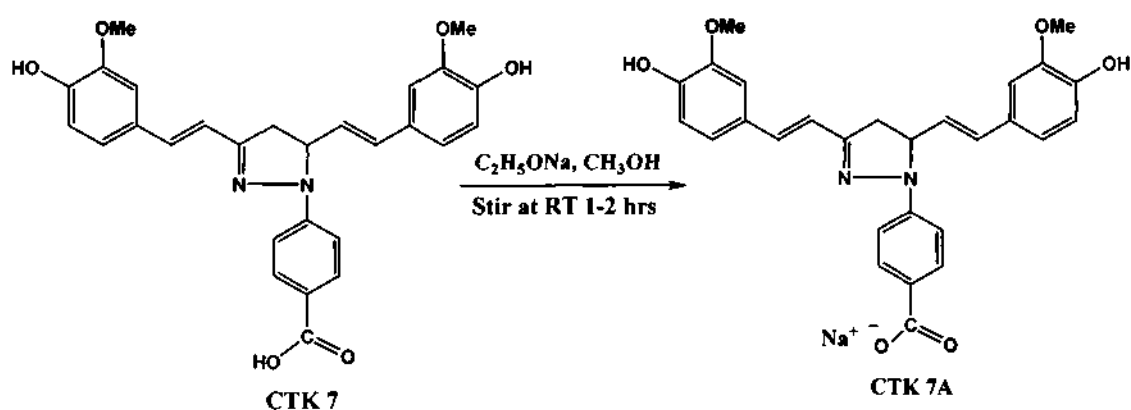
2.2. Cloning and protein purification:

2.2.1. Cloning of p300 HAT domain point mutants S1396 to A1396, Y1397 to F1397, G1626 to A1626 and R1627 to K1627:

The introduction of single point mutations in the p300 HAT domain at S1396, Y1397, G1626 and R1627amino acid residues in to pET-28b p300 HAT domain bacterial construct was achieved by performing site directed mutagenesis using Quick-Change

Table 2.1: Primer sets used to clone single point mutant p300 HAT domain in the pET-28b bacterial expression vector.

Name of the construct	Fw. primer (5' to 3')	Rw. primer (5' to 3')
p300HDS1396A	5'-AGG AGA GTA TAC ATA GCT TAC CTCGATAGTGTT-3'	5'-AAC ACTA TCG AGG TAA GCT ATG TAT ACT CTC CT-3'
p300HDY1397F	5'-AGA GTA TAC ATA TCT TTC CTC GAT AGT GTT CAT-3'	5'-ATG AAC ACT ATC GAG GAA AGA TAT GTA TAC TCT-3'
p300HDG1626A	5'-TGC GAT CTG ATG GAT GCT CGG GAT GCG TTT CTC-3'	5'-GAG AAA CGC ATC CCG AGC ATC CAT CAG ATC GCA-3'
p300HDR1627K	5'GAT CTG ATG GAT GGT AAG GAT GCG TTT CTC ACG-3'	5'-CGT GAG AAA CGC ATC CTT ACC ATC CAT CAG ATC-3'

site-directed mutagenesis kit (Stratagene). pET-28b p300 HAT domain (a.a 1284-1673) was used as template DNA together with the below given set of primers. After initial denaturation at 95°C for 1 min, the cycling parameters were 50 seconds at 95°C followed by 50 seconds at 60°C and 7 mins at 68°C (18 cycles) and the final extension at 68°C for 7 mins. The reaction mixtures were placed on ice for 2 mins, and then the parental supercoiled double-stranded DNA was digested with 0.5 µl of *Dpn I* at 37°C for 1 hour before being transformed into *E. coli* XL Gold competent cells. Mutations were verified by DNA sequencing (Figure 2.1).

5'G T A T A C A T A G C T T A C C T C G A T 3'

p300HD S1396A

5'T A C A T A T C T T T C C T C G A T A G T 3'

p300HD Y1397F

5' C G C A T C C C G A G C A T C C A T C A G 3'

p300HD G1626A

5' A A A C G C A T C C T T A C C A T C C A T 3'

p300HD R1627K
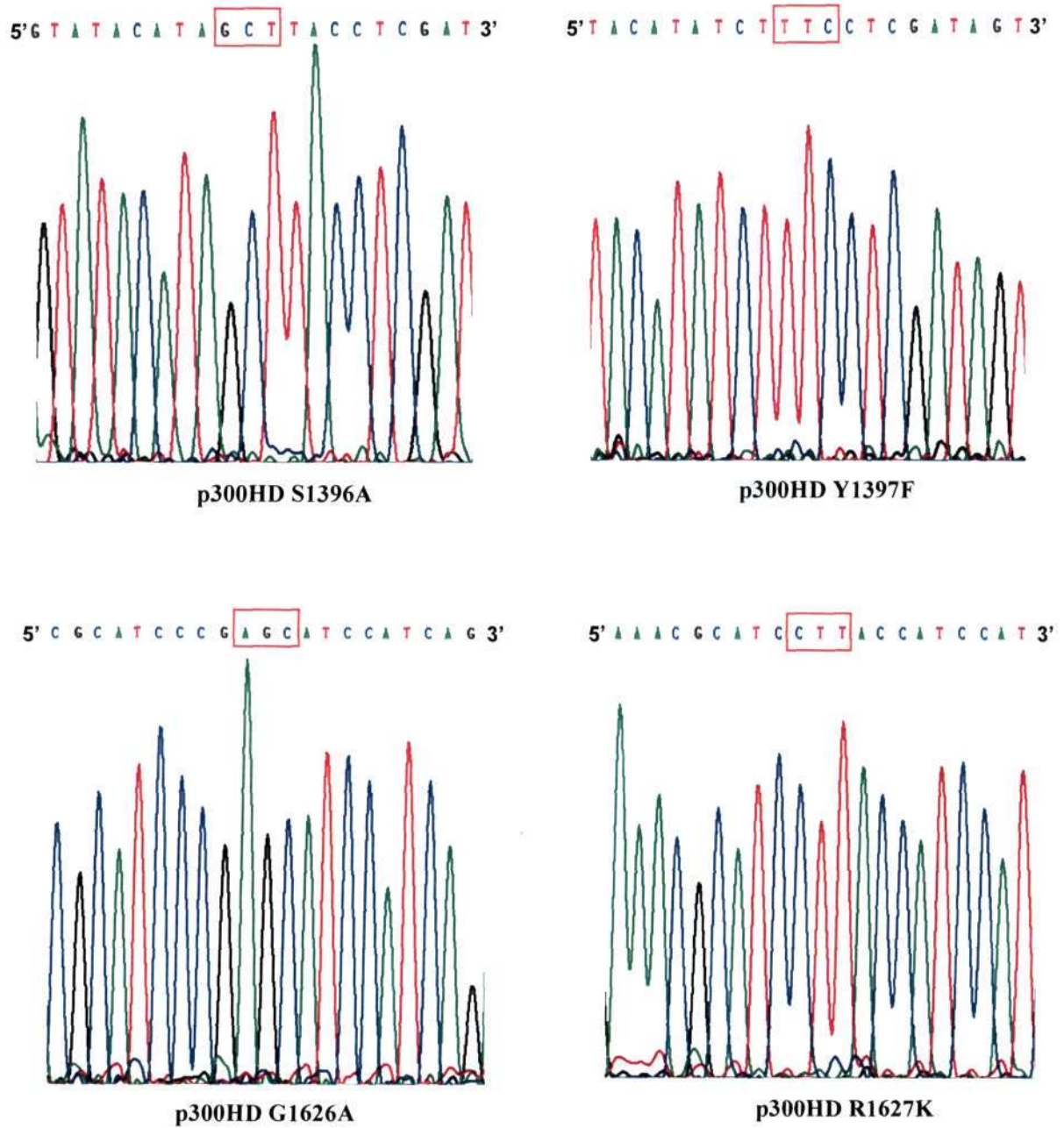
Figure: 2.1. Chromatogram showing the point mutations made at **S1396, Y1397, G1626** and **R1627** amino acid residues in p300 HAT domain as confirmed by DNA sequencing.. Red boxes on the sequence show the change in residues after mutation.

2.2.2. Cloning of human SirT2:

Full-length recombinant GST-SirT2 was cloned in pGEX-CD vector (Figure 2.2) and constructed by PCR amplification of gene corresponding to human SirT2 gene (Variant 1) using HEK 293 cell cDNA as template with the indicated primers. The amplified product was cloned in to pGEX-CD at *NcoI* and *XhoI* sites with an N-terminal GST-tag. The sequences of the primers are:

Forward Primer: 5′ CAT GCC ATG GCA GAG CCA GAC CCC TC 3′

Reverse Primer: 5′ CCG CTC GAG ATC ACT GGG GTT TCT CCC 3′

Clones were confirmed by PCR amplification of the positive clone and by restriction analysis (Fig. 2.3).
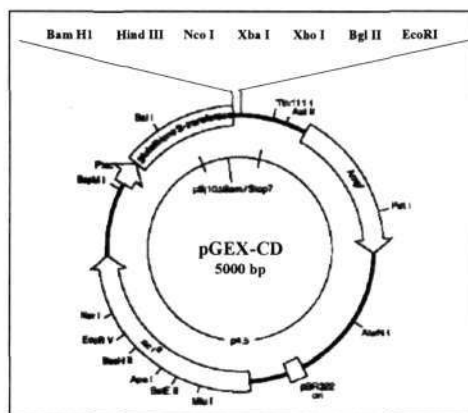
Figure 2.2: Schematic representation of pGEX-CD vector bacterial expression vector.
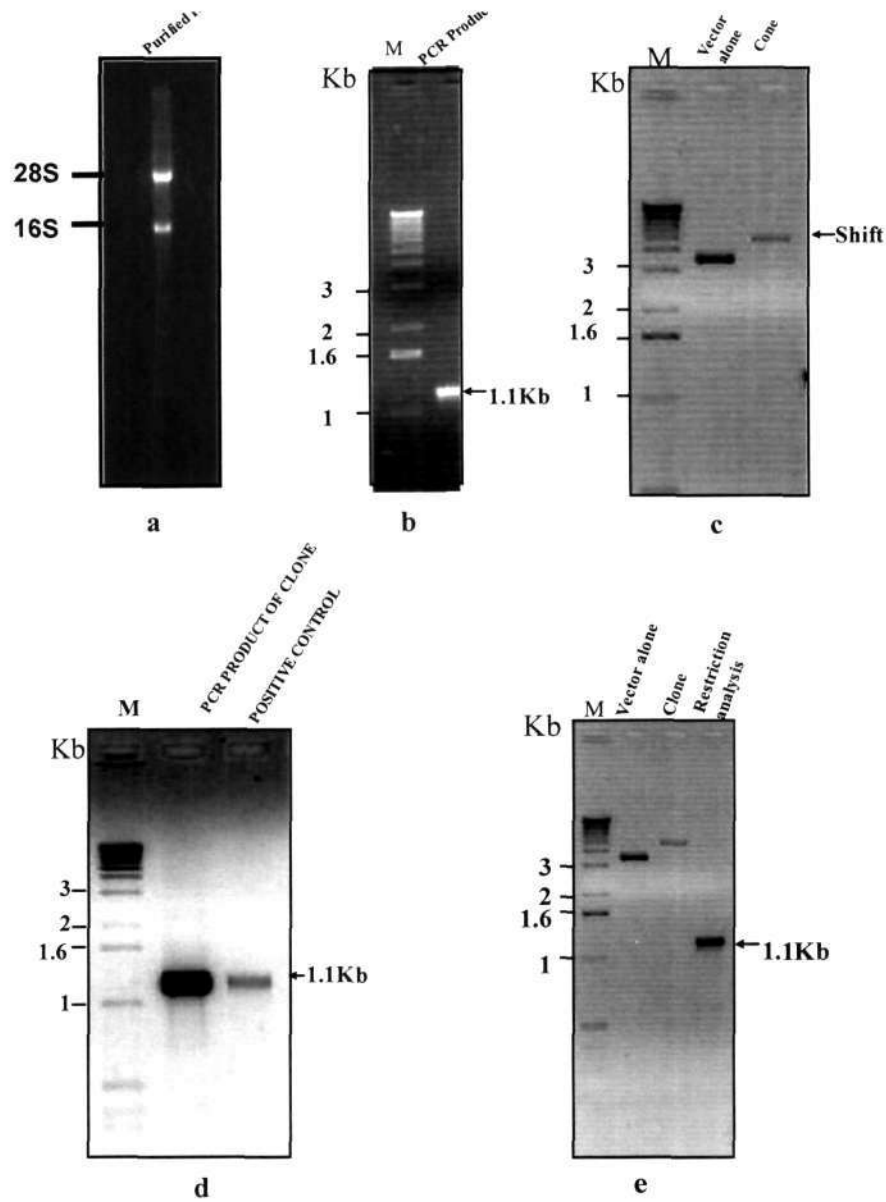
Figure 2.3: a. Schematic representation of GST SirT2 cloning. a. Total RNA was isolated from Hela cells (see method) for the c-DNA synthesis. RNA was checked on 1% agarose gel. b. PCR product obtained from the c-DNA. c. Shift in the agarose gel was observed of the positive clone. Vector alone was used to compare. d. Cloning was further confirmed by the PCR done on the positive clone. Purified PCR product of (b) was used as a control. Full-length SirT2 specific primers as mentioned in the text, were used to amplify the genes corresponding amino acids from SirT2 full length cDNA clone. e. Restriction analysis of GST-SirT2 with *Nco I* and *Xho I* The amplicons were separated on 0.8% agarose gel and visualized by Ethidium bromide (EtBr) staining.

2.2.3. Purification of GST-SirT2:

The GST-SirT2 was expressed in *E. coli* and GST-SirT2 sepharose beads were prepared. *E. coli* BL21 DE3 cells were transformed with GST-SirT2 expression vectors and grown in 100 ml LB medium containing 100 μg/ml Ampicillin and grown for 12 hrs at 37°C. The culture was inoculated into 900 ml LB containing 100 μg/ml Ampicillin and grown at 37°C followed by induction at 0.4 OD_{600} with 0.1 mM IPTG for 3 hrs. The cells were harvested, homogenized in BC300 (20 mM Tris-HCl pH7.4, 20% Glycerol, 0.2mM
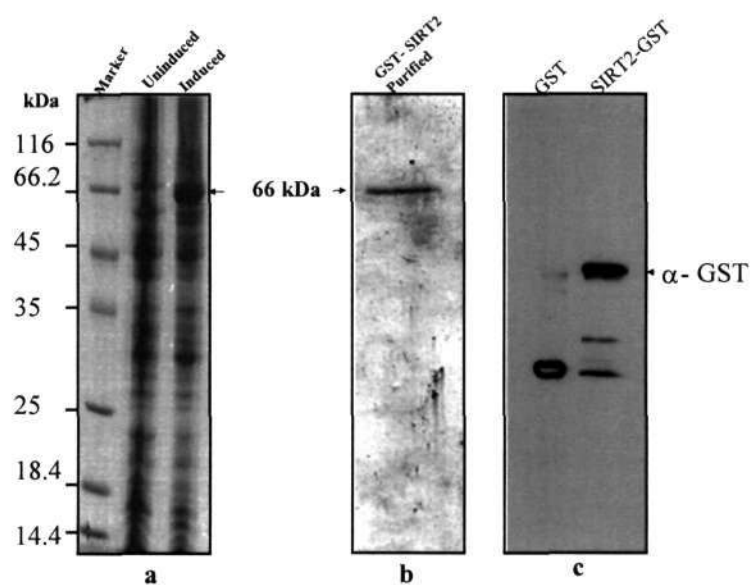
Figure 2.4: a. Schematic representation of GST SirT2 purification. a. Induction of protein is observed in the IPTG added culture as mentioned in the text. b. Purification profile of GST-SirT2 from *E. coli*. Molecular mass of the GST-SirT2 was 66 kilodalton as expected (SirT2 is 40 kDa and GST is 26 kDa). c. Western blot analysis of the purified GST-SirT2 using GST specific antibody was done to confirm the protein.

EDTA, 300 mM KCl, 0.1% NP40, 2 mM PMSF and 2mM β Mercaptoethanol), sonicated. Triton X-100 was added to the sonicated samples at a final concentration of

1% and incubated at 4°C for 30 mins. and centrifuged to clear the prepared cell lysates. Pre-equilibrated GST beads (Pharmacia) were incubated with the cleared lysate for 3 hrs at 4°C in an end-to-end shaker. After incubation the beads were pelleted at 2000 rpm/10 mins/4°C, washed with 10 ml of BC500 (20 mM Tris-HCl pH7.4, 20% Glycerol, 0.2mM EDTA, 500 mM KCl, 0.1% NP40, 2 mM PMSF and 2mM β Mercaptoethanol) (7 times). Protein was eluted with elution buffer (50 mM Tris-HCl pH 7.9and 10 mM reduced glutathione pH 8) analyzed by a 12% SDS PAGE (Fig. 2.4).and dialysed in BC100 before storing it in -80°C. Protein activity was checked by SirT2 HDAC assay (see Methods), (Fig. 2.5).
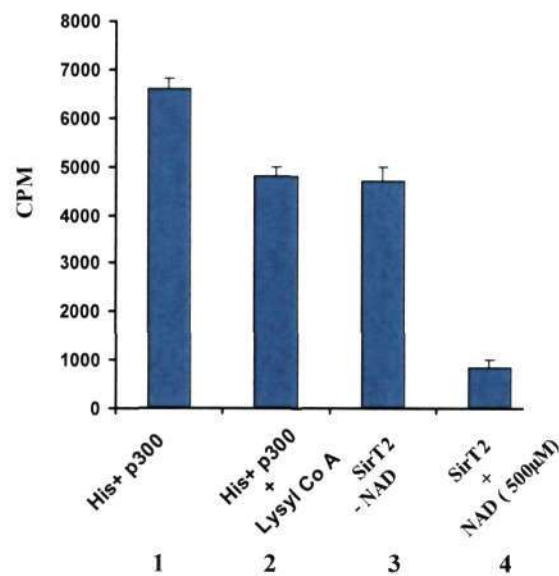
Figure 2.5 SirT2 deacetylase assay. Filter binding assay for testing the activity of the purified GST-SirT2 was done using core histones, p300 acetyl CoA in the absence and presence of SirT2. Reactions 1, 2- core histones incubated with ^{3}[H] Acetyl-CoASH and p300 in absence or presence of p300 specific inhibitor Lysyl CoA. Lane 3 and 4. Reactions were carried out as in case of lane 2 but in presence of SirT2 and in absence and presence of SirT2 cofactor NAD$^+$ (lane 3) and (lane 4). It can be seen that SirT2 in presence of NAD$^+$ can deacetylates the core histones. Error bars indicate standard deviation from two independent experiments.

2.2.4. Purification of Human Histone Acetyltransferase p300:

Recombinant full length His_6 tagged p300 was purified from baculovirus (p300) infected infect 4 x 10^6 *Spodoptera frugiperda* (Sf21) insect ovary cell line in a 150mm diameter dish. The infection time was around 72 hrs. Subsequently cells were harvested and
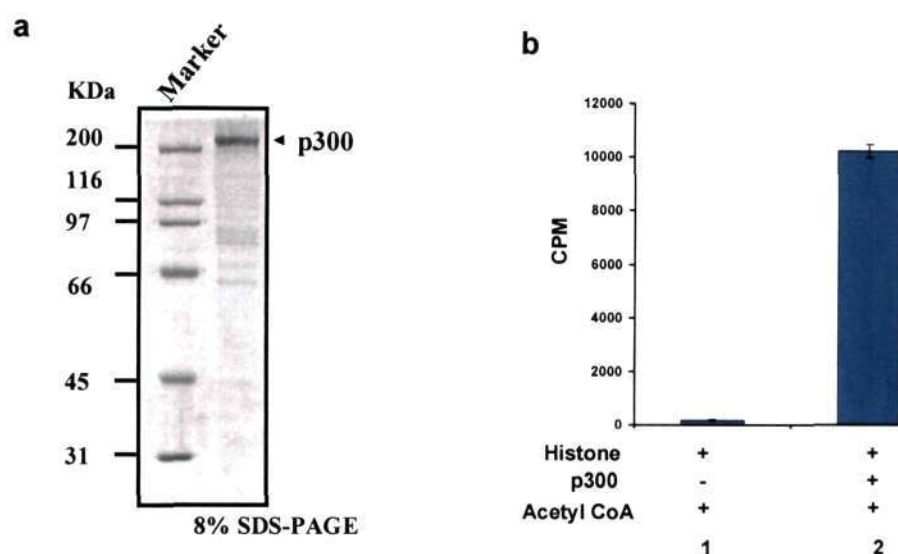
Figure 2.6 . (a) Purified protein profile of human full length p300. (b) Filter binding assay for testing the activity of the purified core histones and p300. Reactions 1, 2- core histones incubated with ^{3}[H] Acetyl CoASH in absence or presence of p300 respectively. Error bars indicate standard deviation from two independent experiments.

pelleted down at 2000 rpm for 10 min and then resuspended in cold homogenization buffer (10 mM Tris HCl pH 7.5, 10% Glycerol, 0.1% NP0, 2 mM β-Mercaptoethanol, 0.2 mM PMSF, 500 mM NaCl, 15 mM Imidazole and 50 μg/ml of each of the protease inhibitors Leupeptin and Aprotinin). Cells were homogenized by series of 10 strokes with a tight pestle, using a Dounce's homogenizer (Wheaton) and a tight pestle for 30 mins at 4°C. The cell lysate was centrifuged 11000 rpm for 15 mins at 4°C. The supernatant was bound to Ni-NTA agarose (Novagen) beads for 2 hrs at 4°C in an end-to-end shaker. The beads were washed 5 times in wash buffer (10 mM Tris HCl pH 7.5, 10% Glycerol, 0.2%NP40, 2 mM β-Mercaptoethanol, 2 mM PMSF, 300 mM NaCl, 15 mM Imidazole). The beads were packed in a USB column (Catalogue No. 13928) and the protein was

eluted in homogenization buffer containing 200mM NaCl and 250mM imidazole. The protein was checked in a 8 % SDS PAGE (Fig. 2.6) , aliquoted and stored at -80°C.

Protein activity was checked by HAT assay (see Methods), (Fig. 2.6).

2.2.5. Purification of Human Histone Acetyltransferase, CREB Binding protein (CBP):

Recombinant full length FLAG-tagged CBP HAT baculoviruses were used to infect 4 x 10^6 Sf 21 (*Spodoptera frugiperda*) insect ovary cell line in a 150 mm diameter dish. The infection time was around 72 hrs. Subsequently cells were harvested and pelleted down at 2000 rpm for 10 min and then resuspended in 8ml of F lysis buffer (20 mM Tris HCl pH 7.9, 500 mM NaCl, 4 mMMgCl$_2$, 0.4 mM EDTA, 2 mM DTT, 20 mM β-glycerophosphate, 20% Glycerol, 0.4 mM PMSF, 1 mM benzamidine, 4 μg/ml Leupeptin

Figure 2.7 . (a) Purified protein profile of human full length CBP. (b) Filter binding assay for testing the activity of the purified core histones and CBP. Reactions 1, 2- core histones incubated with ³[H] Acetyl CoASH in absence or presence of CBP respectively. Error bars indicate standard deviation from two independent experiments.

and 2μg/ml Aprotinin). The cells were homogenized using a Dounce's homogenizer (Wheaton) (pestle B, by 3 series of 10 strokes over 30 mins at 4°C). The cell lysate was

centrifuged 11000 rpm for 10 mins at 4°C. The lysate was diluted using the dilution buffer (10 mM Tris HCl pH 7.9, 10% Glycerol and 0.02 % NP-40) and incubated with 200 µl of FLAG M2-agarose resin (1:1 slurry in F Lysis Buffer), with constant rocking for 4 hrs. at 4°C. The resin was pelleted and washed four times with the F wash buffer (20 mM Tris HCl pH 7.9, 150 mM NaCl, 2 mM MgCl$_2$, 0.2 mM EDTA, 1 mM DTT, 20 mM β-glycerophosphate, 20% Glycerol, 0.4 mM PMSF, 1 mM benzamidine, 4 µg/ml Leupeptin and 2µg/ml Aprotinin and 0.01 % NP-40). The resins were packed in a USB column (Catalogue No. 13928) and the protein was eluted with three successive rounds in F Elution Buffer (F Wash Buffer containing 0.2 mg/ml FLAG peptide; Sigma). The protein was checked in a 8 % SDS PAGE (Fig. 2.7) , aliquoted and stored at -80°C.

Protein activity was checked by HAT assay (see Methods), (Fig. 2.7).

## 2.2.6. Purification of Human Histone Acetyltransferase, p300/ CBP Associated Factor (PCAF):

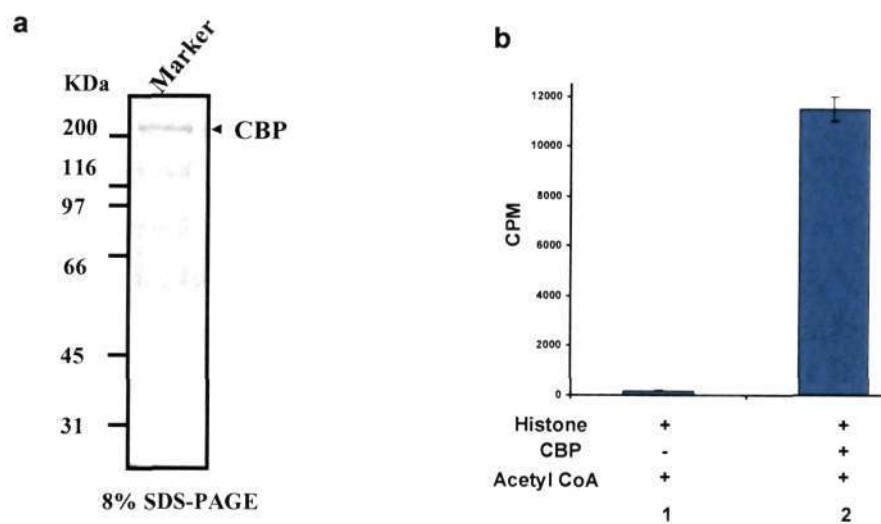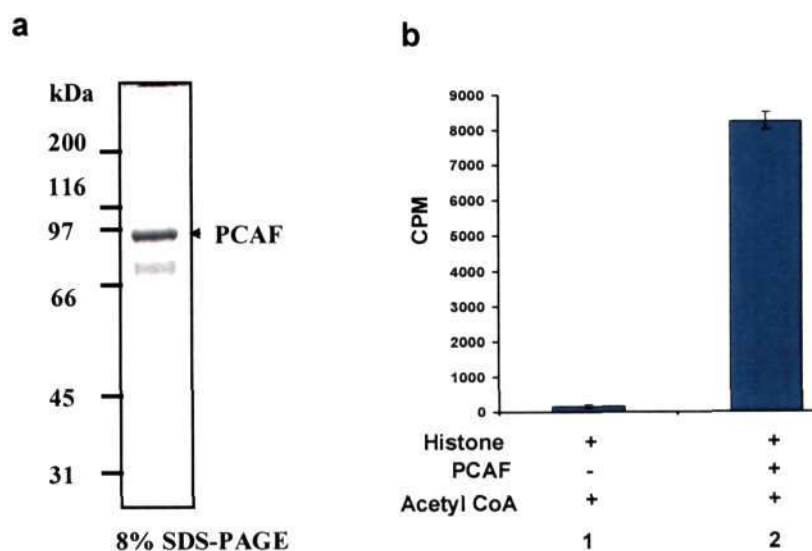**Figure 2.8.** (a) Purified protein profile of human PCAF. (b) Filter binding assay for testing the activity of the purified core histones and PCAF. Reactions 1, 2- core histones incubated with 3[H] Acetyl CoASH in absence or presence of PCAF. Error bars indicate standard deviation from two independent experiments.

Recombinant full length FLAG-tagged PCAF baculoviruses were used to used to infect 4 x 10^6 Sf 21 (*Spodoptera frugiperda*) insect ovary cell line in a 150 mm diameter dish. The infection was allowed to proceed for 70 hrs, after which the cells were harvested and the FLAG purification carried out as described above. The protein was analysed on a 8% (Fig. 2.8) SDS-PAGE. Protein activity was checked by HAT assay (see Methods), (Fig. 2.8).

2.2.7. Purification of bacterial expressed p300 HAT domain:

6His – tagged p300 HAT domain (a.a 1284- 1673) was purified from cells cotransformed with p300 HAT domain and SirT2 in *E.coli* BL21 (DE3). Kanamycin A (50µg/ml final) and ampicillin (100µg/ml final) were used for antibiotic selection of the p300HD and GST-SirT2 expression construct respectively. Cells were grown at 37°C to an A_{600} of 0.55 at which point protein expression was induced by the addition of IPTG (0.5mM final) and induction was done for 3 hrs. Cells were harvested by centrifugation (5000g),
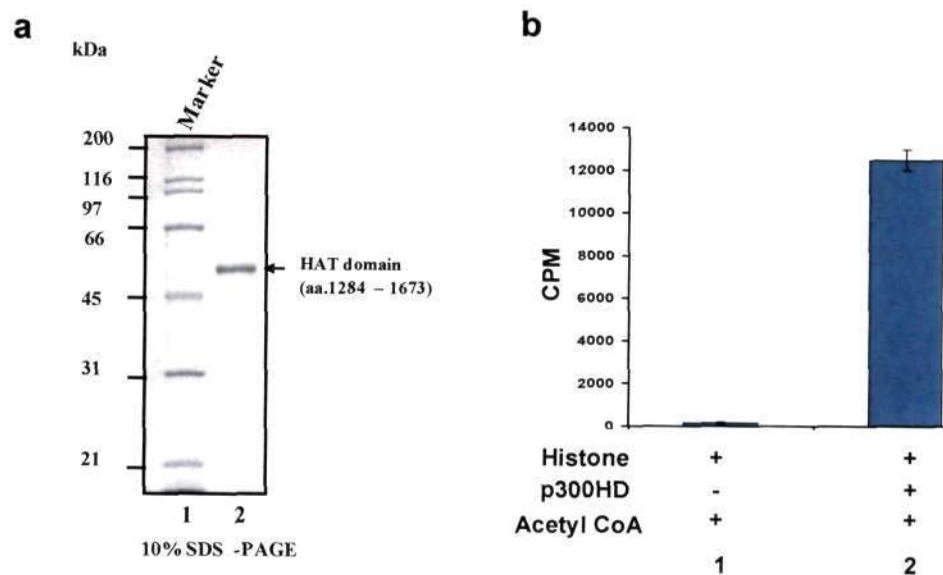
Figure 2.9- (a) Purified protein profile of p300 HAT domain (p300HD)(aa 1284-1673). Lane 1 is protein molecular weight marker; lane 2 is purified protein. (b) Filter binding assay for testing the activity of the purified core histones and p300HD. Reactions 1, 2- core histones incubated with ^{3}[H] Acetyl CoASH in absence or presence of p300HD respectively. Error bars indicate standard deviation from two independent experiments.

resuspended by sonication. The 6His-tagged p300 HAT domain was affinity purified through the Ni-NTA column (Novagen) after a stepwise washing upto 1M NaCl.. Bound proteins were eluted with 250mM imidazole along with 100mM NaCl. Fractions containing p300HD were pooled and dialysed against the BC100 buffer (20 mM Tris-HCl [pH 7.9], 100 mM KCl, 20% glycerol, 0.1 mM DTT). In some cases the pooled proteins were desalted and applied to the RESOURCE Q column (Amesrsham Biosciences) and was purified using the linear gradient of increasing concentration of NaCl.

For biophysical studies p300HD were further dialysed against20 mM Tris-HCl of pH 7.5, 0.2 mM EDTA, and 100 mM KCl. The protein was analysed on a 10% (Fig. 2.9) SDS-PAGE. HAT assays were performed to check the enzyme activity before any *in vitro* study (Fig. 2.9).

2.2.8. Purification of human core histones:

Human core histones were purified from HeLa nuclear pellet. The pellet was homogenized with a Dounce's homogenizer (Wheaton) with pestle B in buffer A

15% SDS-PAGE
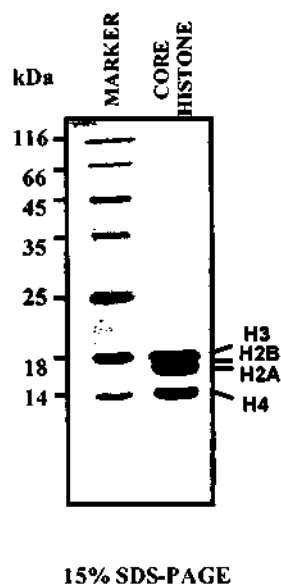
Figure 2.10 . Purification profile of the HeLa nuclear core histone. Lane 1 is the protein molecular weight marker; lane 2 is purified HeLa core histone.

(0.1 M potassium phosphate [pH 6.7], 0.1 mM EDTA, 10% glycerol, 0.1 mM phenylmethylsulfonyl fluoride, 0.1 mM dithiothreitol (DTT) containing 0.63 M sodium chloride and centrifuged at 14,000 rpm at 4°C. The supernatant was incubated with previously swollen Hydroxyapatite Biogel-HTP resin (DNA grade; Bio-Rad) for 3 h. The resin was then packed into an Econo column (Bio-Rad) and washed overnight with buffer A containing 0.63 M NaCl. The bound core histones were eluted with buffer A containing 2 M NaCl and dialyzed first against buffer B (10 mM potassium phosphate [pH 6.7], 150 mM KCl, 10% glycerol) for 3 h and then against BC100 buffer (20 mM Tris-HCl [pH 7.9], 100 mM KCl, 20% glycerol, 0.1 mM DTT) for 3 h. The protein was analysed on a 15% (Fig. 2.10) SDS-PAGE.

2.3. Protocols for the various assays and biophysical techniques:

2.3.1. Immunoprecipitation assay:

In vivo protein-protein interactions were detected by immunoprecipitation assays. Indicated amount of antibody was incubated with Protein-G Sepharose overnight on a rotary shaker at 4°C. The beads were pelleted and washed 3 times with 1 ml of cold PBS and final wash was done with lysis buffer. Antibody bound protein-G sepharose was incubated with 500 µg whole cell lysate overnight at 4°C on a end to end rotary shaker. The beads were then pelleted and washed 3 times with lysis buffer. The protein bound beads were loaded on 10% SDS PAGE gel followed by immunoblotting with indicated antibodies. For p300, 8% SDS PAGE was used. In cases where cells were treated with HDAC inhibitors, 5 mM sodium butyrate, 5 mM nicotiamide and 100 ng ml⁻¹ TSA were added 10 h before cells were harvest (Thompson et al. 2004).

2.3.2. Chromatin immmunoprecipitation assay (ChIP):

The pull-downs for ChIP assay was performed using anti-acetylated H3 (H3AcK9AcK14) (Santa Cruz) antibody. KB cells were maintained in DMEM supplemented with 10% FBS were treated with CTK7A (100 µM) and cells were grown

for 24 hrs. For ChIP assay cells were processed as described elsewhere (Bandyopadhyay et al. 2002). The pulldown was done using antibody against the above mentioned antibody and the immunoprecipitated samples were deproteinized and ethanol-precipitated to recover the DNA. Real-time PCR analysis was performed using primers for the cyclin E promoter region. PCR primers for the cyclin E promoter region were 5'-GGCGGGACGGGCTCTGGG-3' and 5'-CCTCGGCATGATGGGGCTG-3'.

2.3.3. Histone Acetyltransferase Assay (HAT assay):

HAT assays were performed as described in an earlier report (2). 1.8 μg of highly purified HeLa core histones were incubated in HAT assay buffer at 30 °C for 10 minutes with or without bacterially-expressed recombinant p300 HAT domain in the presence and absence of Silver nanoparticle and HATi followed by addition of 1 μl of 4.7 Ci/mmol [^{3}H] acetyl CoA (NEN-PerkinElmer) and were further incubated for another 10 min in a 30 μl reaction. The radio labeled acetylated histones were visualized by resolving on 15% SDS-PAGE and subjected to fluorography followed by autoradiography.

For kinetic analysis of HAT inhibitors mediated inhibition of p300 HAT domain, filter binding assays were performed in the presence (1 and 5 μM) for garcinol and IG and (10 and 20 μM) of LTK14 or in absence of these inhibitors. For CTK7A similar assays were performed in presence of 30 and 50 μM of CTK7A. Of the two substrates, core histones and the acetyl group donor tritiated acetyl CoA, the concentration of one substrate was kept constant and the other was varied. Concentration of core histones was kept constant at 1.6 μM and ^{3}H-acetyl CoA was varied from 1.08 μM to 8.66 μM in the first assay. H^3-acetyl CoA was kept constant at 2.78 μM and core histones was varied from 0.003 μM to 0.068 μM in the second assay. The incorporation of the radioactivity was taken as a measure of the reaction velocity recorded as counts per minute (cpm). Each experiment was performed three times and reproducibility was within 15%. Weighted averages of the values obtained were plotted as a lineweaver burk plot using

Graphpad Prism software. The slope and intercept were replotted from the primary inhibition kinetic data to evaluate the inhibition constant, K_i.

2.3.4. Histone Methyltransferase Assay (HMT assay):

Histone methyltransferase assays were performed in a 30-μl reaction. The reaction mixture containing highly purified HeLa core histones, with or without histone methyltransferases in the HMT assay buffer 20 mM Tris, 4 mM EDTA, pH 8.0, 200 mM NaCl, along with varying concentrations of HAT inhibitors for 10 min at 30 °C. After the initial incubation, 1 μl of 15 Ci/mmol [^{3}H] (S)-adenosyl methionine (Amersham) was added to the reaction mixtures, and the incubation continued for 15 minutes. The reaction mixture was then blotted onto P-81 (Whatman) filter paper, and radioactive counts were recorded on a PerkinElmer Wallac 1409 liquid scintillation counter.

2.3.5. Histone Deacetylase assay (HDAC Assay):

The deacetylation assay was performed as per standard protocol ((Balasubramanyam et al., 2004, Balasubramanyam et al., 2004, Mantelingu et al., 2007). HeLa core histones were incubated in HAT buffer without NaBu, with p300 and 1 μl of 4.7 Ci/mmol [^{3}H] acetyl-CoA for 30 min at 30 °C. The activity of p300 was inhibited by incubating the reaction mixture with 30 μM p300-specific inhibitor Lysyl-CoA (Lau et al. 2000) for 15 min at 30 °C, after which 50 ng of HDAC1 was added in the presence or absence of HAT modulator and incubated further for 45 min at 30 °C. The reaction mixture was then blotted onto P-81 (Whatman) filter paper, and radioactive counts were recorded on a PerkinElmer Wallac 1409 liquid scintillation counter.

2.3.6. SirT2 - Deacetylase Assay:

This is the modified form of the above described HDAC assay. HeLa core histones were incubated in HAT buffer without NaBu, with p300 and 1 μl of 4.7 Ci/mmol [^{3}H] acetyl-CoA for 30 min at 30 °C. The activity of p300 was inhibited by incubating the reaction mixture with 30 μM p300-specific inhibitor Lysyl-CoA (Lau et al. 2000) for 15 min at 30 °C, after which 50 ng of SirT2 was added in the presence or absence of cofactor NAD$^+$ and HAT modulators and incubated further for 45 min at 30 °C. The reaction mixture was then blotted onto P-81 (Whatman) filter paper, and radioactive counts were recorded on a PerkinElmer Wallac 1409 liquid scintillation counter.

2.3.7. Immunohistochemistry:

Patient tissues were obtained from Bangalore Institute of Oncology. All the 31 samples were collected with informed consent of the patients and prior institutional review board approval. All of the samples were histologically confirmed by pathologists for the tumor and the adjacent normal tissue. Hematoxylin and eosin staining (H&E staining) was done to confirm the pathological state. Cellular invasiveness (lost cellular boundary identity), increase vasculature and cellular atypia were used by the pathologists to confirm the nature of the tissue (tumor vs adjacent normal). All sample tissues were collected in three separate vials (a).for IHC (fixed in 10% formalin) ; (b). for protein isolation (in protease inhibitor cocktails; Roche) ; (c). for RNA isolation (in RNA latter solution; Ambion). Tissues samples except for IHC were quick frozen in liquid nitrogen and stored at -80°C. Patient samples to be used in IHC were fixed in 10% formalin for 1–2 hr and transferred to 70% ethanol overnight followed by paraffin embedding. Paraffin blocks of fixed oral tissues were sectioned at 5 μm. The sections were mounted on silane coated glass slides. The deparaffinization was done by keeping the slides at 42°C hot platform (overnight), hydrated and heated by microwave for 5 min at 93–98 °C in citric buffer (10mM, pH 6.0).The slide were further incubated in same buffer for 20 min at room temperature (RT). The slides were washed with PBS (3 min, two times). Blocking was done at RT with 5% fat free milk. Slides were again washed with PBS (3 min, four times). The sections were then incubated overnight at RT with different antibodies as mentioned in

the text (1:30 dilution). Then, the Envision kit (Dako, Denmark) was used according to the manufacturer's recommendations. Sections were counterstained with Mayer's hematoxylin, mounted in DPX and air dried. Slides were evaluated by two independent pathologists. For statistical analysis, cells (100 cells from a total of 5-6 independent fields) were counted from both normal and tumor tissue sections and scored for percentage of positive cells (brown colour) for the indicated antibodies (see text, Chapter 5). For comparison one-way ANOVA was performed using "Sigmaplot Software". P-value < 0.01 was considered as statistically significant, n= 31.

2.3.8. Xenograft growth assay:

Animal experiments were performed with the approval by authorized ethics Committee. Sixteen nude mice (BALB/c) were included in the experiments (10 male and 6 female mice). Mice were kept in isolators in a pathogen free environment. All nude mice were 3-4 weeks old at the start of the experiments. KB cells (oral cancer cell), 2×10^6 cells were inoculated in each mice in the right and left flanks, respectively. Mice were then divided in two groups (5 males and 3 females) in each group. After the tumors grown to palpable in size, CTK7A treatment were given intraperitoneally (i.p) with 100mg/kg body weight/twice a day. Tumors were measured once in three days with a caliper and their volumes were calculated by the formula: $0.52 \times D1 \times (D2)^2$, where 'D1' and 'D2' are, respectively, the longest and shortest dimension. The last dose of the compound (CTK7A) was administered four hour before sacrificing it. Tumors were removed and put into liquid nitrogen or were fixed in 10% formalin for 1–2 h to make blocks to used for IHC. For comparing tumor sizes between treated and control one-way ANOVA was performed using "Sigmaplot Software". P- value < 0.05 was considered as statistically significant.

2.3.9. Fluorescent Activated Cell Sorting (FACS):

KB cells were grown in the presence or absence of CTK7A for 24 h with the indicated concentration (see Chapter 5). Cells were grown in presence of CTK7A for 2 h in absence fo serum followed by addition of 10% Serum. Briefly cells were harvested by mild trypsinization (0.25%) followed by centrifugation at 2000 rpm for 10 mins at 4^OC. Cells were washed with cold PBS by centrifugation at 2000 rpm for 10 mins at 4^OC. Cells were fixed in cold 70% Ethanol which was added dropwise along with mild vortexing. Samples were left for 12 hrs, after which Ethanol was removed followed by two washes in cold PBS. RNase (100 µg/ml) treatment was subsequently given at $37^OC/30$ mins to ensure only DNA staining. 50 µg/ml Propidium Iodide was added for staining. Cells were sorted and analyzed by flow cytometry for the cell cycle distribution using inbuilt software of BD FACScalibur instrument. Analysis was done in FL2 channel.

2.3.10. In vitro Wound-Healing assay:

Cells in medium containing 10% FBS were seeded in 30 mm dishes. After the cells grew to confluence, wounds of constant diameter were made by sterile plastic pipette tip (200-µl) by scratching the monolayers. Cells were washed with the serum free medium twice and refreshed with medium with or without 10% FBS. Cells were treated with or without the HAT inhibitor for 24 h along with 10% serum. The wound photographs were taken under phase-contrast microscope. Serum positive and negative cells act as positive and negative control for the experiments respectively. The experiments were repeated three times.

2.3.11. Senescence-associated β-gal (SA-β-gal) activity analysis:

Cells were grown in 60 mm dishes. Cells were then treated with CTK7A (100µM) for 24 hours. SA-β-gal activity was analyzed in KB cells as described earlier (Dimri et al., 1995). Cells were washed with PBS and fixed with 2% (v/v) formaldehyde for 5'. Cells were again washed in PBS two times. Staining solution was added to cover the cells in the culture dish and incubated for 12 h at 37°C (do not incubate in a CO_2 incubator).Cells were again washed with PBS and then photographed under the microscope. A blue color is visible within 2 hr; however, staining is maximum at between 12 to 16 h. Blue stain is indicative of senescence-associated β-galactosidase activity.

Staining solution

Chemical concentration	Stocks
1 mg/ml X-gal	40 mg/ml
150 mM NaCl	5 M
2 mM MgCl2	1M
5 mM $K_3Fe(CN)_6$	100 mM
5 mM $K_4Fe(CN)_6$	100 mM
40 mM Citric Acid/Phosphate Buffer, pH 6.0	0.1M

Citric Acid/Phosphate Buffer 0.1 M Citric Acid was prepared using 0.2 M Sodium Phosphate Dibasic (Na_2HPO_4) and pH was set at 6.0. In this case proper pH is very important.

2.3.12. [^{3}H]Thymidine Incorporation Assay:

Cells were grown in 24-well plate and were treated with the compound for 16 h followed by addition of 1 micro curie [^{3}H] thymidine (NEN, Perkin Elmer). Cells were grown for

an additional period of 8 h. Following this media was aspirated and cells were washed with 1 ml ice cold PBS. Cells were lysed by repeated freeze thawing (2 times). DNA was isolated using cell harvester and scintillation counting was done using liquid scintillation counter.

2.3.13. Determination of the specific activity of the p300HD:

Approximately 3.0 Units/mg total protein was used for the assay. 1 Unit is defined as the transfer of 1nmol of $[^3H]$-acetate/ minute to the HeLa core histones. p300 full length with similar specific activity were also used and were in comparable range with p300HD. HAT assays were performed to determine the specific activity.

2.3.14. Absorbance and Fluorescence Measurement:

Absorption spectra were recorded with CECIL 7500 spectrophotometer. Fluorescence measurements were performed with PerkinElmer LS55 Luminescence Spectrometer using 1 cm path length quartz cuvettes. Excitation and emission slits with a band-pass of 10 nm, each were used for all measurements. During fluorescence measurements, absorbance of the samples did not exceed 0.05 at 295 nm. Therefore, no correction for optical filtering effect was done.

2.3.15. Binding Analysis:

Results from fluorometric titrations were analyzed by the following method. The apparent dissociation constant (K_d) was determined using a nonlinear curve fitting analysis (eqs 1 and eqs 2). Experimental points for the binding isotherm were fitted by the least-squares method (Chakrabarty et al. 1998).

$K_d = [C_p - (\Delta F/\Delta F_{max}) C_p][C_l - (\Delta F/\Delta F_{max}) C_p]/[(\Delta F/\Delta F_{max}) C_p]$ (1)

$C_p (\Delta F/\Delta F_{max})^2 - (C_p + C_l + K_d)(\Delta F/\Delta F_{max}) + C_l = 0$ (2)

where ΔF is the change in fluorescence emission intensity at 340 nm ($\lambda_{ex} = 295$ nm) for each point of titration curve, ΔF_{max} is the same parameter when the protein is totally bound to the ligand (HATi), C_l is the concentration of the HATi and C_p is the initial concentration of the protein. A double reciprocal plot of $1/\Delta F$ against $1/(C_p-C_l)$ was used for determination of ΔF_{max}.

$1/\Delta F = 1/\Delta F_{max} + K_d/[\Delta F_{max} (C_p - C_0]$ (3)

2.3.16. Fluorescence Quenching Experiment:

Fluorescence quenching experiments were carried out by recording fluorescence intensities at 340 nm ($\lambda_{ex} = 295$ nm) at 20°C. Aliquots from a stock solution of a neutral quencher acrylamide were added successively to p300HD (1.2 µM) preincubated with 2.5 µM of HATi for 2 min at room temperature in 20 mM Tris-HCl of pH 7.5, 0.2 mM EDTA, and 100 mM KCl. Quenching data were analyzed according to the Stern-Volmer equation (Lakowicz, 1999), $F_o/F = 1 + K_{sv} [Q]$, where F_o and F are the initial and final fluorescence intensities, respectively. K_{sv} is the quenching constant, and $[Q]$ denotes the input concentration of acrylamide. A modified Stern-Volmer plot was also done to estimate the accessible (f_e) fraction of tryptophan residues according to the below given equation

$$F_o/(F_o - F) = 1/(K_{sv} f_e [Q]) + 1/f_e$$

2.3.17. Circular Dichroism Spectroscopy:

Circular Dicrhroism (CD) measurements were carried out in a JASCO J-810 spectropolarimeter (Jasco Corporation, Tokyo, Japan) at 20°C equipped with a temperature controller. The CD scans were recorded for the wavelength range of 200-250

nm at sensitivity set to 10 mdeg and scan speed 10 nm per minute with step size of 0.5 nm. The time constant was 8 second and band-width was 2 nm. All measurements were carried out in a quartz cuvette of 1mm path length in a reaction volume of 250 μl in 20 mM Tris-HCl of pH 7.5, 0.2 mM EDTA, and 100 mM KCl at 20°C. In a reaction mixture containing 1.2 μM p300HD, individual titration for each HAT inhibitors was performed to achieve a concentration range of 2.88 μM. The reaction mixture was incubated for 15 minutes prior to scanning. All spectra are average of six runs. They are subtracted from appropriate buffer blank containing the ligands when required. They were smoothed within the permissible limits by the inbuilt software of the instrument.

2.3.18. Isothermal Titration Calorimetry (ITC):

ITC experiments were carried out in a VP-ITC system (Microcal LLC) at 20°C temperature. Samples were centrifuged and degassed prior to titration. Titration of HAT inhibitors (HATi) against the protein (p300HD) was carried out by injecting 30-35 μM HATi in 20 mM Tris-HCl of pH 7.5, 0.2 mM EDTA, and 100 mM KCl buffer against 3μM p300HD. A two minute interval was allowed between injections for equilibration; sufficient for the return of the heat signal to baseline. A total of 35 injections were carried out to ensure complete titration. The protein concentration was chosen to achieve sufficiently high heat signals with a minimum enthalpy of dilution. To minimize the error associated with diffusion from the syringe during baseline equilibration, the first injection was only 1 μl and the associated small heat change was not considered for data analysis.

Blank experiments involving the titration of HATi against the buffer and the buffer against buffer were carried out and used for subtraction of the background heat change. The corrected heat change were plotted against molar ratio of the titrated products and analyzed using manufacturer's software which yielded the stoichiometry n (in terms of number of molecule of HATi /protein) and equilibrium constant (K_a). From the relationship $\Delta G° = -RT \ln K_a$ and the Gibbs-Helmholtz equation, the free energy of binding and the entropy of association ($\Delta S°$) were calculated.

2.3.19. Isobologram studies:

Isobologram analysis was performed as previously reported (Milne et al. 2007). The effect of the combination of IG versus garcinol and IG versus LTK14 was determined using the filter binding assays as described above. A concentration matrix of the 2 compounds was created and tested against p300HD. The % inhibition of core histone acetylation was determined at each of the combinations present in the matrix. The resulting Isobologram was used to evaluate the effect of the combination. For the analysis, a plot in Cartesian coordinates of a dose combination that produce the same effect level is the basis for an Isobologram. If two compounds have variable potency, a constant relative potency (R) - which is the amount of compound needed to achieve the same fold activity (e.g. IC_{50} for IG vs garcinol and IC_{50} for IG vs LTK14) - is selected for the X and Y intercepts for Isobologram analysis. The concentration of both compounds which corresponds to the respective IC_{50} value is used as an intercept on both the X and Y axes. Using these two intercepts, a theoretical line called the line of additivity is drawn between the two points. Experimental data obtained by the logarithmic titration of the two compounds mixed as a dose pair in a matrix which yield the same effect level (IC value), is plotted on the Isobologram. Statistical comparison of the line of additivity and the curve arising from experimental two drug dose combinations indicates if an effect is additive. Points falling below and above the line of additivity are subjected to regression analysis. Experimental data that is higher than the line of additivity is interpreted antagonistic and experimental data that is lower is interpreted as synergistic, and experimental data that fall on the line of additivity is considered additive.

2.3.20. Molecular calculation and computational strategy for IG structure optimization:

The Gaussian 03 program was used for all the ab inito molecular orbital calculations. Electron correlation was accounted for using the Becke's three parameter hybrid method

and the Lee–Yang–Parr correlation functional (B3LYP) at the 6-31+G (d) basis set (Becke et al. 1993; Lee et al. 1998).

2.3.21. Docking studies:

Crystal structure of p300 HAT domain has been extracted from PDB (PDB id: 3BIY). The HAT domain was docked with the structure of garcinol (Pub Chem CID 5281560), IG and LTK14 to find out their interaction sites on HAT domain. Molecular simulation and the docking of p300HD with different HAT inhibitors were performed using Hex 4.5 software (Mustard et al. 2005). The docking calculations were done using 3D parametric functions of both the protein (p300HD) and the chemical structures (inhibitors), which were used to encode surface shape and electrostatic charge and potential distributions. The parametric functions are based on expansions of real orthogonal spherical polar basis functions. The docking was performed in full rotation mode; both domain and inhibitor were taken at 180 ranges for 20,000 solutions. Crystal structure of PCAF HAT domain (PDB-id: 1CM0.) is used to dock the HAT inhibitors using AutoDock 4 software.

2.3.22. Experimental details for the SERS studies of p300 and p300HD:

2.3.22. a. Raman Spectroscopy:

The Raman excitation light (632.8 nm), provided by a He-Ne laser (model 25-LHR-151-230, Melles-Griot, U.S.A.), traversed a band-pass filter (XL12- 633NB4, Omega Optical Inc., U.S.A.) and was launched into an epi-illuminated microscope (Nikon 50i, Nikon, Japan; axial resolution ~1µm) for micro-Raman experiments. The microscope objective both focused the excitation light and collected the Raman-scattered light in a backscattering geometry. A dichroic beam splitter (660DCLP, Chroma Technology Corp.) redirected the Raman-scattered light from the microscope to a 100 µm single-core, multimode optical fiber atop the microscope. The light passed through an edge filter

(XR3003, Omega Optical Inc., VT) kept before the optical fiber. The optical fiber was f-number matched to a 0.55 m spectrograph (Jobin-Yovn 550 Triax, Instruments SA, NJ) attached with a liquid nitrogen cooled CCD detector. The spectrograph itself had a computer controlled adjustable slit and a turret, which held three gratings for a range of measurements. For the Raman studies, a holographic 1800 grooves mm^{-1} grating was used along with the 500 μm spectrograph entrance slit setting, providing ~4 cm^{-1} resolution. A digital camera (Nikon Coolpix 5400, Nikon, Japan) atop the microscope allowed for registration of the focused laser spot and focusing the image of the laser spot onto the optical fiber. Typically, for Raman studies on liquid samples, a 60× infinity-corrected water immersion objective (Nikon Fluor, Japan, numerical aperture (NA) 1.00) was used. In the case of solid samples, a 60× infinity-corrected objective (Nikon Plan Apo, Japan, NA 0.9) was used. The laser power used at the sample was 6 mW. The typical accumulation time used was 180 s.

2.3.22. b. Silver Colloid Preparation and Characterization:

Silver colloids were prepared by the standard Lee and Meisel method (Lee et. al. 1982). Transmission electron microscopy (TEM) images of Ag were recorded using a JEOL-3010 microscope operating at 300 keV. The TEM images of Ag colloids are shown in Figure 2.13. The average size of the spherical colloids was found to be ~50 nm. There are
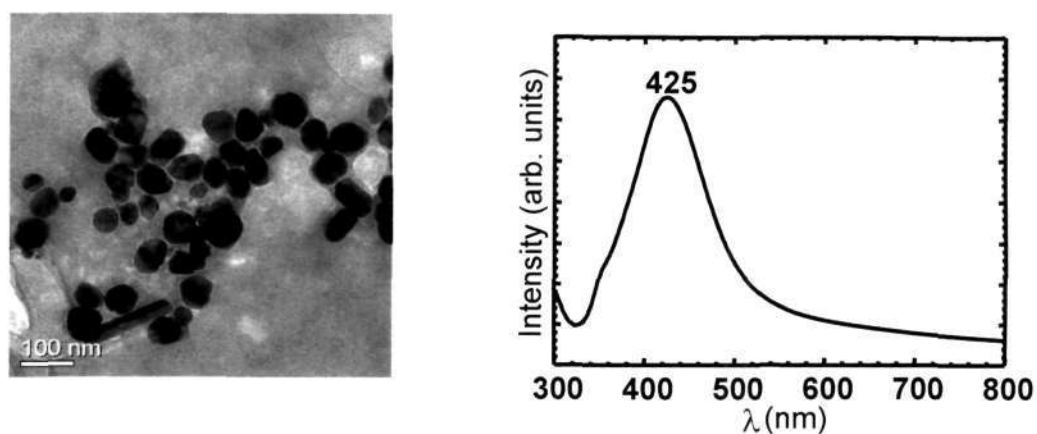
Figure 2.13: TEM images and their corresponding plasmon resonance plots of citrate reduced Ag nanoparticles prepared by Lee-Meisel method (Lee, et al. 1982).

some rod like structures present, whose numbers are negligible when compared to those of the spherical colloidal particles. Figure 2.13 shows the extinction spectrum of the Ag colloids, which has the maxima around 425 nm, confirming the expected nature of the Ag colloid.

2.3.22. c. Processing of p300 for SERS studies:

The details of the expression and purifcation of full-Length recombinant human p300 and purifcation of Human (HeLa) Core Histones was done as described above. The protein was dialyzed against BC100 (20 mM Tris-HCl (pH 7.9),10% glycerol, 0.2 mM EDTA (pH 8.0), 100 mM NaCl, 0.5 mM PMSF, 0.01 M 2-mercaptoethonol, and 0.1% NP40) to remove the imidazole for performing the SERS experiments. To deuterate the protein, p300 was incubated in D_2O before performing the SERS experiments. The nanoparticles in D_2O solution were used for the deuterated protein experiments. In order to check the activity of the protein, HAT assay was performed. The indicated amounts of highly purified human core histones were incubated in HAT assay buffer containing 50 mM Tris-HCl, pH 8.0, 10% (v/v) glycerol, 1 mM dithiothreitol, 1 mM PMSF, 0.1 mM EDTA, pH 8.0, 10 mM sodium butyrate, and 1 μL of 3.3 Ci/mmol [3H]acetyl coenzyme A (acetyl-CoA) (Perkin-Elmer-NEN) at 300C for 30 min. The final reaction volume was 30 μL. The reaction was stopped by incubating the mixture on ice for 10 min before blotting onto P-81 (Whatman) filter papers. The radioactive counts were recorded on a Wallac 1409 liquid scintillation counter. To visualize the radiolabeled acetylated histones, the reaction mixtures were resolved on 15% SDS-polyacrylamide gel and processed for fluorography as described earlier.

2.3.22. d. SERS of the p300 in Aqueous Sample:

p300 solution (protein concentration approx- imately 40 ng/ μL) was mixed with Ag colloidal solution (prepared by Lee and Meisel method, 1982) in the ratio of 1:4 on a glass slide with a cavity in it. After allowing the mixture to settle for 5 min, SERS measurements were performed using the water immersion objective lens of the Raman microscope. To find out the effect of chloride ion in the SERS experiments, NaCl solution was mixed with the above suspension in the ratio of 1:10 (NaCl/suspension). The final concentration of NaCl was 0.3 mM in the solution mixture.

2.3.22. e. SERS of p300 on a Glass Substrate:

Two methods were used to perform SERS on p300 deposited over the glass substrate. Figure 2.12 shows the schematic of both the methods.
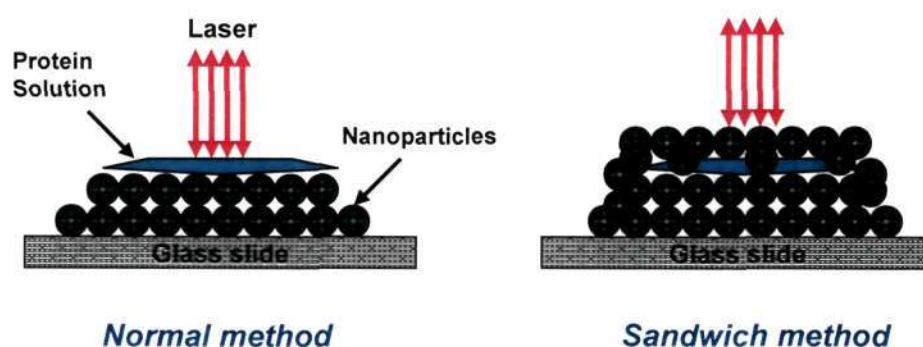
Figure 2.12: Schematic depicting the two configurations of SERS measurements.

2.3.22. e. i. Normal Method:

A 100 μL solution of Ag colloid was deposited on a flat glass slide and dried overnight at room temperature. A brown-colored ring was observed over which 20 μL of p300 solution (40 ng/ μL) was dropped, and the sample was dried at room temperature for 5 h. SERS measurements were performed by focusing the objective onto the uppermost layers of the deposited mixture as shown in the schematic diagram in Figure 2.12. Proper care was taken to avoid any contact with the objective while focusing the laser.

2.3.22. e. ii. Sandwich Method:

A 50 μL solution of Ag colloid was deposited on a flat glass slide and dried overnight at room temperature. On the ring formed by the colloidal solution, 20 μL of p300 solution of the same concentration as mentioned above was deposited followed by 50 μL of Ag colloidal solution as shown in Figure 2.12. The sample was left to dry at room temperature for 5 h. The SERS measurements were performed as discussed in the normal method.

2.3.22. f. SERS of p300 HAT domain:

SERS of p300 HAT domain was done similar to that of the p300 full length SERS. To perform SERS of p300HD, it was adsorbed on the silver nanoparticles prepared by Lee and Meisel method (Lee, et al. 1982). All the measurements were performed using the water immersion objective of custom built Raman microscope. For the present study, 532 nm frequency doubled Nd-YAG laser was used. The typical size of the Ag nanoparticles was found to be ~ 50 nm by Transmission Electron Microscopy (as shown above). p300 HAT domain solution (protein concentration ~ 50 ng/μl) was mixed with Ag nanoparticles solution in the ratio of 1:4 and put on to a cavity glass slide. The deuterated SERS spectrum was obtain by the same method as explained for p300 full length, without any modifications. The mixture was allowed to settle for 5 minutes before recording the SERS using a water immersion high magnification objective.

2.3.22. g. p300 Autoacetylation assay:

Autoacetylation reactions of p300 HAT domain were carried out in HAT assay buffer at 30 °C for 10 minutes with or without HAT inhibitor or silver nanoparticle followed by addition of 1 μl of 4.7 Ci/mmol [^{3}H] acetyl CoA (NEN-PerkinElmer) and

were further incubated for another 10 min in a 30 μl reaction. The radios labeled acetylated p300HD were visualized by fluorography followed by autoradiography.

2.1.43. h. Autoacetylation of p300 HAT domain for SERS experiments:

Autoacetylation reactions of p300 HAT domain were carried out using cold acetyl-CoA. The p300 HAT domain were preincubated in the HAT buffer for 10 min at 30°C then the reaction was started with the addition of cold acetyl-CoA (125μM). The reaction was incubated further for 2hrs at 30°C. In order to get the fully autoacetylated p300 HAT domain, the cold acetyl-CoA was gain added to the above reaction mixture and incubated for an additional time of 2 hrs. Following the reaction, all the reaction mixtures were pooled together. In order to remove the free acetyl-CoA and other small molecules from the autoacetylated p300 HAT domain, which would otherwise hinder the SERS study, autoacetylated p300 HAT domain was again affinity purified through the Ni- NTA column. This was followed by dialysis to remove the imidazole and glycerol. p300HD activity was checked by filter binding assay (HAT assay) . MALDI-TOF was done to confirm autoacetylation of p300 HAT domain (see Chapter 4).

Chapter **3**

This chapter presents the results and discussion of an effort to elucidate mechanisms of p300-HAT activity inhibition by different classes of inhibitors.

3.1. Rational of the study:

Previously we have discovered that the polyisoprenylated benzophenone, garcinol isolated from *Garcinia indica* (an edible fruit), is a potent nonspecific inhibitor of histone acetyltransferase p300 (KAT3B). Further we made several garcinol derivatives out of which some were specific towards p300 (e.g. LTK14) and some were not like isogarcinol. It was surprising to us that even though the structures of these HAT inhibitors were very similar they showed difference in specificity. In the present study we analyzed the biochemical and biophysical reasons for the differential nature of inhibition brought about by these HAT inhibitors. These data provide precise mechanisms of HAT inhibition by these small molecule compounds which could be useful in designing more therapeutically potential HAT inhibitors.

3.2. Introduction:

Among different HATs, the histone acetyltransferase, p300 is the most thoroughly studied. It is a highly potent enzyme that acetylates histones and several other proteins (Ogryzko et al. 1996; Bannister et al. 1996). Mechanistically, p300 act as transcriptional coactivator through the direct interaction with a diverse set of transcription factors and RNA polymerase II transcription machinery (Goodman et al. 2004). The intrinsic HAT

activity of p300 plays an important role in the transcriptional coactivation of several transcription factotrs and proteins which include CREB, c-Jun, c-Fos, c-Myb, p53, Stats, nuclear receptors, RelA GATA, p73 etc (Shikama et al. 1997; Ogryzko et al. 1996; Costanzo et al. 2002; Zhou et al. 2004).

A proper balance of acetylation and deacetylation is important for the normal cellular growth and differentiation. Therefore, dysfunction of p300 has been implicated in diseases, like inflammatory processes, Huntington disease, cardiac diseases, diabetes mellitus, AIDS and cancer (Swaminathan et al. 2007; Zhou et al. 2004; Varier et al. 2006). These observations lead to consider small molecule modulators (activators and inhibitors) of p300 as potential new generation therapeutics. These small molecule compounds would also be highly useful to probe the functional significance of the histone acetyltransferase activity *in vivo*.

The first synthetic HAT modulators to be designed were the peptide CoA conjugates. Of these, Lys-CoA was specific for p300 and H3-CoA was specific for PCAF. These compounds are now used as biological tools to study HAT function in vitro and in cellular studies (Lau et al., 2000, Zheng, Y., et al., 2004). A detailed analysis of the p300 selective inhibitor Lys-CoA showed that it exhibited slow, tight-binding kinetics. It was shown that p300/CBP preferentially acetylates longer peptide substrates and the importance of nearby positively charged residues in lysine targeting was also shown (Thompson, P.R., et al., 2001). Recently isothiazolone based modulators have also been designed that inhibit p300 and PCAF (Stimons et al., 2005). More recently, epigallocatechin-3-gallate (EGCG), a major polyphenol found in green tea, was found to be a non-specific HATi with global specificity for the majority of HAT enzymes but with no activity towards other epigenetic enzymes like HDAC, SIRT1, and HMTase (Choi K.C., et al., 2009). Anacardic acid was the natural small molecule modulators of HATs isolated from cashew nut shell liquid and was proved as a potent inhibitor of p300 and PCAF. Anacardic acid was found to ba a non-competitive type of p300 inhibitor (Balasubramanyam K, et al. 2003). Recent work on anacardic acid suggest its role in potentially preventing or treating cancer through modulation of NF-kappaB signaling pathway (Sung B., et al., 2008). Furthermore, CTPB (N-(4-chloro-3-trifluoromethylphenyl)-2-ethoxy-6-pentadecyl-benzamide), an amide derivative of

100

anacardic acid was reported to be the first known activator of HAT p300 (Balasubramanyam K, et al. 2003). Kinetically CTPB was able to activate the HAT activity of p300 by decreasing the K_m of the acetyl-CoA for the HAT p300 .It was speculated that the binding of the activator to the enzyme p300 altered the enzyme structure in such a way that its affinity towards acetyl-CoA increased which in turn led to the activation of the enzyme activity (Mantelingu K., et al., 2007). Further, it was found that CTPB was able to activate the transcription from the chromatin template in vitro while anacardic acid inhibited the transcription (Balasubramanyam K, et al. 2003). We have recently developed a glucose-derived carbon nanospheres which posses intrinsic fluorescence property. The cell permeability property of nanosphere was used to deliver the cell impermeable CTPB molecule to the HeLa cells and also in mice system. Biochemical analyses such as Western blotting, immunohistochemistry, and gene expression analysis confirmed the induction of the hyperacetylation of p300 (autoacetylation) as well as of histones upon CTPB delivery. These promising results established for the first time an alternative path for the activation of gene expression mediated by the induction of HAT activity instead of histone deacetylase (HDAC) inhibition (Selvi BR, et al., 2008).

Curcumin (diferuloylmethane), a major curcumanoid present in the spice turmeric was found to be a specific inhibitor of the p300/CREB-binding protein (CBP) HAT activity but not of p300/CBPassociated factor (PCAF) (Balasubramanyam K., et al. 2004). It specifically repressed the p300/CBP HAT activity-dependent transcriptional activation from chromatin but not from the DNA template. Curcumin was found to inhibit the acetylation of HIV-Tat protein in vitro by p300 as well as repressed the syncytia formation of the virus in SupT1 cells. It was also further shown that curcumin is a noncompetitive inhibitor of the HAT p300 (Balasubramanyam K., et al. 2004). The p300 HAT inhibition ability of curcumin was used to elucidate the role of p300 in the transcriptional preinitiation complex (PIC) assembly. It was demonatrated that autoacetylation and curcumin induce similar conformational changes in the catalytic domain of (Black, J. C., et al., 2006). .

Recently, a few successful attempts have been made to understand the mechanisms of p300 mediated acetylation of histones (Thompson et al. 2001; Thompson et al. 2004; Karanam et al. 2006), including the co-crystalization of p300 HAT domain and p300 specific, synthetic inhibitor Lys-CoA. It has been shown that p300 follows an unusual the hit-and-run (Theorell-Chance) mechanism of enzyme action (Liu et al. 2008). p300 gets extensively autoacetylated in an intermolecular fashion, which is highly cooperative in nature (Karanam et al. 2006). Autoacetylation of multiple lysines at the proteolytic sensitive loop was found to be important for the regulation of its catalytic activity (Thompson et al. 2004). Presumably, the distal protein contacts or a particular loop conformation may influence p300 autoacetylation (Karanam et al. 2007). Autoacetylation of p300 is closely linked to the p300 mediated transcriptional regulation (Thompson et al. 2004). The acetylation of p300 is essential to initiate the transcription. It was predicted that the autoacetylated p300 gains a favorable structural change to dissociate from the transcriptional pre-initiation complex (PIC), leading to initiation of activator dependent transcription (Black et al. 2006). By employing Surface Enhanced Raman Spectroscopy (SERS), we have shown that indeed the autoacetylation of p300 induces a significant structural alteration in the p300HAT domain (see chapter 4 and Arif et al. 2007).

Previously, our laboratory have shown that the polyisoprenylated benzophenone, garcinol (Figure 3.1, panel b), isolated from *Garcinia indica* (an edible fruit), is a potent nonspecific inhibitor of histone acetyltransferase p300 (Balasubramanyam et al. 2004). In order to find out more potent, specific and less toxic inhibitors several garcinol derivatives, based on isogarcinol (IG), a product of intramolecular cyclization of garcinol (Figure 3.1, panel b) was synthesized. IG was also found to be a nonspecific inhibitor of HATs (Mantelingu et al. 2007). Remarkably, a methoxy monosubstitution at C-14 position (Mantelingu et al. 2007) (Figure 3.1, panel b) converted the IG to a highly specific inhibitor (LTK14) of p300 HAT activity. IG and LTK14 are characterized by the presence of a lactone ring. Furthermore, LTK14 was shown to inhibit HIV multiplication in SupT1 cells by inhibiting histone acetylation and hence have the potential to be a lead molecule for therapeutics (Mantelingu et al. 2007). The significant alteration in the
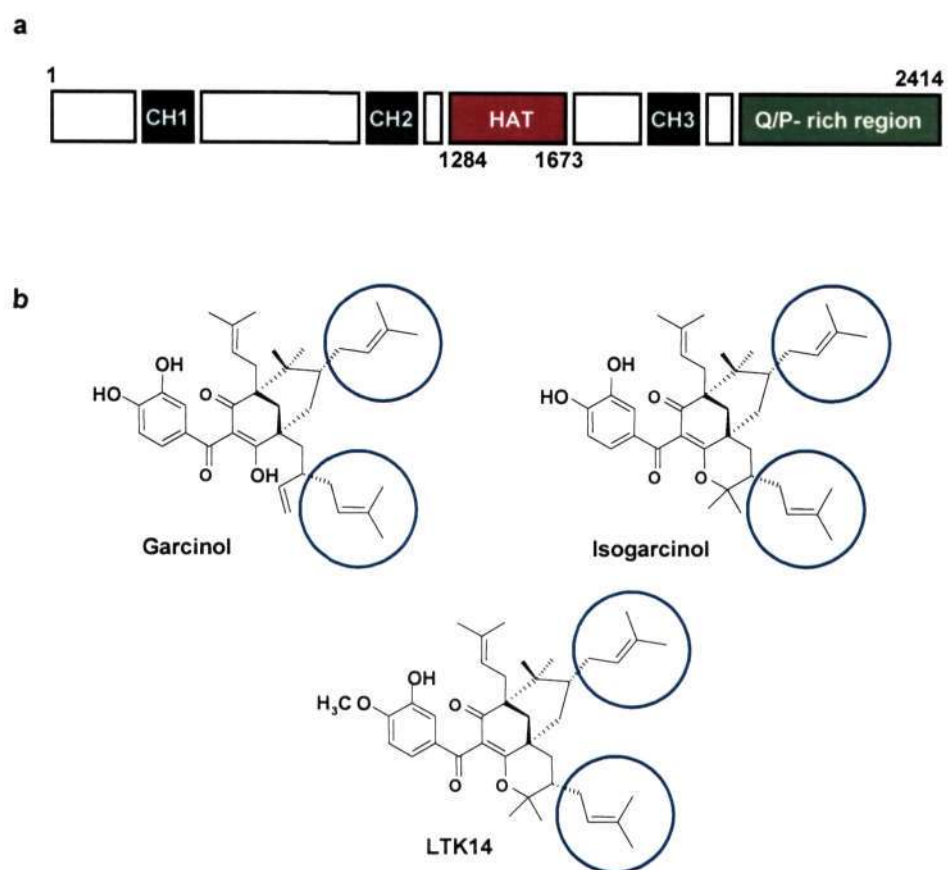
Figure 3.1: **a)** Schematic representation of p300 domain structure: The functional domains of p300 include CH1, CH2, CH3, HAT domain and Q/P-rich region. Note that p300 HAT domain used in this work encompasses amino acid residue 1284 – 1673 as shown. **b)** Chemical structures of Garcinol, IG and LTK14. The blue circled moieties represent the region of structural difference between garcinol and the other two inhibitors (IG and LTK14) in their three dimensional orientation.

specificity has lead us to investigate the molecular mechanisms responsible for the differential nature of HAT inhibition by these structurally close related inhibitors (Figure 3.1, panel b and Figure 3.2). Since, it is difficult to obtain highly purified full length p300 (p300fl) from eukaryotic expression system in a sufficient quantity for biocalorimetry and other biophysical studies, we have used p300 HAT domain (p300HD) (1284-1673aa) (Figure 3.1, panel a) in the present studies. Recombinant p300HD was
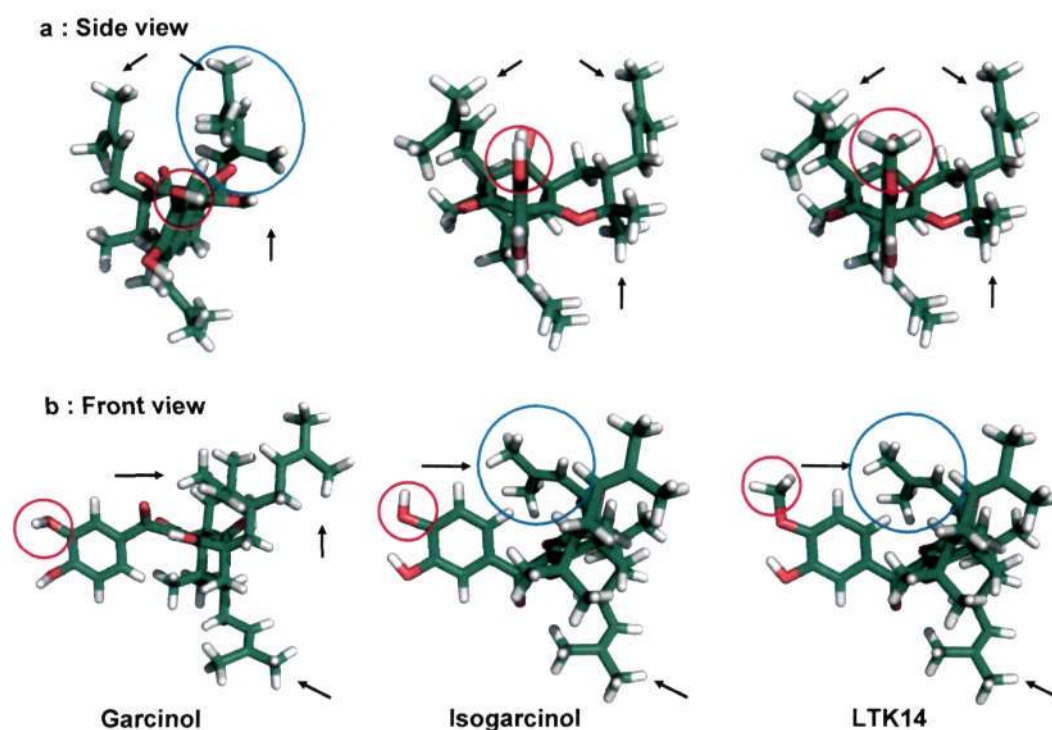
Figure 3.2. 3-D structure model of the p300 HAT inhibitors. Panel a and b, shows the side and the front view of the molecules respectively. Pink circle indicate the position of chemical substitution for each of the inhibitor molecule and the blue circles and black arrows indicate the position of major structural differences observed (see text also). Note the high similarity in 3-D structure of IG and LTK14 as compared to garcinol. Stick model of molecules were generated by PyMol (DeLano, W. L.; 2002).

over expressed upon co-transformation of human histone deacetylase SirT2 with p300HD construct and purified from *E.coli* (Figure 3.3, panel a). It is pertinent to point out here that mechanistic and substrate selectivity parameters for p300fl and that of p300HD were reported to be quite similar which justifies our choice of p300HD in the present studies (Thompson et al. 2001; Thompson et al. 2004). We believe that this is the first report which attempt to throw light on the molecular mechanism of differential nature of the inhibition of p300 HAT brought about by nonspecific (e.g. garcinol and IG) and specific inhibitor (e.g. LTK14) of natural origin.

104

3.3. Results and Discussion:

3.3.1. p300 HAT domain is the target of garcinol derivatives:
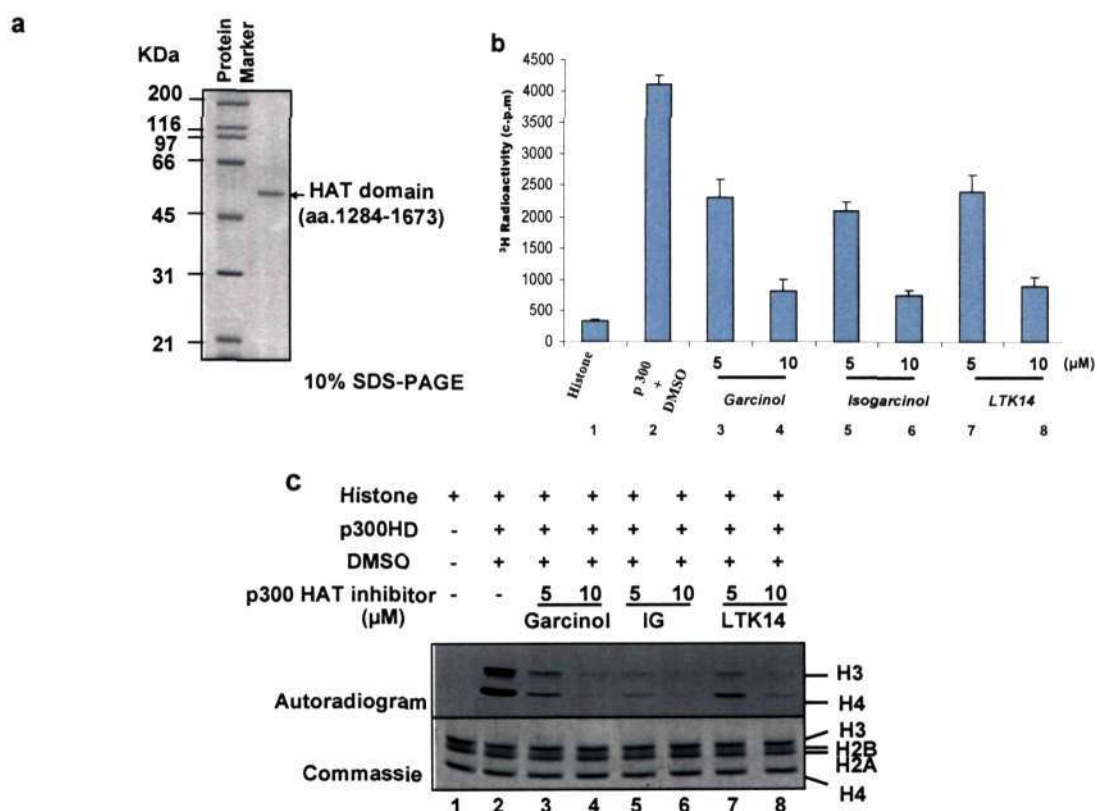
Figure 3.3: a) Purification profile of recombinant p300 HAT domain (p300HD) (aa. 1284 – 1673). **b)** Garcinol derivatives inhibit p300 HAT domain: HAT assays were performed by using highly purified HeLa core histones in the absence (lane1); and presence of solvent control DMSO (lane2); (lane 3 and 4, 5 and 6 , 7 and 8) histone with HAT in the presence of garcinol, IG and LTK14 at 5 and 10 μM concentrations respectively. Filter binding assays were performed. **c)** HAT assays were performed as described for (b) and reaction mixtures were resolved on 15% SDS-PAGE and processed for fluorography.

The dose dependent inhibition of the p300HD HAT activity by different inhibitors was investigated by gel fluorography/autoradiography assay. Figure 3.3, panel b represents the profile of HAT activity in the presence of the three inhibitors. Results show that all three ligands: garcinol, IG and LTK14 inhibit the HAT activity of p300HD in a concentration dependent manner (compare lanes 2 vs. 3 and 4, 5 and 6, 7 and 8 of

Figure 3.3, panel b and c). Similar degree of inhibition was also observed for p300fl (Balasubramanyam et al. 2004; Mantelingu et al. 2007). Taken together, these results suggest that the inhibition of p300fl is executed through the direct inhibition of p300HD HAT activity which could be the direct target of the p300 HAT inhibitors. These results justify the use of p300HD as the appropriate model to understand the molecular basis of the inhibition of the HAT activity of p300fl by these small molecules. Hence, we carried out biophysical and kinetic studies with p300HD to understand the mechanism of p300 inhibition.

3.3.2. *In vitro* characterization of p300 HAT inhibitors interaction to the p300HD:

The nature of binding of p300HD with the different HAT inhibitors were estimated from the ligand concentration dependent decrease in fluorescence emission (at 340 nm) of the protein. The resulting binding curves suggest non-cooperative mode of binding. Dissociation constants were found to be $1.8 \pm 0.27\mu M$, $1.1 \pm 0.03\mu M$ and $1.4 \pm 0.05\mu M$ for garcinol, IG and LTK14, respectively (Figure 3.4, panel a). The dissociation constant values are in the same range (micromolar) necessary for the inhibition of HAT activity. Furthermore, they fall in the same range for the IC_{50} values reported for these ligands with PCAF and p300 (Balasubramanyam et al. 2004; Mantelingu et al. 2007). Binding stoichiometry was also estimated from the intersection of the two straight lines of a least-squares fit plot of the normalized decrease in fluorescence against the ratio of input concentrations of respective ligand and the p300 HAT domain (Majee et al. 1997). The abscissa values corresponding to the intersection of the two straight lines for garcinol, IG and LTK14 are 1.6, 1.7 and 0.98, respectively (Figure 3.4, panel b).

Acrylamide quenching of tryptophan fluorescence of the protein was used to detect the ligand-induced alteration in the tertiary structure of the protein, if any. Tryptophan accessibility and Stern-Volmer constants of the free and ligand-bound protein (summarized in Table 3.1 and for plot see Figure 3.5) was estimated from modified Stern-Volmer plot (Lakowicz et al. 1999). Results suggest that the change in accessibility is significant upon addition of LTK14 (Table 3.1). The alteration in the accessibility value originates from the ligand-induced change in tertiary structure of the protein. It may
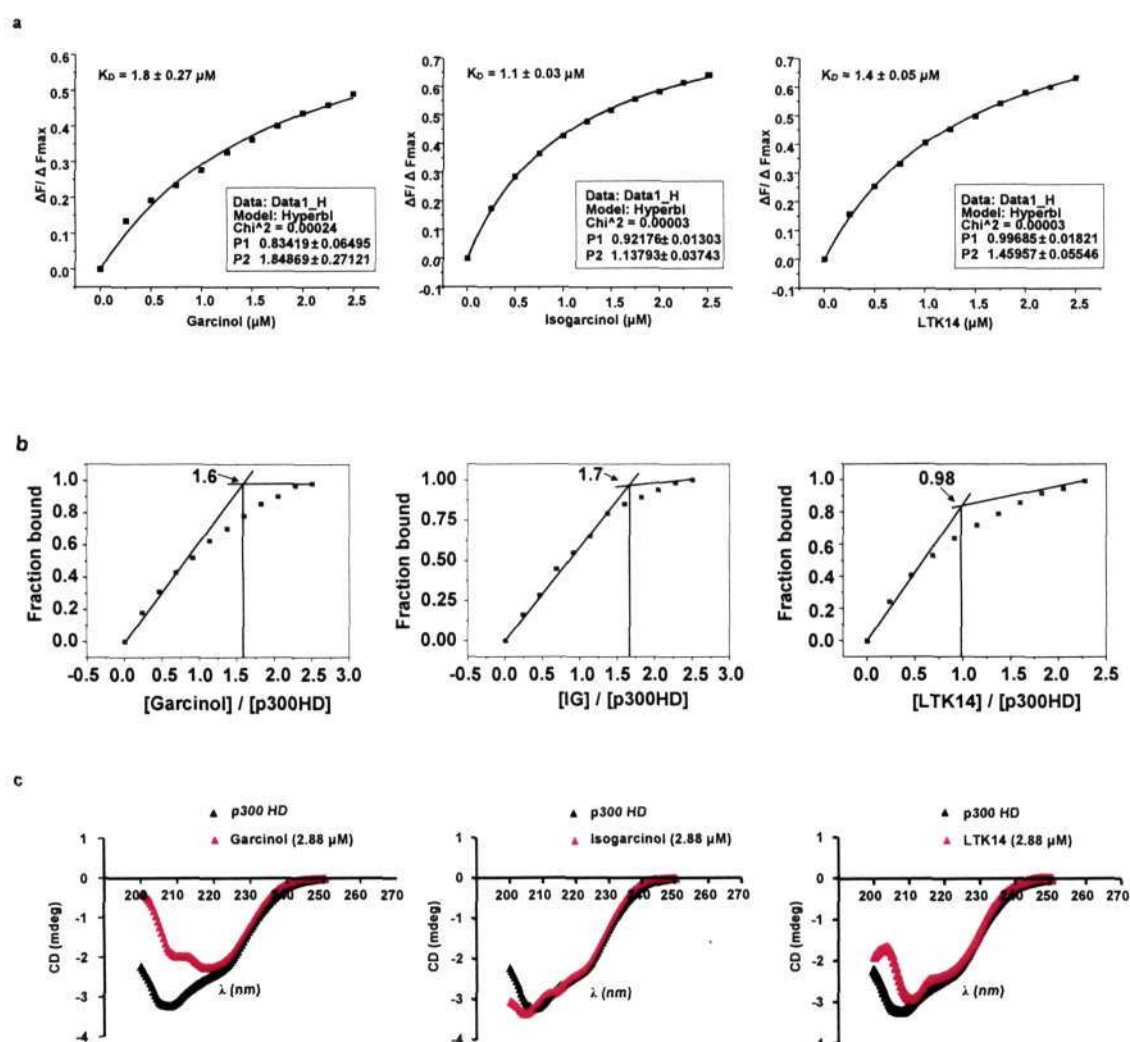
Figure 3.4: a) Curve fitting analysis to evaluate the dissociation constant for the association of the different HATi with p300 HAT domain (p300HD). 1) Garcinol. 2) IG and 3) LTK14. The concentration of the protein was 1.2 µM in all the three cases. K_d value obtained from Non-linear least square method are 1.8 µM, 1.1 µM and 1.4 µM for garcinol, IG and LTK14, respectively. **b)** Method to determine binding stoichiometry associated with the binding of ligands with p300 HAT domain. The abscissa values corresponding to the intersection of the two straight lines for garcinol, IG and LTK14 are 1.6, 1.7 and 0.98, respectively. **c)** Far-U.V C.D spectra of 2.88 µM of different HAT inhibitors and in the presence of 1.2 µM of p300HD in the buffer at 25°C. Panel 1, 2 and 3 corresponds to garcinol, IG and LTK14 respectively. The black spectra denotes for the p300HD alone in all the cases. The spectra recorded over the wavelength range shown.

be suggested that the association of the other two ligands does not lead to a major alteration in the tertiary structure of the protein. The extent of change, however, does not suggest any radical alteration of the tertiary structure for p300HD even in case of LTK14. On the other hand, we noticed a change in the secondary structure of p300HD upon interaction with garcinol and LTK14 from far UV CD (200-250nm). Results are shown in Figure 3.4, panel c. Shape of the CD spectrum of the protein suggests a preponderance of beta-sheet in the protein. Addition of garcinol and LTK14 changes the secondary structure which results in alteration of the shape in the CD spectra though not to a major extent. The change is not marked in case of IG. Earlier reports have shown that that the specific and nonspecific inhibitors of p300 bind to the amide groups of a helix and thereby differentially alter the enzyme structure. Present data are consistent with earlier reports from ligand-induced alteration of SERS for the p300fl (Mantelingu et al. 2007). It should be mentioned that CD spectra of p300HD in presence of the ligands were monitored under non-saturating concentrations of the ligands due to presence of DMSO solvent necessary for solubilizing the ligands. It also prevented us from monitoring the

Table 3.1 Modified Stern-Volmer plot for the acrylamide quenching of p300HD alone and after pre-incubated with different HAT inhibitors.

System	Ksv (M^{-1})	% Accessibility (1/f_a)
Control HAT (1.2μM)	21.9 ± 0.3	80 ± 1.2
HAT (1.2μM) + Garcinol (2.5μM)	15 ± 0.5	78 ± 1.1
HAT (1.2μM) + IG (2.5μM)	16.3 ± 0.7	75 ± 1
HAT (1.2μM) + LTK14 (2.5μM)	15.8 ± 0.9	67 ± 2
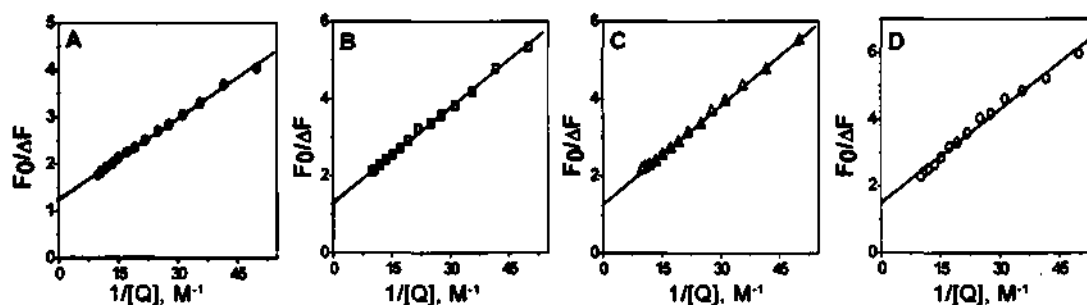
Figure 3.5. Modified Stern-Volmer plot for tryptophan quenching of p300 HAT domain in absence (panel A) and in presence of IG (panel B), garcinol (panel C) and LTK14 (panel D).

CD spectra of the protein beyond 200 nm. Therefore, we refrained from any quantitive estimation of the relative percentages of the secondary structure, because all available programs require CD data upto 190 nm.

3.3.3. Isothermal titration calorimetry (ITC) studies of the HAT inhibitors to p300HD:

In order to have insights regarding molecular nature of the interaction between the inhibitors and the protein, isothermal titration calorimetry was performed. Representative binding isotherms for all three are shown in Figure 3.6 and the results are summarized in Table 3.2. Dissociation constants agree to a reasonable degree with the value obtained from fluorescence method. In addition to the associated thermodynamic parameters, isothermal titration calorimetry indicated an important difference in the binding modes for garcinol, IG and LTK14. It is clear from Table 3.2 that only one molecule of LTK14
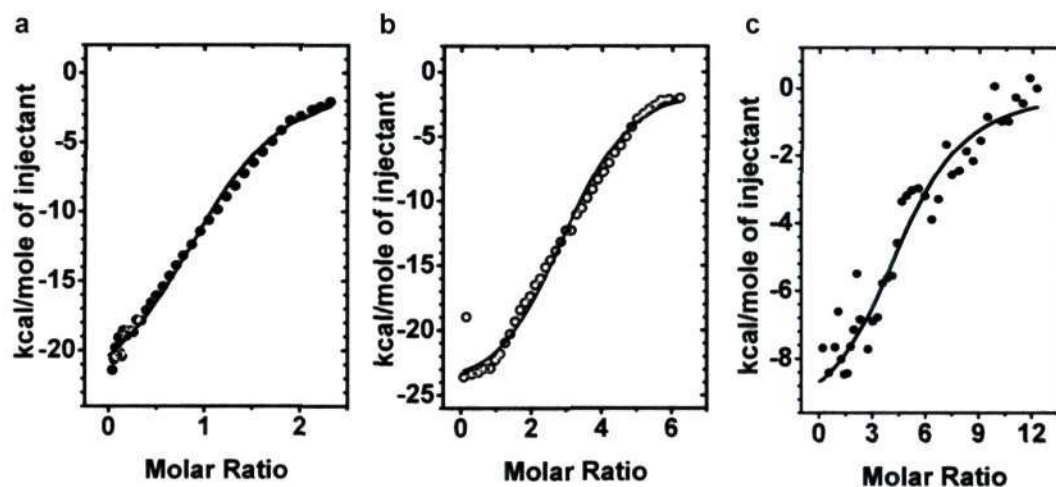
Figure 3.6: ITC titration of different HAT inhibitors with the p300HD. Figure 4 a, b and c shows the ITC titration of garcinol, IG and LTK14 with the p300HD at 20°C respectively. The data were fitted to a "one set of sites"-binding model to obtain the thermodynamic parameters Solid line represents the fit of the binding isotherm.

binds to the p300HD. In contrast, two molecules of garcinol and IG bind to the protein. These results are consistent with the stoichiometry obtained from fluorescence titration curve obtained from the progressive addition of the ligands to the protein (Figure 3.4, panel b). The affinity constant values could be grouped similarly in two classes. Garcinol and IG have relatively higher affinity than LTK14. All interactions are enthalpy driven. It implies that the complex formation takes place due to enthalpy driven non-covalent interactions like H-bonding and/or stacking interactions. This is partially compensated by negative entropy change. The unusually high negative value of ΔH in the range of 18-22 kcal/mol for garcinol and IG (Table 3.2) could be ascribed to the following parsing of enthalpy: $\Delta H_{total} = \Delta H_{site\ 1} + \Delta H_{site\ 2}$, the subscripts refer to the enthalpy change associated with the first and second binding site, respectively. Similar explanation could also account for the high negative entropy change. In the reported crystal structure of the complex of GCN5 and acetyl-CoA, multiple hydrogen bonds have been observed to stabilize the association (Clements et al. 1999). Large values of negative entropy changes might originate from ordering of water molecules at the protein-ligand binding interface.

Table 3.2 Thermodynamic parameters for the interaction of HAT inhibitors with p300HD

System	N	K_d (µM)	ΔG (kcal/mol)	ΔH (kcal/mol)	ΔS (e.u)
HAT + Garcinol	1.87 ± 0.06	6.6 ± 0.2	- 7.03 ± 0.15	- 21.1 ± 0.89	- 48.2 ± 1.25
HAT + IG	2.1 ± 0.09	5.9 ± 0.1	-7.8 ± 0.09	- 23 ± 0.95	- 57.9 ± 1.65
HAT + LTK14	1.08 ± 0.08	9.1 ± 0.2	- 6.3 ± 0.10	-18.2 ± 0.98	- 37.7 ± 1.23

As reported in the crystal structure of a ternary complex, HAT domain of Tetrahymena GCN5 (tGCN5) bound with its physiologically relevant ligands (Poux et al. 2002) coenzyme A (Co A) and a histone H3 peptide, water mediated hydrogen bonds is a potential source of localization of water molecule. Conformational change of the small ligands, another potential source of negative entropy could also be possible. In terms of the enthalpy and entropy change LTK14 exhibits a difference from garcinol and IG. The lower value of enthalpy change in this case could be ascribed to the absence of two binding sites. Relatively lower value of negative entropy change also characterizes the LTK14 and protein association.

3.3.4. Kinetic characterization of the mode of inhibition of p300 HAT inhibitors:

In order to further understand the nature of inhibition, kinetics analyses were done. We then compared the inhibition kinetics of p300HD HAT activity by the three ligands for both substrate; acetyl-CoA and core histone. Double reciprocal plots were constructed to find the nature of inhibition. Results are summarized in Figure 3.7. Inhibition kinetics studies clearly demonstrate the difference in the mechanism of inhibition caused by specific, LTK14 and non-specific (garcinol and IG) inhibitors. They show that the inhibition pattern for the garcinol and IG are similar. Both of them show competitive inhibition for the acetyl-CoA binding site on p300HD and non-competitive for the histone binding site (Figure 3.7, panel a and b respectively). In contrast, LTK14 was found to be the non-competitive inhibitor for both acetyl-CoA and histone binding sites (Figure 3.7, panel c), which is consistent with the earlier report with p300fl (Mantelingu et al. 2007). These difference in the nature of inhibition could be attributed to the chemical modifications in LTK14 (compare structures of Figure 3.1, panel b). It should be noted that the three dimensional (3-D) structure of IG and LTK14 are very similar (Figure 3.2). Further the inhibitor constant (Ki) values for all the three inhibitors were determined using the slope and the intercept replots obtained from the primary plots. Ki values for garcinol, IG and LTK14 are $4.9 \pm 0.2\mu M$, $3.9 \pm 0.2\mu M$ and $5.1 \pm 0.3\mu M$ respectively. The observed Ki values are in the similar range (micromolar) of K_d values determined from the ITC and the fluorescence titration results (Table 3.2 and Figure 3.4, panel a). These are also in the same range (micromolar) necessary for the inhibition of HAT activity.

3.3.5. Mechanism of inhibition of p300HD with garcinol derivatives:

Based on the data obtained from thermodynamic studies and inhibition kinetic studies we proposed a mechanism (Scheme 3.1) of inhibition by both specific and non-specific inhibitors. Isothermal calorimetric titration yields a binding stochiometry of two for both garcinol and IG per molecule of the enzyme. Out of these two, at least one molecule binds to acetyl-CoA binding site (Scheme 3.1, panel a.1): since these inhibitors exhibit competitive mode of inhibition in presence of excess of histones. The other binding site

Garcinol
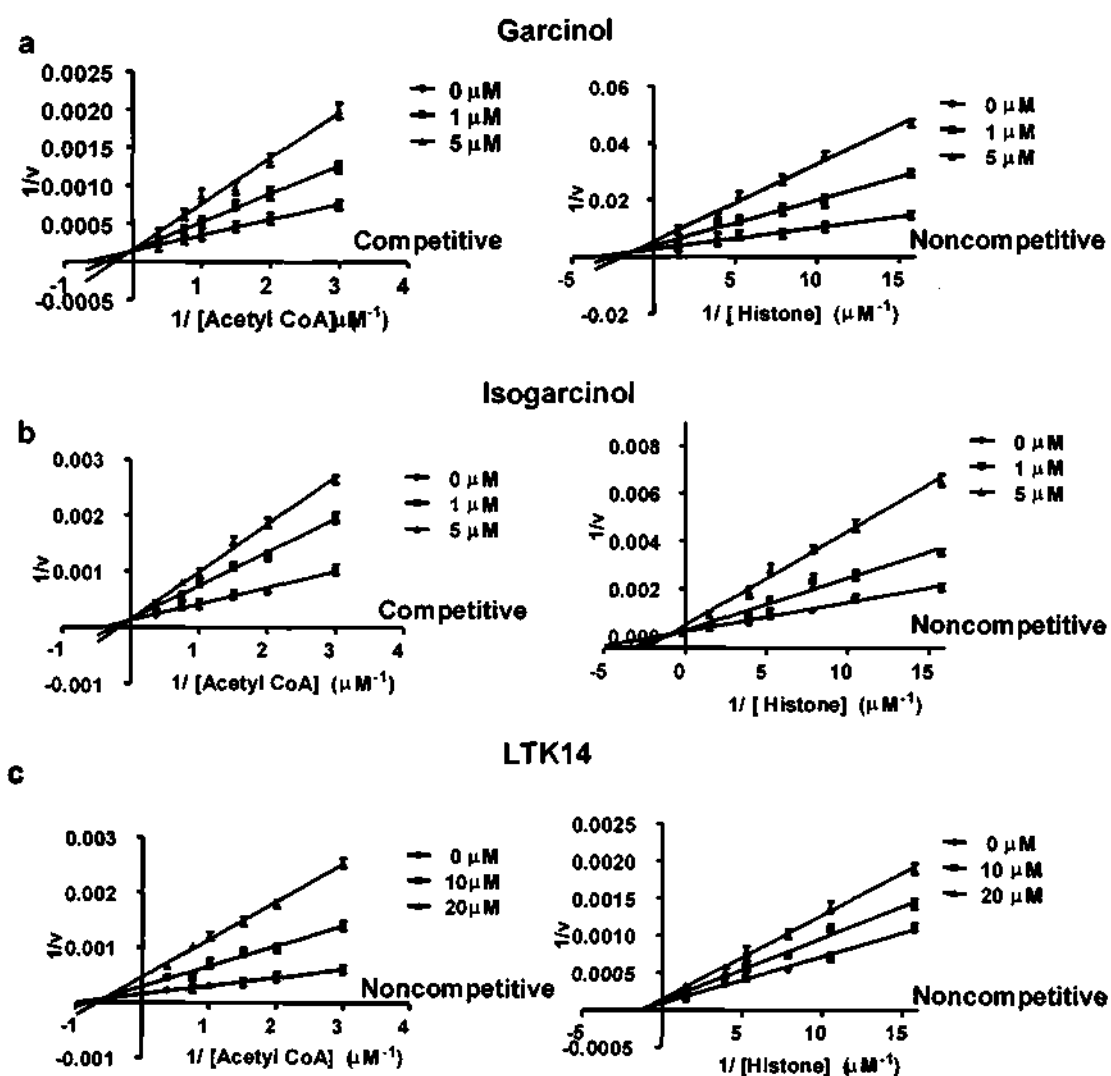
Isogarcinol

LTK14

Figure 3.7: Inhibition kinetics of garcinol, IG and LTK14 with p300HD. Lineweaver-Burk plot for garcinol, IG and LTK14 are shown in panel a, b and c respectively. Each experiment was performed three times and reproducibility was within 15%.

would be a site other than histone binding site (Scheme 3.1, panel a.2), because these inhibitors exhibit non-competitive mode of inhibition in the presence of excess acetyl-

CoA. However, the remote possibility of the second molecule binding to structurally altered p300HD under the influence of substrate(s) binding cannot be excluded. In contrast, LTK14, which shows 1:1 stochiometry of binding, neither binds to histone binding site nor to acetyl-CoA binding site (Scheme 3.1; panel b.1 and b.2) as the ligand exhibits non-competitive mode of inhibition towards both the substrates. It is apparent that conversion of phenolic hydroxyl group at C-14 to a methoxy group (a bulky group) in LTK14 has led to the reduction in its binding stochiometry for p300HD. In addition, the comparison of the inhibition kinetics pattern suggests that unlike garcinol and IG, LTK14 does not bind to acetyl-CoA binding site in the p300HD. It implies that -OH at the C-13 and C-14 position in garcinol and IG would have a role in binding to the acetyl-CoA binding site of the p300HD, since both of them compete for the acetyl-CoA binding site. Similarly, the bulky group at the C-14 position of LTK14 may be an unfavorable structural choice which could not be accommodated and hence cannot bind to the acetyl-CoA binding site because of probable steric hindrances. It should be noted that the 3-D

Scheme 3.1. Proposed mechanism of inhibition by Garcinol, IG and LTK14

a.1

E + G   EG

\+   In excess of Histone

A

[E(A)]

b.1

E + L   EL

\+   In excess of Histone

A

[E(A)] + L   [E(A)] L

a.2

[E(A)] + G   [E(A)] G

\+

H   In excess of Acetyl-CoA

[E(A)(H)] + G   [E(A)(H)] G

b.2

[E(A)] + L   [E(A)] L

\+

H   In excess of Acetyl-CoA

[E(A)(H)] + L   [E(A)(H)] L
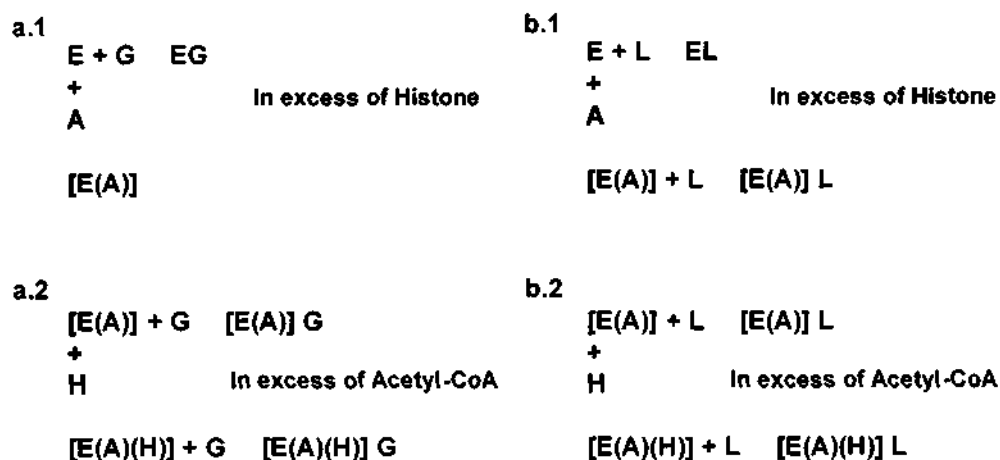
| E= p300 HAT |
| A= Acetyl-CoA |
| H= Histone |
| G= Garcinol or IG |
| L= LTK14 |

Table 3.3 Putative HATi interacting residues in p300HD

HATi	Acetyl-CoA Site	Second binding site
Garcinol	L1398, S1400, H1402, K1407, R1410, T1411, Y1414, D1454, K1456, I1457, P1458, R1462, L1463, W1466, K1469,Q1555, K1459	K1331, T1332, S1396, S1506, D1625, G1626, R1627
IG	D1399, H1402, R1410, T1411, P1439, P1440, Q1455, K1456, I1457, P1458, R1462	H1377, Q1379, S1396, Y1397, Y1446, I1447, E1505, G1506, D1625, G1626, R1627
LTK14	NA[a]	K1331, V1333, T1357, H1377, V1378, Q1379, S1396, Y1397, E1505, G1506, D1625, G1626, R1627, D1628, A1629

All amino acid residue shown are present at H-bonding distance from the respective HAT inhibitors at the respective docking site. In second column residues in red are known to interact via H-bonding or hydrophobic interaction with Lys-CoA. In third column residues in red have a role in making the putative substrate binding site. Residues underlined were mutated in the present study. Data were generated using PyMol (Becke et al. 1993; Lee et al. 1998).
[a]NA, not applicable

structure of IG and LTK14 are very similar (Figure 3.2). Therefore, it suggest that their exist a strict structural requirement for the interacting ligand (i.e. inhibitor in the given case) to the acetyl-CoA binding site. This is further supported by the fact that strict structural requirement exist at the ADP–ribose portion of Lys-CoA where adenosine ring exist in a well ordered form (Liu et al. 2008). This is supported by the fact that the entropy is relatively lower in case of garcinol and IG than LTK14 (Table 3.2) which is a reflection of the proposed strict structural requirement at the acetyl-CoA binding site (Liu et al. 2008). At the same time it should be noticed that there is a difference of -3 to -5 kcal/mole binding enthalpy between the two classes of ligands (Table 3.2). The value is equivalent to the enthalpy required for the formation of an H-bond. It is therefore, rational to propose that –OH group at C-13 and C-14 in garcinol and IG plays key role in binding to the acetyl-CoA binding site via H-bonding with the appropriate amino acid

side chain or peptide backbone of p300HD in the vicinity of acetyl-CoA binding site (Figure 3.9, and Table 3.3). Such interactions along with the structural complementarity to the acetyl-CoA binding site would further stabilize the above interactions and hence the observed p300HD inhibition. Other part(s) in the structure of the three inhibitors might be responsible for binding to another site (i.e. second binding site).

3.3.6. Characterization of the site of molecular interaction of p300HD with HAT inhibitors:

To further verify the characteristic binding of non-specific (garcinol and IG) versus specific (LTK14) inhibitors to the enzyme and the above proposed mechanism of the HAT inhibition, an isobologram analysis was performed (Milne et al. 2007) (Figure 3.8).
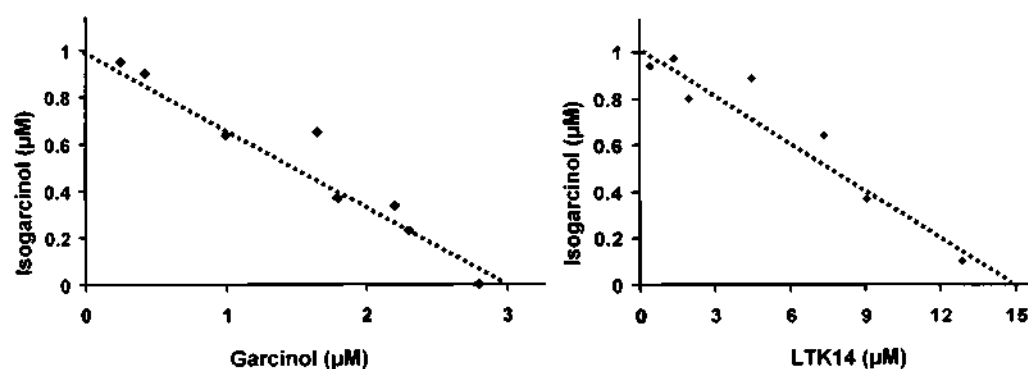

Figure 3.8: a) Isobologram analyses of IG versus garcinol and IG versus LTK14 are shown in the first and the last column. The experimental data are best fit to the theoretical line of additivity (dashed line).

A concentration matrix of two compounds, IG versus garcinol (Figure 3.8, left panel) and IG versus LTK14 (Figure 3.8, right panel), was examined to determine whether the

116

combination was antagonistic, additive or synergistic. IG was taken as a common inhibitor in both the matrix as the structure of IG, closely resembles both garcinol and LTK14. In both the cases the compound combination resulted in an additive effect, consistent with the hypothesis that both the molecules of garcinol and IG binds to the same site on p300HD and that a second binding site exists on the p300HD to which, probably one molecule of each garcinol, IG and LTK14, binds (Figure 3.8). The above observation correlates positively with the logic that structurally very similar molecules interact with the similar region on the protein or receptor.

Further, in the absence of the 3D X-ray crystal structure of IG, the following computational strategy was adopted to obtain the optimized geometry of IG based on LTK14 due to the structural similarity. The structure of LTK14 (depository number CCDC645420) as obtained from the crystallographic data (Mantelingu et al. 2007), was optimized to get rid of any unnatural structural constrains. Following this, -OCH3 was replaced by -OH to construct the initial geometry of IG. In Figure 3.2, middle row in both top and bottom parts, we present the optimized geometry of IG. All the above calculations were performed using Gaussian 03 suite of programs as mentioned in methods section (Frisch et al. 2004). It is noted that 3D geometries (i.e., the spatial arrangement of atoms) of both IG and LTK14 are very similar and they mainly differ at the above-mentioned side group; -OH is present in IG at the C-14 position, while -OCH3 in LTK14 is at the same position (Figure 3.2; see middle and the rightmost parts in both rows). Further, we performed molecular docking of all the three inhibitors onto the crystal structure of p300HD (Liu et al. 2008) using Hex 4.5 software (Mustard et al. 2005) (Figure 3.9). Significantly, an identical binding site was found for both garcinol and IG (Figure 3.9, top rows in the middle and the bottom column) which overlaps with acetyl-CoA binding site. In addition to this site, a second binding site also exists to which one molecule of each LTK14, garcinol, and IG could be docked (Figure 3.9, lower rows in the middle and the last column) (Table 3.3 for the putative HAT inhibitor interacting

Garcinol docked onto p300HD

IG docked onto p300HD

LTK14 docked onto p300HD

118
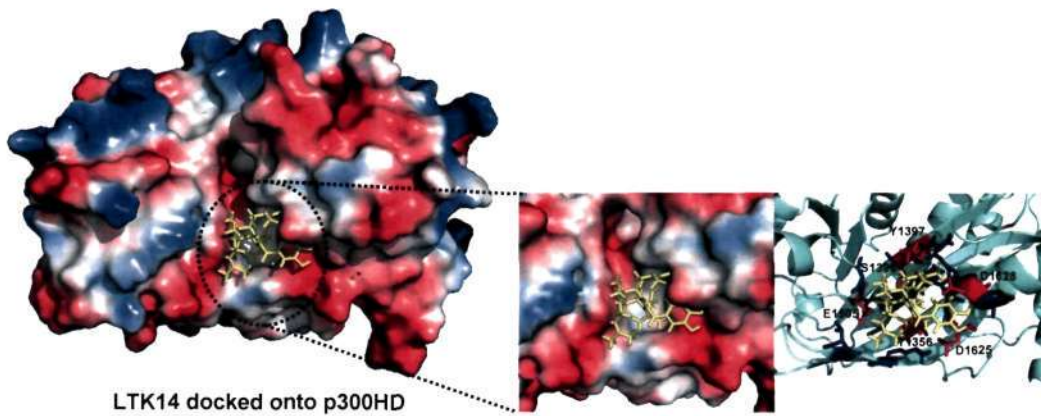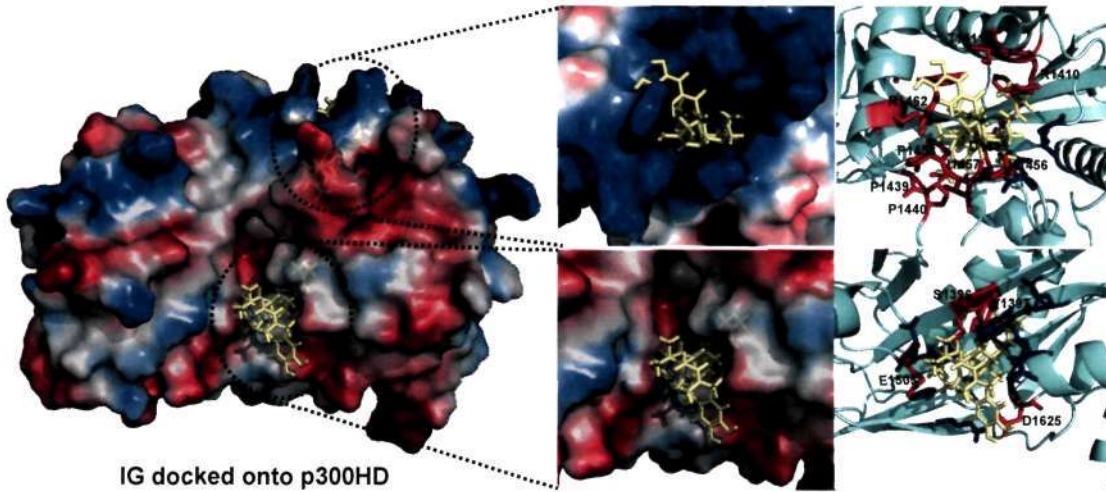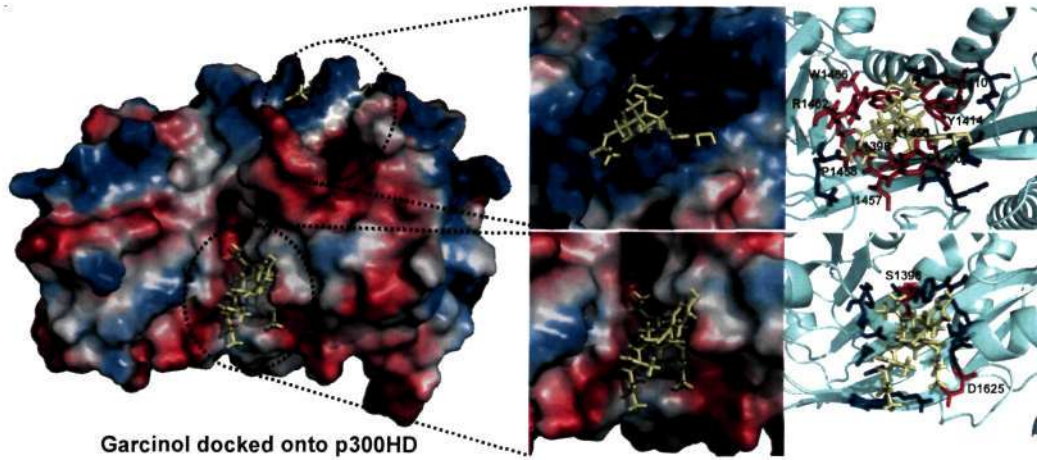
residues). These observations further support the above hypothesis and provide clues regarding the nature of the second binding site. It appears that the second binding site is present close to the proposed site of acetylation reaction (Liu et al. 2008) (Figure 3.9; see blown up images at the bottom and Table 3.3). It is noted that the docking studies have been done using the p300HD structure (Liu et al. 2008) lacking the autoinhibitory autoacetylation loop (Thompson et al. 2004; Karanam et al. 2007), which has been proposed to fold back in cis and block the protein substrate binding at this site (Liu et al. 2008). The kinetic studies suggest a noncompetitive mode of inhibition at the histone binding site for all three inhibitors. Since, the native protein has the autoinhibitory loop present that led us to speculate that the HAT inhibitors could be positively affecting the loop movement at this site which would further block the substrate binding and hence mediate its HAT inhibitory function.

To further support our hypothesis and to test our docking model, we selected four different amino-acids on the p3000HD; S1396, Y1397, G1626 and R1627 which we predicted to make contacts with the inhibitors (e.g. LTK14) at the propose second binding site (Figure 3.9, panel b, see blown up images at the bottom and Table 3.3). We performed single amino-acid mutagenesis on mentioned residues, S1396A, Y1397F, G1626A and R1627K. All the mutants were active and were further used for the inhibition assay using p300 specific inhibitor, LTK14. Interestingly, LTK14 failed to inhibit the HAT activity of all the four mutant p300HD even at 100µM concentration

Figure 3.9: The Crystal structure of p300HD (PDB-ID, 3BIY) is used to dock the HAT inhibitors using HEX 4.5 software. Top, middle and bottom rows represent p300HD-garcinol complex, p300HD-IG complex and p300HD- LTK14 complex respectively. The ligand is shown in yellow stick figure representation whereas the protein has been shown with surface electrostatic potential as generated by PyMol.[34] Respective blow-up images are shown in right hand side in both surface electrostatic potential and in cartoon form where top blow-up image is of acetyl-CoA active site and the bottom is for the second binding site. See Table 3.3 for the amino acid residue labeling.

(Figure 3.10). Taken together, these data support the existence of the second binding site close to the propose site of the acetylation reaction (Liu et al. 2008) where LTK14 binds specifically.
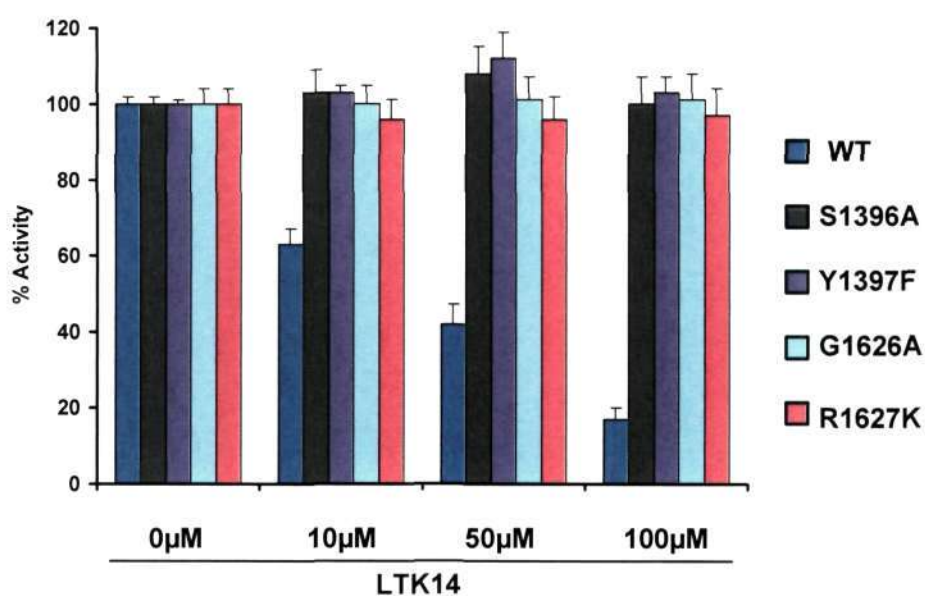
Figure 3.10: Mutagenesis study showing the percent inhibition of different putative LTK14 binding p300HD mutants. HAT inhibition assays were performed using 10, 50 and 100µM of LTK14.

3.3.7. Effect of garcinol and its derivative on PCAF stability:

The high degree of p300 selectivity of LTK14 is quit unexpected as all the three inhibitors are very closely related to their structure and posses the similar hydrogen donors and acceptors. In order to understand the basis for the activity and selectivity of these polyisoprenylated benzophenones to p300 with respect to PCAF, we performed filter binding assays with increasing concentration of HAT inhibitors (Figure 3.11, panel a). As reported earlier (Mantelingu et al. 2007), LTK14 do not inhibit the PCAF HAT

activity up to 80 µM concentration (compare DMSO treated vs. LTK14, of Figure 3.11, panel a), while garcinol could inhibit around 90% of the PCAF HAT activity at 40 µM (Figure 3.11, panel a, compare DMSO vs. garcinol treated). Interestingly, IG which also inhibits PCAF HAT activity can only inhibit up to 50% at the highest concentration tested (compare DMSO vs. IG treated, of Figure 3.11 panel a). These observations led us to suggest that molecular cyclization of garcinol to IG and LTK14 plays an important role in introducing the selectivity towards p300 by not allowing LTK14 to interact with PCAF efficiently and thereby inhibit the HAT activity.

Earlier work on PCAF has shown that it is an unstable enzyme that under commonly used assay conditions is rapidly and irreversibly inactivated (Herrera et al. 1997). Stabilization of PCAF requires its cofactor acetyl-CoA. We have shown that nonspecific inhibitor garcinol inhibits the PCAF HAT activity more potently than that of p300 (Balasubramanyam et al. 2004). This led us to hypothesize that garcinol could be mediating its PCAF HAT inhibitory activity by destabilizing the enzyme irreversibly. Examination of the time course of inactivation (Figure 3.11, panel b) revealed that two minute of pre-incubation of PCAF with garcinol(10 µM), in the absence of acetyl-CoA ,is sufficient to bring down the enzyme activity by 80%. In contrast, no significant loss of enzymatic activity was observed under similar condition in the presence of LTK14 as compared to the DMSO solvent control. As expected and suggested above, the molecular cyclization of the non-specific HAT inhibitor, IG can inactivate the PCAF HAT activity only up to 50% even after 15 minutes of preincubation. This observations are in agreement with the above made conclusion that molecular cyclization has a role to play in creating specificity towards p300. In order to strengthen our above made observations, we performed molecular docking of all three inhibitors onto the crystal structure of PCAF HAT domain (PDB id: 1CM0) (Clements et al. 1999). Surprisingly, LTK14 was unable to make any hydrogen bonding with the PCAF HAT domain where as the very similar molecule IG can make one hydrogen bond with the residue T587 whereas garcinol can make two hydrogen bonds with the D610 of the PCAF HAT domain. (Figure 3.12). Hence, these data suggest that indeed molecular cyclization restricts the ligands to

a

b
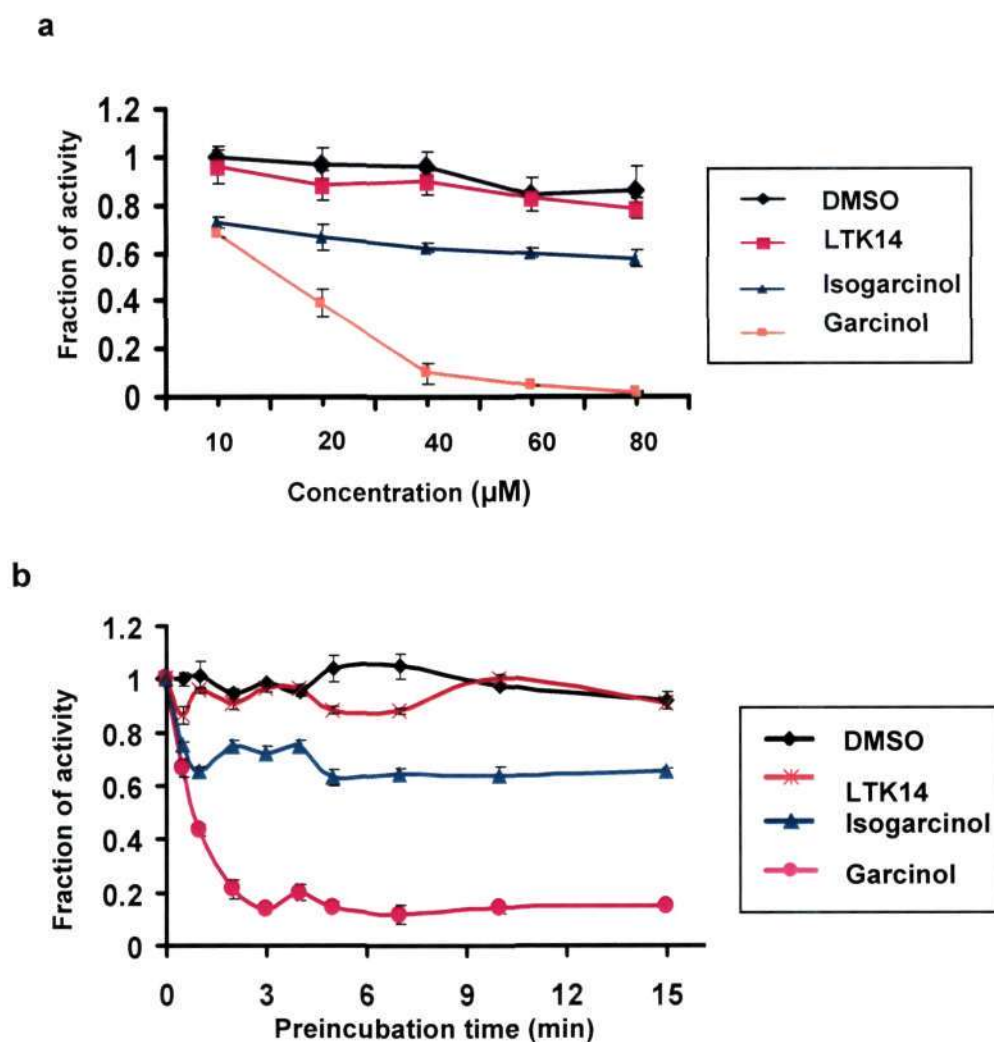
Figure 3.11: a) Concentration dependent inhibition of PCAF HAT activity by different HAT inhibitors. HAT assays were performed in triplicate by using highly purified HeLa core histones. **b)** Time course of the inactivation of PCAF in the presence of different HAT inhibitors at a constant concentration (10μM). HAT assays were performed in triplicate by using highly purified HeLa core histones. Data is plotted as the fractional activity in both the above assays.

interact properly with the PCAF and which results in poor PCAF inhibitory activity of the LTK14 and IG as shown above. At the same time it also makes garcinol a potent PCAF inhibitor.

Garcinol docked onto PCAF HAT domain

Isogarcinol docked onto PCAF HAT domain

LTK14 docked onto PCAF HAT domain
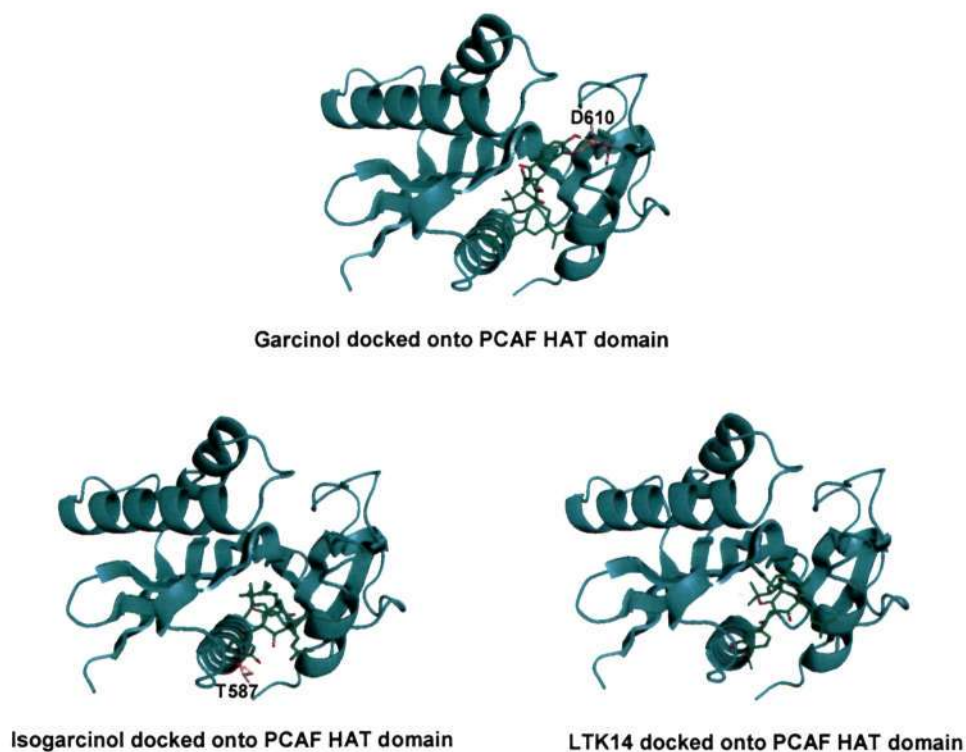
Figure 3.12. Crystal structure of PCAF HAT domain (PDB-id: 1CM0.) is used to dock the HAT inhibitors using AutoDock 4 software. Garcinol, IG and LTK14 docked onto PCAF HAT domain are shown from left to right respectively. The ligand is shown in green stick figure representation whereas the protein has been shown in cartoon form in aquamarine as generated by PyMol.[34] Hydrogen bonding between protein and ligand is shown in dashed orange line with the shown amino acid. Note that garcinol and IG make 2 and 1 hydrogen bonds with the PCAF HAT domain respectively. LTK14 do not make any hydrogen bond.

3.3.8. Summary:

Structure- activity relationships (SARs) obtained from our studies is summarized in Figure 3.13. Present study suggests that Garcinol and LTK14 induce alteration in the secondary structure of the protein. Such alteration in case of garcinol may be confined to the ordered segment of the protein. In contrast, LTK14 induces an alteration in the

tertiary structure. It also stands out in exhibiting non-competitive inhibition kinetics for both acetyl-CoA and histone substrates. The binding stochiometry of one LTK14 per complex with p300HD further implies that there is a high affinity enthalpy driven binding site in the p300HD for LTK14. Binding to this site culminates in the non-competitive inhibition for both acetyl-CoA and histone. Our data suggest that these binding site overlaps with the second binding site for garcinol and IG in the protein which was also confirmed using p300HD mutants that totally abrogate the LTK14 interaction with the p300HD. However, present data also emphasize the role of C-13 and C-14 –OH group in garcinol and IG in their recognition of the acetyl-CoA binding site. The three dimensional structure of the three ligands show that garcinol differ from the other two in the orientation of the blue circled moieties (Figure 3.1, panel b and Figure 3.2). It further corroborates the proposition that the aromatic ring in garcinol and IG is required for the specific recognition of the acetyl-CoA binding site. On the other hand, the circled non-aromatic moieties are responsible for the non-competitive inhibition for the histone substrate. Remarkably, p300HD cannot accommodate the bulky group of LTK14 at the acetyl-CoA binding site which showed the low structural tolerance at the acetyl-CoA binding site which is in contrast to the observed broad sequence selectivity (Liu et al. 2008) i.e. higher structural tolerance at the other active site (protein binding site) for protein substrate. Hence, binding of HAT inhibitors (especially LTK14) to the proposed highly electronegative site may be a useful tool to further elucidate the role of acetylation reaction in the context of the p300 autoinhibitory loop movement. Our data further suggest that cyclization of garcinol leading to the formation of lactone ring present in IG and LTK14 does not play a role in the recognition of p300HD .On the other hand; it has a role in imparting specificity towards p300 by not allowing HAT inhibitors to interact with PCAF. It might reduce the *in vivo* oxidation, thereby, reducing the possibility of toxic quinone type metabolic intermediate (Sarli et al. 2007). Thus, IG and LTK14 have better therapeutic potential.

**Alkylation Reduces toxicity
Increases steric hindrance**

Role in binding to allosteric site

**Binds to active site
(Acetyl CoA site)**

**Increases specificity
Reduces interaction with PCAF**
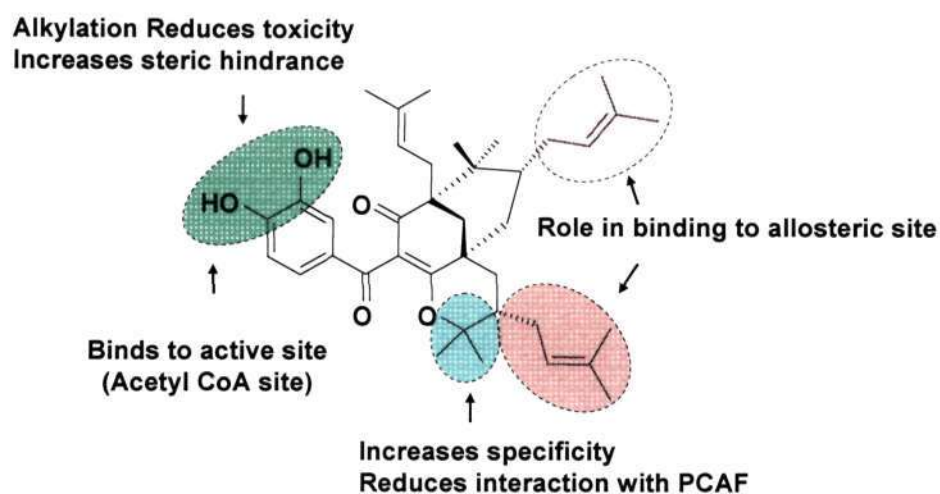
Figure 3.13: Summary of SAR for p300 HAT inhibitors. Arrows indicates the position and nature of each substitution tested in biochemical and biophysical studies.

The combination of biochemical, biophysical and *in vitro* binding assays elucidates the mechanisms of p300 HAT inhibition and also demonstrates that the molecular scaffold of LTK14 is a potentially promising scaffold for further elaboration to obtain potent and specific p300 inhibitors. It may serve as a useful mechanistic probe to understand the role of the master regulator p300. Further these data could also be useful to design p300 (HAT) targeted therapeutics for AIDS, cancer, cardiac hypertrophy and diabetes.

.

Chapter **4** *This chapter presents the results and discussion of understanding of p300 structural dynamics in the context of autoacetylation of the enzyme*

4.1. Rational of the study:

p300 is very large multidomain protein with several unique structural features, ranging from the KIX domain, cysteine/histidine-rich zinc finger domain to C-terminal glutamine rich region. It is one of the very important HAT in the cell and has been implicated in many diseases. The autoacetylation of p300 is one of the key regulators of its catalytic activity which is mediated by its HAT domain. This study is the first attempt to obtain direct information into the structure of full length p300 and its HAT domain in solution. Difficulty in obtaining large amount of p300 full length and it's HAT domain is an important factor hindering its structural studies. Although autoacetylation mediated structural alteration of p300 HAT domain has been realized as one of the key mechanisms of action, the direct evidence for the conformational changes was not shown. Here, we report about the SERS experiments carried out on p300 and it's HAT domain (both, partially and fully autoacetylated) which shed light on autoacetylation mediated structural dynamics of p300. In the SERS spectra, it was possible to identify modes related to various functional groups of the protein, which would provide a key to understand protein-drug interactions. We have also utilized SERS as an effective probe to determine the subtle structural change in p300 HAT domain.

4.2. Introduction:

4.2.1. Raman spectroscopy to understand HAT and small molecule modulator intractions:

4.2.1.1. Raman Scattering:

When photons are incident on molecules, there are various energy pathways for the molecules to be excited. Due to this excitation, the electrons in the molecules make transition from their ground state to an excited state. This excited state has a finite life time, and hence the molecules relax back to their ground state by emitting photons. These emitted photons can be a resultant of either elastic or an inelastic interaction between the photons and molecular vibrations. The former is generally categorized as Rayleigh scattering, and the latter may be due to various interactions between photons and vibrational states of a molecule, where exchange of energy between them is prevalent. One such interaction which is essentially due to an inelastic scattering mechanism is known as Raman scattering. In Raman scattering, the photons can either gain or loss energy upon interaction with vibrational energy states of a molecule. The Raman scattered radiation is classified either as Stroke or anti-stroke radiation depending on whether the photon has lost or gained energy, respectively. In 1928, Sir C.V. Raman and K.S. Krishnan experimentally discovered the ''Raman Effect'' (Raman and Krishnan, 1928). Sir C.V. Raman won the Nobel Prize in 1930 for this discovery.

4.2.2. Surface Enhanced Raman Scattering (SERS):

Upon adsorption of molecules on metallic nano-surfaces having atomic scale roughness, the Raman signal intensity of the molecule is enhanced by many orders of magnitude. This phenomenon is called as Surface Enhanced Raman Scattering (SERS). (Moskovits

128

1985; Campion et al. 1998). It was first observed in 1974 (Fleischmann et al. 1974) and latter, correctly interpreted in 1977(Albrecht et al. 1977; Jeanmaire et al. 1977). Earlier to the discovery of SERS, laser Raman scattering was not an ideal candidate to study vibrational spectroscopy of molecules at low concentrations because the Raman cross section was too small when compared to other optical processes of a molecule. In a situation where florescent molecule is under Raman scattering study, there is always possibility that the Raman signal being masked due to the fluorescent background. This is because the non-resonant Raman cross section of a molecule is around 10^{-26} cm^2, whereas the fluorescence cross section of a molecule is around 10^{-17} cm^2 per molecule (Kneipp et al. 1997). All these reasons had hampered the usage of Raman scattering for ultra trace analysis of molecules. SERS has the ability to circumvent this problem because the Raman cross section is no more the same as that for the conventional Raman scattering, but would be drastically changed to values comparable to fluorescence (Nie et al. 1997). Since its discovery, this enhanced Raman cross section in SERS has been utilized as a tool for ultra trace analysis of molecules (Graham et al. 2000; Moore et al. 2004; Podstawka et al. 2004; Stewart et al. 1999; Podstawka et al. 2004; Fabriciova et al. 2004; Ermishov et al. 2000; Streltsov et al. 2003).

It is important to unveil the reason behind this increased cross section in SERS, as it has a significant bearing on understanding of metal-molecule interaction (Otto et al. 1992). As the Raman intensities scale as the product of the incident field intensity and polarizability derivative, there are two commonly considered mechanisms for SERS, one of which involves enhancements in the field intensity as a result of Plasmon resonance excitation and other is the enhancement in polarizability due to chemical effects such as charge-transfer excited states and formation of resonant intermediates (Campion et al, 1998). These two important enhancement mechanisms underlying the SERS phenomenon are known as Electromagnetic and Chemical enhancement.

In Electromagnetic enhancement, the surface plasmons (are collective oscillations of free electrons on the surface of a metal) present on the surface of a metal results in a strong electric field due to the plasmon resonance (Moskovits et al. 1985; Otto et al. 1992; Aroca et al. 2006). Any molecule residing in the vicinity of a metallic surface is under the influence of this strong electric field and hence has strong

Raman signal (Moskovits et al. 1985; Otto et al. 1992; Baker et al. 2005). Therefore metals like Ag, Au and Cu exhibit SERS properties. The electromagnetic enhancement is a distance dependent mechanism. Interestingly, it is not necessary for the molecule to be in contact with the metal surface to exhibit enhancement. Whereas in chemical enhancement molecule and metal surface need to be in contact with each other (Campion et al, 1998). This mechanism is mainly attributed to electronic coupling between molecule and metal which leads to formation of an adsorbate-surface complex, resulting in an increased Raman cross section of the adsorbed molecule in the complex compared with the cross section of a free molecule in a normal Raman experiment.

4.2.3. Nanoparticles for SERS studies:

Two of the main prerequisites to observe considerable enhancement in Raman signal are intense surface Plasmon resonance and atomic scale roughness of the metallic surface used (Moskovits et al. 1985; Campion et al, 1998; Otto et al. 1992). Metallic nanoparticles are ideal candidates possessing the above properties. Since the surface to volume ratio of a nanoparticle is high, most of their atoms reside on the surface. This feature not only facilitates Plasmon oscillation on the surface, but also provides the required surface roughness. The most commonly used nanoparticles for SERS applications are gold and silver. Silver and gold are coinage metals with intense surface Plasmon resonance in visible wavelength, and their preparation is simple. The most popular one is the citrate reduced method (Lee et al. 1982), where citrate ions act as the capping agent and provide stability. For the present study we have used this method because of its stability and performance. This method leads to nanoparticles with an average diameter of 50μm. The maximum SERS enhancement factor is of the order of 10^6 to 10^7. Although silver nanoparticles facilitate high SERS enhancements, they have not been extensively used for biomolecular detection, especially for in vivo experiments due to their bio-incompatibility. In such a case, gold nanoparticles have been used because of the inertness. Recently, we have done a thorough investigation on the Ag core-Au shell (core-shell) nanoparticles as a possible SERS candidate for biological

130

systems has been done (Kumar et al. 2007). This is because with Ag nanoparticles, one can obtain a very large enhancement in Raman intensities, but it is not preferred for in vivo studies in biological systems because of toxicity. In contrast, Au nanoparticles are used for in vivo studies of biological systems, but they provide moderate enhancement in SERS experiments. The hot spots (which are nanopinholes formed because of the incomplete filling of Au shells over Ag nanoparticles) facilitate enhanced optical fields, which in turn contribute to the electromagnetic enhancement when a molecule is in the vicinity of these spots.

4.2.4. SERS as a Biomolecular-detection tool:

SERS has been used as an effective tool for bimolecular detection and characterization. In recent years, people have developed new techniques which utilizes SERS as probe to study interactions of biomolecules (Ermishov et al. 2000; Streltsov et al. 2003). SERS detection of antigen-antibody interactions with multiplexing abilities has also been demonstrated (Dou et al.1997). By employing Raman markers (molecules with a large Raman cross-section) for the first time they have shown important applications in immunoassays and diagnostics. Based on this work, various research groups have come up with strategies to detect relevant molecules related to diseases like HIV and Cancer. SERS has also been used as glucose sensor inside mice at physiological conditions (Stuart et al. 2006; Shafer-Peltier et al. 2003). Some researchers have also used SERS to detect molecules on the surface of bacteria and other organisms (Kahraman et al. 2007; Jarvis et al. 2006; Premasiri et al 2005). Apart from this, SERS has been used for in vivo studies, wherein gold nanoparticles are introduced into the cell, which further help in enhancing the Raman signatures of different cellular components (Huang et al 2007; Kneipp et al. 2002). The single molecule detection sensitivity of SERS is similar to the chemical imaging capabilities have added new dimensions to biodetection and sensing (Kneipp et al. 2002). In recent years, these extraordinary abilities of SERS has been utilized for ultra-trace analysis of molecules of biological interest. It should be noted that

physiological concentrations of biomolecules are scare and hence a very sensitive tool like SERS is of primary importance.

4.2.4.a SERS to understand p300 and small molecule interaction:
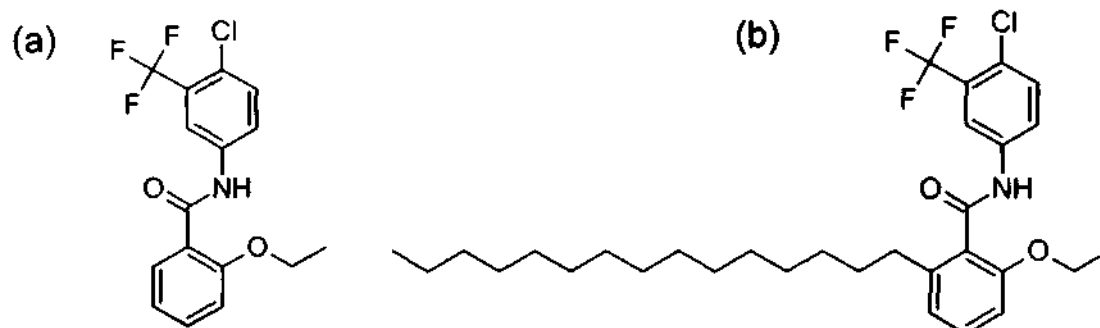
Figure 4.1: Schematic representation of the molecular structure of (a) CTB and (b) CTPB.

Earlier we have performed Raman and surface enhanced Raman spectroscopy on CTPB and its pentadecane hydrocarbon tail deleted derivative, CTB. Both the small molecule compounds are specific activator of p300 histone acetyltransferase activities. A complete Raman and SERS band assignments have been performed for both the molecules (Kumar et al. unpublished). Further, to understand the interaction between the small molecule activators and the p300, SERS experiments were performed (Kumar et al. 2006). In the case of CTPB (Figure 4.1), the SERS spectrum of p300 does not show large-scale changes (Figure 4.2b). The appearance or increase in intensity of the Raman modes 1654, 1335, and 960 cm^{-1} suggests that the binding of CTPB is predominant to the amide groups of the α-helix and β-sheets. In the case of CTB (Figure 4.1), comparatively larger change in the SERS spectra of p300 was observed (Figure 4.2c). CTB also binds to the amide groups of the α-helix and β-sheets like CTPB. Note that CTB induces greater change to SERS spectra of p300 than CTPB.

132
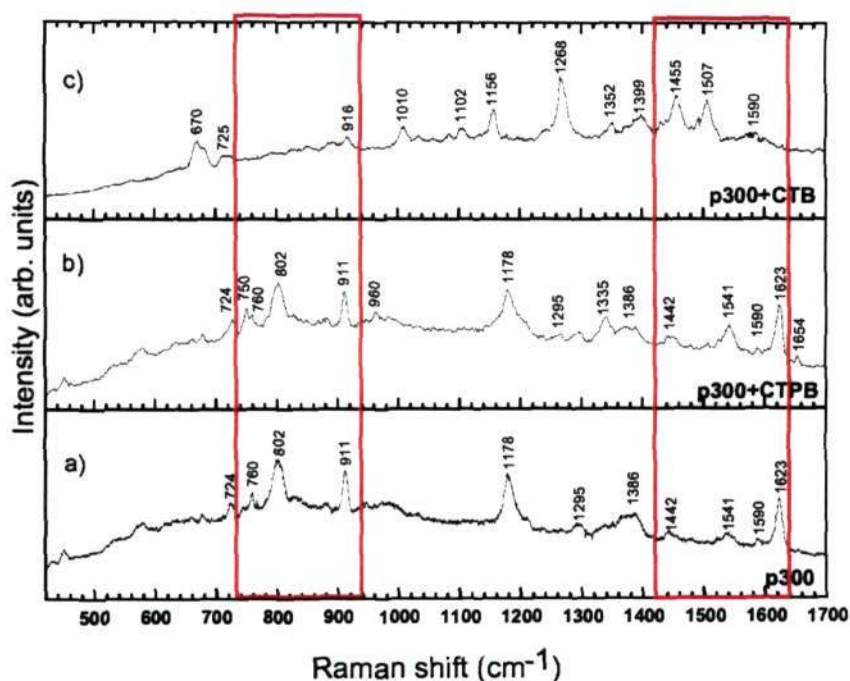
Figure 4.2: SERS spectra of (a) p300; (b) p300 bound to CTPB; (c) p300 bound to CTB. Red boxes shows the region of major change in spectra.

In a similar study (Mantelingu et al.2007), SERS was successfully used to understand the differential nature of activation of derivatives of CTB molecule which were similar to each other in structure, except for the positions of a Cl atom, and a CF3 group (Figure 4.3, left panel). It was found that CTB1 activates p300 to maximum followed by CTB3. Whereas, CTB2 showed no significant activation (Figure 4.3, right panel). In order to reveal the interaction of these derivatives with p300, SERS studies were performed which can also be used to correlate them to small structural changes in p300 (Mantelingu et al. 2007). It was observed that the SERS spectra of p300 bound to CTB1 shows a significant change in the intensity and band position when compared to SERS spectra of p300 alone. The SERS spectra of p300 interacting with CTB3 (which shows the least or no HAT activation) is

(a)   **(b)**

CTB1

N-[4-chloro-2-(trifluoromethyl)phenyl]-2-ethoxybenzamide

CTB2

N-[5-chloro-2-(trifluoromethyl)phenyl]-2-ethoxybenzamide

CTB3

N-[2-chloro-4-(trifluoromethyl)phenyl]-2-ethoxybenzamide
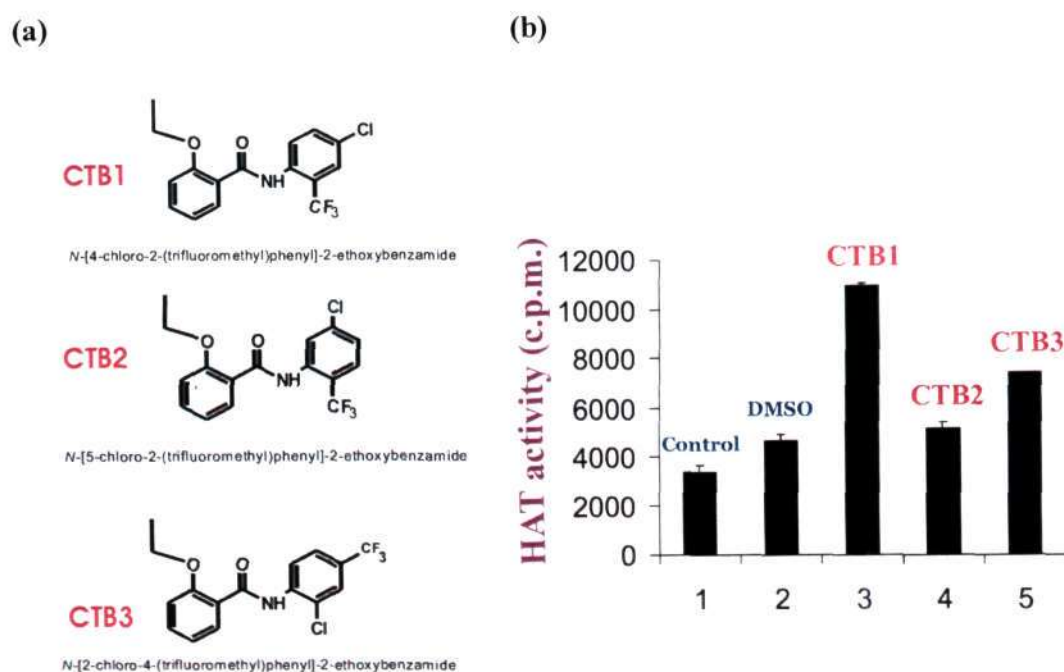
Figure 4.3: Molecular formulae of CTB derivatives (a) and their respective affect on HAT activity of p300 (b) (Mantelingu et al. 2007).

very similar to SERS spectrum of molecule-free p300 (Figure 4.4). Both CTB1 and CTB2 have electronegative groups, namely, Cl and CF_3 groups at the para position of the phenyl group of the CTB. Therefore, we infer that the presence of the CF_3 group at the meta position also plays an important role in the activation. It also implies that substitution at the meta and para positions in the phenyl group of CTB with strong electronegative group, such as F, may lead to stronger activation of p300 HAT activity. The SERS spectra also showed an increase in the random coils at the expense of α-helix (compare intensities of 1623, 1295, and 1654 cm^{-1}) as well as large changes to ring-structured amino acids like Trp, Tyr, His, and Phe in the structure of the p300 upon addition of these compounds(compare Figure 4.4 a, b, and d). These results led to believe that, in general, the activators of p300 mainly induce changes to the α-helix and the ring-structured amino acids of the protein p300.

134
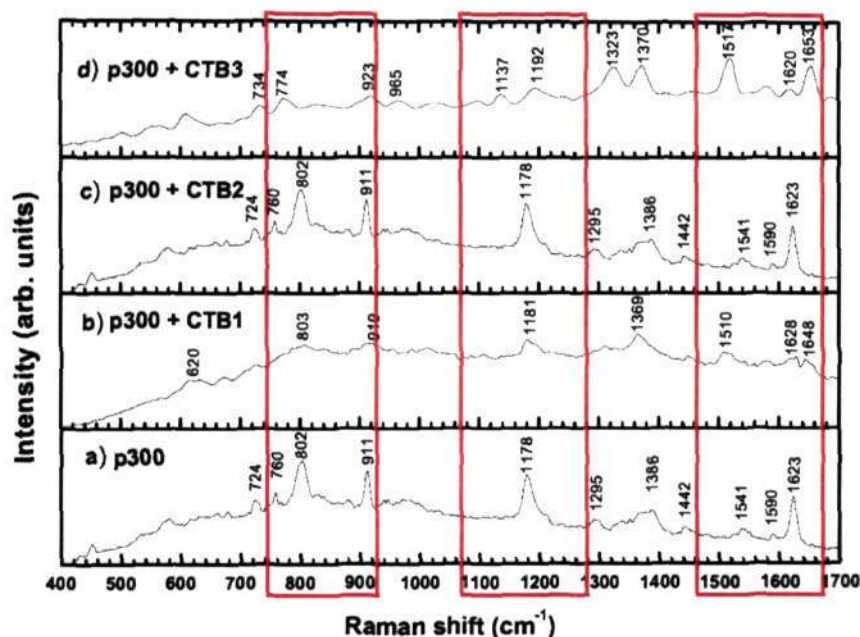
Figure 4.4: SERS spectrum of molecule-free p300 compared with SERS spectrum of p300+CTB1, p300+CTB1 and p300+CTB3 (Mantelingu et al. 2007). Red boxes shows the region of major change.

The above examples clearly show the importance of SERS in understanding the small molecule (activator in this case) interaction with the enzyme (e.g. p300). It would be otherwise be very difficult to study such an interaction in detail specially due to lack of structural information (e.g. X-ray crystal structure) of the full length p300. All the above experiments were carried out in a shorter time and with very minimum amount of protein sample (~ 0.5 µg / assay) as compared to other available biomolecular detection techniques. Similar studies were also done with different histone histone acetyltransferase inhibitors and p300 (Mantelingu et al. 2007). It was found that the specific (LTK13,14 and 19) and nonspecific inhibitors (garcinol, isogarcinol) of p300 bind to the amide groups of α helix and thereby differentially alter the enzyme structure. Whereas, the inactive inhibitor (LTK15 lost the ability to interact with the enzymes

In this chapter we have used SERS as an effective tool to probe different aspects of histone acetyltransferase p300 and it's catalytic active domain i.e. p300 HAT domain. It should be noted that the structure of p300 full length in still not solved by X-ray crystallography or by any other method and that of HAT domain has very recently been solved in 2008(Liu et al. 2008). The SERS experiments carried out on

p300 and it's HAT domain (and its autoacetylated form) show the complete vibration spectral analysis, which throws light into the protein structure. In the SERS spectra, it is possible to identify modes related to various functional groups of the protein, which would provide a key to understanding the protein drug interactions. In addition to this, we have also studied the effect of chloride ion on the SERS of p300 protein. Chloride ion provides a better aggregation of silver nanoparticles around the molecule resulting in large enhancement in Raman signals. To make a comparative study of the effect of silver nanoparticles on aqueous and dry samples of p300, we have performed SERS on p300 dried on a glass substrate in the presence of silver nanoparticles. The last part of this chapter would constitute the SERS studies on p300 HAT domain and the fully autoacetylated HAT domain. We show that SERS can also used to probe specific structural changes in protein upon modifications like autoacetylation.

4.3. Results and Discussion:

4.3.1. Effect of silver nanoparticle on p300 HAT activity:

Although p300 is one of the most important multifunctional proteins in humans, very little is known about the structural dynamics of it. However, the structural and functional domain organization of p300 indicates that the protein presumably undergoes vibrational reorganization at the amino acid level to achieve diverse functional ability.

136
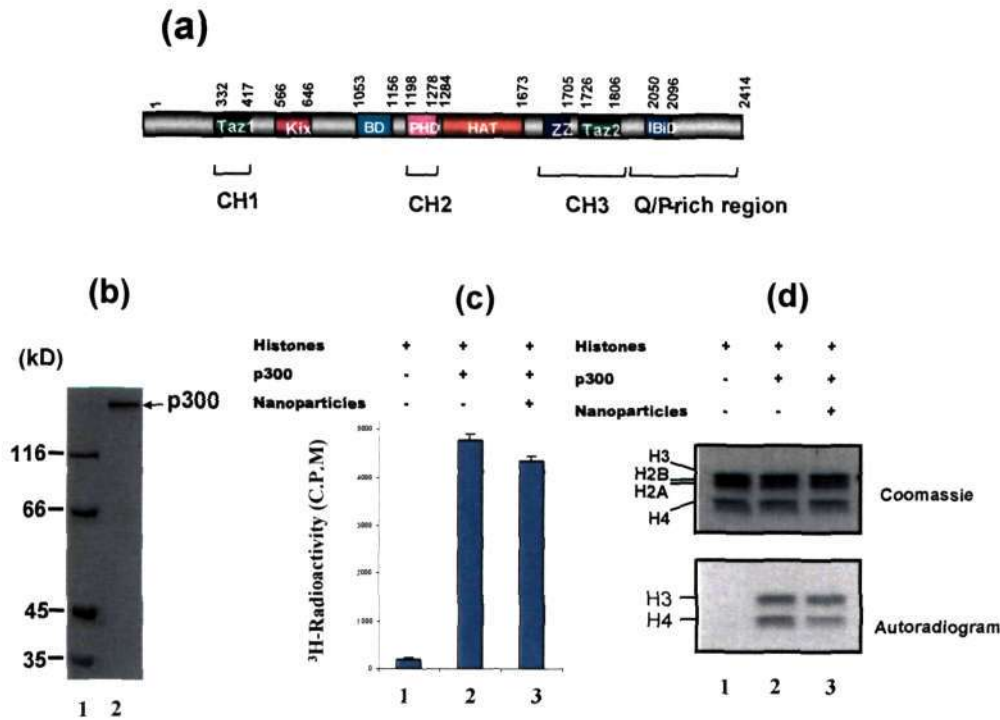
Figure 4.5: (a) Schematic diagram showing the structural and functional domain organization of p300 protein: The functional domains of p300 include CH1, CH2, CH3, KIX, Bromodomain (BD), HAT domain and Q/P-rich region. The N- and C-terminal domains can act as transactivation domains: 1-2414 represents the amino acids in the protein. (b) Full-length recombinant His$_6$-tagged p300 protein used in the experiment: Lane 1 is the protein molecular weight marker represented in kDa, and lane 2 is the purified dialyzed p300 protein analyzed on 8% SDS-polyacrylamide gel. (c) Filter binding assay: HAT assay was performed by using highly purified HeLa core histones (800 ng) in the absence (lane 1) and presence (lane 2) of enzyme p300 (5 ng) and the enzyme (p300) incubated with silver nanoparticles (lane 3). The results represent the average values with error bars (SD) of three independent experiments. (d) Fluorographic analysis of acetylated histones. HAT assays were performed by using highly purified HeLa core histones (1.2 μg) in the absence (lane 1) and presence (lane 2) of p300 enzyme (5 ng) and the p300 enzyme incubated with silver nanoparticles (lane 3). The radiolabeled acetylated histones (H3, H2B, H2A, and H4) were resolved on 15% SDS-polyacrylamide gel and visualized by coomassie blue staining and subjected to fluorography followed by autoradiography.

The functional domains of p300 include nuclear hormone receptor (Nr) cysteine/histidine-rich zinc finger domains CH1 (347-413), CH2 (1195-1451), and CH3

(1669-1807), the KIX domain, the bromo domain (Br), the histone acetyltransferase (HAT) domain, and the minimal HAT domain (1284-1669) (Figure 4.5a). The N and C-terminal domains can act as transactivation domains. As shown in Figure 4.5b, the recombinant full-length human p300 was expressed in Sf-21 insect cell line and purified as described in the Materials and Methods. The protein was dialyzed against BC100 buffer to remove imidazole. The HAT activity of p300 was assayed by filter binding and fluorography of radiolabeled acetylated histones (Figure 4.5, panel c and d). SERS of p300 was carried out with the protein adsorbed on silver nanoparticles. Therefore, it was essential to find out the effect of the silver surface on the functional activity of p300. The HAT activity of p300 incubated with silver nanoparticles was assayed by both filter binding and fluorography. As depicted in Figure 4.5, panel c and d, the HAT activity of p300 adsorbed on the silver nanoparticle surface remained almost the same as compared to that of the mock incubated enzyme (lane 2 vs 3). These data suggest that the SERS of p300 shown in this report represent the structural dynamics of the functional enzyme.

4.3.2. SERS Spectra of p300 Protein in the Aqueous Phase.

At first, we took a very high concentration of p300 in solution and carried out a normal Raman experiment. As seen from curve 1 of the inset on the left of Figure 4.6a, we were unable to see any Raman signature from the p300. If we add silver nanoparticles to this solution, we get very strong Raman signals, which resemble the spectrum shown in curve i of Figure 4.6a. To determine that these modes are not arising from the nanoparticles or the buffer, we recorded the Raman spectra of the nanoparticles in solution and the SERS of the buffer, separately. In the case of nanoparticles we do not observe any Raman peaks as shown in curve 2 of the inset on the left of Figure 4.6a. The buffer in the presence of nanoparticles gives strong Raman signals as shown in curve 3 of the inset on the left of Figure 4.6a. On comparison of this spectrum with the spectrum shown in curve i of Figure 4.6a, we observe that there are no Raman modes which resemble each other in both the spectra. This suggests that the spectrum in curve i of Figure 4.6a is indeed coming from the protein p300. Table 4.1 shows the observed frequencies of the most

important Raman bands and their proposed band assignments for the Raman spectrum shown in curve i of Figure 4.6a. The band assignments have been carried out in accordance with the existing literature pertaining to SERS spectra of amino acids and proteins (Podstawka et al. 2004; Stewart et al. 1999; Podstawka et al 2004). We describe some of the characteristic SERS vibrations observed in the spectrum. As expected, aromatic rings, amides, and carboxylic group vibrations dominate the SERS spectrum of p300.
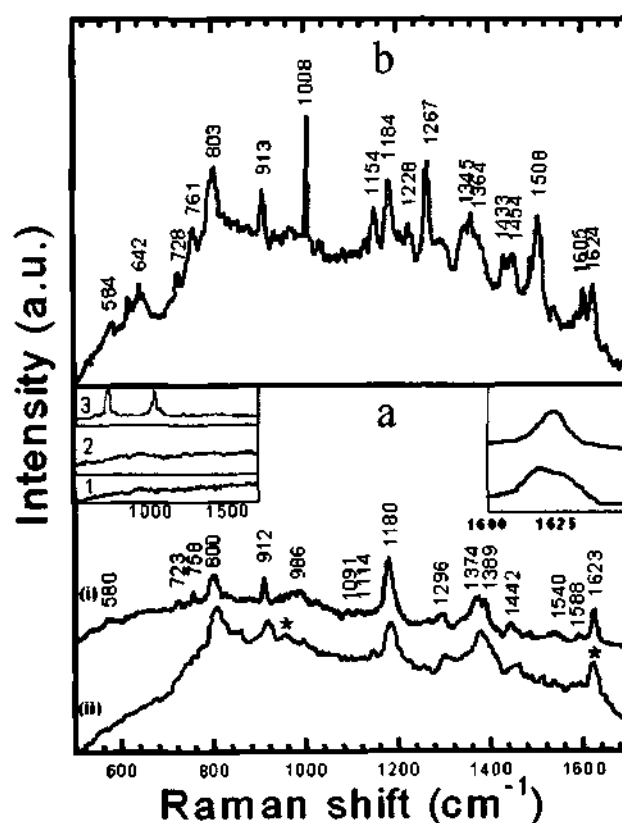
Figure 4.6: SERS of p300. (a) The inset on the left shows the Raman spectra of pure p300 solution (curve 1), nanoparticles (curve 2) and buffer with nanoparticles (curve 3). Curve (i) shows the SERS spectra of p300, and the curve (ii) shows the SERS spectra of deuterated p300. The * has been placed on curve (ii) to show the shifted/new bands in deuterated p300. The inset on the right shows the Amide I region for clarity. (b) SERS spectra of p300 in the prescence of 0.3 mM of NaCl. The concentration of the p300 was ~ 40 ng/μL for all the above cases.

i. Polypeptide Backbone Vibrations. Figure 4.6a (curve i) shows three Raman bands associated with the polypeptide backbone at around 1623, 1540, and 1296 cm^{-1}. The 1623 cm^{-1} is associated with vibrations of the amide I band. These generally appear in the protein spectra when the α-helix of the protein is in close vicinity of the silver surface. It

Table 4.1: Assignment of Raman Bands in the SERS spectra of p300 shown in curve (i) of Fig. 4.6 a.

Raman Shift (cm^{-1})	Raman band assignment
1623	Amide I
1588	v_{as} (COO$^-$), His, Trp, and/or Phe (v_{8a})
1540	Trp and/or Amide II
1442	His and/or Trp
1389	v (COO$^-$)
1374	δ (CH)
1296	Amide III (a helix) and/or δ (CC$_\alpha$H)
1180	Tyr and/or Phe (v_{9a})
1114	v_{as} (C$_\alpha$CN)
1091	v (C$_\alpha$N)
912	v (C–COO$^-$)
800	Tyr and/or v_{as} (C–S–C)
758	Trp or His
723	δ (COO$^-$)
580	Trp

v– stretching; as– asymmetric; δ– deformation.

has been seen that most of the common proteins are adsorbed to the silver surface through the α-helix (Stewart et al. 1999; Podstawka et al 2004). The next band, viz., 1540 cm^{-1}, is due to the amide II vibration. In normal Raman spectra these modes of vibrations are Raman inactive. In the SERS experiments there is a modification in the selection rules giving rise to this band (Moskovits et al. 1985). This is due to the changes in the bond angles, which induce changes in the polarizability of the vibrations in the presence of the nanoparticles. However, there are 12 tryptophan (Trp) residues in p300. Therefore, the possibility of this mode overlapping with the Trp cannot be ruled out. The amide III vibration is seen around 1296 cm^{-1}. The amide III band often overlaps with the δ (CC$_\alpha$ H) vibrations, and hence the Raman band at 1296 cm^{-1} could have contributions from both of these vibrations.

To confirm these observations, we have performed SERS on deuterated p300. In the deuterated p300, the hydrogens in the amide are replaced by heavy deuteriums. Hence, the vibrational frequencies of the amide bands should decrease in deuterated p300. Curve ii of Figure 4.6a shows the SERS spectra of deuterated p300. Significantly, curves i and ii of Figure 4.6a closely resemble each other. Since the deuteration happens only at the amide group, this observation is on the expected lines. Upon deuteration, we observe a decrease in the amide I band frequency by ~7 cm^{-1}. The inset on the right of Figure 4.6a shows the amide I band region. There is a clear shift from 1623 to 1616 cm^{-1}. Since the deuteration is not complete, we do observe a reduced intensity of the 1623 cm^{-1} present in the spectra. In curve ii of Figure 4.6a, we do observe distinct changes in the regions around 1540 and 1296 cm^{-1}. This supports our earlier statement that these peaks are a superposition of the Raman bands of the amide groups and that of other functional groups in the same region. We observe a new mode around ~950 cm^{-1} in the deuterated p300 spectra (see Figure 4.6a, curve ii). It is known that upon deuteration the amide III band shifts from 1296 to 950 cm^{-1} (~340 cm^{-1}) (Tuma et al. 1998). These observations confirm the amide band assignments.

It is interesting to note that we do not observe any amide bands pertaining to β-sheet or random coil of p300 protein. The crystal structures of p300 and CBP (a close homolog of p300) are not known. The solution structure of the CH1 domain of p300 (Freedman et al. 2002; Dial et al. 2003), CH3 (De Guzman et al. 2000,

Legge et al. 2004), and KIX (Radhakrishnan et al. 1997) domains of CBP reveal that indeed in these domains there is no β-sheet or random coil. However, on the basis of the primary structure, it could be predicted that p300 may contain very short stretches of β-sheet as well as random coils. Since none of the structural information available so far is from the full-length protein, our spectral analysis may reflect more realistic structural information about p300. These discrepancies can only be solved by the high resolution full-length crystal structure of CBP/p300. It should be noted that in the recently solved p300 HAT domain structure a central β-sheet comprising seven β-strands has been found surrounded by nine α-helices and many loops (Liu et al. 2008).

ii. Vibrations Associated with the Aromatic Side Chain. The SERS spectrum of p300 is dominated by aromatic side chain vibration of tyrosine (Tyr), tryptophan (Trp), and phenylalanine (Phe). Table 4.1 gives the detailed assignments of these modes. It is necessary to point out here that p300 is quite rich in these aromatic amino acids. There are 12 Trp, 46 Tyr, and 44 Phe present in the primary structure of p300. We do not observe the phenyl ring-breathing mode of Phe as well as the indole ring mode of Trp. This could be due to the fact that these groups may not be in close proximity to the silver surface. This kind of behavior has been observed previously in the SERS spectra of lysozymes adsorbed to silver, where the short-range component of SERS (chemical enhancement) was predominant (Chumanov et al. 1990). It could also be due to the orientation of the molecules with respect to the silver surface. There is a direct implication, of the orientation of the molecule on the silver surface, on the enhancement of the Raman signal (Moskovits et al. 1985).

iii. Aliphatic Side Chain Vibrations. The carboxylate groupof the aspartic acid (Asp), glutamine (Glu), and/or the Cterminus group in protein interacts with the silver surface to give strong enhancements of these Raman bands (Grabbe et al. 1989) The bands at 1588 and 1389 cm^{-1} are assigned to the asymmetric and symmetric stretching modes of the COO- group, respectively. In the SERS spectra a strong Raman feature at 912 cm^{-1} is seen, which is due to the C-COO$^-$ stretching. One also observes the Raman band at 723 cm^{-1} due to δ (COO$^-$) vibrations. There are two weak bands around 1091 and 1114 cm^{-1}, which are due to the symmetric stretching of (C$_\alpha$N) and the asymmetric stretching of

142

$(CC_\alpha N)$ groups, respectively. This observation suggests that the p300 adsorbs to the silver nanoparticles through the nitrogen groups. This could be one of the reasons for the presence of strong amide bands in the SERS of p300.

4.3.3. SERS Spectra of p300 Protein in the Presence of Colloidal Aggregating Agent:

Although the role of aggregating agents in SERS has been studied earlier with respect to small molecules, (Li et al. 2001; Flauds et al. 2004) proteins are yet to be investigated in great detail. Upon addition of a small quantity of NaCl or KCl to the solution containing the analyte and nanoparticles, one observes a large enhancement in the SERS signal. As it is known, the enhancement of Raman bands in SERS is governed by both electromagnetic enhancement and the chemical enhancement. (Moskovits et al. 1985) Upon addition of small concentrations of Cl$^-$ ions to the protein nanoparticle composite there is an aggregation of nanoparticles around the protein molecule. This will cause a further enhancement in the above-mentioned mechanisms due to (i) an enhanced plasmon coupling as a result of the aggregation of the nanoparticles, (ii) an increased charge-transfer pathway between the metal-protein system, and (iii) the anion-induced reorientation of adsorbed protein (Li et al. 2001). These will not only account for the enhanced Raman signal intensity but also for the appearance of new modes of vibrations upon the addition of Cl$^-$ ions in the solution. Figure 4.6b shows the SERS spectrum of p300 in the presence of 0.3 mM NaCl. Table 4.2 shows the frequencies of the most important SERS bands and their proposed band assignments. We observe new modes of vibrations arising upon the addition of Cl$^-$ ions (see Figure 4.6b). We can clearly see new Raman bands around 1008, 1267, 1508, and 1605 cm^{-1}, which have been assigned to the groups Phe, C=O stretching of the α- helix, histidine (His)/Trp, and Tyr and/or Phe, respectively. Note that p300 contains 68 His residues along with several Trp, Tyr, and Phe as mentioned earlier; hence, the SERS spectra of p300 reported here are realistic. Predicted structural data (Freedman et al. 2002; Dial et al. 2003; De Guzman et al. 2000; Legge et al. 2004; Radhakrishnan et al. 1997) also suggest the presence of stretches of the

143

Table 4.2: Assignment of Raman bands in the SERS spectra of p300 + 0.3 mM NaCl shown in Fig. 4.6 b.

Raman Shift (cm^{-1})	Raman band assignment
1624	Amide I
1605	Trp, Tyr and/or Phe (v_{8a})
1508	His
1454	δ (CH$_2$)
1433	His and/or Trp
1364	Trp
1345	δ (CH) and / or Trp
1267	v (C = O) (a helix)
1184	Tyr and Phe
1153	v (C–N)
1008	Phe (v_{12})
913	v (C–COO$^-$)
803	Tyr
761	Trp or His
728	δ (COO$^-$)
642	Tyr
584	Trp

α-helix throughout the p300 structure. It is to be noted that there is a strong resemblance in the spectra with and without Cl⁻ ion as shown in Figure 4.6, panel a and b. This suggests that the Cl⁻ ion effect could be used in the studies of proteins using SERS.

4.3.4. SERS Spectra of p300 Adsorbed to Silver Nanoparticles Dried over a Glass Substrate:

The SERS spectra of p300 obtained by method I (see the Experimental Details) is shown in Figure 4.7a. Enhanced Raman signals for the bands around 634, 721, 1013, and 1268 cm⁻¹ are observed. These bands are stretching vibrations of Phe and C=O and are absent in SERS spectra of p300 recorded in the aqueous solution (compare with Figure 4.6a). It
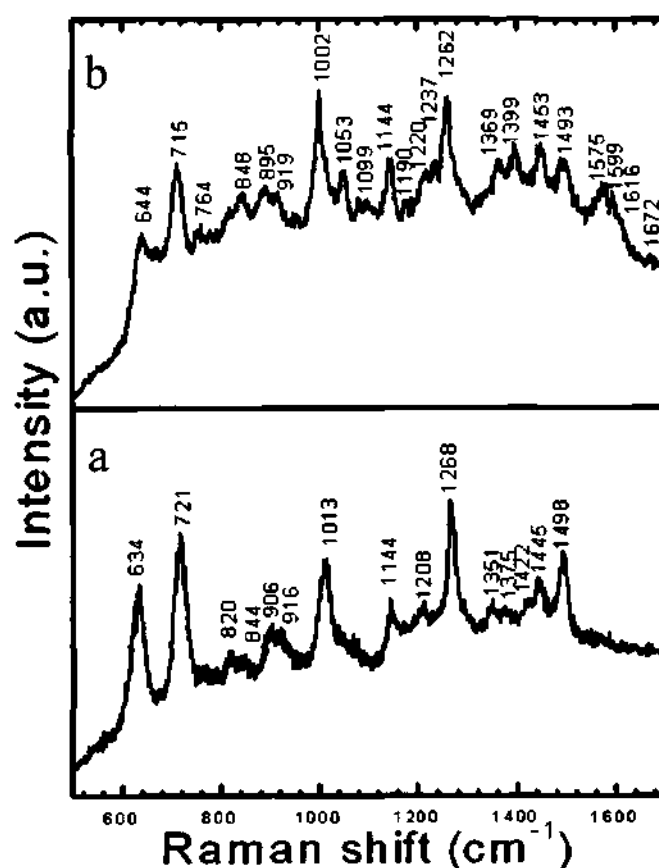

Figure 4.7: SERS spectra of p300 in nonaqueous form on substrates prepared by (a). Method I (b) Method II (See experimental section for substrate preparation). The concentration of the p300 was ~ 40 ng/μL.

is important to note the absence of the amide vibration in Figure 4.7a. The absence of amide bands could be due to the fact that these groups are not in the close proximity to silver surface, since the silver collides are immobilized on the glass slides apriori. This also could be due to screening of the amide groups by the aromatic groups on the protein surface (Tuma et al. 1998)). In the absence of a short-range component of the SERS mechanism, the amide bands can disappear in the SERS spectra. SERS spectra were also obtained by preparing the sample using method II (see the Experimental Details), which we call the "sandwich technique". Figure 4.7b shows the SERS spectra of p300 obtained by method II. Here, we observe a weak amide I band around 1672 cm^{-1} along with many other modes, which were absent in the SERS spectra obtained by method I. It is interesting to observe that the Raman spectrum of p300 prepared by the "sandwich technique" (Figure 4.7b) resembles the Raman spectrum of the p300 in aqueous solution in the presence of chloride ion (Figure 4.6b). Since, in the "sandwich" case, we add the nanoparticles along with the protein on top of a dried silver nanoparticle layer, this allows a better adsorption of the protein to the silver surface and provides an environment to retain minute amounts of water between the silver nanoparticles. Although the enhancement of the Raman signal obtained by this method is less when compared to that of the spectra obtained in aqueous form, this technique may still facilitate a unique opportunity to perform SERS studies in "chemically pure" conditions, especially under ultrahigh vacuum conditions.

4.3.5. Silver nanoparticles do not affect HAT and autoacetylation activity of p300 HAT domain:

In order to perform SERS of p300 HAT domain (a.a 1284-1673), p300HD, it was adsorbed on silver nanoparticles. The HAT and autoacetylation activities of p300HD incubated with silver nanoparticles were assayed by fluorography. As depicted in Figure 4.8a, the HAT activity of p300HD adsorbed on the silver nano surface remained almost the same as compared to that of the mock-incubated enzyme (Figure 4.8a, lanes 2 vs. 4).
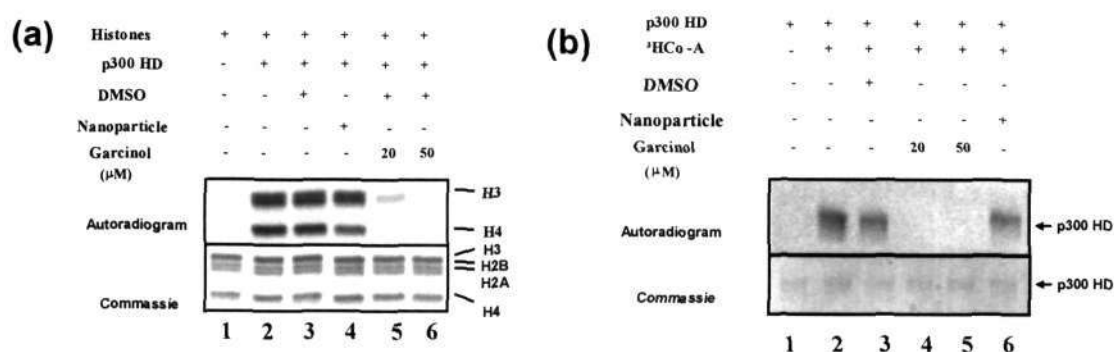
Figure 4.8: (a) Effect of silver nanoparticle and garcinol on the p300HD catalytic activity: HAT assays were performed by using highly purified HeLa core histones in the absence (*lane 1*) and presence of p300HD (*lane 2*), the p300HD incubated with silver nanoparticle (*lane 4*); *lane 3*, histones with the HAT in presence of DMSO, *lane 5* and 6; histones with the HAT and in the presence of 20 and 50 μM of garcinol, respectively. (b) Effect of silver nanoparticle and garcinol on the p300HD autoacetylation activity: Autoacetylation assays were performed using p300HD in the absence of [^{3}H] acetyl CoA (*lane 1*) and in the presence of [^{3}H] acetyl CoA with silver nanoparticle (*lane 6*), (*lane 3*); in the presence of DMSO as solvent control, *lane 4* and 5, HAT in the presence of 20 and 50 μM of garcinol, respectively. Reaction mixtures were resolved on SDS-PAGE and processed for fluorography.

Similarly, the autoacetylation activity of the p300HD was also not affected in the presence of silver nanoparticles (compare Figure 4.8b, lanes 2 vs. 6). Interestingly, we observe that the potent natural HAT inhibitor, garcinol (Balasubramanyam et al. 2004). could inhibit the HAT activity of p300HD (Figure 4.8a, lanes 3 vs. 5 and 6) as well as the autoacetylation of p300HD (Figure 4.8b, lanes 3 vs. 4 and 5).Presumably, the p300 HAT inhibitory function of garcinol is exhibited through the inhibition of p300 autoacetylation and hence the substrate acetylation.

4.3.6. Surface Enhanced Raman Spectroscopic studies of p300 HAT domain (a. a 1284-1673)

Further, to understand the structural details of p300HD in the absence of high resolution crystal structure, we performed SERS of bacterially purified p300HD (see Materials and Methods). Figure 4.9a show the SERS spectra of HAT domain, in the range 400 cm^{-1} to
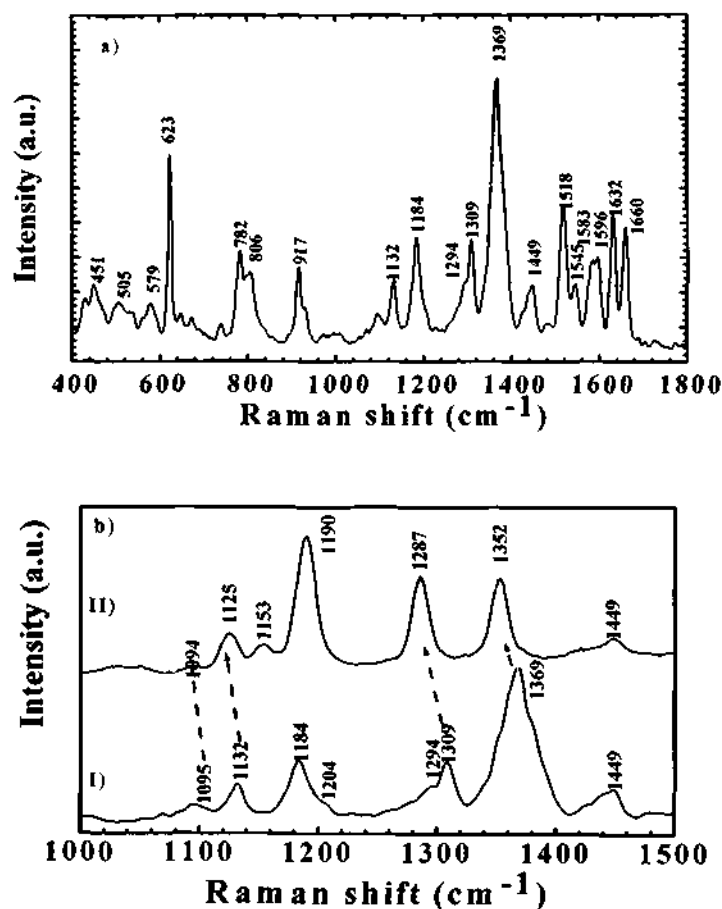
Figure 4.9: (a) SERS of HAT domain. (b) SERS of I) HAT domain compared with II) autoacetylated HAT domain. The red arrows indicate the red shifting of some modes.

1800 cm⁻¹. In order to confirm the amide band positions, we have performed SERS of the deuterated HAT domain. As expected, we observed a red shift in amide bands (Figure 4.9 b, I and II). To confirm that the SERS spectrum of the HAT domain is not contaminated with the spectra of the buffer, we have carried out the SERS of the neat buffer solution and are presented in Figure 4.10,c. Table 4.3 shows the SERS band assignments of the HAT domain. Modes have been assigned in comparison to the SERS spectra of the parent protein p300 as shown above, and using the standard amino acids and proteins band assignments. It is evident that the spectrum is dominated by SERS modes of ring-structured amino acids: Tryptophan (Trp), tyrosine (Tyr) and phenylalanine (Phe), which are characteristic of SERS of any protein. It should be noted that in the case of SERS of p300 HAT domain we were able to see the modes pertaining to α-helix and random coil

148

(Figure 4.9 and Table 4.3) which is consistent to the published report of p300 HAT domain structure (Liu et al. 2008) which made up of nine α-helices and several loops. Here it should be noted that the p300 HAT domain structure was solved in the absence of the 32 residues (1523-1554) proteolytically sensitive autoacetylation loop which is present in our study. In the present study we have used the p300 HAT domain consisting of residues (1284-1673) in contrast to the semisynthetic HAT domain (residues 1287-1666) used to solve the crystal structure. Because both the HAT domains are of comparable size therefore the results can be faithfully interpreted to a good extent. In this case also we do not observe any amide bands pertaining to β-sheet which is similar to the observation made for the SERS of full length p300. Presence of β-sheet away from the surface of the protein as compared to loops and α-helix may be one of the reason. To investigate the structural changes associated with the fully acetylated p300HD using SERS, we performed autoacetylation reactions (see Materials and Methods).The autoacetylation was confirmed by mass spectrometry analysis. It was found that fully acetylated p300HD was acetylated
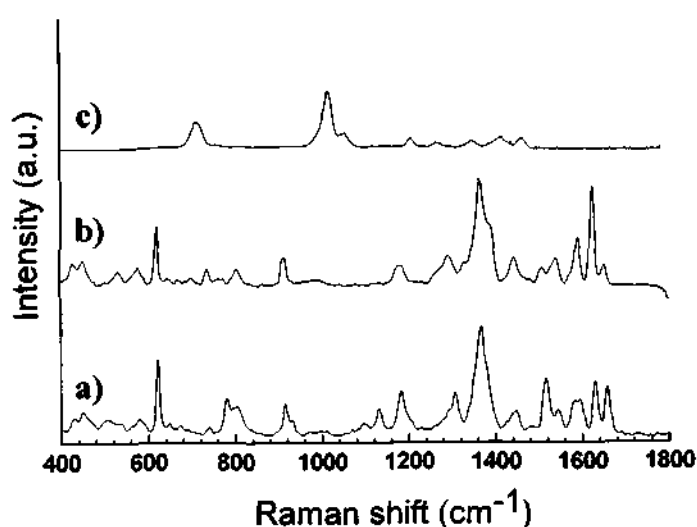
Figure 4.10: SERS of a) HAT domain; b) deuterated HAT domain; c) Only buffer

in all the available 37 sites (Figure 4.11 a and b). We have performed SERS of fully-autoacetylated p300HD and compared it with normal, partially acetylated HAT domain.

This is shown in Figure 4.9 b (I & II). There is a marked change in the modes pertaining to symmetric stretching of COO$^-$ (1369 cm^{-1}), Amide III (1294 cm^{-1}), v_{9a} of Phe (1184 cm^{-1}) and asymmetric stretching of $C_{\alpha}CN$ (1132 cm^{-1}). We observe not only a change in intensity of these modes, but also some softening (Figure 4.9b). Softening, in fact signifies bond weakening, and would be due to the interaction between various groups

Table 4.3: SERS band assignments of p300HAT domain

SERS band (cm^{-1})	assignment
1660	Amide I (α helix)
1632	Amide I (random coil)
1596	Trp,Tyr, and/or Phe
1583	v_{as}(COO$^-$),His, Trp
1545	Trp,Tyr, and/or Phe
1518	Amide II and/or Trp
1449	δ(CH$_2$)
1369	v_s(COO$^-$)
1303	ω(CH$_2$)
1294	Amide III (α helix)
1184	Phe(v_{9a})
1132	v_{as}(C$_{\alpha}$CN)
917	v(C - COO$^-$)
806	Tyr and/or v_s(C-S-C)
782	Trp(w_{18})
623	Phe (v_{6b})
579	Trp
505	v(S-S)

upon autoacetylation. Hence, these changes indicate structural reorganization of the HAT domain after the complete autoacetylation. It is to be noted that, unlike conventional Raman spectroscopy, SERS probes vibrational modes of groups which are in close proximity to the metal surface. This would be reflected as intensity changes due to the
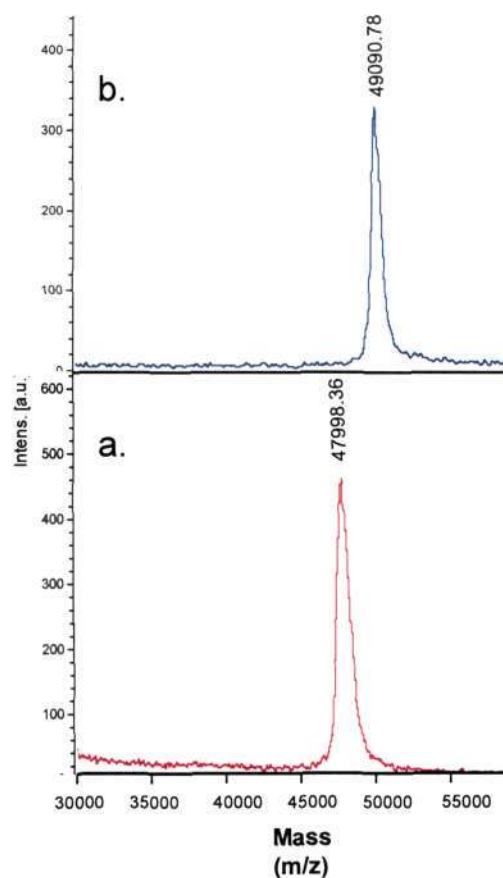
Figure 4.11: MALDI-TOF mass spectroscopy of purified p300HD. The observed mass of recombinant protein is 47,998.36 Da and that of fully autoacetylated is 49,090.78 Da. The expected mass of p300HD is 47,536 Da. Because single acetyl modification is 42 AMU, so the recombinant p300HD has about 11 sites modified (a) and 37 in the fully autoacetylated p300HD (b).

distance dependent electromagnetic enhancement and the surface selection rules, where the orientation of the molecule on metal surface determines the enhancement of the vibrational modes. Therefore, all these conditions suffice to make SERS sensitive to probe the structural modifications of macromolecules near the surface of nanoparticles, as in the present case. Furthermore, these data also suggest that the SERS could be used to

monitor the structural changes in the other self-modifying proteins like kinases, methyltransferases and glycosyltransferases (Thompson et al. 2004).

4.4. Summary:

For the first time, SERS was performed on p300 and it's HAT domain in aqueous medium. The SERS spectra suggest the presence of α-helix, random coil, aromatic ring structures like Phe, Tyr, Trp, His, and aliphatic structures such as Asp, Glu, and C-terminus groups in p300. The presence of these Raman bands in the SERS of the protein provides an important tool for studying drug-protein interactions. In the absence of full-length crystallographic data of proteins, SERS could provide a very useful technique to obtain structural information. The presence of small concentrations of NaCl leads to aggregation of nanoparticles leading to a better adsorption of silver nanoparticles to the proteins. The chloride ion could increase the sensitivity of SERS experiments due to larger enhancement in Raman signals more or less retaining the Raman spectra of the proteins. In this work, we demonstrate a new method called the "sandwich technique", which could provide an alternate method for recording SERS spectra of proteins without the aqueous medium. In the present case, we were able to record the Raman spectra of p300, which resembles its spectra in the aqueous medium. This method could pave the way to perform SERS experiments in ultrahigh vacuum conditions. In the present study, autoacetylation induced specific structural changes in p300 HAT domain was also probed through SERS. Remarkably, for the first time it also establishes that autoacetylation of p300 alters its structure, which is significantly important for the autoacetylation mediated regulation of the p300 HAT activity, especially in the regulation of gene expression in humans. Furthermore, SERS analysis can be used to study protein-ligand interactions, like p300-HAT modulator interaction (as mentioned above), which would have immense implications in drug design. This technique may be further used to study site specific structural changes in protein, especially at the surface. It is important to note that all the above mentioned experiments were performed in solution phase at low concentrations of protein. This provides a significant advantage to study subtle secondary structural

changes of protein under physiological conditions, which is not viable to probes like X-ray crystallography. Although the in vitro studies like these show promising results, the final aim should be to perform experiments in vivo. Many research laboratories around the world are aiming to achieve the same.

Chapter **5**

> *This chapter presents the incidents of histone hyperacetylation and its molecular mechanism in oral cancer manifestation. Possibility of targeting HATs for the antineoplastic therapy by small molecule HAT inhibitor has also been explored.*

5.1. Rational of the study:

Altered histone acetylation pattern is associated with several diseases including cancer. The dysfunction of histone deacetylases (HDACs) and the consequent hypoacetylation of histone as well as nonhistone proteins have been causally related to cancer manifestation. However, we observed that histones are hyperacetylated in the oral cancer cell line. This observation lead us to investigate the status of histone acetylation in oral cancer patient samples. In agreement with the cell line based data histones were found to be dramatically hyperacetylated in all the grade II oral cancer sample tested. We further investigate the molecular mechanisms behind the hyperacetylation and also explore the possibility of targeting the acetyltransferase, p300 by a water soluble, small molecule inhibitor to control tumor progression.

5.2. Introduction:

Oral cancer is one of the most common type of human cancer, with an annual incidence of 274,000 cases world wide (Parkin et al. 2005). Tobacco use and alcohol intake are the major risk factor for the development of oral cancer. However, the exact mechanism by which tobacco carcinogen and alcohol induces transformation and malignant progression

of the epithelial cells in oral cancer is not well understood (Mao et al. 2004; Decker and Goldstein, 1982).

Rapidly increasing research works now suggest the pivotal role of chromatin structure-function in several disease manifestations (Quina et al. 2006; Thorne al. 2009). This is evident from the fact that genetic alterations and/or a more diverse group of epigenetic changes may result in disease pathogenesis (Fraga et al. 2005, Varambally et al. 2002, Seligson et al. 2005; Das et al. 2009; Pfister et al. 2008; Quina et al. 2006; Thorne al. 2009; Esteller M. 2007) . Chromatin being a dynamic entity plays a critical role in all the nuclear related phenomenon like transcription, repair and replication etc (Eberharter et al. 2002; Carrozza et al. 2003). Post translational modifications of chromatin play an important role in the maintaining chromatin structure–function and hence regulate gene expression, cell growth and differentiation. It has been suggested that perturbation of the transcriptional state of a cell can lead to developmental defects (Berger, S. L. et al. 2002). Further it has also been shown that dysfunction of different chromatin components and covalent modifications of histones can lead to disease pathogenesis (Quina et al. 2006; Bhaumik et al. 2007; Thorne al. 2009).

Histone acetylation is one of the well characterized epigenetic modifications and is controlled by histone acetyltrasnferases (HATs) or lysine (K)-Acetyltransferases (KATs) and histone deacetylases (HDACs), which affect the acetylation of histone and non-histone proteins thereby affecting the down stream biological functions (Das et al. 2005; Spange et al. 2009). Altered HAT and HDAC activity are now known to play important role in several diseases including cancer (Seligson et al. 2005; Glozak et al. 2007; Das et al. 2009; Pfister et al. 2008; Van Beekum et al. 2007). The histone acetyltransferase, p300 is a global transcriptional coactivator and is a major HAT in the cell (Shikama et al. 1997). High levels of p300 has been observed in some tumors (Debes et al. 2003, Ishihama et al.2007). Further, mutations in p300 acetyltransferase were found in primary tumors and cell lines (Gayther et al. 2000). Similarly, loss of heterozygocity at the p300 locus is associated with the colorectal, breast cancer and with brain cancer (gliobastoma) (Gayther et al. 2000; Giles et al. 1998; Muraoka et al. 1996). Although these data indicate the involvement of CBP, p300 and PCAF genes, HAT activities of these acetyltransferases have not been established as the

cause of the malignancy (Van Beekum et al. 2007). However, increased acetylation of H3K56, a target of CBP/p300 was observed in multiple cancers (Das et al. 2009).

Recently, alteration of histone modifications in different cancers have been reported. The loss of Lys 16 acetylation and Lys 20 methylation of H4 is found to be associated with primary tumors and tumor cell lines (Fraga et al. 2005). In an another study changes in bulk histone modifications of cancer cells were found to be predictive of clinical out come in prostate cancer (Seligson et al. 2005). Hyperacetylation of histones has been observed in hepatocellular carcinoma (Bai et al. 2008). Apart from cancer, dysfunction of p300 has been implicated in other diseases: inflammatory processes, Huntington disease, cardiac disease, diabetes and AIDS (Varier et al. 2006; Davidson et al. 2005; Zhou et al. 2004; Rouaux et al. 2003). These observations suggest that specific and relatively non-toxic HAT inhibitors could be considered as new generation therapeutic agent, specially, cancer. Several HAT inhibitors have been discovered, which has indeed potential clinical impact in HIV and cardiac disease (Mantelingu et al. 2007, Balasubramanyam et al. 2004; Davidson et al. 2005, Morimoto et al. 2008). However, effect of HAT inhibitor in cancer manifestation has not been tested yet.

Cancer is marked by hyperproliferative cells which have evaded the apoptotic machinery of the cells and hence have overexpression of antiapoptotic proteins. B23 (NPM1) and GAPDH are two of those genes which are known to get frequently highly upregulated in many cancers. Both of these proteins are suggested to be positive regulators of cell proliferation (Grisendi at al. 2006, Lim et al. 2006).

Here, we report that histones (H3) are hyperacetylated in oral cancer patient samples and is positively correlated to the upregulated B23 and GAPDH proteins. We also present a novel mechanism to explain how hyperacetylation of H3 could be regulated by B23 and GAPDH in a nitric oxide (NO) dependent manner involving p300 acetyltransferase. Further, we also report for the first time that a novel water soluble HAT inhibitor, CTK7A can inhibit tumor cell growth in nude mice.

5.3. Results and Discussion:

5.3.1. Hyperacetylation of histone at H3K14 is linked to the overexpression of B23 and GAPDH in oral cancer:

To investigate the status of histone acetylation in different cell lines, histones were isolated from the cells and subjected to immunoblotting with anti-acetylated histone H3 (K9 and K14) antibodies. We observed that histones are predominatly hyperacetylated in oral cancer cell line, KB cells and the liver (HepG2) (Figure 5.1, compare lanes 3 and 4 vs lanes 1, 2 and 5). Hyperacetylation of histones in hepatocarcinoma is well documented (Bai et al. 2008). Hyperacetylation of histones in oral cancer cell line was almost equivalent to the liver cancer cells, HepG2 was quite surprising. This result encouraged us to find out the acetylation levels of histone in tissues from oral cancer patient samples. Next the global levels of histone acetylation in tissues from patient samples were determined. Oral cancer tissue samples (grade II, total sample studied 31) were obtained from Bangalore Institute of Oncology. All samples were collected with informed consent of the patients and prior institutional review board approval. Cancer grading was done by the qualified pathologist. In all the cases adjacent normal tissue was taken for the control (normal) from each patient and histopathological
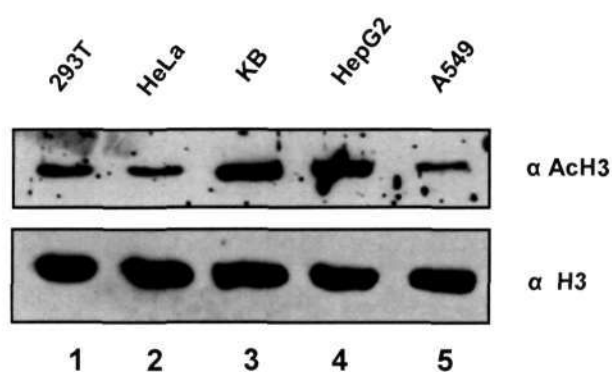
Figure 5.1 State of histone acetylation in different cell lines. Histones were isolated from different cell lines as indicated (lane 1 to 5) and histone acetylation was analysed by western blotting with anti-acetylated H3 antibody (upper panel). Anti-H3 was used as a loading control (lower panel).
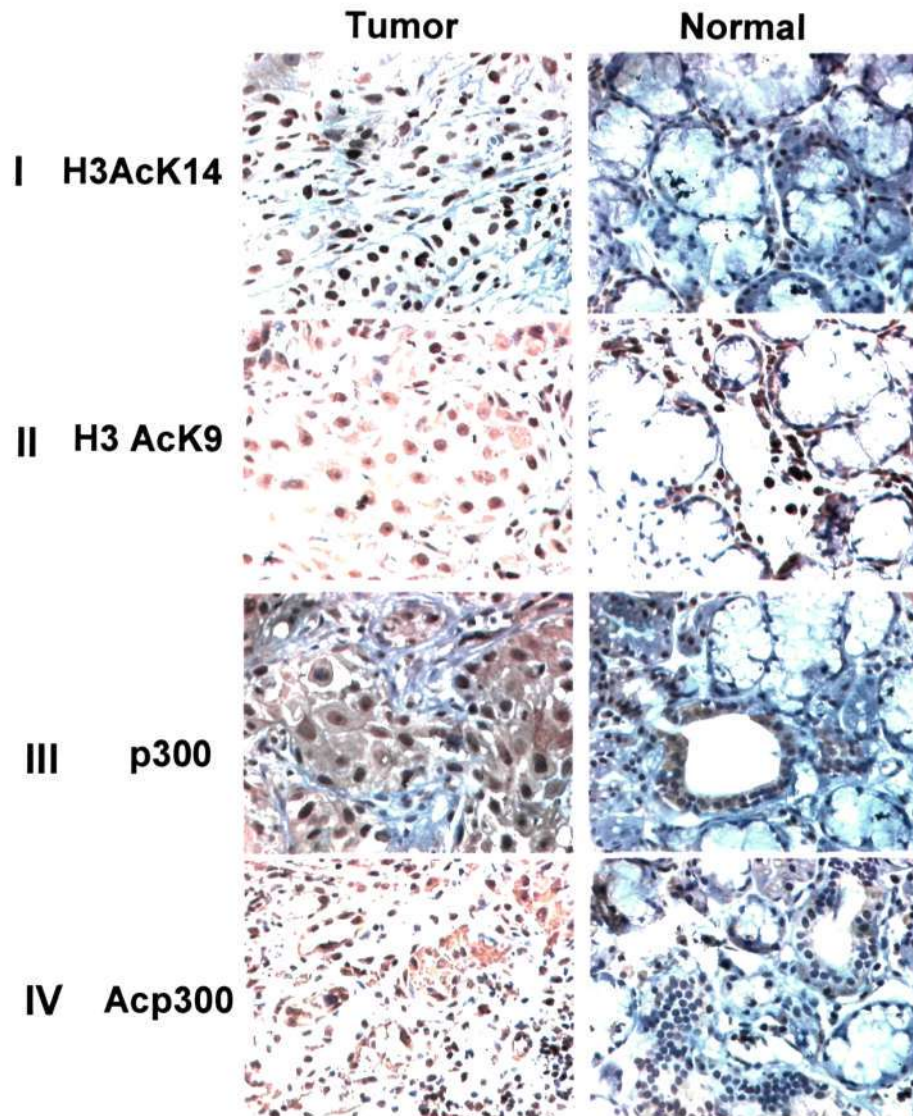
Figure 5.2. Histone hyperacetylation is associated with hyperacetylation and upregulation of p300 in human oral cancer. Immunohistochemical detection of p300 expression, acetylated-p300 (ac-p300), H3K14 acetylation and H3K9 acetylation in malignant oral tumor and respective adjacent normal tissue. Images acquired at 40X magnification.

condition of tissue were determined by the pathologist (see Materials and Methods for detail). Tumors were harvested and fixed in 10% formalin for 1–2 hr and transferred to 70% ethanol overnight followed by paraffin embedding. Other part of the same tissue

kept in protease inhibitor cocktail was used for western analysis. Paraffin blocks of fixed oral tissues were sectioned and mounted (see Materials and Methods for detail). Immunohisto-chemistry (IHC) and western analysis were performed using specific antibodies. Cells stained with dark brown color were considered as positive. It was found that H3K14 (anti-H3AcK14, Abcam) was predominantly hyperacetylated (80% cells, p< 0.001, one-way ANOVA, see Materials and Methods) in cancer tissues as compared to normal counterpart (compare normal vs tumor in Figure 5.2, panel I). Further the levels of H3K9 acetylation (anti-H3AcK9, Upstate) was also found to be marginally higher (40% cells, p< 0.01, one-way ANOVA) which is a target of PCAF (compare normal vs tumor in Figure 5.2, panel II). Significantly, the levels of H3K14 acetylation was found to be much higher than that of H3K9 acetylation (compare normal vs tumor in Figure 5.2, panel I and II respectively). As the H3K14 is the only known invivo target of p300 among lysine 9 and 14 of histone H3, we next look at the expression levels of histone acetyltransferase, p300. It was found that the p300 levels were higher than the adjacent normal tissue (72 % cells, p< 0.001, one-way ANOVA) (compare normal vs tumor in Figure 5.2, panel III). Further it is known that autoacetylation of p300 augments its catalytic (i.e HAT) activity (Thompson et. al. 2004). This led us to investigate the autoacetylation status of p300 in oral cancer samples. For this we generated autoacetylated specific antibody (Thompson et. al. 2004) against residue lysine-1499 of p300 using an acetylated heptapeptide (see Materials and Methods) which is known to get acetylated during the course of p300 activation via autoacetylation (Thompson et. al. 2004). Interestingly, p300 was also found to be hyperacetylated in oral cancer samples (72 % cells, p< 0.001, one-way ANOVA) (compare normal vs tumor in Figure 5.2, panel IV). Taken together these results suggest that in grade II oral cancer samples histones are predominantly hyperacetylated at H3K14 and overexpression and also hyper-autoacetylation of p300 could be involved in the histone hyperacetylation at H3K14.

Next, we looked into the protein levels of GAPDH and B23 which are known to get highly expressed in different cancers (Grisendi at al. 2006, Lim et al. 2006; Majumder et al. 2004; Altenberg et al. 2004; Vilà et al. 2000). As expected, a sharp increase in the GAPDH (80% cells, p< 0.001, one-way ANOVA) and B23 (83 % cells,

p< 0.001, one-way ANOVA) levels were found in malignant tumors compared to corresponding normal tissue in each case (patient sample) tested (compare normal vs tumor in Figure 5.3, panel I and II respectively). Subsequently, we took six different tissue pair samples (tumor and corresponding adjacent normal tissue) and determined the levels of protein overexpression by western blotting analysis. Tissue lysates were prepared and western were performed using specific antibodies as indicated in Figure 5.4. It was observed that in all the six pairs of tissue samples histones H3 were hyperacetylated as probed by H3AcK9AcK14 acetylation specific antibody (compare normal vs tumor in Figure 5.4.a, in each case 1-6, respectively). Surprisingly, both GAPDH and B23 were found to get overexpressed in all tumor tissue samples tested as
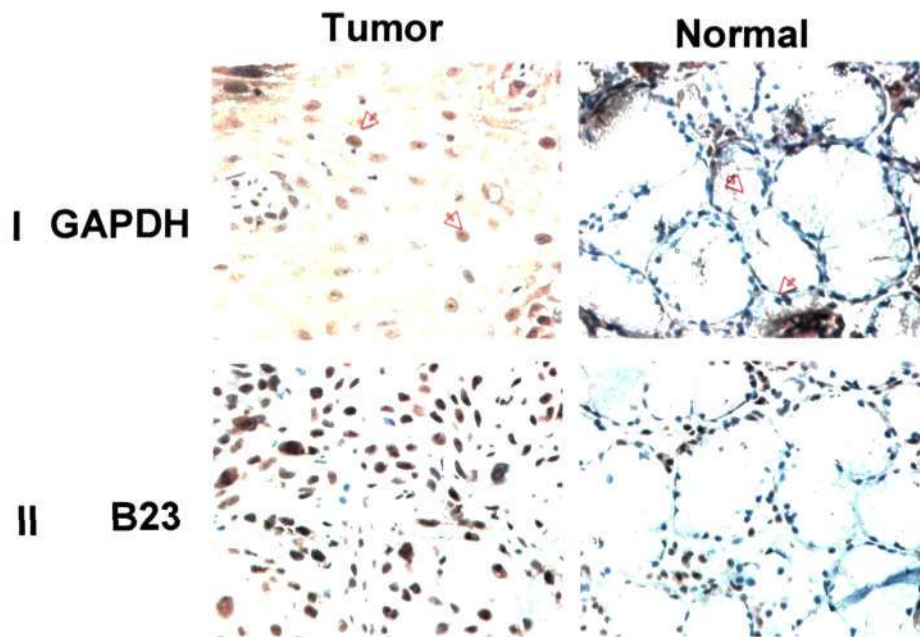

Figure 5.3. Immunohistochemical detection of GAPDH and B23 expression in oral cancer samples. Immunohistochemical detection was performed in malignant oral tumor and respective adjacent normal tissue using indicated antibody. In case of GAPDH in tumor sample, arrow marks indicate the nuclear localization of GAPDH. Images acquired at 40X magnification.

determined by western analysis (compare normal vs tumor in Figure 5.4, in each case 1-6, respectively). These results were found to be statistically significant (see Figure 5.4 b). It was noticed that H3 hyperacetylation follows the same pattern of B23 and GAPDH overexpression in all cancer tissue samples tested as compared to their adjacent normal tissue counterpart, suggesting a strong correlation between overexpression of B23 and GAPDH and histone hyperacetylation (Figure 5.4).

Taken together these data suggest that overexpression of GAPDH and B23 are positively correlated to histone hyperacetylation in oral cancer. Further the role of p300 levels in cancer manifestation is rarely associated (Debes et al., 2003; Ishihama et

(a) **(b)**
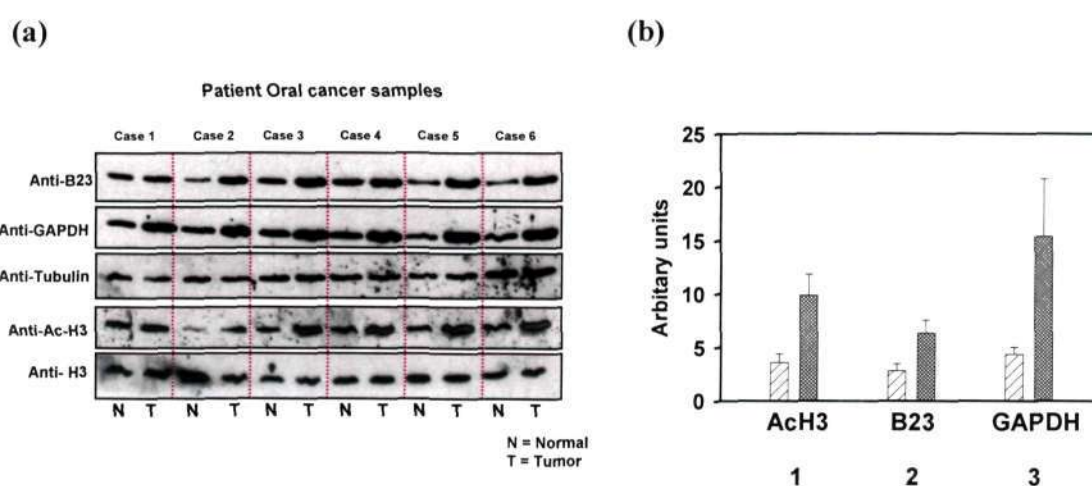
Figure 5.4. Western blot comparing protein levels and acetylation status of histone H3 in normal and respective adjacent normal tissue of the different patient samples. (a) For western blot analysis against B23 and GAPDH, tissue lysate were used and tubulin was taken as loading control. Histones isolated from the same patient tissue were used for the western blotting using anti-H3 and anti-acetylated H3 antibodies. A global antibody to histone H3 was used as a loading control. Western blotting done with six different patient samples (case 1 to 6) as shown. In figure (5.2) IHC was done with case 3 tissue as is also used in figure (5.3 and 5.5) and is shown as a representative figure of IHCs done with several tissue samples. (b) Quatification of bands from of Figure 5.3.a was done using phosphoimager (Fuji). One way ANOVA revealed that tumor samples are significantly different ($p < 0.05$) from the corresponding normal tissue group. Light shaded column and deep shaded columns in lane 1,2 and 3 Figure 5.4 b shows the difference in acetylation of H3, B23 and GAPDH expression in control (adjacent normal tissue) and corresponding tumor tissue, respectively.

al. 2007). However, consistent hyperacetylation of histones, predominantly at H3K14 which is a target of p300 and p300 autoacetylation, together with overexpression of

162

GAPDH and B23 suggest a possible link between these proteins. These results also suggest that increase in H3K14 hyperacetylation levels in oral cancer could be mediated by p300. The autoacetylation of p300 may fine tune the histone hyperacetylation.

5.3.2. NO induced H3K14 acetylation is associated with B23 and GAPDH overexpression via p300 autoacetylation:
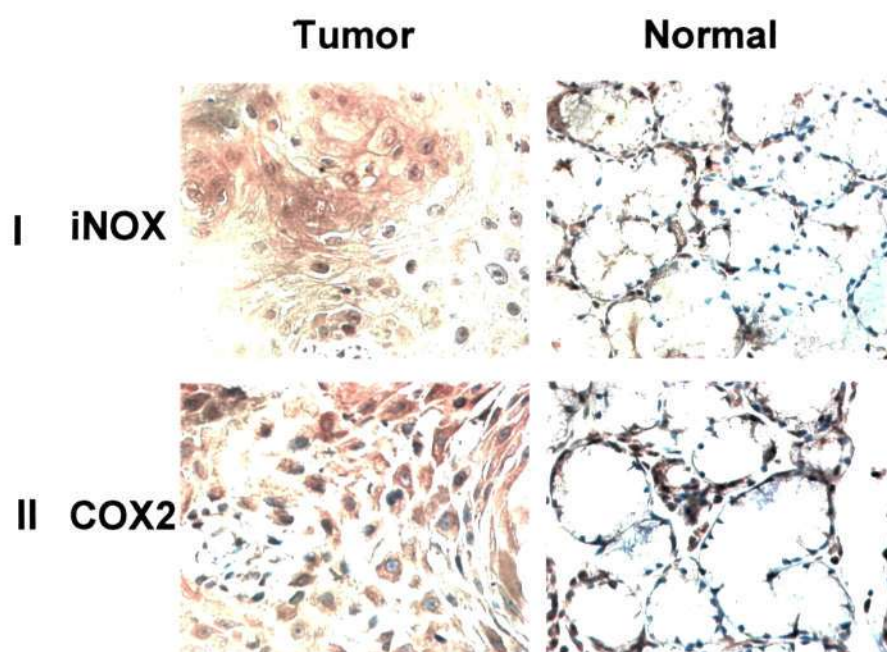
Figure 5.5. Immunohistochemical detection of iNOS and COX-2 expression in human oral cancer. Immunohistochemical detection was performed in malignant oral tumor and respective adjacent normal tissue using indicated antibody. Images acquired at 40X magnification.

The free radical gas, nitric oxide (NO), is generated by nitric oxide synthase (NOS) family of enzymes. NO is a plieotropic signaling molecule that has been identified as mediator for numerous physiological and pathophysiological conditions (Moncada et al .1991; Knowles et al. 1994). NOS activity has been detected in human tumor cell lines (Jenkins et al. 1994; Asano et al. 1994) tumor cells of various histogenetic origins (Ambs

et al. 1998; Thomsen et al. 1998; Zhao et al. 1998) and has been associated with tumorogenesis, proliferation and expression of important signaling components linked to cancer development (Xu et al. 2002, Wink et al. 1998; Fukumura et al. 2006; Shin et al. 2008). Interestingly, various studies have also shown that NO has both
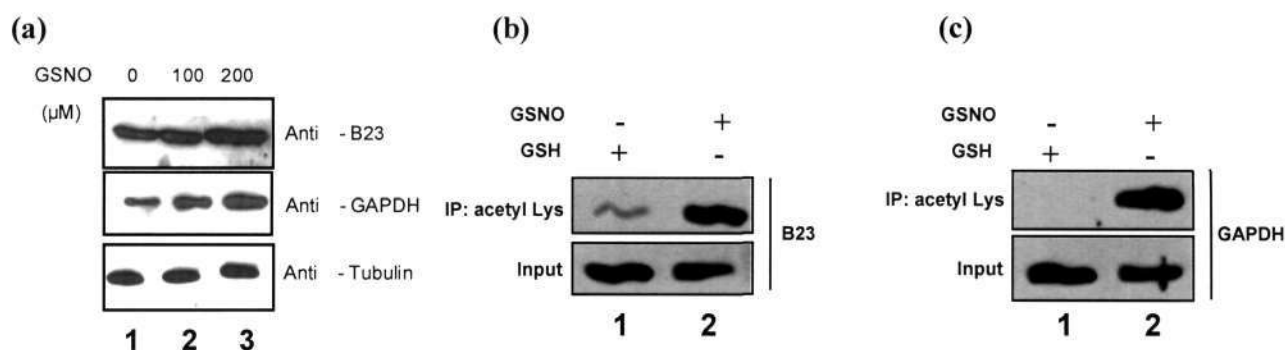
Figure 5.6. Nitric oxide enhances histone acetylation and is linked to B23 and GAPDH overexpression. **(a)** B23 and GAPDH level increased in a GSNO concentration dependent manner. KB cells were treated with indicated concentration of GSNO for 24 h (lane 1 to 3). Cell lysate were used to perform the western blotting using anti-B23 (top panel) and anti-GAPDH antibody (middle panel). Tubulin was used as a loading control (lower panel). **(b)** and **(c)** KB cells were grown in presence of 200μM GSNO or GSH for 24 h. Cell lysates were immunoprecipitated with anti-acetyl Lysine antibody and the immunoprecipitate were analysed by western blotting with an anti-B23 (panel b) and anti-GAPDH (panel c) antibodies.

pro- and anti-tumor effect which are mainly concentration, duration and context dependent (Jenkins et al. 1995; Forrester et al. 1996; Ambs et al. 1998; Xu et al. 2002, Wink et al. 1998). Since role of NO has also been demonstrated in oral cancer (Shin et al. 2008; Gallo et al. 1998; Czesnikiewicz et al. 2008), we next determined the levels of inducible nitric oxide synthase (iNOS) in the oral tumor tissue samples. Interestingly, the iNOS levels (85 % cells, $p < 0.001$, one-way ANOVA) were also found to be upregulated in tumor tissue samples and were found to be positively correlated to the B23 and GAPDH levels (compare normal vs tumor in Figure 5.5, panel I). COX2 levels were also found to be higher in tumor tissue samples (86 % cells, $p < 0.001$, one-way ANOVA) (compare normal vs tumor in Figure 5.5, panel II), which is induced in many cell types by different stimulus, cytokines and by tumor promoters and has been found to be

upregulated in many cancers including oral cancer (Wallace et al. 2002; Mallery et al. 2008; Chan et al. 1999; Gallo et al. 2002; Connelly et al. 2005). These results suggest a possible role these proteins in oral cancer manifestation. It should be mentioned here that all the IHC data shown here are of same tissues samples and are representative IHC data for the experiments done with several tissue samples.

Recent works suggest NO dependent role of GAPDH in the proapoptotic response where NO mediated nuclear translocation of GAPDH activates p300 autoacetylation and mediates p53 dependent apoptosis (Sen et al. 2008). In contrast to this, some reports also suggest that nuclear GAPDH do not cause apoptosis (Dastoor et al. 2001). As the nuclear GAPDH is known to activate p300 catalytic activity and our observation also suggest increase of GAPDH levels in oral cancer samples with a concomitant increase in histone acetylation, we next investigated the localization of GAPDH in oral cancer tissue samples. Surprisingly, GAPDH was found in the nucleus of oral cancer patient samples (90% cells, $p< 0.0001$, one-way ANOVA) (compare normal vs tumor in Figure 5.3, panel I, red arrow in tumor sample indicate the presence of nuclear GAPDH). This observation led us to determine the role of NO on the B23 and GAPDH protein expression levels. KB cells were treated with the NO donor, S-nitroso-glutathione (GSNO) for 24h. It was found that, NO increased the B23 and GAPDH levels in concentration dependent manner in KB cells (Figure 5.6, panel a, compare lanes 2,3 vs lane 1). Tubulin was used as a loading control. Taken together these observations suggest a role of NO signaling in oral cancer manifestation.

It has been reported that GAPDH get acetylated by p300 in a NO dependent manner (Sen et al. 2008), this led to determine the role of NO in B23 acetylation. It is pertinent to point out at this juncture that our laboratory has found that B23/NPM1 gets acetylated by p300, which is essential for its transcriptional coactivator ability from chromatin template (Swaminathan et al. 2005). B23 was also found to be overexpressed and hyperacetylated in oral cancer samples (Shandilya J and Kundu T.K., unpublished). However, next we treated KB cells with the indicated amount of GSNO or glutathione (GSH) (Figure 5.6 b and c). Cell lysate were immunoprecipitate with anti-acetyl Lysine antibody and the immunoprecipitate were analysed by western blotting with the indicated antibodies. Consistently it was found that B23 and GAPDH get acetylated in a NO

dependent manner in KB cells (Figure 5.6 b and c, compare lane 2 vs 1). These data further suggest that NO signaling has a role in oral cancer manifestation, specially the involvement of acetylation of B23 and GAPDH.

Oral cancer is an inflammatory related disease which can lead to NO production and can have impact on initiation and progression stages of cancer (Gallo et al. 1998; Shin et al. 2008; Xu et al. 2002; Wink et al. 1998). Interferon γ (IFNγ) is a proinflamatory cytokine with plieotropic effect and has roles in cell proliferation and apoptosis which is known to

(a)   **(b)**
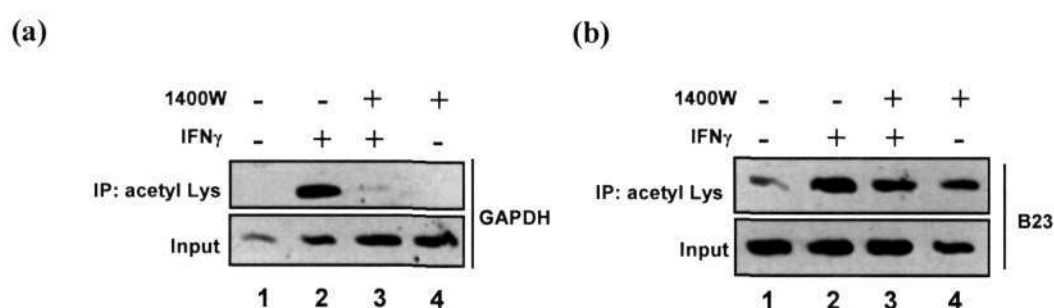
Figure 5.7. IFNγ dependendent acetylation of GAPDH and B23. Increased acetylation of GAPDH (a) (left panel) and B23 (b) (right panel) in KB cells treated with IFNγ (10 ng ml⁻¹) for 16 h. Acetylation is inhibited by the iNOS inhibiotor 1400W (100 μM). Anti-acetyl Lysine antibody were used to immunoprecipitate the cell lysate which were analysed by western blotting with the indicated antibodies.

activate iNOS gene expression to produce NO (Fukumura et al. 2006). Recent work suggests the role of IFNγ on GAPDH acetylation in macrophage RAW264.7 cells (Sen et al. 2008).This led to investigate the affect of IFNγ on GAPDH and B23 acetylation. KB cells were treated with IFNγ for 16 h and cell lysates were prepared. Cell lysate were immunoprecipitate with anti-acetyl Lysine antibody and the immunoprecipitate were analysed by western blotting with the
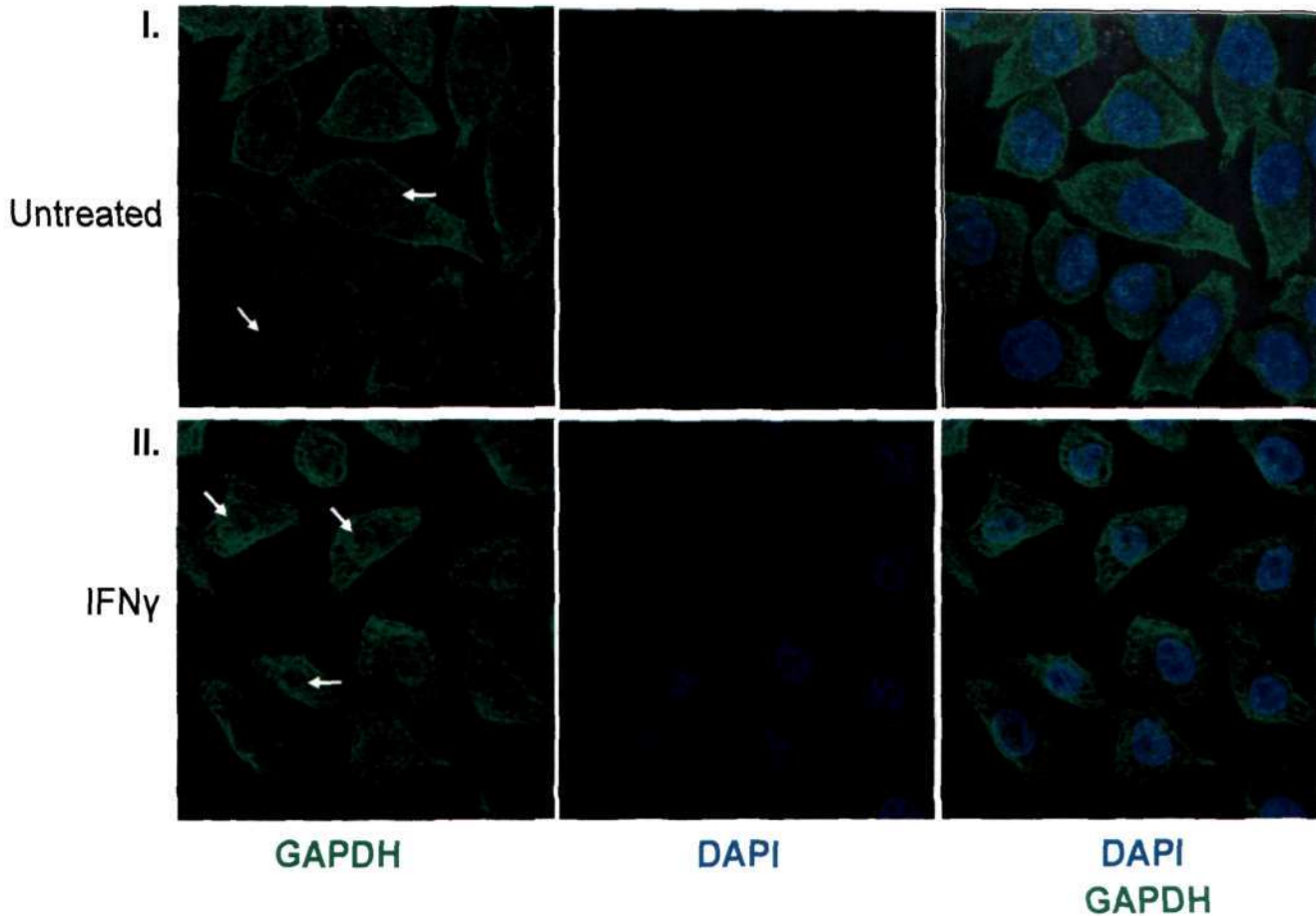
Figure 5.8 GAPDH translocates to the nucleus of KB cells after exposure to IFNγ. KB cells were treated with IFNγ (10 ng ml⁻¹) for 16h and stained with immunofluorescent anti-GAPDH antibodies and DAPI (green, GAPDH; blue, DAPI). IFNγ caused the nuclear translocation of GAPDH (panel II) as compared to untreated control (panel I). White arrows indicate very low level of GAPDH in the nucleus of untreated cells while increased nuclear localization in IFNγ treated cells.

indicated antibodies (Figure 5.7 a and b). It was found that IFNγ treatment enhanced the GAPDH and B23 acetylation in NO- dependent manner in KB cells (compare lane 2 vs 1 and 3 in Figure 5.7 a and b respectively). In these experiments a specific iNOS inhibitor , N-(3-(Aminomethyl)benzyl)acetamidine (1400W) was used as a control which is a highly selective inhibitor of inducible nitric-oxide synthase, iNOS. GAPDH is a cytosolic protein and is known to translocate to nucleus of macrophage RAW264.7 cells activated

with interferon-γ (IFNγ) (Hara et al. 2005). We next determined the affect of IFNγ on GAPDH localization in KB cells. KB cells were treated with IFNγ for 16 h and stained with immunofluorescent anti-GAPDH antibodies. In KB cells GAPDH translocated to the nucleus of KB cells (Figure 5.8, compare panel II vs I). Surprisingly, in untreated KB cells also a weak presence of GAPDH in the nucleus was noticed (Figure 5.8, see panel I). This is consistent to some report where presence of GAPDH in the nucleus has been observed (Dastoor et al. 2001; Sirover et al. 1999; Harada et al. 2007). Consistently, several studies have demonstrated that GAPDH serves to a number of non-glycolytic nuclear processes such as nuclear tRNA transport, apoptosis, DNA repair, and DNA replication (Sirover et al. 1999) and has been identified as a component of the eukaryotic transcription machinery (Zheng et al. 2003). We also observed the nuclear presence of GAPDH in oral cancer samples (Figure 5.3) where iNOS levels were high (Figure 5.5).

Taken together these results suggest the involvement of NO- signaling in the overexpression of B23 and GAPDH and their acetylation in KB cells in oral cancer manifestation. These data is also supported from the fact that in oral tissue samples B23, GAPDH and iNOS levels are overexpressed (as mentioned above).
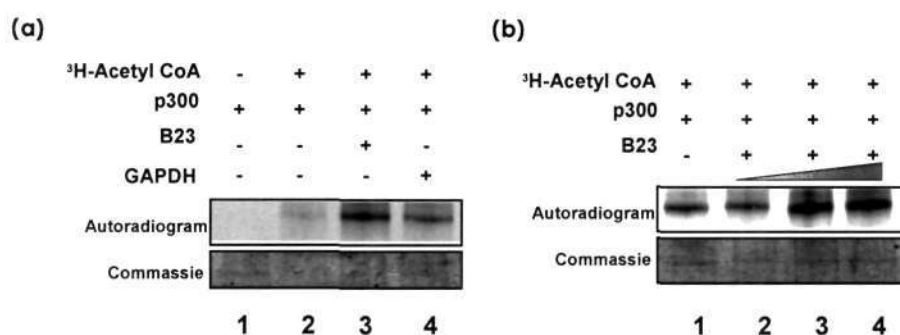
Figure 5.9. B23 enhances the autoacetylation of full length p300 (p300fl) *in vitro*. Left panel (a), autoacetylation of p300fl was examined with ³H-acetyl CoA in presence or absence of B23. GAPDH (600 ng) was used as a positive control. Right panel (b), B23 enhances the p300 autoacetylation in concentration dependent manner. Autoacetylation of p300fl (100ng) with B23 (300, 600 and 900 ng) was performed in presence of ³H-acetyl-CoA which was subjected to fluorography followed by autoradiography.

The increase levels of B23 and GAPDH in NO dependent manner and a similar pattern observed in oral cancer tissue samples (where B23, GAPDH and iNOS levels are high)

with concomitant levels of hyperacetylated histone H3K14 prompted us to investigate the role of B23 on p300 autoacetylation. Autoacetylation reaction of p300 was performed in the presence of B23 and ^{3}H-acetyl-CoA. B23 was found to activate the autoacetylation of p300 (Figure 5.9 a, compare lane 3 vs 2). GAPDH was used as a positive control (Figure 5.8 a, compare lane 4 vs 2) as suggested earlier (Sen et al. 2008). As expected, B23 also augmented autoacetylation of p300 in dose dependent manner (Figure 5.9 b, compare lanes 2,3 and 4 vs 1). These observations suggest the role B23 in enhancing the autoacetylation of p300 which is similar to that of GAPDH mediated autoacetylation of p300 (Sen et al. 2008).

Physiological activation of catalytic activity of p300 by B23 and GAPDH (Sen et al. 2008) should lead to enhance substrate acetylation. Histone being a major physiological substrate of HAT p300, so we next looked into the role of NO on H3K14 acetylation level in KB cells. KB cells were treated with increasing concentration of
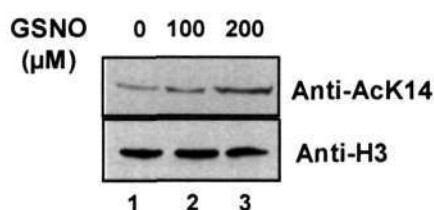
Figure 5.10. NO caused the hyperacetylation of Histone H3K14. Histones were isolated from the indicated concentration of GSNO treated KB cells for 24 h (lane 1 to 3). Histone acetylation was analysed by western blotting with anti-acetylated H3K14 antibody (upper panel). Anti-H3 antibody was used as a loading control (lower panel).

GSNO, histones were isolated and western analysis were performed (Figure 5.10). It was found that H3K14 acetylation increased in NO dependent manner (Figure 5.10, compare lanes 2 and 3 vs 1) with a concomitant increase in B23 and GAPDH levels as shown earlier (Figure 5.6 a). These data stabilishes the role of B23 and GAPDH in enhancing the H3K14 acetylation by activating p300 HAT activity via autoacetylation in NO dependent manner in oral cancer. This is similar to the increased p300 HAT activation upon GAPDH nuclear translocation as suggested earlier (Sen et al. 2008).

Overexpression of B23 and GAPDH is known to have antiapoptotic effect and an increase in B23 and GAPDH levels upon NO signaling may help the fast growing cell to cope up with the growing needs of the cancerous cells which involve energy requirement and increase ribosome biosynthesis. At the same time presence of nuclear GAPDH in the oral cancer samples suggest that antiapoptotic forces in oral cancer cells are dominant which is evident from the enhanced levels of B23 in these cancer samples. Further, an increase NO generation in oral cancer cells may further select mutant p53 cells which can drive the clonal selection of mutant p53 cells where apoptosis is impaired, which may lead to cancer. It has been shown that p53 is mutated in about 50% of oral cancer (Xu et al. 2002). In this context, it should also be noted that NO-triggered GAPDH cell death pathway is p53 dependent (Sen et al. 2008), consistant to which it is also reported that losses of p53 function by inactivating mutations abrogate NO-induced apoptosis in human lymphoblastoid cells (Li et al. 2004) which also support the present findings.

5.3.3. CTK7A is a histone acetyltransferase (HAT) inhibitor:

Previously, we have shown the development and use of HAT inhibitors (HATi) for therapeutic purposes (Balasubramanyam et al. 2004; Mantelingu et al. 2007; Swaminathan et al. 2007) Therapeutic use of HATi is limited because of the solvent toxicity and solubility problems. While working with above problem we wish to use HATi in mice system to study the potential clinical impact. Curcumin is one of the major constituent of plant *Curcuma longa* which has been shown to be a specific inhibitor of HAT p300 (Balasubramanyam et al. 2004). Further, curcumin is also known to have anticancer properties (Aggarwal et al. 2003; Sharma et al. 2005). Using curcumin as synthon a water soluble derivative, CTK7A was synthesized (Figure 5.11 a) (For synthesis and characterization please see Materials and Methods). CTK7A was found to inhibit HAT p300/CBP and PCAF but no observed affect on other histone modifying enzyme like G9a, CARM1, Tip60, HDAC1 and SIRT2 (Figure 5.11 b). Further kinetic analysis revealed that CTK7A follows non-competitive type of inhibition pattern for both

(a)

CTK 7A

(b)

(c)
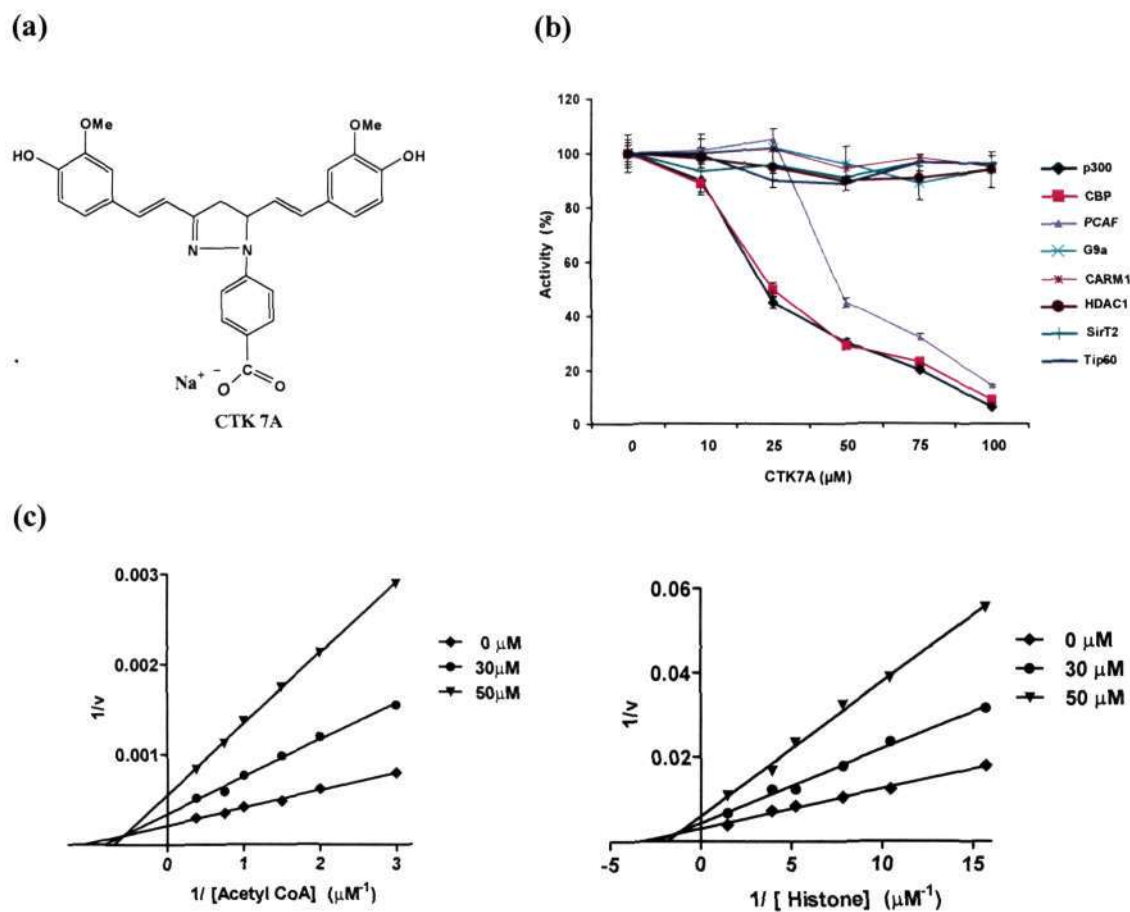
Figure 5.11. CTK7A is a water soluble HAT inhibitor. **(a)** Structural formula of CTK7A, Sodium 4-(3,5-bis(4-hydroxy-3-methoxystyryl)-4,5-dihydropyrazol-1-yl)benzoate **(b)** Inhibition curves for various recombinant HATs, HMTs and HDACs. Respective assays were performed as described in Materials and Methods. Reactions were done in duplicate and error bars reflect the standard deviation from at least two different experiments. **(c)** CTK7A is a non-competitive inhibitor of p300. Lineweaver-Burk plots for effect of CTK7A on p300 mediated acetylation of highly perified HeLa core histones. Filter binding assays were performed in the presence and absence of 30 and 50 μM CTK7A with different substrate concentrations as mentioned in Materials and Methods. Each experiment was performed three times, and reproducibility was within 15%. Representative figure is shown.

(a)

HAT	+	+	+	+	+	+	+	+
³H-Acetyl CoA	-	+	+	+	+	+	+	+
CTK7A (μM)	-	-	25	50	75	100	-	-
Curcumin	-	-	-	-	-	-	-	100
DMSO	-	-	-	-	-	-	+	+

Autoradiogram

p300

Commassie

1 2 3 4 5 6 7 8

(b)

HAT	+	+	+	+	+	+	+	+
³H-Acetyl CoA	-	+	+	+	+	+	+	+
CTK7A (μM)	-	-	25	50	75	100	-	-
Curcumin	-	-	-	-	-	-	-	100
DMSO	-	-	-	-	-	-	+	+

PCAF

Autoradiogram

Commassie

1 2 3 4 5 6 7 8
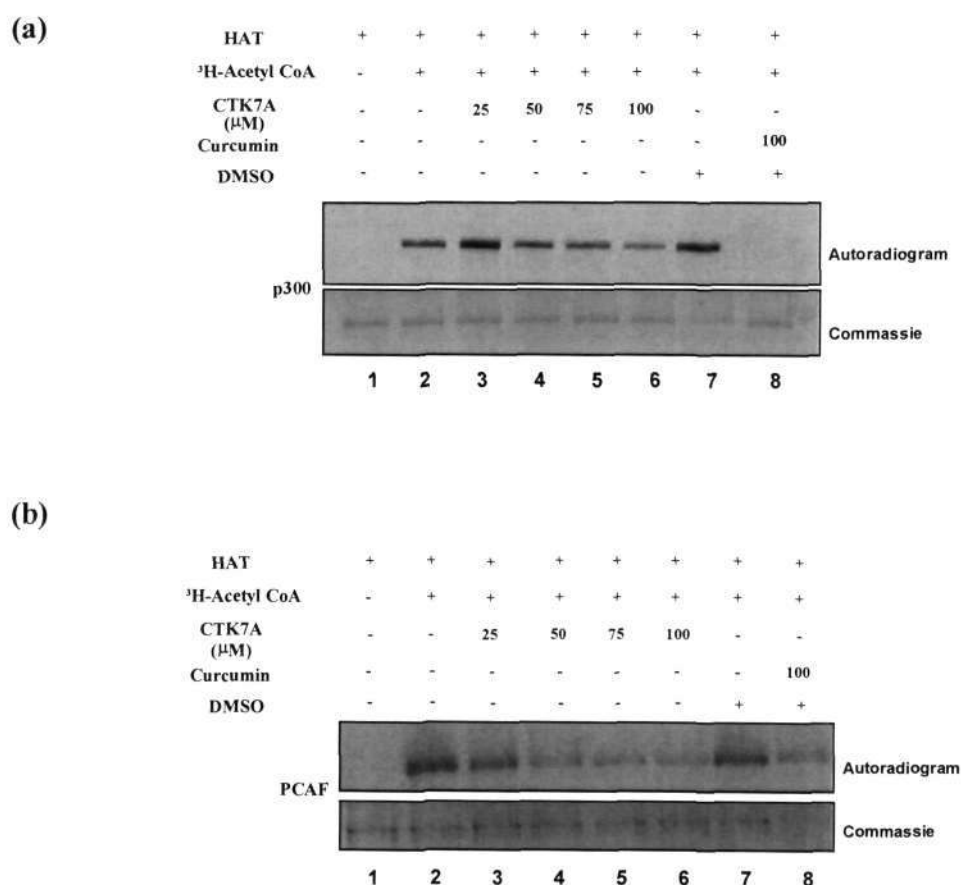
Figure 5.12. CTK7A inhibits p300fl and PCAF autoacetylation *in vitro*. **(a)** Autoacetylation assays were performed using p300fl in the absence and in the presence of ³H-acetyl CoA with indicated concentration of CTK7A. Curcumin was used as a positive control while DMSO acts as a solvent control for curcumin. Reaction mixtures were resolved on 8 % SDS-PAGE and processed for fluorography. **(b)** CTK7A inhibits PCAF autoacetylation in vitro. Autoacetylation assays were performed using PCAF in the absence and in the presence of ³H-acetyl CoA with indicated concentration of CTK7A. DMSO acts as a solvent control for curcumin. Reaction mixtures were resolved on 10 % SDS-PAGE and processed for fluorography.

the substrate, acetyl-coA and core histone when tested for p300 (Figure 5.11 c). This is similar to the inhibition pattern of curcumin for p300 (Balasubramanyam et al. 2004). As mentioned earlier, p300 autoacetylation augments its acetyltransferase activity (Thompson et al. 2004). So next the affect of CTK7A on p300 autoacetylation was determined. CTK7A inhibited the autoacetylation of p300 (Figure 5.12 a, compare lane 3,

4, 5, and 6 vs2) and PCAF (Figure 5.12 b, compare lane 3, 4, 5, and 6 vs 2) in vitro in concentration dependent manner.

Since p300 and its HAT activity was found to get upregulated in oral cancer so the relevance of these invitro findings to the inhibition of p300 in vivo (in KB cells) were investigated. Different experiments in cellular systems were performed.
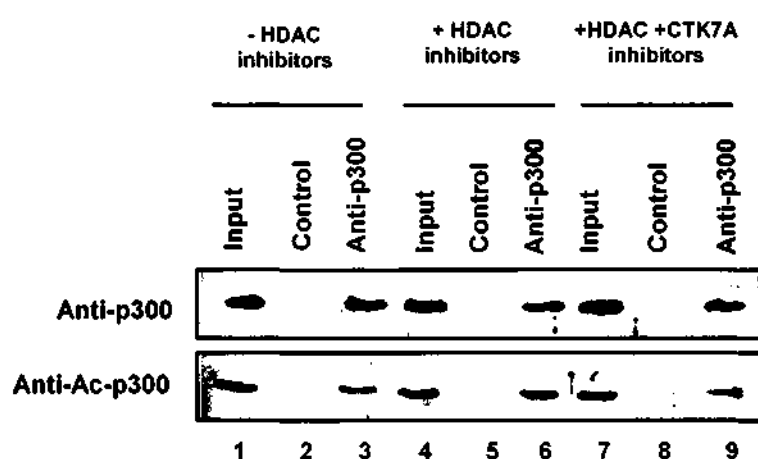
Figure 5.13. CTK7A inhibits p300 autoacetylation *in vivo*. Cell lysate were prepared from KB cells without any treatment (lane to 3), treated with cocktail HDAC inhibitors without (lane 4 to 6) and with CTK7A (lane 7 to 9) and immunoprecipated with anti-p300 and control (IgG) antibody. Immunoprecipitates were analysed by western blotting with anti-ac-p300 antibody (lower panel) and anti-p300 monoclonal antibody (upper panel). Cocktail HDAC inhibitors were used as a positive control.

p300 was immunoprecipitated from KB cells which can be recognized by monoclonal p300 antibody (Sigma). CTK7A inhibited the enhanced autoacetylation mediated by cocktail HDAC inhibitor (Figure 5.13, compare lane 9 vs 6). Cocktail of HDAC inhibitors were used to increased the autoacetylation levels of p300 in cells (Thompson et al. 2004; Black et al. 2008). Here it should be mentioned that human SirT2 has recently been identified as a deacetylase for the autoacetylated p300 in cells (Black et al. 2008). This suggests that indeed CTK7A inhibit the p300 autoacetylation in cells. Next to see the affect of CTK7A on the inhibition of histones acetylation in cells, KB cells were

(a)

DMSO	-	+	+	-
Curcumin (µM)	-	-	100	-
CTK7A (µM)	-	-	-	100

α AcH3

α H3

1 2 3 4

(b)

DMSO	-	+	+	-
Curcumin (µM)	-	-	100	-
CTK7A (µM)	-	-	-	100

α AcH3

α H3

1 2 3 4

(c)

DMSO	-	+	+	-
Curcumin (µM)	-	-	100	-
CTK7A (µM)	-	-	-	100

α AcH3

α H3

1 2 3 4
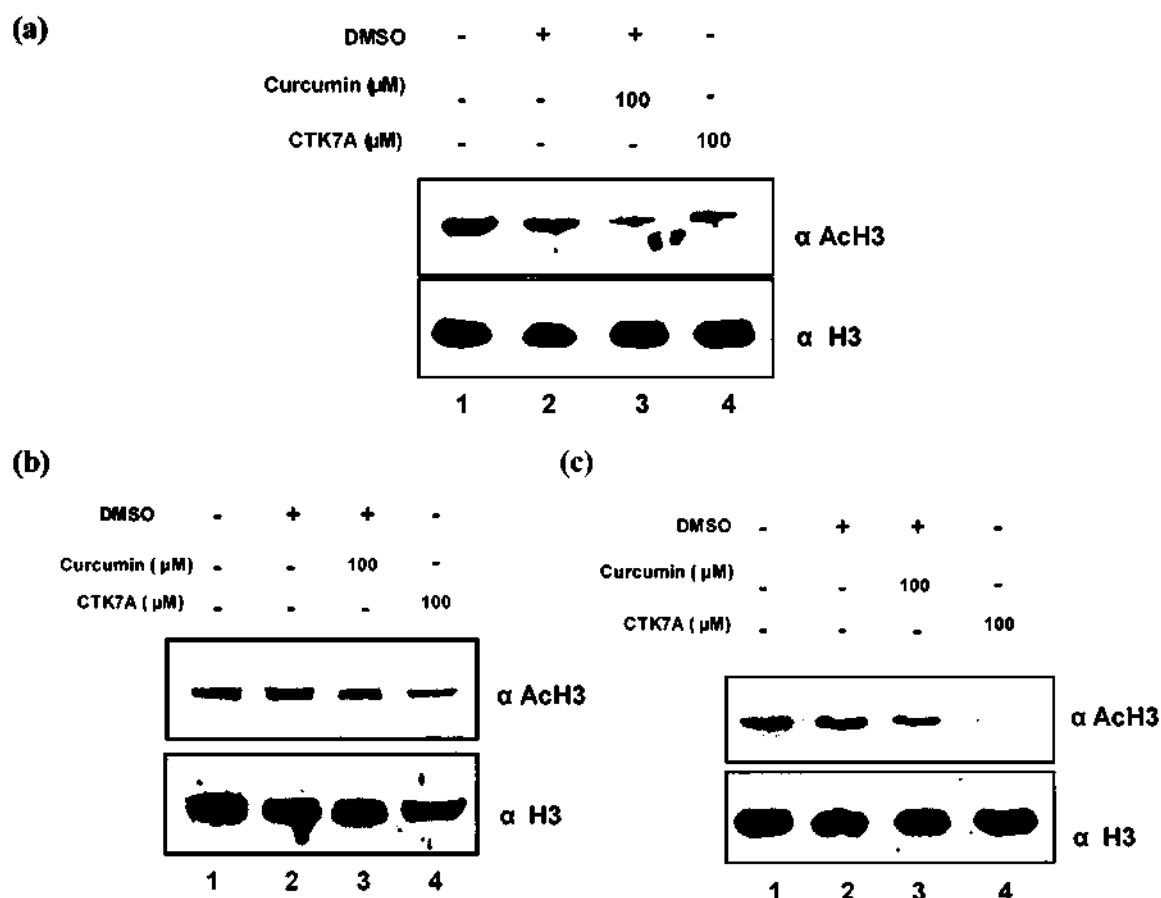
Figure 5.14. CTK7A inhibits histone acetylation in vivo. CTK7A inhibits histone acetylation in KB cells (a), HepG2 cells (b), and in Hela cells (c). Histones were isolated from these cells after treatment with CTK7A or curcumin at indicated concentration after 24 h. Histone acetylation was analysed by western blotting with anti-acetylated H3 (top panel) antibody. Anti-H3 was used as a loading control (lower panel).

treated with 100µM of CTK7A and as expected it could potently inhibit the histone acetylation in KB cells (Figure 5.14 a , compare lane 4 vs 1). Curcumin could also potently inhibit the histone acetylation in KB cells (Figure 5.14 a, compare lane 3 vs 2), which is consistent to earlier report (Balasubramanyam et al. 2004). Similar results were found with HepG2 and Hela cells (Figure 5.14 b and c respectively, compare lane 4 vs 1).

Taken together these results that water soluble HATi, CTK7A inhibited histone acetylation via inhibiting p300 autoacetylation. These results further suggest a possible use of CTK7A for therapeutic use as in the case of oral cancer as shown here.

5.3.4. CTK7A inhibits cell proliferation and induces senescence like growth arrest:
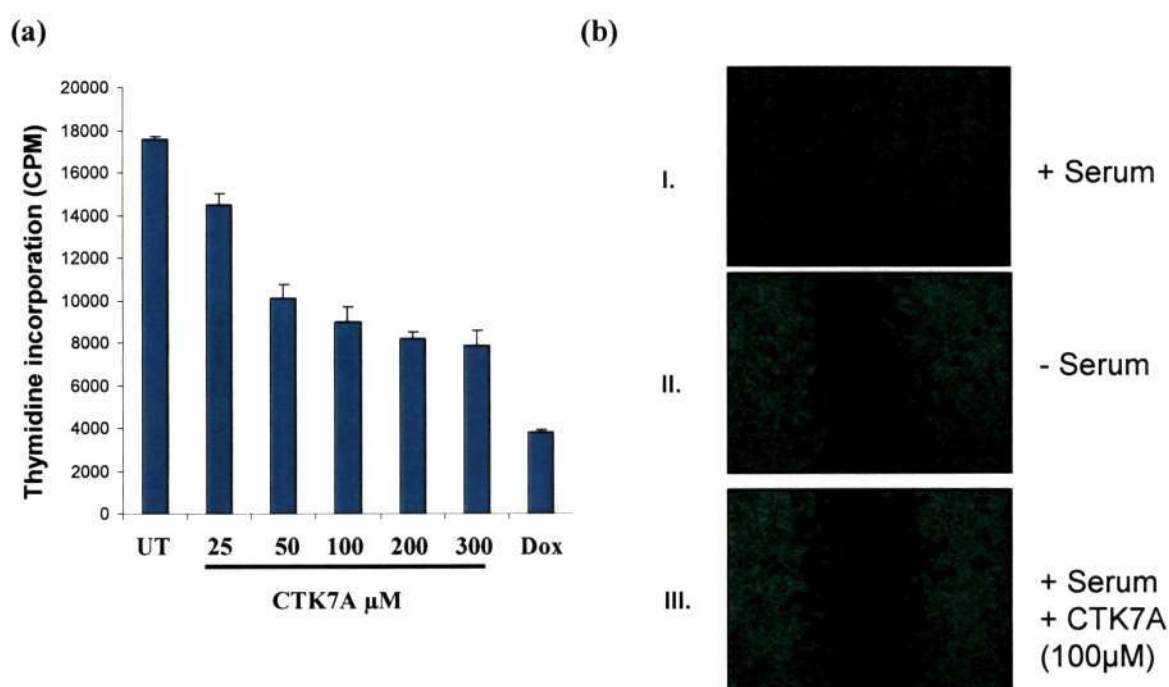
Figure 5.15. CTK7A inhibits the growth of KB cells and induces Senescence-like growth arrest. (a) CTK7A inhibits the growth of KB cells. Cell proliferation was examined by [3H]thymidine incorporation assay after treatment with different concentration of CTK7A as indicated. Doxorubicin (100 µM) was used as positive control. Each experiment was performed in duplicate and error bars reflect the standard deviation from three different experiments. (b) CTK7A inhibits wound healing. Post-confluent KB cells were used in this experiment. Wounds with a constant diameter were made. Cells were treated with CTK7A (100 µM) for 24 h along with 10% serum. The wound photographs were taken under phase-contrast microscope. Serum positive and negative cells act as positive and negative control respectively.

p300/CBP is a master regulator and its role in cell cycle progressionproliferation, differentiation and in maintaining tissue homeostasis is well stabilished. (Goodman et al. 2000). Next the growth inhibitory properties of CTK7A in cells was investigated. KB
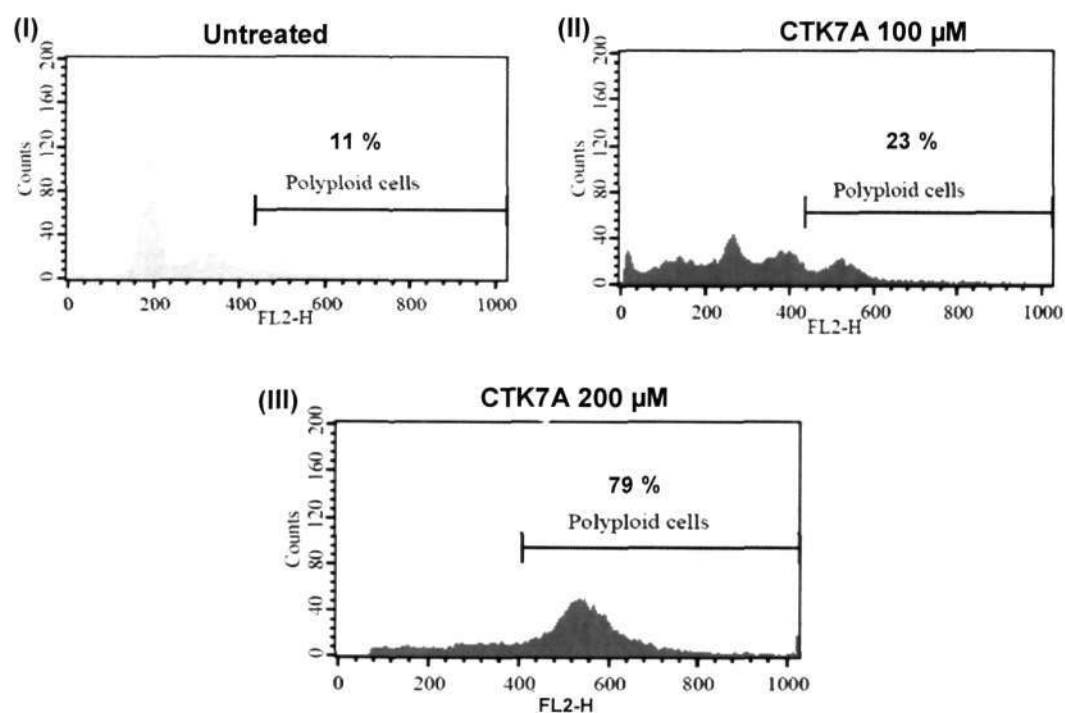
Figure 5.16. CTK7A induces polyploidy in KB cells. KB cells were incubated with the indicated doses of CTK7A for 24 h and were analysed by flow cytometry. In CTK7A treated cells, cell population with DNA content >4N (polyploidy) were increased (panel II and III) compared with untreated KB cells (control) (panel I).

cells were treated with CTK7A and assayed for the growth inhibitory properties using the thymidine-incorporation assay (see Materials and Methods). CTK7A caused a dose dependent inhibition of proliferation of KB cell (Figure 5.15 a). Doxorubicin was used as positive control (Figure 5.15 a). Antiproliferative activity of CTK7A was further assessed in wound healing assay. Post-confluent KB cells were used in these experiments. Wounds with a constant diameter were made using sterile 200µl pipette tip. Cells were treated
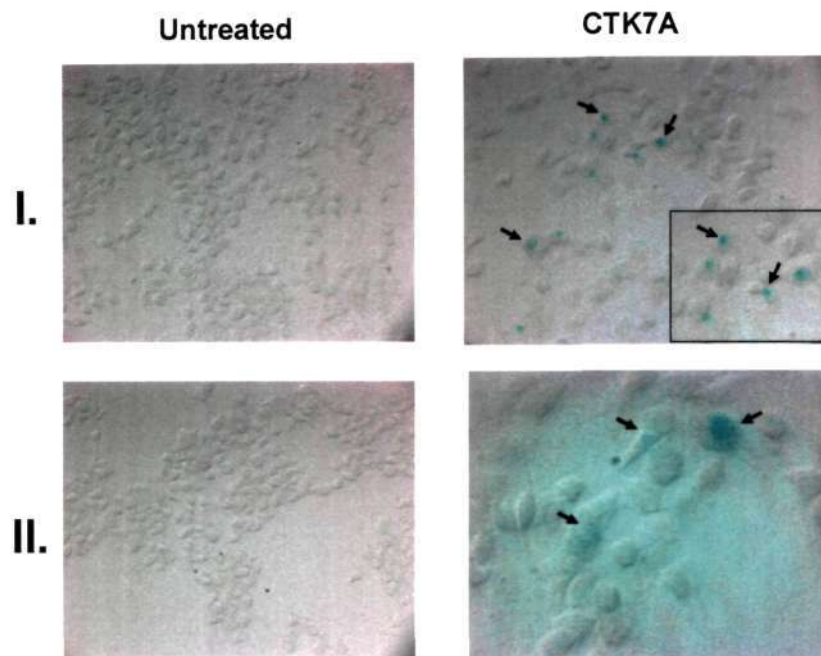
Figure 5.17. CTK7A induces Senescence-associated β-gal expression (SA-β-gal) in KB cells. KB cells were incubated with 100 μM of CTK7A for 24 h. Cells were stained for SA-β-gal. CTK7A treatment induces the SA-β-gal expression in treated cells (right panel) as compared to untreated, control (left panel). Images in the panel I and panel II are of two different experiments. Panel II in CTK7A treated the figure is the magnified image of the cells expressing SA-β-gal.

with CTK7A (100 μM) for 24 h along with 10% serum. The wound photographs were taken under phase-contrast microscope. Serum positive and negative cells were used as positive and negative controls, respectively (Figure 5.15, panel I and II respectively). CTK7A treated cells inhibited the healing of wound in the presence of serum (Figure 5.15 b, compare panel III vs I). These results suggest the antiproliferative role of CTK7A in KB cells. Based on the above results, the affect of CTK7A on cell cycle of KB cells was also determined. KB cells were treated with the increased concentration of CTK7A (Figure 5.16) which caused a dramatic increase in the percentage of polyploidy cells (>4N) in concentration dependent manner (see Figure 5.16, compare panels III and II vs I). These results suggest the role of CTK7A in the induction of polyploidy and hence augmenting the antiproliferative affect on KB cells.

Senescence is known to have antitumor process (Campisi, J. 2005). Induction of senescence is known to contribute to the treatment of chemotherapy, ionization radiation and is also shown to contribute to the antitumor efficacy of HDAC inhibitors (Mathon et al. 2001; Wang et al. 2003; Ben-Porath et al. 2004; Kahlem et al. 2004; Pelicci et al. 2004; Sharpless et al. 2004; Shay et al. 2004; Ota et al. 2006).

Essential role of p300 regulating proliferation and senescence in cells are also shown in human melanocytes where the exposure of p300 specific HATi, lysyl-coA (a
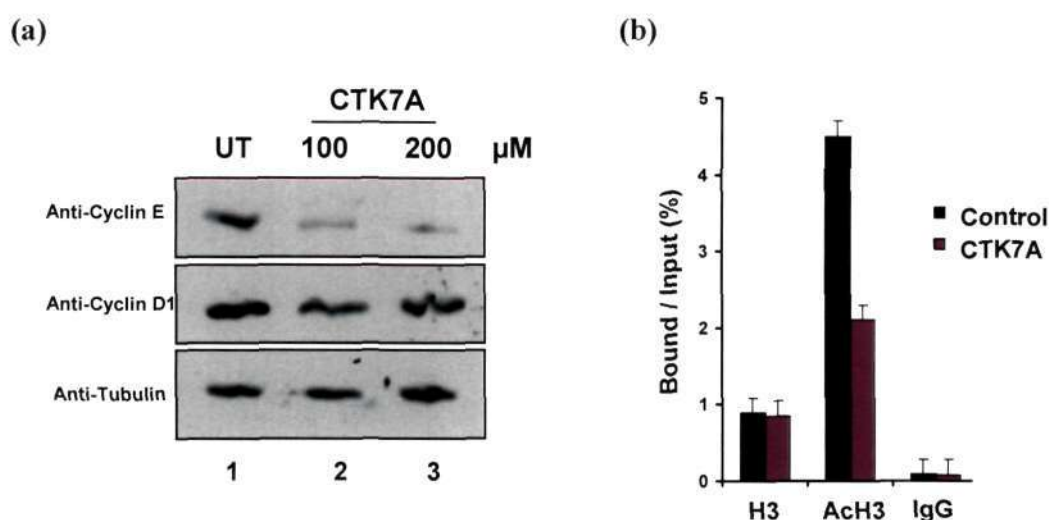
Figure 5.18. CTK7A affects cell cycle progression by inhibiting cyclinE expression. (a) KB cells were treated with the indicated concentration of CTK7A for 24 h. Cell lysates were prepared and analysed by western blotting with anti-cyclinE and anti-cyclinD1 antibodies. Tubulin was used as a loading control. CTK7A reduces the H3 acetylation at cyclinE promoter. (b) KB cells were treated with CTK7A (100 µM) for 24 h. ChIP analysis at the promoter of cyclinE using antiH3 and anti-acetylated H3 antibodies were performed. IgG was used as a loading control. Values are relative to immunoprecipitated input DNA. Error bars indicate standard deviation from three independent ChIP experiments.

substrate analog of acetyl-CoA) is shown to inhibit proliferation and induces senescence-like growth arrest with expression of senescence associated beta-galactosidase (SA-β-gal) (Bandyopadhyay et al. 2002). This led us to determine whether CTK7A induced polyploidy could undergo senescence. It was found that CTK7A treated cells induced the expression of SA-β-gal which is a marker for senescence (Figure 5.17, compare CTK7A

treated vs untreated columns in panel I and II). These results suggest that CTK7A induced polyploidy lead to senescence like phenotype in KB cells. Further it can also be suggested that CTK7A mediated p300 HAT inhibition is directly involved in this process as mentioned above.

Cyclin E is a critical regulator of senescence because under overexpression condition it is sufficient to escape from BRG1 and RAS- induced senescence (Peeper at al. 2002; Shanahan et al. 1999).Given that p300/CBP regulate expression of many cell cycle genes. Next the affect of CTK7A on the expression of cyclin E was determined. It was found that cyclin E is down regulated in KB cells in a dose dependent manner while cyclin D1 was affected marginally (Figure 5.18 a, compare lane 2and 3 vs 1). Earlier work suggest that cyclin E promoter in human tumor cells and in mouse embryonic fibroblast is regulated by acetylation and deacetylation cycles (Brehm et al. 1998; Sambucetti et al. 1999; Morrison et al. 2002). Hence, to address the affect of CTK7A on acetylation status at the cyclin E promoter chromatin immunoprecipitation (ChIP) assays were performed as reported earlier (Bandyopadhyay et al. 2002). ChIP assays clearly demonstrated that CTK7A inhibited the acetylation of H3 at the cyclin E promoter (Figure 5.18 b). These results further confirms that cyclin E down regulation appears to be a direct cause of p300 HAT inhibitory activity of CTK7A which would be responsible for the senescence-like growth arrest in KB cells.

5.3.5. CTK7A inhibits tumor growth:

The in vitro and cell line based studies prompted us to study the role of CTK7A in xenograft mice. The most important test of drug specificity and efficacy for in vivo cancer administration, which allows of the drug toxicity towards different types of normal cells versus tumor cells. CTK7A was well tolerated in mice after intraperitoneal (i.p) administration with no observed weight loss at doses up to 100 mg/kg body weight/ twice a day during 1 month.

In order to test the affect of CTK7A on tumor growth, KB cells (2x 10^6 cells) were inoculated in nude mice in the right and left flanks, respectively and were treated intraperitoneally with 100 mg/kg body weight/ twice a day (for detail see Materials and

Methods). Mice were divided into 2 groups and each group contained 8 mice. After CTK7A treatment for about 3 weeks tumor samples were used for histopathological and immunohistochemistry (IHC) studies according to the standard procedure.
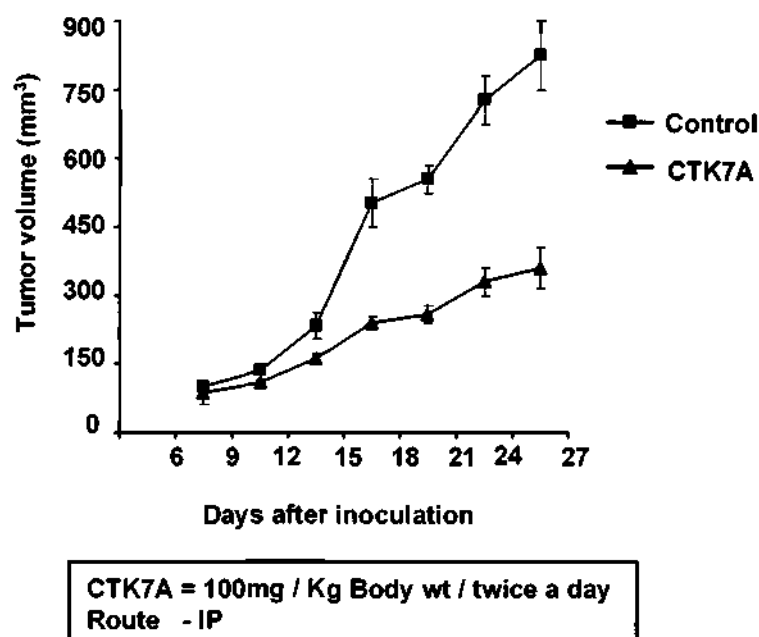
Figure 5.19. CTK7A inhibits oral tumor growth in nude mice. Nude mice carrying the KB cell xenografts were treated with phosphate buffered saline (control) or with CTK7A intraperitonially with 100 mg/Kg body weight/ twice a day. Tumor volumes (mm^3) were determined every third day from sixth day onwards as described in Materials and Methods. One-way ANOVA revealed that tumor sizes were significantly different ($p < 0.05$).

CTK7A showed a strong antitumor activity (Figure 5.19). KB cell tumors were 50% smaller in mice treated with CTK7A than in control untreated mice. The differences in the tumor size between xenografts (Control vs treated) was statistically significant ($p < 0.05$). The levels of H3 acetylation and that of other proteins (e.g. B23, GAPDH, p300) were determined as mentioned earlier using IHC. CTK7A treated mice tumors showed marginal affect on p300 expression (Figure 5.19, compare control vs treated of panel I). It was found that CTK7A decreased the levels of ac-p300 (autoacetylated p300) (86 % cells in treated were -ve staining, $p< 0.001$, one-way ANOVA), H3K9 and K14

180

acetylation (as probed by H3AcK9AcK14) (70% cells in treated were -ve staining, p< 0.001, one-way ANOVA) (see Figure 5.20, compare control vs treated of panel II and III respectively). Further to see the site specific affect of CTK7A mediated HAT inhibition on histone acetylation. IHC were done with site specific antibodies. It was found that CTK7A inhibited the H3K14 acetylation (71% cells in treated were -ve staining, p< 0.001, one-way ANOVA) more potently than H3K9
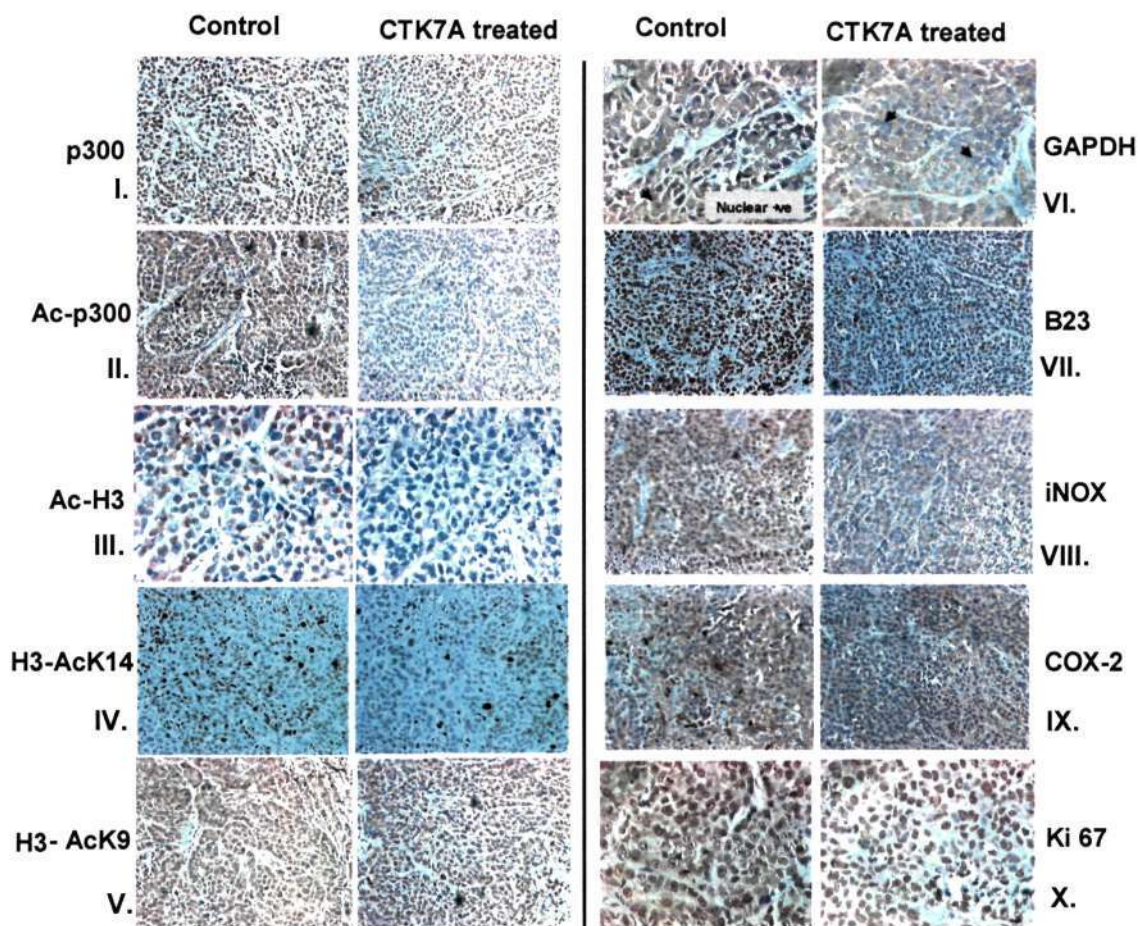
Figure 5.20. CTK7A inhibits histone acetylation in nude mice. KB cell tumors from control and CTK7A treated mice were used for immunohistochemical detection with indicated antibodies as performed earlier. In case of control tumor sample arrow mark indicates the nuclear localization of GAPDH while it is absent in CTK7A treated tumor. Images acquired at 40X magnification. IHC were done with tissues obtained from different mice and shown is a representative figure of IHCs done with several tissue samples.

acetylation (50% cells in treated were -ve staining, p< 0.01, one-way ANOVA) (Figure 5.20, compare control vs treated of panel IV and V respectively). These data further suggest that CTK7A mediates inhibition of histone acetylation mainly via inhibition of p300 autoacetylation in mice cancer tissue which could lead to tumor growth inhibition. These data are also consistent with the antiproliferative affect of CTK7A on KB cells (Figure 5.15). Further, the levels of GAPDH, B23 and iNOS (60%, 75% and 73% cells in treated were -ve staining, p< 0.01, one-way ANOVA) were also found to be down regulated in CTK7A treated mice which could be because of antiproliferative affect of CTK7A on mice tumors (Figure 5.20, compare control vs treated panels of panel VI, VII and VIII respectively). Moreover, the levels of COX2, which is induced in many cell types by mitogens, growth factors, cytokine and tumor promoters and has been implicated in many cancers which includes oral cancer was also found to be suppressed in CTK7A treated tumors (72 % cells in treated were -ve staining, p< 0.01, one-way ANOVA) (Figure 5.20, compare control vs treated panels of panel IX). Next we determined the expression levels of the proliferation marker, Ki-67. Ki-67 expression levels were found to be down regulated in CTK7A treated tumors (70% cells in treated were -ve staining, p< 0.01, one-way ANOVA) (Figure 5.20, compare control vs treated panels of panel X). It should be noted here that in the control mice we observed the presence of nuclear GAPDH while nuclear GAPDH were absent or very faintly present in the CTK7A treated mice (74% cells in treated were -ve staining, p< 0.01, one-way ANOVA). This could be because of the downregulation of iNOS levels where reduced NO production could not stimulate the translocation of cytosolic GAPDH to the nuclei.

These results suggest that CTK7A inhibited the tumor growth in nude mice in HAT dependent manner. Induction of polyploidy by CTK7A in cells has antitumor mechanism by inducing senescence like growth arrest since senescence like growth arrest has been suggested to have antitumor activity as mentioned above. Because p53 abnormalities are common in human tumors so as in oral cancer, this pathway may play an important role in the antitumor mechanism of CTK7A.

Further these results clearly shows the involvement of B23, GAPDH, iNOS and histone hyperacetylation could be associated to tumor growth in oral cancers in human and have prognostic values. These studies also support the idea of a

feed-forward activation mechanism (Sen et al. 2008) wherein p300 acetylates and augments the ability of B23 and GAPDH to stimulate the autoacetylation of p300, which further acetylates B23 and GAPDH (Figure 5.21). This cascade is consistent with recent reports that acetylated B23 is present predominantly in the nucleoplasm of oral cancer patient samples and similar observation were made in KB cells where acetylated B23
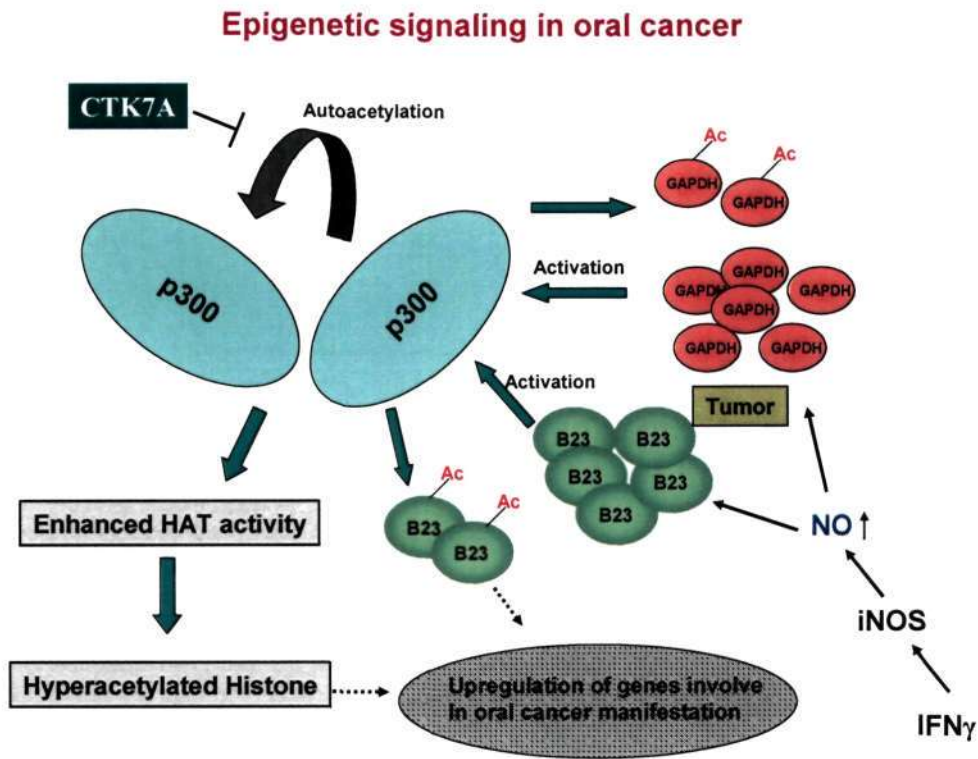
Figure 5.21. Schematic diagram of NO dependent B23-GAPDH-p300 signaling pathway in oral cancer. NO triggers the upregulation of B23 and GAPDH which in turn get acetylated by p300. B23 and GAPDH enhance the HAT activity of p300 which leads to hyperacetylation of histones. Hyperacetylation of histone may lead to upregulation of genes involved in oral cancer manifestation.

colocalizes with the active transcription foci (Shandilya J and Kundu T.K., unpublished). In this context it should be mentioned that B23 get specifically acetylated by p300 (Swaminathan et al. 2005; Shandilya J and Kundu T.K., unpublished), which is essential for the activation of transcription, in conjunction with histone acetylation where the acetylated B23 acts as a better histone chaperone activating the transcription from the

chromatin template (Swaminathan et al. 2005). Recent report suggested that autoacetylation of p300 to be prerequisite for the PIC formation by VP16 (Black et al. 2006). Based on these facts, it is tempting to speculate that B23 mediated autoacetylation of p300 may further enhance the PIC formation by allowing autoacetylated p300 to dissociate from the promoter while the acetylated B23 can further facilitate the histone removal from the promoter region, resulting in enhanced transcription (Swaminathan et al. 2005). This transcription regulation of B23 may have role in oral cancer gene manifestation (Figure 5.21 and Shandilya J and Kundu T.K., unpublished). Similarly GAPDH may also facilitate PIC formation as suggested above and may have role in gene regulation specific for oral cancer.

5.4. Summary:

Histone acetylation is one of the well studied histone modifications and the enzymes that regulate it i.e. HATs and HDACs show altered activities in cancer (Seligson et al. 2005). Here we report for the first time antitumor activity using a water soluble HATi, CTK7A. As suggested (Roth et al. 2001) and predicted (Thompson et al 2004, Liu et al. 2008, Balasubramanyam et al. 2004; Balasubramanyam et al. 2004; Mantelingu et al. 2007) previously, we have successfully demonstrated the antitumour activity of a non-toxic HATi, which has been developed based on the parent molecule curcumin. Curcumin has been shown to have anticancer activity but its solubility in organic solvent like ethanol and DMSO limits its therapeutic use. These results establish a fundamental role for histone hyperacetylation and p300 in maintaining the tumorogenic state in oral cancer. These data correlate the overexpression of cell proliferative marker genes like B23 and GAPDH to the transcription state of the tumorogenic cells as in the case of oral cancer. Present work also convincely delineate the basic link between the metabolic enzyme like GAPDH and nucleolar protein B23 to the master regulator p300 in oral cancer. Our results also show a direct link between the nitric oxide (NO) signaling to oral cancer as suggested earlier (Gallo et al. 1998; Shin et al. 2008; Xu et al. 2002; Wink et al. 1998) which is supported from the fact that iNOS levels were high in oral cancer patient

samples (Figure 5.5, panel I). Given that oral cancer may originate from chronic inflammation that can lead to the production of chemical intermediated like NO (Xu et al. 2002; Wink et al. 1998), which in turn enhances the expression B23 and GAPDH and which further activates p300 catalytic activity that results in aberrant hyperacetylation of histone. These events can further lead to aberrant gene expression involved in tumorogenesis (Figure 5.21). Our observations also get supported from the fact that B23 and iNOS has oncogenic properties (Lim et al. 2006; Grisendi et al. 2006; Fukumura et al. 2006; Xu et al. 2002; Wink et al. 1998)and iNOS and B23 inhibitors have been shown to have antitumor activities (Fukumura et al. 2006; Qi et al. 2008). This work also suggest a role of water soluble HATi in cancer prevention as shown in the nude mice model. In the light of the recent discoveries of different small molecule modulators of histone-modifying enzymes for the treatment of different diseases (Cole P.A. 2008) the new HATi CTK7A may open a new avenue for the use of HATi in cancer therapy.

Thesis Summary

Chromatin is a highly dynamic entity present in the nucleus of eukaryotic cells. It is the physiological template for all the nuclear related processes like transcription, replication, recombination, chromosomal segregation and repair. The dynamic interconversion of chromatin between transcriptionally active euchromatin and transcriptionally repressed heterochromatin plays an important role in transcription regulation. It has been shown that the establishment of distinct chromatin region can be achieved through specific covalent modification of histones (e.g. acetylation, methylation and phosphorylation), dynamic nucleosome assembly with histone variants (e.g. H2A.Z, CENPA) or with the help of nucleosome binding non-histone proteins (e.g. HP1, PARP-1 & PC4). Reversible acetylation of histone and non-histone proteins plays an important role in the regulation of gene expression and cellular homeostasis. A balance between acetylation and deacetylation of these proteins are maintained by histone acetyltransferases (HATs) and histone deacetylases (HDACs). Among different HATs, p300/CBP is the most widely studied chromatin modifying enzymes. p300 is involved in several physiological processes like cell growth, regulation of gene expression, development, and tumor suppressor, and therefore its dysfunction causes different diseases, like inflammatory processes, Huntington disease, cardiac disease, diabetes mellitus, AIDS and cancer. These observations lead to consider small molecule modulators (activators and inhibitors) of p300 as potential new generation therapeutics. These small molecule compounds would also be highly useful to probe the functional significance of the histone acetyltransferase activity *in vivo*.

This research work has been initiated with the elucidation of the mechanism of p300 HAT inhibition by specific and non-specific HAT inhibitors: garcinol, IG and LTK14. Among these three polyisoprenylated benzophenones, garcinol and IG inhibit the HAT activity nonspecifically and thereby induce toxicity in human cells, whereas a C-14 monosubstituted methoxy-isogarcinol, LTK14 specifically inhibits the p300 HAT activity with minimal toxicity. Mechanistically, LTK14 behaves as a non-competitive inhibitor for both acetyl-CoA and histone binding site, unlike garcinol and IG, which are competitive for acetyl-CoA binding site but are non-competitive for histone binding site. Furthermore, the ITC data suggest that there is a high affinity enthalpy driven single binding site for LTK14 on p300HAT domain in contrast to two binding sites for both garcinol and IG. It was also found that garcinol and LTK14 induce alteration in the secondary structure which is not marked in case of IG. Furthermore, isobologram and molecular simulation based docking studies suggest that indeed the non-specific inhibitors binds at the acetyl-CoA binding site and the specific inhibitors binds at an allosteric site, a site which could also be common for non-specific inhibitors. Based on these observations, we have proposed the mechanism of specific versus non-specific HAT inhibition by these small molecule HAT inhibitors, which may be useful to design therapeutically favorable HAT inhibitors.

The HAT activity of p300 is regulated by different posttranslational modifications and protein-protein interactions. Among these, autoacetylation of p300 is one of the key regulators of its catalytic activity. Mechanistically, autoacetylation induced structural changes in the p300 HAT domain acts as a master switch. We have shown that the natural HAT inhibitor Garcinol,

isogarcinol and LTK14 could potently inhibit the autoacetylation activity. Furthermore, for the first time, we demonstrate that indeed autoacetylation induces structural changes in p300 HAT domain, as probed by surface-enhanced Raman scattering.

Alteration in HATs and HDACs are associated with several diseases which include cancer. Oral cancer is one of the most common cancers in developing countries, especially in India. The prevalence of oral cancer is particularly high among men. It is the eighth most common cancer worldwide. In India, the age standardized incidence rate of oral cancer is 12.6 per 100 000 population. Smokeless tobacco use has been implicated for the etiology of the oral pre-cancerous and cancerous lesions. Traditional forms like betel quid, tobacco with lime and tobacco tooth powder are commonly used. However, cancer is a disease caused by genetic or somatic mutation. Alteration of genome organization and epigenetic marks are hallmark of cancer. Post translational modification of chromatin is causally related to cancer manifestation. Incidentally we have found that histones are unusually hyperacetylated in a few cancer cell lines, one of which is oral cancer cells. These findings prompted us to look into the acetylation status of histones in oral cancer patient samples. In agreement with the cell line data histone hyperacetylation was also found to be associated with oral cancer patient samples, specially the H3K14 acetylation was found to be more predominant. H3K14 is a known target for p300. We assumed that overexpression and /or hyperactive p300 (autoacetylated) could be directly responsible for the histone hyperacetylation in the patient samples. As predicted, we found the p300 is overexpressed and is predominantly enhanced autoacetylated in the patient samples. We could also find the upregulation of GAPDH and B23 in patient oral cancer tissue samples. Both B23 and GAPDH are well

known to get upregulated in several other cancers. Significantly, we observed that the autoacetylation of p300 is induced by GAPDH and B23 *in vitro*. We have found that histones get hyperacetylated in oral cancer cells (KB cells) occurs in response to nitric oxide (NO) signaling which is dependent on IFNγ. NO treatment could also upregulate the GAPDH and B23 protein levels as well as histone H3 hyperacetylation in concentration dependent manner. We further designed a novel, non-toxic water soluble HAT inhibitor (CTK7A) which could inhibit histone acetylation and p300 autoacetylation in the oral cancer cell line. CTK7A was found to cause senescence like growth arrest in cells. The small molecule HAT inhibitor was also found to inhibit the tumor growth in the mouse tumor xenograft model with a characteristic suppression of histone acetylation in these samples. These data raises the possibility of HATs as a target for the oral cancer therapy.

In summary, we have elucidated the mechanisms of p300 HAT inhibition by small molecule compounds. These inhibitors target one of the mode of p300 activation, autoacetylation. The autoacetylation of p300 is induced by GAPDH and B23 in oral cancer, in response to NO, resulting in hyperacetylation of histones. Inhibition of p300 HAT activity by small molecules such as CTK7A could be a potential therapeutic strategy against oral cancer.

List of Publications from the Thesis:

1. **Arif M**, Vedamurthy M, Pradhan S K, Thanuja G R, Dipak Dasgupta and Tapas K Kundu. (2009), Mechanism of p300 Specific Histone Acetyltransferase Inhibition by Small Molecules. J Med Chem. Jan 22;52(2):267-77.

2. **Arif M**, Kumar GV, Narayana C, Kundu T.K. (2007) Autoacetylation induced specific structural changes in histone acetyltransferase domain of p300: probed by surface enhanced Raman spectroscopy. J. Phys. Chem. B. 111(41):11877-9.

3. Pavan Kumar, G. V., Ashok Reddy, B. A., **Arif M**, Kundu, T. K., Narayana C. (2006) Surface-enhanced Raman scattering studies of human transcriptional coactivator p300. J Phys Chem. B. 110(33):16787-92.

4. **Arif M**, Vedamurthy B M, Mantelingu K, Ramesh C, Gopinath K S, and Tapas K Kundu (2009), Nitric oxide signaling and NPM1/GAPDH induced p300 autoacetylation in oral cancer manifestation: Putative therapeutic target of a novel water soluble HAT inhibitor. (Manuscript under preparation).

References

Abraham, J., Kelly, J., Thibault, P., and Benchimol, S. (2000) Post-translational modification of p53 protein in response to ionizing radiation analyzed by mass spectrometry. Mol. Biol. 295, 853–864

Aggarwal BB, Kumar A and Bharti AC, Anticancer potential of curcumin: preclinical and clinical studies. Anticancer Res 23(1A): 363–98, 2003.

Aggarwal, B. D., and Calvi, B. R. (2004) Chromatin regulates origin activity in Drosophila follicle cells. Nature 430, 372–376.

Ait-Si-Ali S, Ramirez S, Barre FX, Dkhissi F, Magnaghi-Jaulin L, Girault JA, Robin P, Knibiehler M, Pritchard LL, Ducommun B, Trouche D, Harel-Bellan A (1998) Histone acetyltransferase activity of CBP is controlled by cycle-dependent kinases and oncoprotein E 1 A. Nature 396:184–186

Ait-Si-Ali S, Carlisi D, Ramirez S, Upeguí-Gonzalez LC, Duquet A, Robin P, Rudkin B, Harel- Bellan A, Trouche D (1999) Phosphorylation by p44 MAP KinaseJERK1 stimulates CBP histone acetyl-transferase activity in vitro. Biochem Biophys Res Commun 262:157–162

Alexiadis, V., Waldmann, T., Andersen, J., Mann, M., Knippers, R., and Gruss, C. The protein encoded by the proto-oncogene DEK changes the topology of chromatin and reduces the efficiency of DNA replication in a chromatin-specific manner. Genes Dev. 2000, 14, 1308-1312

Altaf M, Utley RT, Lacoste N, et al. Interplay of chromatin modifi ers on a short basic patch of histone H4 tail defi nes the boundary of telomeric heterochromatin. Mol Cell 2007 ; 28 (6): 1002 -14

Altenberg, B. & Greulich, K. O. Genes of glycolysis are ubiquitously overexpressed in 24 cancer classes. Genomics 84, 1014–1020 (2004).

Ambs, S. et al. Frequent nitric oxide synthase-2 expression in human adenomas: implication for tumour angiogenesis and colon cancer progression. Cancer Res. 58, 334–341 (1998).

Ambs, S. et al. p53 and vascular endothelial growth factor regulate tumor growth of NOS2-expressing human carcinoma cells. Nature Med. 4, 1371–1376 (1998).

Anzick SL, Kononen J, Walker RL, et al. AIB1, a steroid receptor coactivator amplify ed in breast and ovarian cancer.Science 1997 ; 277 (5328): 965 -8

An W, Kim J, Roeder RG. Ordered cooperative functions of PRMT1, p300, and CARM1 in transcriptional activation by p53. Cell 2004; 117(6): 735-48

Arany Z, Newsome D, Oldread E, Livingston DM, Eckner R (1995) A family of transcriptional adaptor proteins targeted by the E1A oncoprotein. Nature 374:81–84

Arany Z, Sellers WR, Livingston DM, Eckner R (1994) E1A-associated p300 and CREB-associated CBP belong to a conserved family of coactivators. Cell 77:799–800

Arents G, Burlingame RW, Wang BC, Love WE, Moudrianakis EN (1991) The nucleosomal core histone octamer at 3.1 A resolution: a tripartite protein assembly and a left-handed superhelix. Proc Natl Acad Sci U S A 88:10148–10152.

Arif, M.; Kumar, G. V. P.; Narayana, C.; Kundu, T. K. Autoacetylation induced specific structural changes in histone acetyltransferase domain of p300: probed by surface enhanced Raman spectroscopy. J Phys Chem B. 2007, 111, 11877-11879.

194

Asano, K. et al. Constitutive and inducible nitric oxide synthase gene expression, regulation, and activity in human lung epithelial cells. Proc. Natl Acad. Sci. USA 91, 10089–10093 (1994).

Aznavoorian S., A.N. Murphy, W.G. Stetler-Stevenson, L.A. Liotta, Molecular aspects of tumor cell invasion and metastasis, Cancer 71 (1993) 1368–1383.
Bai X, Wu L, Liang T, Liu Z, Li J, Li D, Xie H, Yin S, Yu J, Lin Q, Zheng S. Overexpression of myocyte enhancer factor 2 and histone hyperacetylation in hepatocellular carcinoma. J Cancer Res Clin Oncol. 2008 Jan;134(1):83-91.

Balasubramanyam K, Swaminathan V, Ranganathan A, Kundu TK. Small molecule modulators of histone acetyltransferase p300. J Biol Chem 2003 ; 278 (21): 19134 -40.

Balasubramanyam K, Altaf M, Varier RA, et al. Polyisoprenylated benzophenone, garcinol, a natural histone acetyltransferase inhibitor, represses chromatin transcription and alters global gene expression. J Biol Chem 2004 ; 279 (32): 33716 -26

Balasubramanyam K, Varier RA, Altaf M, et al. Curcumin, a novel p300/CREB-binding protein-specific inhibitor of acetyltransferase, represses the acetylation of histone/nonhistone proteins and histone acetyltransferase-dependent chromatin transcription. J Biol Chem 2004 ; 279 (49): 51163 -71

Ballestar, E. et al. Methyl-CpG binding proteins identify novel sites of epigenetic inactivation in human cancer. EMBO J. 22, 6335–6345 (2003).

Bandyopadhyay D, Okan NA, Bales E, Nascimento L, Cole PA, Medrano EE. Down-regulation of p300/CBP histone acetyltransferase activates a senescence checkpoint in human melanocytes. Cancer Res. 2002 Nov 1;62(21):6231-9.

Bannister, A. J.; Kouzarides, T. The CBP co-activator is a histone acetyltransferase. Nature 1996, 384, 641-643.

195

Becke, A.D.J. A new mixing of Hartree–Fock and local density-functional theories Chem. Phy 1993, 98, 1372-1377

Ben-Porath I, Weinberg RA. When cells get stressed: an integrative view of cellular senescence. J Clin Invest. 2004 Jan;113(1):8-13. Review

Berger, S. L. Histone modifications in transcriptional regulation. Curr. Opin. Genet. Dev. 2002, 12, 142-148.

Bernardi, R., Scaglioni, P. P., Bergmann, S., Horn, H. F., Vousden, K. H., and Pandolfi, P. P. (2004) PML regulates p53 stability by sequestering Mdm2 to the nucleolus. Nat. Cell Biol. 6, 665–672.

Bestor, T. H. (1998) Gene silencing. Methylation meets acetylation. Nature 393, 311–312

Bhaumik, S.R., and Green, M.R. (2001). SAGA is an essential in vivo target of the yeast acidic activator Gal4p. Genes Dev. 15, 1935–1945

Bhaumik SR, Smith E, Shilatifard A. Covalent modifications of histones during development and disease pathogenesis. Nat Struct Mol Biol. 2007 Nov;14(11):1008-2007 Review

Biel M, Wascholowski V, Giannis A. Epigenetics – an epicenter of gene regulation: histones and histone-modifying enzymes. Angew Chem Int Ed Engl 2005 ; 44 (21): 3186 -216

Bhaumik SR, Smith E, Shilatifard A. Covalent modifications of histones during development and disease pathogenesis. Nat Struct Mol Biol. 2007 Nov;14(11):1008-16.. Review.

Bilsen M. van, K. R. Chien, Cardiovasc. Res. 1993, 27, 1140–1149.

Black JC, Mosley A, Kitada T, Washburn M, Carey M. The SIRT2 deacetylase regulates autoacetylation of p300. Mol Cell. 2008 Nov 7;32(3):449-55

Black, J. C.; Choi, J. E.; Lombardo, S. R.; Carey, M. A Mechanism for Coordinating Chromatin Modification and Preinitiation Complex Assembly. Mol. Cell 2006, 23, 809-818.

Blander, G., Zalle, N., Daniely, Y., Taplick, J., Gray, M. D., and Oren, M. (2002) DNA damage-induced translocation of the Werner helicase is regulated by acetylation. J. Biol. Chem. 277, 50934–50940.

Borrow J, Stanton VP, Jr., Andresen JM, Becher R, Behm FG, Chaganti RS, Civin CI, Disteche C, Dube I, Frischauf AM, Horsman D, Mitelman F, Volinia S, Watmore AE, Housman DE (1 996) The translocation t(8; 16)(p 1 1;p 13) of acute myeloid leukaemia fuses a putative acetyltransferase to the CREB-binding protein [see comments]. Nat Genet 14:33–41

Borrow J, Stanton VP Jr, Andresen JM, et al. The translocation t(8;16)(p11;p13) of acute myeloid leukaemia fuses a putative acetyltransferase to the CREB-binding protein. Nat Genet 1996 ; 14 (1): 33 -41

Boutillier, A. L., Trinh, E., and Loeffler, J. P. (2003) Selective E2F-dependent gene transcription is controlled by histone deacetylase activity during neuronal apoptosis. J. Neurochem. 84, 814–828.

Bordoli L, Netsch M, Luthi U, Lutz W, Eckner R (2001b) Plant orthologs of p300lCBP: conservation of a core domain in metazoan p300lCBP acetyltransferaserelated proteins. Nucleic Acids Res 29:589–597

Brachmann CB, Sherman JM, Devine SE, et al. The SIR2 gene family, conserved from bacteria to humans, functions in silencing, cell cycle progression, and chromosome stability. Genes Dev 1995 ; 9 (23): 2888 -902

Brown CE, Lechner T, Howe L, Workman JL. The many HATs of transcription coactivators. Trends Biochem Sci. 2000 Jan;25(1):15-9. Review

Brennan, J., Boyle, J., Koch, W., Goodman, S., Hruban, R., Eby, Y., Couch, M., Forastiere, A., and Sidransky, D. (1995). Association between cigarette smoking and mutation of the p53 gene in head and neck squamous carcinoma. N. Engl. J. Med. 332, 712–717.

Brown, C.E., Howe, L., Sousa, K., Alley, S.C., Carrozza, M.J., Tan, S., and Workman, J.L. (2001). Recruitment of HAT complexes by direct activator interactions with the ATM-related Tra1 subunit. Science 292, 2333–2337

Brown, D.T. (2003). Histone H1 and the dynamic regulation of chromatin function. Biochem. Cell Biol. 81, 221–227.

Buratowski, S., Hahn, S., Guarente, L. and Sharp, P.A. (1989) Cell 56, 549–561.

Kim, Y.J., Bjorklund, S., Li, Y., Sayre, M.H. and Kornberg, R.D. (1994) Cell 77, 599–608.

Bustin M, Catez F, Lim, JH (2005). The dynamics of H1 function in chromatin.Mol.Cell17:617–620.

Campisi, J. (2005). Senescent cells, tumor suppression, and organismal aging: Good citizens, bad neighbors. Cell 120, 513–522.

198

Carrozza MJ, Utley RT, Workman JL, Côté J. The diverse functions of histone acetyltransferase complexes. Trends Genet. 2003 Jun;19(6):321-9. Review.

Caterino TL, Hayes JJ. Chromatin structure depends on what's in the nucleosome's pocket. Nat Struct Mol Biol. 2007 Nov;14(11):1056-8.

Chan G, Boyle JO, Yang EK, et al. Cyclooxgenase-2 expression is up-regulated in squamous cell carcinoma of the head and neck. Cancer Res 1999;59:991–4.

Chan HM, La Thangue NB (2001) p300ICBP proteins: HATS for transcriptional bridges and scaffolds. J Cell Sci 114:2363–2373

Chakrabarti SK, Francis J, Ziesmann SM, et al. Covalent histone modifications underlie the developmental regulation of insulin gene transcription in pancreatic beta cells. J Biol Chem 2003; 278: 23 617–23 623.

Chakrabarty, S.; Roy, P.; and Dasgupta, D., Interaction of the antitumor antibiotic chromomycin A3 with glutathione, a sulfhydryl agent, and the effect upon its DNA binding properties. Biochem. Pharmacol. 1998, 31, 3379-3386.

Champagne N, Bertos NR, Pelletier N, Wang AH, Vezmar M, Yang Y, Heng HH, Yang XJ (1999b) Identification of a human histone acetyltransferase related to monocytic leukemia zinc finger protein. J Biol Chem 274:28528–28536

Chen LF, GreeneWC. Shaping the nuclear action of NF-kappaB. Nat Rev Mol Cell Biol 2004;5(5):392–401.

Chevillard-Briet M, Trouche D, Vandel L (2002) Control of CBP co-activating activity by arginine methylation. EMBO J 21:5457–5466

Cheung P, Tanner KG, Cheung WL, et al. Synergistic coupling of histone H3 phosphorylation and acetylation in response to epidermal growth factor stimulation. Mol Cell 2000 ; 5 (6): 905 -15

Chodaparambil, J.V. et al. Nat. Struct. Mol. Biol. 14, 1105–1107 (2007).

Cremer T, Cremer C. Chromosome territories, nuclear architecture and gene regulation in mammalian cells. Nat Rev Genet. 2001 Apr;2(4):292-301. Review.

Chrivia JC, Kwok RP, Lamb N, Hagiwara M, Montminy MR, Goodman RH (1993) Phosphorylated CREB binds specifically to the nuclear protein CBP. Nature 365:855–859.

Clements, A.; Rojas, J. R.; Trievel, R. C.; Wang, L.; Berger, S. L.; Marmorstein, R. Crystal structure of the histone acetyltransferase domain of the human PCAF transcriptional regulator bound to coenzyme A. EMBO J. 1999, 18, 3521-3532

Connelly ST, Macabeo-Ong M, Dekker N, Jordan RC, Schmidt BL. Increased nitric oxide levels and iNOS overexpression in oral squamous cell carcinoma. Oral Oncol 2005; 41:261–7.

Cosma, M.P., Tanaka, T., and Nasmyth, K. (1999). Ordered recruitment of transcription and chromatin remodeling factors to a cell cycleand developmentally regulated promoter. Cell 97, 299–311.

Cosío BG, Mann B, Ito K, Jazrawi E, Barnes PJ, Chung KF, Adcock IM. Histone acetylase and deacetylase activity in alveolar macrophages and blood mononocytes in asthma. Am J Respir Crit Care Med. 2004 Jul 15;170(2):141-7.

Costanzo, A.; Merlo, P.; Pediconi, N.; Fulco, M.; Sartorelli, V.; Cole, P. A.; Fontemaggi, G.; Fanciulli, M.; Schiltz, L.; Blandino, G.; Balsano, C.; Levrero, M. DNA damage-

dependent acetylation of p73 dictates the selective activation of apoptotic target genes. Mol. Cell 2002, 9, 175-186.

Cramer, P. (2002) Curr. Opin. Struct. Biol. 12, 89–97.

Croft, J. A. et al. Differences in the localization and morphology of chromosomes in the human nucleus. J. Cell Biol. 145, 1119–1131 (1999).

Cramer, P., Bushnell, D.A. and Kornberg, R.D. (2001) Science. 292, 1863–1876.

Cremer T, Cremer M, Dietzel S, Müller S, Solovei I, Fakan S. Chromosome territories--a functional nuclear landscape. Curr Opin Cell Biol. 2006 Jun;18(3):307-16.Review.

Cullis PM, Wolfenden R, Cousens LS, Alberts BM. Inhibition of histone acetylation by N-[2-(S-coenzyme A)acetyl] spermidine amide, a multisubstrate analog. J Biol Chem 1982 ; 257 (20): 12165 -9.

Czesnikiewicz-Guzik M, Lorkowska B, Zapala J, Czajka M, Szuta M, Loster B, Guzik TJ, Korbut R. NADPH oxidase and uncoupled nitric oxide synthase are major sources of reactive oxygen species in oral squamous cell carcinoma. Potential implications for immune regulation in high oxidative stress conditions. J Physiol Pharmacol. 2008 Mar;59(1):139-52

Das C, Hizume K, Batta K, Kumar BR, Gadad SS, Ganguly S, Lorain S, Verreault A, Sadhale PP, Takeyasu K, Kundu TK. Transcriptional coactivator PC4, a chromatin-associated protein, induces chromatin condensation. Mol Cell Biol. 2006 Nov;26(22):8303-15.

Das C, Kundu TK. Transcriptional regulation by the acetylation of nonhistone proteins in humans -- a new target for therapeutics. IUBMB Life. 2005 Mar;57(3):137-49. Review.

201

Das C, Lucia MS, Hansen KC, Tyler JK.CBP/p300-mediated acetylation of histone H3 on lysine 56. Nature. 2009 Mar 8.

Dastoor, Z. & Dreyer, J.L. (2001) Potential role of nuclear translocation of glyceraldehyde-3-phosphate dehydrogenase in apoptosis and oxidative stress. J. Cell Sci. 114, 1643–1653.

Davidson SM, Townsend PA, Carroll C, Yurek-George A, Balasubramanyam K, Kundu TK, Stephanou A, Packham G, Ganesan A, Latchman DS. The transcriptional coactivator p300 plays a critical role in the hypertrophic and protective pathways induced by phenylephrine in cardiac cells but is specific to the hypertrophic effect of urocortin. Chembiochem. 2005 Jan;6(1):162-70.

Decker, J., and Goldstein, J.C. (1982). Risk factors in head and neck cancer.
N. Engl. J. Med. 306, 1151–1155.

DeLano, W. L.; The PyMOL Molecular Graphics System.2002, http://www.pymol.org

Dimri GP, Lee X, Basile G, Acosta M, Scott G, Roskelley C et al. (1995). A biomarker

that identifies senescent human cells in culture and in aging skin in vivo. Proc Natl Acad

Sci USA 92:9363–9367.

Ding HF, Bustin M, Hansen U (1997) Alleviation of histone H1-mediated transcriptional repression and chromatin compaction by the acidic activation region in chromosomal protein HMG-14. Mol Cell Biol 17:5843–5855.

Dormeyer W, Ott M, Schnölzer M. Probing lysine acetylation in proteins: strategies, limitations, and pitfalls of in vitro acetyltransferase assays. Mol Cell Proteomics. 2005 Sep;4(9):1226-39.

Dornan, D., Shimizu, H., Perkins, N.D., and Hupp, T.R. (2003). DNA-dependent acetylation of p53 by the transcription coactivator p300. J. Biol. Chem. 278, 13431–13441

Eckner R, Ewen ME, Newsome D, Gerdes M, DeCaprio JA, Lawrence JB, Livingston DM (1994) Molecular cloning and functional analysis of the adenovirus E1A-associated 300-kD protein (p300) reveals a protein with properties of a transcriptional adaptor. Genes Dev 8:869–884.

Eberharter A, Becker PB. Histone acetylation: a switch between repressive and permissive chromatin. Second in review series on chromatin dynamics. EMBO Rep. 2002 Mar;3(3):224-9. Review.

Edelmann, P., Bornfleth, H., Zink, D., Cremer, T. & Cremer, C. Morphology and dynamics of chromosome territories in living cells. Biochim. Biophys. Acta 1551, M29–M39 (2001).

Esteller M. Cancer epigenomics: DNA methylomes and histone-modification maps. Nat Rev Genet. 2007 Apr;8(4):286-98. Review.

Esteller, M. & Herman, J. G. Generating mutations but providing chemosensitivity: the role of O6-methylguanine DNA methyltransferase in human cancer. Oncogene 23, 1–8 (2004).

Fahrner, J. A., Eguchi, S., Herman, J. G. & Baylin, S. B. Dependence of histone modifications and gene expression on DNA hypermethylation in cancer. Cancer Res. 62, 7213–7218 (2002).

Felts SJ, Weil PA, Chalkley R (1990) Transcription factor requirements for in vitro formation of transcriptionally competent 5S rRNA gene chromatin. Mol Cell Biol 10:2390–2401.

Forastiere, A., Koch, W., Trotti, A., and Sidransky, D. (2001). Head and neck cancer. N. Engl. J. Med. 345, 1890–1900.

Forastiere, A.A., Goepfert, H., Maor, M., Pajak, T.F., Weber, R., Morrison, W., Glisson, B., Trotti, A., Ridge, J.A., Chao, C., et al. (2003). Concurrent chemotherapy and radiotherapy for organ preservation in advanced laryngeal cancer. N. Engl. J. Med. 349, 2091–2098.

Forrester, K. et al. Nitric oxide-induced p53 accumulation and regulation of inducible nitric oxide synthase expression by wild-type p53. Proc. Natl Acad. Sci. USA 93, 2442–2447 (1996).

Fraga, M. F. et al. Loss of acetylation at Lys16 and trimethylation at Lys20 of histone H4 is a common hallmark of human cancer. Nature Genet. 37, 391–400 (2005).

Frisch, M. J.; Trucks, G. W.; Schlegel, H. B.; Scuseria, G. E.; Robb, M. A.;. Cheeseman, J. R.; Montgomery, J. A.; Vreven, Jr., T.; Kudin, K. N.; Burant, J. C.; Millam, J. M.; Iyengar, S. S.; Tomasi, J.; Barone, V.; Mennucci, B.; Cossi, M.; Scalmani, G.; Rega, N.; Petersson, G. A.; Nakatsuji, H.; Hada, M.; Ehara, M.; Toyota, K.; Fukuda, R.; Hasegawa, J.; Ishida, M.; Nakajima, T.; Honda, Y.; Kitao, O.; Nakai, H.; Klene, M.; Li, X.; Knox, J. E.; Hratchian, H. P.; Cross, J. B.; Bakken, V.; Adamo, C.; Jaramillo, J.; Gomperts, R.; Stratmann, R. E.; Yazyev, O.; Austin, A. J.; Cammi, R.; Pomelli, C.; Ochterski, J. W. ; Ayala, P. Y.; Morokuma, K.; Voth, G. A.; Salvador, P.; Dannenberg, J. J.; Zakrzewski, V. G.; Dapprich, S.; Daniels, A. D.; Strain, M. C.; Farkas, O.; Malick, D. K.; Rabuck, A. D.; Raghavachari, K.; Foresman, J. B.; Ortiz, J. V.; Cui, Q.; Baboul, A. G.; Clifford, S. ; Cioslowski, J.; Stefanov, B. B.; Liu, G.; Liashenko, A.; Piskorz, P.; Komaromi, I.;

Martin, R. L.; Fox, D. J.; Keith, T.; Al-Laham, M. A.; Peng, C. Y.; Nanayakkara, A.; Challacombe, M.; Gill, P. M. W.; Johnson, B.; Chen, W.; Wong, M. W.; Gonzalez, C.; Pople, J. A., 2004, Gaussain 03, revision B.05; Gaussian, Inc.: Wallingford, CT.

Frønsdal K, Engedal N, Slagsvold T, Saatcioglu F. CREB binding protein is a coactivator for the androgen receptor and mediates cross-talk with AP-1. J Biol Chem. 1998 Nov 27;273(48):31853-9. Erratum in: J Biol Chem 1999 Aug 27;274(35):25188.

Fu, M., Wang, C., Zhang, X., and Pestell, R. G. (2004) Acetylation of nuclear receptors in cellular growth and apoptosis. Biochem. Pharmacol. 68, 1199–1208

Fukumura D, Kashiwagi S, Jain RK. The role of nitric oxide in tumour progression. Nat Rev Cancer. 2006 Jul;6(7):521-34. Review

Gallo O, Masini E, Morbidelli L, Franchi A, Fini-Storchi I, Vergari WA, Ziche M. Role of nitric oxide in angiogenesis and tumor progression in head and neck cancer. J Natl Cancer Inst. 1998 Apr 15;90(8):587-96

Gallo O, Masini E, Bianchi B, Bruschinini L, Paglierani M, Franchi A. Prognostic significance of cyclooxygenase-2 pathway and angiogenesis in head and neck squamous cell carcinoma. Hum Pathol 2002; 33:708–14.

Gay, F., Calvo, D., Lo, M. C., Ceron, J., Maduro, M., Lin, R., and Shi, Y. (2003) Acetylation regulates subcellular localization of the Wnt signaling nuclear effector POP-1. Genes Dev. 17, 717–722.

Gayther SA, Batley SJ, Linger L, et al. Mutations truncating the EP300 acetylase in human cancers. Nat Genet 2000 ; 24 (3): 300 -3.

Germond JE, Hirt B, Oudet P, Gross-Bellark M, Chambon P (1975) Folding of the DNA double helix in chromatin-like structures from simian virus 40. Proc Natl Acad Sci U S A 72: 1843–1847.

Giles, R. H., Peters, D. J. & Breuning, M. H. Conjunction dysfunction: CBP/p300 in human disease. Trends Genet. 14, 178–183 (1998).

Gillison, M.L., Koch, W.M., Capone, R.B., Spafford, M., Westra, W.H., Wu, L., Zahurak, M.L., Daniel, R.W., Viglione, M., Symer, D.E., et al. (2000). Evidence for a causal association between human papillomavirus and a subset of head and neck cancers. J. Natl. Cancer Inst. 92, 709–720.

Girdwood D, Bumpass D, Vaughan OA, Thain A, Anderson LA, Snowden A W, Garcia-Wilson E, Perkins ND, Hay RT (2003) P300 transcriptional repression is mediated by SUMO modification. Mol Cell 11:1043

Glozak MA, Seto E. Histone deacetylases and cancer. Oncogene. 2007 Aug 13;26(37):5420-32. Review

Goodman, R. H.; Smolik, S. CBP/p300 in cell growth, transformation, and development. Genes Dev. 2000, 14, 1553-1577.

Gray SG, De Meyts P. Role of histone and transcription factor acetylation in diabetes pathogenesis. Diabetes Metab Res Rev. 2005 Sep-Oct;21(5):416-33. Review

Gray SG, Ekstrom TJ. The human histone deacetylase family. Exp Cell Res 2001; 262: 75–83.

Grigoryev, S. A. Role of the M-loop and reactive center loop domains in the folding and bridging of nucleosome arrays by MENT. J. Biol. Chem. 2003, 278: 43384-93

Grisendi S, Mecucci C, Falini B, Pandolfi PP. Nucleophosmin and cancer. Nat Rev Cancer. 2006 Jul;6(7):493-505. Review.

Gu, W., and Roeder, R. G. (1997) Activation of p53 sequence-specific DNA binding by acetylation of the p53 C-terminal domain. Cell 90, 595–606.

Guccione, E., Martinato, F., Finocchiaro, G., Luzi, L., Tizzoni, L., Dall' Olio, V., Zardo, G., Nervi, C., Bernard, L., and Amati, B. (2006). Mycbinding- site recognition in the human genome is determined by chromatin context. Nat. Cell Biol. 8, 764–770.

Gusterson R., B. Brar, D. Faulkes, A. Giordano, J. Chrivia, D. Latchman, J. Biol. Chem. 2002, 277, 2517– 2524.

Gusterson R. J., E. Jazrawi, I. M. Adcock, D. S. Latchman, J. Biol. Chem. 2003, 278, 6838 – 6847

Hahn, S. (2004). Structure and mechanism of the RNA polymerase II transcription machinery. Nat. Struct. Mol. Biol. 11, 394–403.

Hara MR, Agrawal N, Kim SF, Cascio MB, Fujimuro M, Ozeki Y, Takahashi M, Cheah JH, Tankou SK, Hester LD, Ferris CD, Hayward SD, Snyder SH, Sawa A. S-nitrosylated GAPDH initiates apoptotic cell death by nuclear translocation following Siah1 binding. Nat Cell Biol. 2005 Jul;7(7):665-74.

Harada N, Yasunaga R, Higashimura Y, Yamaji R, Fujimoto K, Moss J, Inui H, Nakano Y. Glyceraldehyde-3-phosphate dehydrogenase enhances transcriptional activity of androgen receptor in prostate cancer cells. J Biol Chem. 2007 Aug 3;282(31):22651-61.

Hassa PO, Haenni SS, Elser M, Hottiger MO. Nuclear ADP-ribosylation reactions in mammalian cells: where are we today and where are we going? Microbiol Mol Biol Rev 2006; 70(3): 789-829.

207

Herman JG, Baylin SB. Gene silencing in cancer in association with promoter hypermethylation. N Engl J Med 2003;349:2042–54

Herrera, J. E.; Bergel, M.; Yang, X. J.; Nakatani, Y.; Bustin, M. The histone acetyltransferase activity of human GCN5 and PCAF is stabilized by coenzymes. J. Biol. Chem. 1997, 272, 27253-27258.

Hong, W.K., and Sporn, M.B. (1997). Recent advances in chemoprevention of cancer. Science 278, 1073–1077.

Hong, W.K., Endicott, J., Itri, L.M., Doos, W., Batsakis, J.G., Bell, R., Fofonoff, S., Byers, R., Atkinson, E.N., Vaughan, C., et al. (1986). 13-cis-retinoic acid in the treatment of oral leukoplakia. N. Engl. J. Med.315, 1501–1505.

Hong, W.K., Lippman, S.M., Itri, L.M., Karp, D.D., Lee, J.S., Byers, R.M., Schantz, S.P., Kramer, A.M., Lotan, R., Peters, L.J., et al. (1990). Prevention of second primary tumors with isotretinoin in squamous-cell carcinoma of the head and neck. N. Engl. J. Med. 323, 795–801.

Horn, P.J., and Peterson, C.L. (2002). Molecular biology. Chromatin higher order folding–wrapping up transcription. Science 297, 1824– 1827.

Horvai AE, Xu L, Korzus E, Brard G, Kalafus D, Mullen TM, Rose DW, Rosenfeld MG, Glass CK. Nuclear integration of JAK/STAT and Ras/AP-1 signaling by CBP and p300. Proc Natl Acad Sci U S A. 1997 Feb 18;94(4):1074-9.

Huang WC, Chen CC. Akt phosphorylation of p300 at Ser-1834 is essential for its histone acetyltransferase and transcriptional activity. Mol Cell Biol. 2005 Aug;25(15):6592-602

Huang, Y., Myers, S. J., and Dingledine, R. (1999) Transcriptional repression by REST: recruitment of Sin3A and histone deacetylase to neuronal genes. Nat. Neurosci. 2, 867–872.

Huletsky, A., de Murcia, G., Muller, S., Hengartner, M., Menard, L., Lamarre, D., and Poirier, G. The effect of Poly(ADP-ribosyl)ation on native and H1-depleted chromatin. J Biol Chem 1989, 264, 8878-8886

Huletsky A, De Murcia G, Muller S, et al. The effect of poly(ADP-ribosyl)ation on native and H1-depleted chromatin. A role of poly(ADP-ribosyl)ation on core nucleosome structure. J Biol Chem 1989 ; 264 (15): 8878 -86.

Ida K, Kitabayashi I, Taki T, Taniwaki M, Noro K, Yamamoto M, Ohki M, Hayashi Y (1997) Adenoviral E 1 A-associated protein p300 is involved in acute myeloid leukemia with t(11;22)(q23;q13). Blood 90:4699–4704

Iizuka, M., and Stillman, B. (1999) Histone acetyltransferase HBO1 interacts with the ORC1 subunit of the human initiator protein. J. Biol. Chem. 274, 23027–23034.

Ikura T, Ogryzko VV, Grigoriev M, et al. Involvement of the TIP60 histone acetylase complex in DNA repair and apoptosis. Cell 2000 ; 102 (4): 463 -73

Impey S, Fong AL, Wang Y, Cardinaux JR, Fass DM, Obrietan K, Wayman GA, Storm DR, Soderling TR, Goodman RH. Phosphorylation of CBP mediates transcriptional activation by neural activity and CaM kinase IV. Neuron. 2002 Apr 11;34(2):235-44.

Ishihama K, Yamakawa M, Semba S, Takeda H, Kawata S, Kimura S, Kimura W. Expression of HDAC1 and CBP/p300 in human colorectal carcinomas. J Clin Pathol. 2007 Nov;60(11):1205-10.

209

Ito K, Barnes PJ, Adcock IM. Glucocorticoid receptor recruitment of histone deacetylase 2 inhibits interleukin-1beta-induced histone H4 acetylation on lysines 8 and 12. Mol Cell Biol. 2000 Sep;20(18):6891-903

Ito A, Kawaguchi Y, Lai CH, Kovacs JJ, Higashimoto Y, Appella E, et al. MDM2-HDAC1-mediated deacetylation of p53 is required for its degradation. EMBO J 2002;21(22):6236-45.

Iyer, N. G., Chin, S. F., Ozdag, H., Daigo, Y., Hu, D. E., Cariati, M., Brindle, K., Aparicio, S., and Caldas, C. (2004) p300 regulates p53-dependent apoptosis after DNA damage in colorectal cancer cells by modulation of PUMA/p21 levels. Proc. Natl. Acad. Sci. U. S. A. 101, 7386–7391.

Izzo, J.G., Papadimitrakopoulou, V.A., Liu, D.D., den Hollander, P.L., Babenko, I.M., Keck, J., El-Naggar, A.K., Shin, D.M., Lee, J.J., Hong, W.K., and Hittelman, W.N. (2003). Cyclin D1 genotype, response to biochemoprevention, and progression rate to upper aerodigestive tract cancer. J. Natl. Cancer Inst. 95, 198–205

Janknecht R, Nordheim A (1996) MAP kinase-dependent transcriptional coactivation by Elk-1 and its cofactor CBP. Biochem Biophys Res Commun 228:831–837

Jenkins, D. C. et al. Human colon cancer cell lines show a diverse pattern of nitric oxide synthase gene expression and nitric oxide generation. Brit. J. Cancer 70, 847–849 (1994).

Jenkins, D. C. et al. Roles of nitric oxide in tumour growth. Proc. Natl Acad. Sci. USA 92, 4392–4396 (1995).

Jeong JW, Bae MK, Ahn MY, Kim SH, Sohn TK, Bae MH, et al. Regulation and destabilization of HIF-1alpha by ARD1-mediated acetylation. Cell 2002;111(5): 709-20.

Johnson JJ, Mukhtar H. Curcumin for chemoprevention of colon cancer. Cancer Lett. 2007 Oct 8;255(2):170-81.

Jiang H, Nucifora Jr FC, Ross CA and DeFranco DB (2003) Cell death triggered by polyglutamine-expanded huntingtin in a neuronal cell line is associated with degradation of CREB-binding protein. Hum. Mol. Genet. 12: 1–12.

Jin K, Mao XO, Simon RP and Greenberg DA (2001) Cyclic AMP response element binding protein (CREB) and CREB binding protein (CBP) in global cerebral ischemia. J. Mol. Neurosci. 16: 49–56

Jones PA, Baylin SB. The fundamental role of epigenetic events in cancer. Nat Rev Genet 2002;3:415–28

Kahlem P, Dörken B, Schmitt CA. Cellular senescence in cancer treatment: friend or foe? J Clin Invest. 2004 Jan;113(2):169-74. Review.

Kaiser, C., and James, S.R. (2004) Acetylation of insulin receptor substrate-1 is permissive for tyrosine phosphorylation. BMC Biol. 2: 23.

Kamei, Y., Xu, L., Heinzel, T., Torchia, J., Kurokawa, R., Gloss, B., Lin,S. C., Heyman, R. A., Rose, D. W., Glass C. K. et al. (1996). A CBP integrator complex mediates transcriptional activation and AP-1 inhibition by nuclear receptors. Cell 85, 403-414.

Kalkhoven E, Roelfsema JH, Teunissen H, den Boer A, Ariyurek Y, Zantema A, Breuning MH, Hennekam RC, Peters DJ (2003) Loss of CBP acetyltransferase activity by PHD finger mutations in Rubinstein-Taybi syndrome. Hum Mol Genet 12:441–450

Karanam, B.; Jiang, L.; Wang, L.; Kelleher, N. L.; Cole, P. A. Kinetic and mass spectrometric analysis of p300 histone acetyltransferase domain autoacetylation. J. Biol. Chem. 2006, 281, 40292-40301.

Karanam, B.; Wang, L.; Wang, D.; Liu, X.; Marmorstein, R.; Cotter, R.; Cole, P. A. Multiple roles for acetylation in the interaction of p300 HAT with ATF-2. Biochemistry 2007, 46, 8207-8216.

Keller W (1975) Determination of the number of superhelical turns in simian virus 40 DNA by gel electrophoresis. Proc Natl Acad Sci U S A 72:4876–4880.

Kellum, R. (2003). HP1 complexes and heterochromatin assembly. Curr. Top. Microbiol. Immunol. 274, 53–77.

Keppler BR, Archer TK. Chromatin-modifying enzymes as therapeutic targets--Part 1. Expert Opin Ther Targets. 2008 Oct;12(10):1301-12. Review

Keppler BR, Archer TK. Chromatin-modifying enzymes as therapeutic targets--Part 2. Expert Opin Ther Targets. 2008 Nov;12(11):1457-67. Review.

Khan N., F. Afaq, H. Mukhtar, Apoptosis by dietary factors: the suicide solution for delaying cancer growth, Carcinogenesis (2006).

Khuri, F., Lee, J.J., Lippman, S.M., Kim, E.S., Cooper, J.S., Benner, S.E., Vokes, E.E., Pajak, T.F., Goepfert, H., and Hong, W.K. (2003). Isotretinoin effects on head and neck cancer recurrence and second primary tumors. Proc. Am. Soc. Clin. Oncol. 22, 90.

Kim MY, Mauro S, Gévry N, Lis JT, Kraus WL. NAD+-dependent modulation of chromatin structure and transcription by nucleosome binding properties of PARP-1. Cell. 2004 Dec 17;119(6):803-14.

Kim SC, Sprung R, Chen Y, Xu Y, Ball H, Pei J, et al. Substrate and functional diversity of lysine acetylation revealed by a proteomics survey.Mol Cell 2006;23(4):607–18.
Knoepfler, P. S., and Eisenman, R. N. (1999) Sin meets NuRD and other tails

of repression. Cell 99, 447–450

Knowles, R. G. & Moncada, S. Nitric oxide synthases in mammals. Biochem. J. 298, 249–258 (1994).

Koipally, J., Renold, A., Kim, J., and Georgopoulos, K. (1999) Repression by Ikaros and Aiolos is mediated through histone deacetylase complexes. EMBO J. 18, 3090–3100

Koleske, A.J. and Young, R.A. 1994. An RNA polymerase II holoenzyme responsive to activators. Nature 368:466–469.

Kornberg RD (1974) Chromatin structure: a repeating unit of histones and DNA. Science 184:868–871

Kouzarides, T. Chromatin modifications and their function. Cell 128, 693–705 (2007).

Kouzarides, T. (2000) Acetylation: a regulatory modification to rival phosphorylation? EMBO J. 19, 1176–1179.

Kouzarides, T. (1999) Histone acetylases and deacetylases in cell proliferation. Curr. Opin. Genet. Dev. 9, 40–48

Kovacs JJ, Murphy PJ, Gaillard S, Zhao X, Wu JT, Nicchitta CV, et al. HDAC6 regulates Hsp90 acetylation and chaperone-dependent activation of glucocorticoid receptor. Mol Cell 2005;18(5):601–7.

Kraus, W. L., and Lis, J. T. PARP goes transcription. Cell. 2003, 113, 677-683

Kundu, T. K.; Palthan, V. B.; Wang, Z.; An, W.; Cole, P. A.; Roeder, R. G.; Activator-dependent transcription from chromatin in vitro involving targeted histone acetylation by p300.Mol. Cell. 2000, 6, 551-561.

Kung AL, Rebel VI, Bronson RT, Ch'ng LE, Sieff CA, Livingston DM, Yao TP (2000) Gene dose-dependent control of hematopoiesis and hematologic tumor suppression by CBP. Genes Dev 14:272–277

Kuo, M. H., and Allis, C. D. (1998) Roles of histone acetyltransferases and deacetylases in gene regulation. Bioessays 20, 615–626

Kurdistani SK. Histone modifi cations as markers of cancer prognosis: a cellular view. Br J Cancer 2007 ; 97 (1): 1 -5.

Lakowicz, R.J., Principles of Fluorescence Spectroscopy. 1999, 2nd ed., pp 242-249, Kluwer Academic/ Plenum Publishers, New York.

Lamonica JM, Vakoc CR, Blobel GA. Acetylation of GATA-1 is required for chromatin occupancy. Blood 2006;108(12):3736–8.

Lanctôt C, Cheutin T, Cremer M, Cavalli G, Cremer T. Dynamic genome architecture in the nuclear space: regulation of gene expression in three dimensions. Nat Rev Genet. 2007 Feb;8(2):104-15. Review.

Landry, J., Sutton, A., Hesman, T., Min, J., Xu, R.M., Johnston, M., and Sternglanz, R. (2003). Set2-catalyzed methylation of histone H3 represses basal expression of GAL4 in Saccharomyces cerevisiae. Mol. Cell. Biol. 23, 5972–5978.

Latchman D. S., Int. J. Biochem. Cell Biol. 2002, 34, 907 –910.

Lau OD, Kundu TK, Soccio RE, et al. HATs off: selective synthetic inhibitors of the histone acetyltransferases p300 and PCAF. Mol Cell 2000 ; 5 (3): 589 -95

Lee JS, Zhang X, Shi Y (1996) Differential interactions of the CREBIATF family of transcription factors with p300 and adenovirus El A. J Biol Chem 271:17666–17674

Lee, C.; Yang, W.; Parr, R. G. Development of the Colle-Salvetti correlation-energy formula into a functional of the electron density Phy. Rev. B 1998, 37,785-789: B3LYP

Legube, G., and Trouche, D. (2003). Regulating histone acetyltransferases and deacetylases. EMBO Rep. 4, 944–947.

Lemasson I, Nyborg JK. Human T-cell leukemia virus type I tax repression of p73beta is mediated through competition for the C/H1 domain of CBP. J Biol Chem. 2001 May 11;276(19):15720-7.

Li B, Carey M, Workman JL. The role of chromatin during transcription. Cell. 2007 Feb 23;128(4):707-19. Review.

Li, C. Q. et al. Apoptotic signaling pathways induced by nitric oxide in human lymphoblastoid cells expressing wild-type or mutant p53. Cancer Res. 64, 3022–3029 (2004).

Li N, Sood S, Wang S, Fang M, Wang P, Sun Z, Yang CS, Chen X. Overexpression of 5-lipoxygenase and cyclooxygenase 2 in hamster and human oral cancer and chemopreventive effects of zileuton and celecoxib. Clin Cancer Res. 2005 Mar 1;11(5):2089-96.

Lim MJ, Wang XW. Nucleophosmin and human cancer. Cancer Detect Prev. 2006;30(6):481-90. Review.

Liotta L.A., E.C. Kohn, The microenvironment of the tumor-host interface, Nature 411 (2001) 375–379.

Liu, L., Scolnick, D. M., Trievel, R. C., Zhang, H. B., Marmorstein, R., Halazonetis, T. D., and Berger, S. L. (1999) p53 sites acetylated in vitro by PCAF and p300 are acetylated in vivo in response to DNA damage. Mol. Cell. Biol. 19, 1202–1209.

Liu, X.; Wang, L.; Zhao, K.; Thompson, P. R.; Hwang, Y.; Marmorstein, R.; Cole, P. A. The structural basis of protein acetylation by the p300/CBP transcriptional coactivator. Nature 2008, 451, 846-850.

Lo WS, Trievel RC, Rojas JR, et al. Phosphorylation of serine 10 in histone H3 is functionally linked in vitro and in vivo to Gcn5-mediated acetylation at lysine 14. Mol Cell 2000 ; 5 (6): 917 -26

Luger K, Mader AW, Richmond RK, Sargent DF, Richmond TJ (1997) Crystal structure of the nucleosome core particle at 2.8 A resolution. Nature 389:251–260.

Luo, K., Vega-Palas, M. A., Grunstein, M. Rap1-Sir4 binding independent of other Sir, yKu, or histone interactions initiates the assembly of telomeric heterochromatin in yeast. Genes Dev. 2002, 16, 1528-39.

Maison, C., and Almouzni, G. HP1 and the dynamics of heterochromatin maintenance. Nature Rev. Mol. Cell. Biol. 2004, 5, 296-304.

Manning, G., Whyte, D.B., Martinez, R., Hunter, T. and Sudarsanam, S. (2002) The protein kinase complement of the human genome. Science. 298: 1912–34.

Mao L, Hong WK, Papadimitrakopoulou VA. Focus on head and neck cancer.Cancer Cell. 2004 Apr;5(4):311-6. Review

Mao, L., El-Naggar, A.K., Fan, Y.H., Lee, J.S., Lippman, S.M., Kayser, S., Lotan, R., and Hong, W.K. (1996b). Telomerase activity in head and neck squamous cell carcinoma and adjacent tissues. Cancer Res.56, 5600–5604

216

McCampbell A, Taye AA, Whitty L, Penney E, Steffan JS and Fischbeck KH (2001) Histone deacetylase inhibitors reduce polyglutamine toxicity. Proc. Natl. Acad. Sci. USA 98: 15179–15184

McGhee JD, Felsenfeld G (1980) Nucleosome structure. Annu Rev Biochem 49:1115–1156.

Madison, D. L., Yaciuk, P., Kwok, R. P., and Lundblad, J. R. (2002) Acetylation of the adenovirus-transforming protein E1A determines nuclear localization by disrupting association with importin-α. J. Biol. Chem. 277, 38755–38763.

Mai A. The therapeutic uses of chromatin-modifying agents. Expert Opin Ther Targets 2007 ; 11 (6): 835 -51.

Majee, S.; Sen, R., Guha, S.; Bhattacharya, D.; Dasgupta, D. Differential interactions of the Mg2+ complexes of chromomycin A3 and mithramycin with poly(dG-dC) x poly(dC-dG) and poly(dG) x poly(dC). Biochemistry 1997, 36, 2291-2299

Majumder, P. K. et al. mTOR inhibition reverses Akt-dependent prostate intraepithelial neoplasia through regulation of apoptotic and HIF-1-dependent pathways. Nature Med. 10, 594–601 (2004).

Mallery SR, Zwick JC, Pei P, Tong M, Larsen PE, Shumway BS, Lu B, Fields HW, Mumper RJ, Stoner GD. Topical application of a bioadhesive black raspberry gel modulates gene expression and reduces cyclooxygenase 2 protein in human premalignant oral lesions. Cancer Res. 2008 Jun 15;68(12):4945-57

Mantelingu K, Reddy BA, Swaminathan V, Kishore AH, Siddappa NB, Kumar GV, Nagashankar G, Natesh N, Roy S, Sadhale PP, Ranga U, Narayana C, Kundu TK.

217

Specific inhibition of p300-HAT alters global gene expression and represses HIV replication. Chem Biol. 2007 Jun;14(6):645-57.

Marks, P. A.; Rifkind, R. A.; Richon, V. M.; Breslow, R.; Miller, T.; Kelly, W. K Histone deacetylases and cancer: causes and therapies.Nat. Rev. Cancer 2001, 1, 194-202.

Martinez-Balbas MA, Bauer UM, Nielsen SJ, Brehm A, Kouzarides T. Regulation of E2F1 activity by acetylation. EMBO J 2000;19(4):662-71.

Marzio, G., Wagener, C., Gutierrez, M. I., Cartwright, P., Helin, K., andGiacca, M. (2000) E2F family members are differentially regulated by reversible acetylation. J. Biol. Chem. 275, 10887-10892

Marambaud P, Wen PH, Dutt A, Shioi J, Takashima A, Siman R and Robakis NK (2003) A CBP binding transcriptional repressor produced by the PS1/ epsilon-cleavage of N-cadherin is inhibited by PS1 FAD mutations. Cell 114: 635-645

Marmorstein R, Trievel RC. Histone modifying enzymes: structures, mechanisms, and specificities. Biochim Biophys Acta. 2009 Jan;1789(1):58-68. Review.

Mathon NF, Lloyd AC. Cell senescence and cancer. Nat Rev Cancer. 2001 Dec;1(3):203-13. Review

Matsudaira P., Actin crosslinking proteins at the leading edge, Semin. Cell. Biol. 5 (1994) 165-174.

McKay LI, Cidlowski JA. CBP (CREB binding protein) integrates NF-kappaB (nuclear factor-kappaB) and glucocorticoid receptor physical interactions and antagonism. Mol Endocrinol. 2000 Aug;14(8):1222-34.

Merrick CJ, Duraisingh MT. Plasmodium falciparum Sir2: an unusual sirtuin with

dual histone deacetylase and ADP-ribosyltransferase activity. Eukaryot Cell 2007;6(11):2081-91.

Miller RW, Rubinstein JH (1995) Tumors in Rubinstein-Taybi syndrome. Am J Med Genet 56:112-115

Milne, J.C.; Lambert, P.D.; Schenk, S.; Carney, D.P.; Smith ,J.J.; Gagne, D.J.; Jin, L.; Boss, O.;Perni, R.B.; Vu, C.B.; Bemis, J.E.; Xie, R.; Disch, J.S.; Ng, P.Y.; Nunes, J.J.; Lynch, A.V.; Yang, H.; Galonek, H.; Israelian, K.; Choy, W.; Iffland, A.; Lavu, S.; Medvedik, O.; Sinclair, D.A.; Olefsky,J.M.; Jirousek, M.R.; Elliott, P.J.; Westphal, C.H. Small molecule activators of SIRT1 as therapeutics for the treatment of type 2 diabetes. Nature 2007, 450, 712-716.

Miska, E. A., Langley, E., Wolf, D., Karlsson, C., Pines, J., and Kouzarides, T. (2001) Differential localization of HDAC4 orchestrates muscle differentiation. Nucleic Acids Res. 29, 3439-3447.

Missero, C., Calautti, E., Eckner, R., Chin, J., Tsai, L. H., Livingston, D. M. and Dotto, G. P. (1995). Involvement of the cell-cycle inhibitor Cip1/WAF1 and the E1A-associated p300 protein in terminal differentiation. Proc. Natl. Acad. Sci. USA 92, 5451-5455.

Moncada, S., Palmer, R. M. & Higgs, E. A. Nitric oxide: physiology, pathophysiology and pharmacology. Pharmacol. Rev. 43, 109-142 (1991).

Morimoto, T. et al. The dietary compound curcumin inhibits p300 histone acetyltransferase activity and prevents heart failure in rats. J. Clin. Invest. 118, 868-878 (2008).

Morris, L., Allen, K. E., and La Thangue, N. B. (2000) Regulation of E2F transcription by cyclin E-Cdk2 kinase mediated through p300/CBP coactivators. Nat. Cell Biol. 2, 232-239

Mosley AL, Ozcan S. Glucose regulates insulin gene transcription by hyperacetylation of histone h4. J Biol Chem 2003; 278: 19 660–19 666.

Muraoka M, Konishi M, Kikuchi-Yanoshita R, Tanaka K, Shitara N, Chong JM, Iwama T, Miyaki M (1996) p300 gene alterations in colorectal and gastric carcinomas. Oncogene 12:1565–1569

Mustard, D.; Ritchie, D. W., Docking essential dynamics eigenstructures. PROTEINS: Struct. Funct. Bioinf, 2005, 60, 269- 274.

Mroz RM, Noparlik J, Chyczewska E, Braszko JJ, Holownia A. Molecular basis of chronic inflammation in lung diseases: new therapeutic approach. J Physiol Pharmacol. 2007 Nov;58 Suppl 5(Pt 2):453-60. Review

Nerup J, Pociot F. A genomewide scan for type 1-diabetes susceptibility in Scandinavian families: identification of new loci with evidence of interactions. Am J Hum Genet 2001; 69: 1301–1313.

Neville, B.W., and Day, T.A. (2002). Oral cancer and precancerous lesions. CA Cancer J. Clin. 52, 195–215.

Nielsen SJ, Schneider R, Bauer UM, Bannister AJ, Morrison A, O'Carroll D, Firestein R, Cleary M, Jenuwein T, Herrera RE, Kouzasrides T (2001) Rb targets histone H3 methylation and HP1 to promoters. Nature 201(9):1367–1373.

Nikolov, D.B. and Burley, S.K. (1997) Proc. Natl. Acad. Sci. USA 94, 15–22.

Nucifora Jr FC, Sasaki M, Peters MF, Huang H, Cooper JK, Yamada M, Takahashi H, Tsuji S, Troncoso J, Dawson VL, Dawson TM and Ross CA (2001) Interference by

huntingtin and atrophin-1 with cbp-mediated transcription leading to cellular toxicity. Science 291: 2423-2428

O'Neill TE, Roberge M, Bradbury EM (1992) Nucleosome arrays inhibit both initiation and elongation of transcripts by bacteriophage T7 RNA polymerase. J Mol Biol 223:67-78.

Ogata, N., Ueda, K., Kawaichi, M., and Hayaishi, O. Poly(ADP-ribose) synthetase, a main acceptor of poly(ADP-ribose) in isolated nulcei. J Biol Chem 1981, 256, 4135-4137

Ogryzko, V. V.; Schiltz, R. L.; Russanova, V.; Howard, B. H.; Nakatani, Y. The transcriptional coactivators p300 and CBP are histone acetyltransferases Cell 1996, 87, 953-959

Ohniwa RL, Morikawa K, Kim J, Kobori T, Hizume K, Matsumi R, Atomi H, Imanaka T, Ohta T, Wada C, Yoshimura SH, Takeyasu K. Atomic force microscopy dissects the hierarchy of genome architectures in eukaryote, prokaryote, and chloroplast. Microsc Microanal. 2007 ;13(1):3-12.

Oike Y, Hata A, Mamiya T, Kaname T, Noda Y, Suzuki M, Yasue H, Nabeshima T, Araki K, Yamamura K (1999) Truncated CBP protein leads to classical Rubinstein-Taybi syndrome phenotypes in mice: implications for a dominant-negative mechanism. Hum Mol Genet 8:387-396

Okada Y, Feng Q, Lin Y, et al. hDOT1L links histone methylation to leukemogenesis. Cell 2005 ; 121 (2): 167 -78

Ota H, Tokunaga E, Chang K, Hikasa M, Iijima K, Eto M, Kozaki K, Akishita M, Ouchi Y, Kaneki M. Sirt1 inhibitor, Sirtinol, induces senescence-like growth arrest with attenuated Ras-MAPK signaling in human cancer cells. Oncogene. 2006 Jan 12;25(2):176-85.

Otto J.J., Actin-bundling proteins, Curr. Opin. Cell. Biol. 6 (1994) 105–109.

Papadimitrakopoulou, V.A., Clayman, G.L., Shin, D.M., Myers, J.N., Gillenwater, A.M., Goepfert, H., El-Naggar, A.K., Lewin, J.S., Lippman, S.M., and Hong, W.K. (1999). Biochemoprevention for dysplastic lesions of the upper aerodigestive tract. Arch. Otolaryngol. Head Neck Surg. 125, 1083–1089.

Parkin DM, Bray F, Ferlay J, Pisani P. Global cancer statistics, 2002. CA Cancer J Clin 2005;55(2):74-108.

Partanen A, Motoyama J, Hui CC (1 999) Developmentally regulated expression of the transcriptional cofactors/histone acetyltransferases CBP and p300 during mouse embryogenesis. Int J Dev Biol 43:487–494

Partin A.W., J.S. Schoeniger, J.L.Mohler, D.S. Coffery, Fourier analysis of cell motility: correlation of motility with metastatic potential, Proc. Natl. Acad. Sci. USA 86 (1989) 1254–1258

Partridge, M., Pateromichelakis, S., Phillips, E., Emilion, G.G., A'Hern, R.P., and Langdon, J.D. (2000). A case-control study confirms that microsatellite assay can identify patients at risk of developing oral squamous cell carcinoma within a field of cancerization. Cancer Res. 60, 3893–3898.

Pelicci PG. Do tumor-suppressive mechanisms contribute to organism aging by inducing stem cell senescence? J Clin Invest. 2004 Jan;113(1):4-7. Review.

Petrij F, Giles RH, Dauwerse HG, et al. Rubinstein–Taybi syndrome caused by mutations in the transcriptional co-activator CBP. Nature 1995 ; 376 (6538): 348 -51.

Petrij, F., Giles, R. H., Dauwerse, H. G., Saris, J. J., Hennekam, R. C., Masuno, M., Tommerup, N., van Ommen, G. J., Goodman, R. H. and Peters D. J. (1995). Rubinstein-Taybi syndrome caused by mutations in the transcriptional co-activator CBP. Nature 376, 348-351.

Pfister S, Rea S, Taipale M, Mendrzyk F, Straub B, Ittrich C, Thuerigen O, Sinn HP, Akhtar A, Lichter P. The histone acetyltransferase hMOF is frequently downregulated in primary breast carcinoma and medulloblastoma and constitutes a biomarker for clinical outcome in medulloblastoma. Int J Cancer. 2008 Mar 15;122(6):1207-13.

Pogribny, I. P. et al. Histone H3 lysine 9 and H4 lysine 20 trimethylation and the expression of Suv4–20h2 and Suv-39h1 histone methyltransferases in hepatocarcinogenesis induced by methyl deficiency in rats. Carcinogenesis 27, 1180–1186 (2006).

Pokholok, D.K., Harbison, C.T., Levine, S., Cole, M., Hannett, N.M., Lee, T.I., Bell, G.W., Walker, K., Rolfe, P.A., Herbolsheimer, E., et al. (2005). Genome-wide map of nucleosome acetylation and methylation in yeast. Cell 122, 517–527

Polevoda, B., and Sherman, F. (2002) The diversity of acetylated proteins. Genome Biol. 5, reviews0006.

Poux, A. N.; Cebrat, M.; Kim, C. M.; Cole, P. A.; Marmorstein, R. Structure of the GCN5 histone acetyltransferase bound to a bisubstrate inhibitor. Proc. Natl. Acad. Sci. U.S.A. 2002, 99, 14065-14070

Puri PL, Sartorelli V, Yang XJ, et al. Differential roles of p300 and PCAF acetyltransferases in muscle differentiation. Mol Cell 1997 ; 1 (1): 35 -45.

Qi W, Shakalya K, Stejskal A, Goldman A, Beeck S, Cooke L, Mahadevan D. NSC348884, a nucleophosmin inhibitor disrupts oligomer formation and induces apoptosis in human cancer cells. Oncogene. 2008 Jul 10;27(30):4210-20.

Quina AS, Buschbeck M, Di Croce L. Chromatin structure and epigenetics. Biochem Pharmacol. 2006 Nov 30;72(11):1563-9. Review.

Ravi R, Mookerjee B, van Hensbergen Y, Bedi GC, Giordano A, El-Deiry WS, Fuchs EJ, Bedi A. p53-mediated repression of nuclear factor-kappaB RelA via the transcriptional integrator p300. Cancer Res. 1998 Oct 15;58(20):4531-6.

Razin, A. (1998) CpG methylation, chromatin structure and gene silencing— a three-way connection. EMBO J. 17, 4905–4908.

Richon, V. M., Sandhoff, T. W., Rifkind R. A. & Marks, P. A. Histone deacetylase inhibitor selectively induces p21WAF1 expression and gene-associated histone acetylation. Proc. Natl Acad. Sci. USA 97, 10014–10019 (2000).

Rea S, Eisenhaber F, O'Carroll D, et al. Regulation of chromatin structure by site-specifi c histone H3 methyltransferases. Nature 2000 ; 406 (6796): 593 -9

Reinke, H., and Horz, W. (2003). Histones are first hyperacetylated and
then lose contact with the activated PHO5 promoter. Mol. Cell 11,1599–1607
Rhodes D, Klug A (1981) Sequence-dependent helical periodicity of DNA. Nature 292:378–380.

Richmond, T.J., and Davey, C.A. (2003). The structure of DNA in the nucleosome core. Nature 423, 145–150

Robert, F., Pokholok, D.K., Hannett, N.M., Rinaldi, N.J., Chandy, M., Rolfe, A., Workman, J.L., Gifford, D.K., and Young, R.A. (2004). Global position and recruitment of HATs and HDACs in the yeast genome. Mol. Cell 16, 199–209.

Roeder RG. Lasker Basic Medical Research Award. The eukaryotic transcriptional machinery: complexities and mechanisms unforeseen. Nat Med. 2003 Oct;9(10):1239-44.

Roeder RG. Transcriptional regulation and the role of diverse coactivators in animal cells. FEBS Lett. 2005 Feb 7;579(4):909-15. Review

Roelfsema JH, White SJ, Ariyurek Y, Bartholdi D, Niedrist D, Papadia F, Bacino CA, den Dunnen JT, van Ommen GJ, Breuning MH, Hennekam RC, Peters DJ (2005) Genetic heterogeneity in Rubinstein- Taybi syndrome: mutations in both the CBP and EP300 genes cause disease. Am J Hum Genet 76:572–580

Roh, M. S., Kim, C. W., Park, B. S., Kim, G. C., Jeong, J. H., Kwon, H. C., Suh, D. J., Cho, K. H., Yee, S. B., and Yoo, Y. H. (2004) Mechanism of histone deacetylase inhibitor Trichostatin A induced apoptosis in human osteosarcoma cells. Apoptosis 9, 583–589

Roopra, A., Sharling, L., Wood, I. C., Briggs, T., Bachfischer, U., Paquette, A. J., and Buckley, N. J. (2000) Transcriptional repression by neuronrestrictive silencer factor is mediated via the Sin3-histone deacetylase complex. Mol. Cell. Biol. 20, 2147–2157.

Rosin, M.P., Cheng, X., Poh, C., Lam, W.L., Huang, Y., Lovas, J., Berean, K., Epstein, J.B., Priddy, R., Le, N.D., and Zhang, L. (2000). Use of allelic loss to predict malignant risk for low-grade oral epithelial dysplasia. Clin. Cancer Res. 6, 357–362.

Roth SY, Denu JM, Allis CD. Histone acetyltransferases. Ann Rev Biochem 2001 ; 70 : 81 -120.

Roth U, Curth K, Unterman TG, et al. The transcription factors HIF-1 and HNF-4 and the coactivator p300 are involved in insulin-regulated glucokinase gene expression via the phosphatidylinositol 3-kinase/protein kinase B pathway. J Biol Chem 2004; 279: 2623–2631.

Rouaux C, Loeffl er JP, Boutillier AL. Targeting CREB-binding protein (CBP) loss of function as a therapeutic strategy in neurological disorders. Biochem Pharmacol 2004 ; 68 (6): 1157 -64

Rouaux, C.; Jokic, N.; Mbebi, C.; Boutillier, S.; Loeffler, J. P.; Boutillier, A. L. Critical loss of CBP/p300 histone acetylase activity by caspase-6 during neurodegeneration. EMBO J. 2003, 22, 6537-6549.

Rouaux C, Jokic N, Mbebi C, Boutillier S, Loeffler JP and Boutillier AL (2003) Critical loss of CBP/p300 histone acetylase activity by caspase-6 during neurodegeneration. EMBO J. 22: 6537–6549

Rubbi, C. P., and Milner, J. (2003) p53 is a chromatin accessibility factor for nucleotide excision repair of DNA damage. EMBO J. 22, 975–986.

Rubinstein JH, Taybi H (1963) Broad thumbs and toes and facial abnormalities. Am J Dis Child 105:588–608

Sadoul K, Boyault C, Pabion M, Khochbin S. Regulation of protein turnover by acetyltransferases and deacetylases. Biochimie 2008;90(2):306–12.

Sakaguchi, K., Herrera, J. E., Saito, S., Miki, T., Bustin, M., Vassilev, A., Anderson, C. W., and Appella, E. (1998) DNA damage activates p53 through a phosphorylation-acetylation cascade. Genes Dev. 12, 2831–2841.

226

Saha RN, Pahan K. HATs and HDACs in neurodegeneration: a tale of disconcerted acetylation homeostasis. Cell Death Differ. 2006 Apr;13(4):539-50. Review

Sampath SC, Marazzi I, Yap KL, Sampath SC, Krutchinsky AN, Mecklenbräuker I, Viale A, Rudensky E, Zhou MM, Chait BT, Tarakhovsky A. Methylation of a histone mimic within the histone methyltransferase G9a regulates protein complex assembly. Mol Cell. 2007 Aug 17;27(4):596-608

Sartorelli, V., and Puri, P. L. (2001) The link between chromatin structure, protein acetylation and cellular differentiation. Front. Biosci. 6, D1024–D1047.

Sarli, V.; Giannis, A. Selective inhibition of CBP/p300 HAT.Chem Biol. 2007, 6, 605-606.

Satchwell SC, Drew HR, Travers AA (1986) Sequence periodicities in chicken nucleosome core DNA. J Mol Biol 191:659–675.

Schalch T, Duda S, Sargent DF, Richmond TJ. X-ray structure of a tetranucleosome and its implications for the chromatin fibre. Nature. 2005 Jul 7;436(7047):138-41.

Schwartz, B.E., and Ahmad, K. (2005). Transcriptional activation triggers deposition and removal of the histone variant H3.3. Genes Dev. 19, 804–814

Seligson DB, Horvath S, Shi T, et al. Global histone modification patterns predict risk of prostate cancer recurrence. Nature 2005 ; 435 (7046): 1262 -6.

Selvi BR, Jagadeesan D, Suma BS, Nagashankar G, Arif M, Balasubramanyam K, Eswaramoorthy M, Kundu TK. Intrinsically fluorescent carbon nanospheres as a nuclear targeting vector: delivery of membrane-impermeable molecule to modulate gene expression in vivo. Nano Lett. 2008 Oct;8(10):3182-8..

Sen N, Hara MR, Kornberg MD, Cascio MB, Bae BI, Shahani N, Thomas B, Dawson TM, Dawson VL, Snyder SH, Sawa A. Nitric oxide-induced nuclear GAPDH activates p300/CBP and mediates apoptosis. Nat Cell Biol. 2008 Jul;10(7):866-73.

Shahbazian, M.D. & Grunstein, M. Functions of site-specific histone acetylation and deacetylation. Annu. Rev. Biochem. 76, 75–100 (2007).

Sharma RA, Gescher AJ, Steward WP. Curcumin: the story so far. Eur J Cancer. 2005 Sep;41(13):1955-68. Review.

Sharpless NE, DePinho RA. Telomeres, stem cells, senescence, and cancer. J Clin Invest. 2004 Jan;113(2):160-8. Review.

Shay JW, Roninson IB. Hallmarks of senescence in carcinogenesis and cancer therapy. Oncogene. 2004 Apr 12;23(16):2919-33. Review.

Shikama, N.; Ivon, J.; La Thangue, N. The p300/CBP family: Integrating signals with transcription factors and chromatin. Trends Cell Biol.1997, 7, 230-236.

Shikama N., W. Lutz, R. Kretzschmar, N. Sauter, J. F. Roth, S. Marino, J. Wittwer, A. Scheidweiler, R. Eckner, EMBO J. 2003, 22, 5175 –5185.

Shilatifard, A. Chromatin modifications by methylation and ubiquitination: implications in the regulation of gene expression. Annu. Rev. Biochem. 75, 243–269 (2006).

Shiio Y, Eisenman RN. Histone sumoylation is associated with transcriptional repression. Proc Natl Acad Sci USA 2003 ; 100 (23): 13225 -30.

Shin KH, Kang MK, Park NH. Heterogeneous nuclear ribonucleoprotein G, nitric oxide, and oral carcinogenesis. Nitric Oxide. 2008 Sep;19(2):125-32. Review

228

Shim JS, Kim DH, Jung HJ, Kim JH, Lim D, Lee SK, Kim KW, Ahn JW, Yoo JS, Rho JR, Shin J, Kwon HJ. Hydrazinocurcumin, a novel synthetic curcumin derivative, is a potent inhibitor of endothelial cell proliferation. Bioorg Med Chem. 2002 Sep;10(9):2987-92.

Sirover MA. New insights into an old protein: the functional diversity of mammalian glyceraldehyde-3-phosphate dehydrogenase. Biochim Biophys Acta. 1999 Jul 13;1432(2):159-84. Review

Sobulo OM, Borrow J, Tomek R, Reshmi S, Harden A, Schlegelberger B, Housman D, Doggett NA, Rowley JD, Zeleznik L (1997) MLL is hsed to CBP, a histoneacetyltransferase, in therapy-related acute myeloid leukemia with a t(11;16)(q23;p13.3). Proc Natl Acad Sci U S A 94:8732–8737

Spange S, Wagner T, Heinzel T, Krämer OH. Acetylation of non-histone proteins modulates cellular signalling at multiple levels. Int J Biochem Cell Biol. 2009 Jan;41(1):185-98.

Stein RW, Corrigan M, Yaciuk P, et al. Analysis of E1A-mediated growth regulation functions: binding of the 300-kilodalton cellular product correlates with E1A enhancer repression function and DNA synthesis-inducing activity. J Virol 1990 ; 64 (9): 4421 -7.
Sterner, D. E., and Berger, S. L. (2000) Acetylation of histones and transcription-related factors. Microbiol. Mol. Biol. Rev. 64, 435–459.

Stiehl DP, Fath DM, Liang D, Jiang Y, Sang N. Histone deacetylase inhibitors synergize p300 autoacetylation that regulates its transactivation activity and complex formation. Cancer Res. 2007 Mar 1;67(5):2256-64.

Strahl, B.D., Grant, P.A., Briggs, S.D., Sun, Z.W., Bone, J.R., Caldwell, J.A., Mollah, S., Cook, R.G., Shabanowitz, J., Hunt, D.F., et al. (2002). Set2 is a nucleosomal histone H3-

selective methyltransferase that mediates transcriptional repression. Mol. Cell. Biol. 22, 1298–130

Sudbo, J., Kildal, W., Risberg, B., Koppang, H.S., Danielsen, H.E., and Reith, A. (2001). DNA content as a prognostic marker in patients with oral leukoplakia. N. Engl. J. Med. 344, 1270–1278.

Suka, N., Luo, K., and Grunstein, M. Sir2p and Sas2p opposingly regulate acetylation of yeast histone H4 lysine16 and spreading of heterochromatin. Nat Genet. 2002, 32, 378-383

Swaminathan, V.; Reddy, B. A.; Ruthrotha Selvi, B.; Sukanya, M. S.; Kundu, T. K. Small molecule modulators in epigenetics: implications in gene expression and therapeutics. Subcell. Biochem. 2007, 41, 397-428

Takahashi, Y., Rayman, J. B., and Dynlacht, B. D. (2000) Analysis of promoter binding by the E2F and pRB families in vivo: distinct E2F proteins mediate activation and repression. Genes Dev. 14, 804–816

Tanaka Y., I. Naruse, T. Hongo, M. Xu, T. Nakahata, T. Maekawa, S. Ishii, Mech. Dev. 2000, 95, 133–145.

Tanaka, Y., Naruse, I., Maekawa, T., Masuya, H., Shiroshi, T. and Ishii, S. (1997). Abnormal skeletal patterning in embryos lacking a single Cbp allele: a partial similarity with Rubinstein-Taybi syndrome. Proc. Natl. Acad. Sci. USA 94, 10215-10220.

Tang Y., M.A. Holbert, H. Wurtele, K. Meeth, W. Rocha, M. Gharib, E. Jiang, P. Thibault, A. Verrault, P.A. Cole, R. Marmorstein, Fungal Rtt109 histone acetyltransferase is an unexpected structural homolog of metazoan p300/CBP, Nat. Struct. Mol. Biol. 15 (2008) 738–745.

Thomas MC, Chiang CM. The general transcription machinery and general cofactors. Crit Rev Biochem Mol Biol. 2006 May-Jun;41(3):105-78. Review.

Thomsen, L. L., Sargent, J. M., Williamson, C. J. & Elgie, A. W. Nitric oxide synthase activity in fresh cells from ovarian tumour tissue: relationship of enzyme activity with clinical parameters of patients with ovarian cancer. Biochem. Pharmacol. 56, 1365–1370 (1998).

Taylor JP, Taye AA, Campbell C, Kazemi-Esfarjani P, Fischbeck KH and Min KT (2003) Aberrant histone acetylation, altered transcription, and retinal degeneration in a Drosophila model of polyglutamine disease are rescued by CREB-binding protein. Genes. Dev. 17: 1463–1468

Thompson NC, Koth LL, Yang YH et al. Active cigarette smoking and asthma. Clin Exp Allergy 2003; 33: 1471-1475

Thompson, P. R.; Kurooka, H.; Nakatani, Y.; Cole, P. A. Transcriptional coactivator protein p300. Kinetic characterization of its histone acetyltransferase activity. J. Biol. Chem. 2001, 276, 33721-33729

Thompson, P. R.; Wang, D.; Wang, L.; Fulco, M.; Pediconi, N.; Zhang, D.; An, W.; Ge, Q.; Roeder, R. G.; Wong, J.; Levrero, M.; Sartorelli, V.; Cotter, R. J.; Cole, P. A. Regulation of the p300 HAT domain via a novel activation loop. Nat. Struct. Mol. Biol. 2004, 11, 308-315.

Thorne JL, Campbell MJ, Turner BM. Transcription factors, chromatin and cancer. Int J Biochem Cell Biol. 2009 Jan;41(1):164-75.

Tilney L.G., P.S. Connelly, K.A. Vranich, M.K. Shaw, G.M. Guild, Why are two different cross-linkers necessary for actin bundle formation in vivo and what does each cross-link contribute?, J Cell. Biol. 143 (1998) 121–133.

Tryndyak, V. P., Kovalchuk, O. & Pogribny, I. P. Loss of DNA methylation and histone H4 lysine 20 trimethylation in human breast cancer cells is associated with aberrant expression of DNA methyltransferase 1, Suv4–20h2 histone methyltransferase and methyl-binding proteins. Cancer Biol. Ther. 5, 65–70 (2006).

Utley, R.T., Cote, J., Owen-Hughes, T., and Workman, J.L. (1997). SWI/SNF stimulates the formation of disparate activator-nucleosome complexes but is partially redundant with cooperative binding. J. Biol. Chem. 272, 12642–12649.

Varambally S, Dhanasekaran SM, Zhou M, Barrette TR, Kumar-Sinha C, Sanda MG, Ghosh D, Pienta KJ, Sewalt RG, Otte AP, Rubin MA, Chinnaiyan AM. The polycomb group protein EZH2 is involved in progression of prostate cancer. Nature. 2002 Oct 10;419(6907):624-9.

Van Beekum O, Kalkhoven E. Aberrant forms of histone acetyltransferases in human disease. Subcell Biochem. 2007;41:233-62. Review.

Van Zandwijk, N., Dalesio, O., Pastorino, U., de Vries, N., and van Tinteren, H. (2000).EUROSCAN, a randomized trial of vitamin A and N-acetylcysteine in patients with head and neck cancer or lung cancer. For the European Organization for Research and Treatment of Cancer Head and Neck and Lung Cancer Cooperative Groups. J. Natl. Cancer Inst. 92, 977–986.

Varier, R. A.; Kundu, T. K. Chromatin modifications (acetylation/ deacetylation/ methylation) as new targets for HIV therapy. Current Pharmaceutical Design 2006, 12, 1975-1993

Vilà MR, Nicolás A, Morote J, de I, Meseguer A. Increased glyceraldehyde-3-phosphate dehydrogenase expression in renal cell carcinoma identified by RNA-based, arbitrarily primed polymerase chain reaction. Cancer. 2000 Jul 1;89(1):152-

Vire, E. et al. The Polycomb group protein EZH2 directly controls DNA methylation. Nature 439, 871–874 (2006).

Vo, N., Fjeld, C., and Goodman, R.H. (2001). Acetylation of nuclear hormonereceptor-interacting protein RIP140 regulates binding of the transcriptional corepressor CtBP. Mol. Cell. Biol. 21, 6181–6188.

Von Lindern, M., Fornerod, M., van Baal, S., Jaegle, M., de Wit, T., Buijs, A., and Grosveld, G. The translocation (6;9), associated with a specific subtype of acute myeloid leukemia, results in the fusion of two genes, dek and can, and the expression of a chimeric, leukemia-specific dek-can mRNA. Mol Cell Biol. 1992, 12, 1687-1697.

Wallace JM. Nutritional and botanical modulation of the inflammatory cascade—eicosanoids, cyclooxygenases, and lipoxygenases—as an adjunct in cancer therapy. Integr Cancer Ther 2002;1:7–37.

Wang, A. H., Bertos, N. R., Vezmar, M., Pelletier, N., Crosato, M., Heng, H. H., Th'ng, J., Han, J., and Yang, X. J. (1999) HDAC4, a human histone deacetylase related to yeast HDA1, is a transcriptional corepressor. Mol. Cell. Biol. 19, 7816–7827

Wang X, Tsao SW, Wong YC, Cheung AL. Induction of senescent-like growth arrest as a new target in anticancer treatment. Curr Cancer Drug Targets. 2003 Apr;3(2):153-9. Review.

Webster GA, Perkins ND. Transcriptional cross talk between NF-kappaB and p53. Mol Cell Biol. 1999 May;19(5):3485-95.

Wink DA, Vodovotz Y, Laval J, Laval F, Dewhirst MW, Mitchell JB. The multifaceted roles of nitric oxide in cancer. Carcinogenesis. 1998 May;19(5):711-21. Review.

Wolffe, A. P., and Guschin, D. (2000) Chromatin structural features and targets that regulate transcription. J. Struct. Biol. 129, 102–122

Wolffe, A. P. Chromatin remodeling: Why it is important in cancer. Oncogene 2001, 20, 2988-2990.

Woodcock, C.L., and Dimitrov, S. (2001). Higher-order structure of chromatin and chromosomes. Curr. Opin. Genet. Dev. 11, 130–135.

Worcel, A., and Burgi, E. On the structure of the folded chromosome of Escherichia coli. J. Mol. Biol. 1972, 71, 127-147.

Workman, J.L., and Kingston, R.E. (1998). Alteration of nucleosome structure as a mechanism of transcriptional regulation. Annu. Rev. Biochem. 67, 545–579.

Workman JL, Kingston RE. Alteration of nucleosome structure as a mechanism of transcriptional regulation. Ann Rev Biochem 1998 ; 67 : 545 -79.

Xiao W. Advances in NF-kappaB signaling transduction and transcription. Cell Mol Immunol 2004;1(6):425–35.

Xiang K, Wang Y, Zheng T, et al. Genome-wide search for type 2 diabetes/impaired glucose homeostasis susceptibility genes in the Chinese: significant linkage to chromosome 6q21-q23 and chromosome 1q21-q24. Diabetes 2004; 53: 228–234.

Xu W, Chen H, Du K, Asahara H, Tini M, Emerson BM, Montminy M, Evans RM (2001) A transcriptional switch mediated by cofactor methylation. Science 294:2507–2511

Xu W, Liu LZ, Loizidou M, Ahmed M, Charles IG. The role of nitric oxide in cancer. Cell Res. 2002 Dec;12(5-6):311-20. Review.

234

Yamauchi T, Oike Y, Kamon J, et al. Increased insulin sensitivity despite lipodystrophy in Crebbp heterozygous mice. Nat Genet 2002; 30: 221–226.

Yang, X. J., Ogryzko, V. V., Nishikawa, J., Howard, B. H. and Nakatani, Y. (1996). A p300/CBP-associated factor that competes with the adenoviral oncoprotein E1A. Nature 382, 319-324.

Yang XJ. The diverse superfamily of lysine acetyltransferases and their roles in leukemia and other diseases. Nucleic Acids Res 2004 ; 32 (3): 959 -76.

Yang XJ, Seto E. Lysine acetylation: codified crosstalk with other posttranslational modifications. Mol Cell. 2008 Aug 22;31(4):449-61. Review.

Yao, T., Oh, S. P., Fuchs, M., Zhou, N., Ch'ng, L., Newsome, D., Bronson, R. T., Li, E., Livingston, D. M. and Eckner, R. (1998). Gene dosagedependent embryonic development and proliferation defects in mice lacking the transcriptional integrator p300. Cell 93, 361-372.

Yao T. P., S. P. Oh, M. Fuchs, N. D. Zhou, L. E. Ch'ng, D. Newsome, R. T. Bronson, E. Li, D. M. Livingston, R. Eckner, Cell 1998, 93, 361– 372.

Yuan LW, Giordano A (2002) Acetyltransferase machinery conserved in p300ICBP-family proteins. Oncogene 21:2253–2260

Yuan LW, Gambee JE. Phosphorylation of p300 at serine 89 by protein kinase C. J Biol Chem. 2000 Dec 29;275(52):40946-51.

Yuen A.P.W., K.Y. Lam, A.C. Chan, W.I. Wei, L.K. Lam, W.K. Ho, C.M. Ho, Clinicopathological analysis of elective neck dissection for N0 neck of early oral tongue carcinoma, Am. J. Surg. 177 (1999) 90–92.

Yuen A.P.W., W.I. Wei, Y.M. Wong, K.C. Tang, Elective neck dissection versus observation in the surgical treatment of early oral tongue carcinoma, Head Neck 19 (1997) 83–88

Yuen A.P.W., W.I. Wei, L.K. Lam, W.K. Ho, D. Kwong, Results of surgical salvage of locoregional recurrence of carcinoma of tongue after radiotherapy failure, Ann. Otol. Rhinol. Laryngol. 106 (1997) 779–782.

Zamore, P. D., and Haley, B. Ribo-gnome: the big world of small RNAs. Science 2005, 309, 1519-1524.

Zink, D. et al. Structure and dynamics of human interphase chromosome territories in vivo. Hum. Genet. 102, 241–251 (1998).

Zhang, Q., Yao, H., Vo, N., and Goodman, R. H. (2000) Acetylation of adenovirus E1A regulates binding of the transcriptional corepressor CtBP. Proc. Natl. Acad. Sci. U. S. A. 97, 14323–14328.

Zhang Y, Reinberg D. Transcription regulation by histone methylation: interplay between different covalent modifi cations of the core histone tails. Genes Dev 2001 ; 15 (18): 2343 -60

Zhao, H. et al. B-cell chronic lymphocytic leukemia cells express a functional inducible nitric oxide synthase displaying anti-apoptotic activity. Blood 92, 1031–1043 (1998).

Zheng L, Roeder RG, Luo Y. S phase activation of the histone H2B promoter by OCA-S, a coactivator complex that contains GAPDH as a key component. Cell. 2003 Jul 25;114(2):255-66.

Zhou, X. Y.; Shibusawa, N.; Naik, K.; Porras, D.; Temple, K.; Ou, H.; Kaihara, K.; Roe, M. W.; Brady, M. J.; Wondisford, F. E. Insulin regulation of hepatic gluconeogenesis through phosphorylation of CREB-binding protein. Nat. Med. 2004, 10, 633-637.

Zhou, M., Halanski, M. A., Radonovich, M. F., Kashanchi, F., Peng, J.,Price, D. H., and Brady, J. N. (2000) Tat modifies the activity of CDK9 to phosphorylate serine 5 of the RNA polymerase II carboxyl-terminal domain during human immunodeficiency virus type 1 transcription. Mol. Cell. Biol. 20, 5077–5086.

Zhou, J., Fan, F.Y., Rangasamy, D. & Tremethick, D.J. Nat. Struct. Mol. Biol. 14, 1070–1076 (2007).

572
P09

237